Analysis of a rolling FRP lock gate

+ stability during movement

P.J. Teengs

August 2017

TU Delft

Cover photo:
Rolling gates for new Panama locks

https://sevenwood.wordpress.com/

Analysis of a rolling FRP lock gate
+ stability during movement

By

P.J. Teengs

In partial fulfilment of the requirements for the degree of

Master of Science
in Civil Engineering

at the Delft University of Technology
to be defended publicly August 17, 2017.

Supervisor:	Prof. dr. ir. S. Jonkman, TU Delft
Thesis committee:	Dr. Ir. F.P. van der Meer, TU Delft
	Ir. W.F. Molenaar, TU Delft

An electronic version of this thesis is available at http://repository.tudelft.nl/.

TU Delft

Preface

This report presents the final version of my master thesis. This graduation project was performed to obtain a Master of Science degree in Civil Engineering at the Delft University of Technology.

I would like to thank my graduation committee, especially Ir. W.F. Molenaar, for their input and patience during the realization of this thesis.

Finally I would like to thank my friends and family for their unconditional support during this long process.

Haarlem, July 2017
Pieter Teengs

Abstract

Fibre-reinforced polymers (FRPs) are becoming a more commonly used building material in many civil engineering applications including locks. One quality of FRPs is the fact that it has a high strength to weight ratio. By applying FRPs in rolling lock gate design, the self-weight of the gate could be significantly reduced. This in turn could lead to less wear-and-tear to the support carriages, mechanical parts and rails. Self-weight is also an important factor in the stability of a rolling lock gate. A minimum weight is required to counter the moment caused by horizontal loads during opening and closing. If FRPs were to be applied in rolling lock gates an optimization of lightweight versus stability will be required. The objective of this thesis is to investigate the technical feasibility of the FRP rolling lock gate and how the gates design is affected by the stability criteria. Also, the question remains if the FRP design can compete with traditional materials, for example steel.

To quantify the problem a case study was chosen: New Lock Terneuzen. A rolling lock gate is set to be constructed to improve the connection between Ghent-Terneuzen. The rolling gates will be very large, with a span of 55 m and a height of approximately 26 m.

Initially, the rolling gate is designed with a box shape. The global dimensions of the box gate are determined with a hand calculation based on the boundary conditions and design input from the chosen case study. Basic strength, deflection and stability checks are performed. The box gate is dimensioned in both FRP and steel. The following dimensions are found for the FRP box gate: Width of 8.96 m, with retaining plates: skin:280 mm, core: 200 mm and webs: skin: 200 mm, core: 200 mm. The table below presents a comparison of applied material volume, mass and costs of the FRP and steel box gates.

	Volume [m³]	**Mass [kg]**	**Cost [€]**
Steel box			
Steel	385	3.022.250	4.533.375
FRP box			
FRP	1435	2.832.690	11.330.760
Foam	1206	120.600	120.600

The dimensions found with the hand calculation serve as input for a 3D model of the design. The model is created with Scia Engineer. With this software the gate is checked with finite element analysis. Some additional checks, fatigue and creep, are performed.

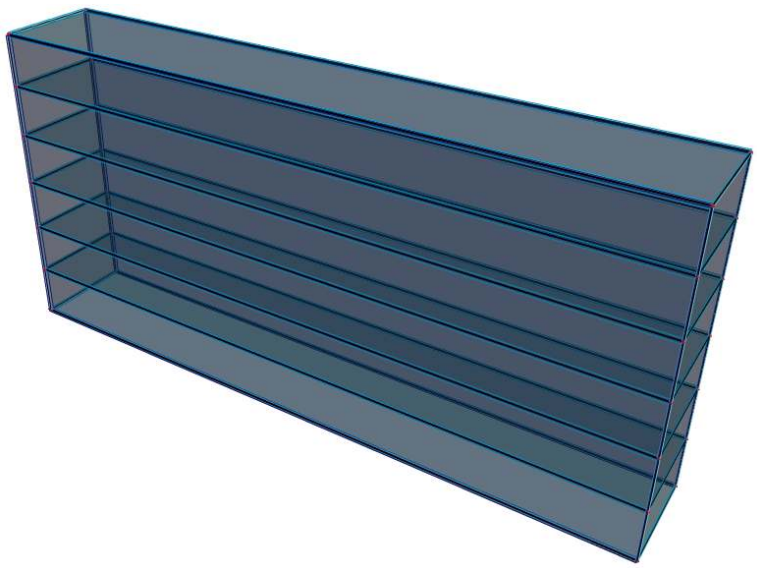

The box gate model is adjusted to resemble the gate during movement. This is achieved by changing the supports, leaving the top right corner unsupported. In addition to a 3D stability check of the designed box gate, the width between the supports, representing the carriage width, is varied (from 0.5 to 12 m) and the impact on the stability is evaluated. This impact is quantified by the required dead weight to guarantee stability.

All the results are used to come up with potential improvements or alternatives to the box gate design. The main objective being a gate with increased stability, which is again quantified by the overweight required. A number of ideas are discussed, where optimizing the shape of the gate is explored further. The following shapes are evaluated.

Model 4a

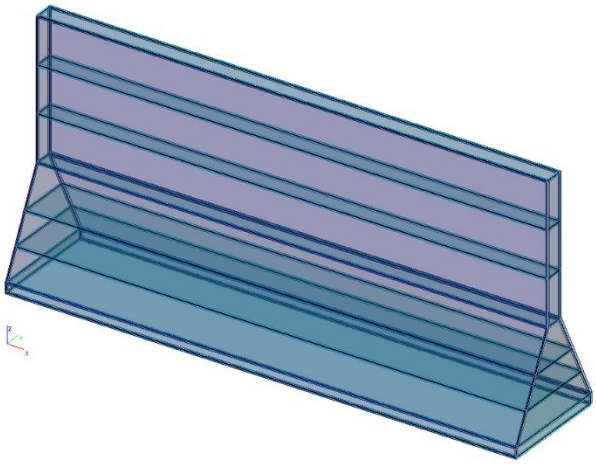

Model 4b

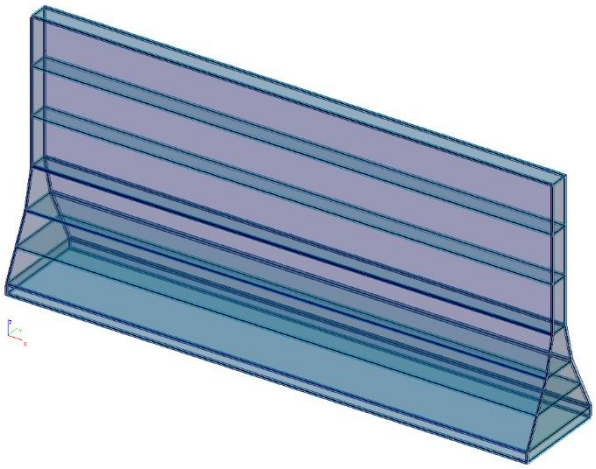

Model 4c

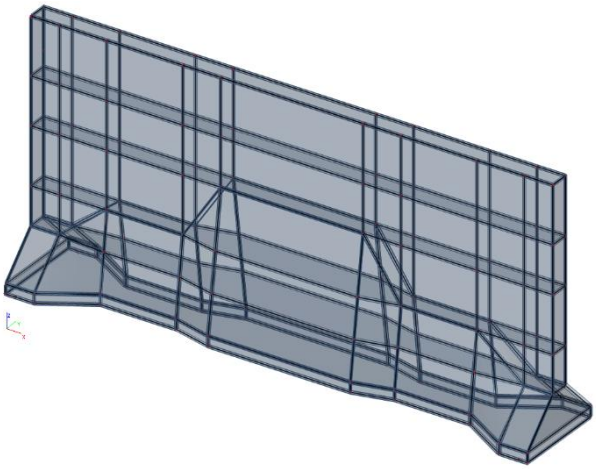

Model 4d

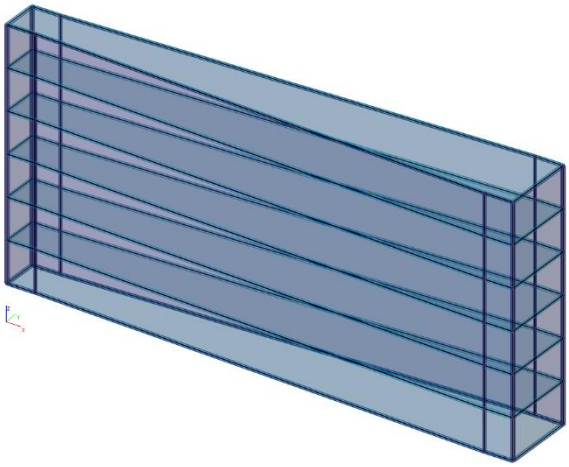

It is found that the required dead weight to achieve stability increased for all evaluated shapes. The main reason is the distribution of the stabilizing moment, which is split up in a horizontal and vertical component. The shape changes result in an shift from horizontal to vertical, which in turn results in more dead weight required to meet the stability criteria.

Gate	Width [m]	Hor. [kNm]	Vert. [kNm]	Required Dead weight [kN]
3a	8	69519	26391	19792
4a	12	57045	41495	20748
4b	10	57178	40613	24368
4c	10	59186	37782	22669
4d	4 - 8	67149	29159	21869

The application of FRP in rolling gate design is technically feasible. However from a stability point of view it's questionable if FRP is the better choice over traditional materials. In the chosen case study, the amount dead weight required to fulfil the stability criteria is significant, and the lightweight quality of FRP cannot be fully taken advantage of. Laminates are designed much thicker when compared to the dimensions required to meet strength and deflection criteria. In other words, material is added primarily for the sake of adding weight.

Reducing the required dead weight was proven to be much harder than anticipated. Even though a wide base gives a larger arm for the vertical couple, which would lead to a smaller force at an equal moment, the required weight is not necessarily reduced. The applied loads, shape of the gate, location of supports and deflections all affect the distribution of loads over the supports, both horizontal and vertical, of the gate. In a structure of this scale, even small differences can have a significant impact on the stability of the gate and the dead weight required to achieve this stability. The required dead weight to meet the stability criteria must be brought down in order for FRP to be a viable option.

Table of Contents

1 Introduction

Locks are an essential part in global waterways, both inland and maritime. With high economic stakes, the demand for efficiently operating locks is always increasing. Operating times must be short while guaranteeing gate stability and safe passage of vessels. In addition, the required maintenance should be limited.

With a successful track record in many different applications, the use of fibre-reinforced polymers (FRPs) in civil engineering is increasing over the last decades. “FRPs are not a “space-age” material anymore, exclusively used in stealth bombers and space shuttles.” (Zoghi, 2013) This composite material has many advantages over traditional construction materials, with a high strength-to-weight ratio, its unique ability to ‘tailor’ the properties to specific needs and excellent corrosion resistance. FRPs could potentially be a competitive alternative for traditional construction materials in locks and specifically lock gates.

In practice, FRPs have been applied in relatively small mitre gates, and research has shown that it’s technically and economically feasible to use FRPs in various types of locks, e.g. mitre and lift gates. There is still much to be learned about the material and its application in lock gates.

1.1 Problem definition

Locks with rolling lock gates are generally large and wide. Scaling up from a relatively small mitre gate could pose a problem in the technical (and economic) feasibility of the rolling gate.

In comparison to mitre gates, consisting of two gates, the rolling gate is one large gate. During opening and closing, the top corner is unsupported, which results in one of the main issues in rolling gate design. The stability of the gate during opening and closing. To guarantee a certain level of stability, some self-weight is required. Using FRP should result in a lighter gate, which is beneficial for many aspects of the design, but not for the stability problem.

One area of the gates design that could benefit from a lighter gate is the operating mechanism, i.e. support carriages, guide rails and operating machinery. These elements require a lot of maintenance and because it is often difficult to reach them, reducing the maintenance of these particular elements is desirable. The forces on these elements will be smaller with a lighter gate, resulting in less wear-and-tear. Also, plastic deformation of the rails is reduced and therefore less maintenance required.

1.2 Hypothesis

Due to the positive results from other research, (Kok, 2013) (Straten, 2013), on the feasibility of FRPs in lock gates, the expectation is that this will also be the case for rolling lock gates.

The stability problem is an issue with gates executed in traditional construction materials. The expectation is that it is possible to design a stable FRP gate, but optimizing the weight reduction will be complicated.

The minimum self-weight required to guarantee stability of the gate is a limiting factor to the potential weight reduction by applying FRP. In turn, the benefits regarding decreased wear-and-tear and maintenance required on various elements of the operating mechanism are limited as well. Therefore it is expected that the benefits of applying FRP will not be that significant in comparison with a steel gate.

1.3 Objective

The objective is to investigate the technical feasibility of the application of FRPs in rolling lock gates and in particular the stability of this gate. How does the stability criteria affect a design in FRP and vice versa, i.e. what is the impact of the application of this lightweight material on the stability of the gate? Finally, gain some insight in the possibilities to fully utilize the potential of FRPs in rolling gates regarding stability.

1.4 Research questions

Primary research question(s):

- *Is it technically feasible to use fibre-reinforced polymers in rolling lock gates?*
- *How do requirements for stability during movement* affect the rolling gates design in FRP?*

* Movement refers to opening and closing of the gate.

Secondary research questions:

- Which elements make up a rolling lock gate design? (Ch. 2)
- What are Fibre-reinforced polymers? Their components and properties? And how are they used in design? (Ch. 3)
- What are the boundary conditions of the case study? (Ch. 5)
- How do you design a lock gate in FRP? (Ch. 7 & 8)
- How is the stability of the gate during opening and closing investigated? (Ch. 7 & 9)
- Can FRP compete with traditional materials in rolling lock gate design? (Ch. 7)
- Is it possible to achieve the full potential of the lightweight qualities of FRP? (Ch. 8 & 9)
- What are possible improvements/alternatives to increase the stability and optimize weight reduction? (Ch. 10)

1.5 Reading guide

Chapter 2
Description of locks and specifically rolling lock gates, its functions and the various structural elements. Gain a basic understanding of the structure.

Chapter 3
Gain basic knowledge about fibre-reinforced polymers, its components, manufacturing methods, properties and mechanics of the material.

Chapter 4
Elaboration of the research method. The chapter is divided into two parts: Part A – Gate design and Part B – Gate stability.

Chapter 5
The introduction of the case New Lock 'Nieuwe Sluis' Terneuzen. Consisting of a description of the current situation and the project. This case is used to quantify the problem, resulting in the requirements/boundary conditions for the design of the lock gate.

Chapter 6
All required design input is calculated with the boundary conditions as established in chapter 5.

Chapter 7
The global dimensions of a box gate are determined with a hand calculation based on the boundary conditions and design input from the previous chapters. The box gate is dimensioned in both FRP and steel. Basic strength, deflection and stability checks are performed.

Chapter 8
A 3D model of the design is made in Scia Engineer. The gate in closed position is checked with finite element analysis. Some additional checks, fatigue and creep, are performed.

Chapter 9
The stability of the gate during opening and closing is investigated in detail.

Chapter 10
By evaluating the results from the previous chapters, potential solutions are presented for a lightweight structure and its stability.

1.6 Structure of thesis

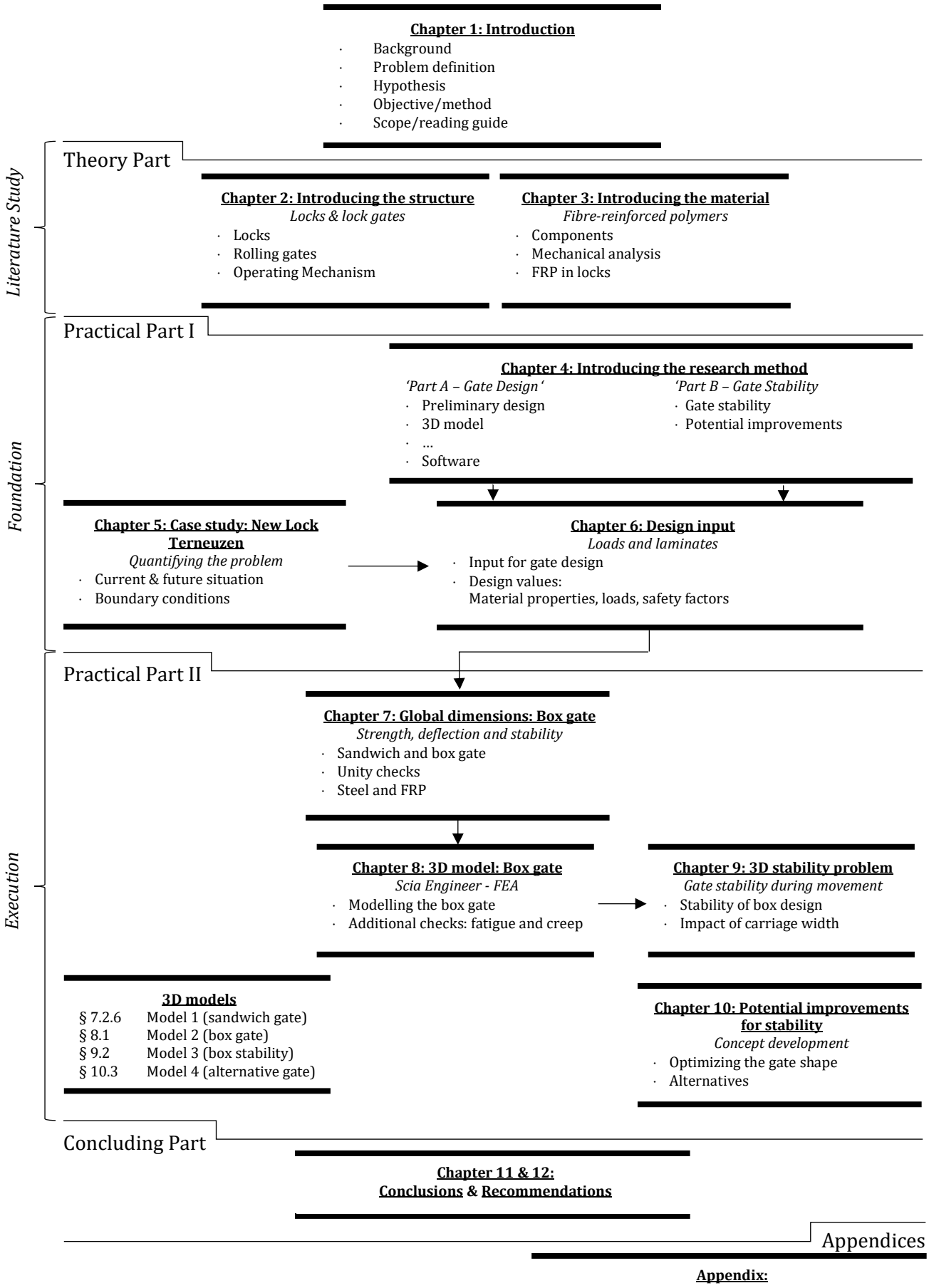

Theory Part

Literature Study

- Introducing the structure – Locks and lock gates
- Introducing the material – Fibre-Reinforced Polymer
- Introducing the research method

2 Introducing the structure

Locks and lock gates

Transport across water (inland and maritime) makes up a large portion of the total transportation of goods worldwide. It's an economically attractive and relatively environmentally friendly way to transport large amounts of goods, but well planned shipping routes and efficient transit of vessels is key. One crucial component in these large water systems is the lock. Locks belong to the sluice family, and there are many different types: Dewatering gate, stop lock, guard lock, storm surge barrier and a navigation lock, to name a few. All of which are constructed with a variety of functions, such as water retention, -locking, -discharge, shore connection and passage of vessels. (Molenaar & e.a., 2011)

This chapter will discuss important aspects concerning locks, like its main functions, general layout and lock gates. The main focus will be on rolling lock gates. In this case, and for the remainder of this thesis, the term lock refers to a *navigation lock*. Most of the information in this chapter is derived from Design of Locks (Vrijburcht & Glerum, 2000).

2.1 Functions of a navigation lock

The main function of a navigation lock, as opposed to other sluice type structures, is allowing vessels to navigate between two sections of a waterway (or reaches) with differing water levels. The water level difference between both sides of the lock is called the lift. To overcome the lift, one or a series of locks (a flight of locks or lock ladder) can be constructed. The aim is to allow for passage as safe and efficient as possible.

Next to the navigation function, locks have a water retaining function and sometimes a water management function. Maritime locks are often part of a flood defence system.

When designing a lock, there are many factors that influence the design process and have to be considered to get from idea initiative to final design and from construction to demolition. An important starting point of the design process is the Program of Requirements, containing the preconditions and (functional) requirements that the lock has to meet. The preconditions describe the current situation of the lock site, including the topography, natural environment and also existing (hydraulic) structures. There are many different requirements, including functional, maintenance and environmental requirements. During development, the requirements can be subject to change.

The main functions regarding navigation locks, each have their own functional requirements.

- *Navigation;* Required capacity of the lock complex, waterway classification, normative vessel and normative combination of vessels. Dimensions are closely related to these requirements.
- *Water retention;* There are requirements concerning overflow, overtopping, strength and stability, but also the reliability of the structure.

- *Water management;* In specific cases, locks can play an important role in water management. Possible requirements include the lock and/or leakage losses, separation of salt and fresh water, and regulation of water discharge or intake.

A lock cycle is defined as a full navigation cycle, which includes the transit of vessels in both directions. The half cycle time, or the transit time, is the time it takes for a vessel to pass through the lock.

Additional requirements for lock design are related to use and operation (water levels, operating times, operating equipment), maintenance (maintenance strategy, related to safety strategy, availability, consequences of failure or delays, spare parts) and the environment (used materials, pollution, aesthetics, recreation).

2.2 General layout

The figure to the right is a top view of a typical navigation lock and shows the general layout of a lock complex. (Molenaar & e.a., 2011)

1. Waiting- or lay-by berths
2. Guard- or guide wall or lead-in jetty
3. Lock gates
4. Lock heads
5. Lock chamber
6. Filling and emptying system
7. Cut-off walls and screens
8. Bottom protection

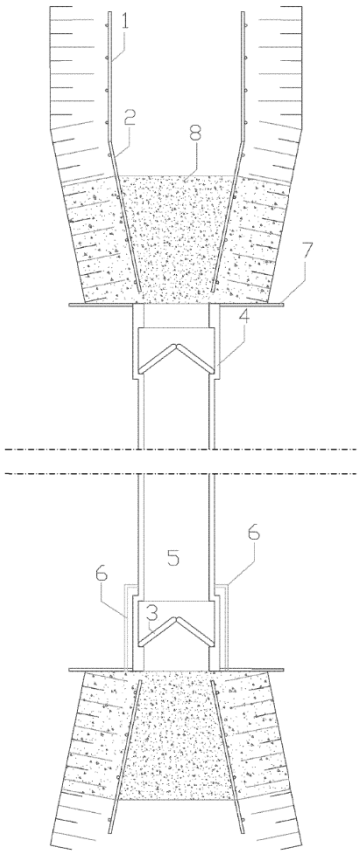

Figure 1. Top view navigation lock

2.2.1 Chamber

The lock chamber is the enclosed space where vessels are moored during the locking process. The primary goal when designing the chamber is for this process to go as safely and efficiently as possible. The two main components of the chamber are the walls and floor, and three functions must be fulfilled:

- Soil and water retention
- Guiding vessels through the lock
- Mooring vessels during locking

A vessel must be able to navigate safely into the lock chamber, moor and remain moored during filling/emptying, and safely navigate out of the lock chamber. For the dimensions (width, length, height) of the chamber, a balance has to be found between the required space for safe and efficient navigation and the smallest possible dimensions for efficient filling/emptying (limit the required quantity of water, short levelling times). The structure has to be able to absorb the soil and water loads, mooring loads, but also forces caused by vessel impact.

2.2.2 Head

The design of the lock head (layout, dimensions, etc.) is linked to the design of the lock gate and the corresponding operating system. The main functions of a lock head are as follows:

- Accommodate the lock gate (open and closed) and
- Water retention
- Load transfer

In the open position, the lock head needs recesses for the gates, to allow vessels to pass into the chamber. The recess is designed in such a way that the gates remain outside of the free profile for navigation and limit the probability of a collision. When closed (retaining position), the heads must be able to absorb the loads transferred from the gates. These loads are transmitted through the walls and floor to the foundation. Proper sealing between the gate and the head structure is required to retain water. Also, the connection between the head and the chamber should be watertight. There are strict requirements for the foundation of the lock head to limit settling. The rail track goes through the lock head into the gate chamber. Therefore the differences in settlement have to be minimised.

2.2.3 Approaches

The function of lock approaches is to guide vessels swiftly into the lock chamber, safe for the vessel and the lock. Approaches form the connection between the lock and the waterway. It's important that they are well oriented and that there is enough space for a line-up- and a waiting area, with appropriate mooring and berthing facilities. Dimensions of the approaches and the various areas depend on the classification of the waterway. Vessels exiting the lock must not be hindered by vessels waiting to enter the lock.

2.2.4 Filling/emptying

Levelling of the water level in the lock chamber is done with the filling and emptying system. To fill, available potential energy is transformed into kinetic energy and water flows from the upper reach into the chamber. When emptying, water flows from the chamber to the lower reach. Different methods are used to accomplish this flow of water. From simple openings in the gate controlled with valves, culverts through the lock heads or longitudinal culvert systems with a stilling chamber. The choice of the system depends on the investment costs, filling/emptying times and safety of vessels during levelling. Filling and emptying through gate openings or the lock heads can result in a very turbulent water zone. In this case, safe mooring and the safety of the lock is a concern. The use of longitudinal culverts distributes the water inflow or discharge over the lock chamber avoiding turbulent water zones.

With each locking cycle, water losses are inevitable. It is desirable or even necessary to minimise these water losses. The use of water-saving basins is an effective method to reduce water losses because in each cycle water is stored in the basin and can be reutilized. Multiple basins can be used for each chamber, but with each additional basin the water reutilization rate decreases. Another downside is the increase in lockage time with each extra basin. The key is to find a balance between the required investment costs, economic consequences of water loss, economic costs due to an increase in lockage times and environmental influences.

2.3 Lock gates

Lock gates are moveable elements of the navigation lock, retaining water in the closed position and allowing the passage of vessels when opened.

For vessels to navigate through the lock, it must be possible to move the gates completely out of the cross sectional area. Operating mechanisms are used to move the gates into recesses. Due to the current economic importance of waterway transport, the operation of the gates must be as quick and efficient as possible. The time needed for a vessel to safely pass a navigation lock has become a dominating factor.

For the water retaining function, the gate must be able to resist the hydrostatic pressure, caused by the water level differences on either side. Retention can be one or two-sided. Throughout the lifetime of a lock, the many different loading cycles can result in fatigue playing a critical role in

the design process of the gates. Another requirement is to prevent water leakage or seepage, especially at the wet perimeter of the gate. Depending on the specific requirements of the project, limited leakage and seepage can be allowed. For maritime locks, strict requirements are often necessary to separate salt and fresh water. Saltwater intrusion can cause major problems on the fresh water supply.

When designing a navigation lock gate, the following general requirements are always applicable:

- When closed, the gate must be able to retain water (ensuring strength and stability), and allowing lockage of vessels.
- The gate must provide a water tight connection, with the lock head and floor, minimising water leakage and seepage losses.
- The gate must be able to efficiently move out of the water profile, remaining stable, and allow safe passage of vessels.
- For maintenance purposes, the gates must be able to retain water with a completely emptied lock chamber.
- The locking process should be as efficient as possible, limiting the water consumption of each cycle.
- A certain level of reliability and safety must be guaranteed.
- Requirements concerning operation capacity, operating times, etc. must be met.
- Removal and transport of gates from the lock head, for large scale repairs, replacement and maintenance, must be made possible.

2.3.1 Gate types

Lock gates come in all shapes and sizes, with each type having its advantages and disadvantages. The most frequently used gate types used in locks are:

1. Mitre gates
2. Single leaf gates
3. Lift gates (Vertical translation)
4. Radial gates
5. Rolling gates (Horizontal translation)

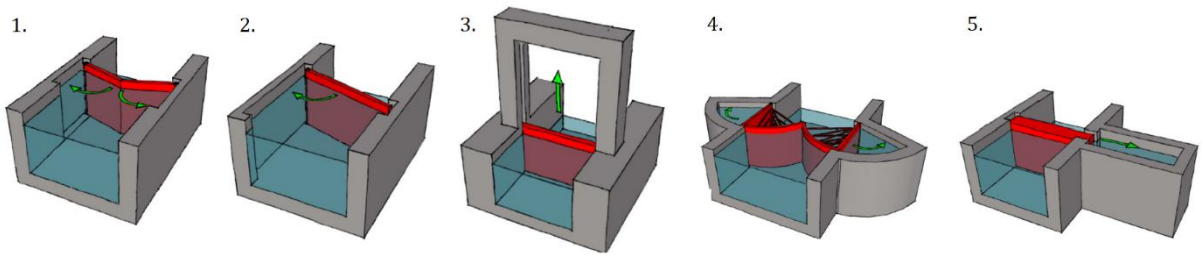

Figure 2. Lock gate types (Doeksen, 2012)

The focus of this thesis is on rolling gates. More information on the other types of gates can be found in Appendix A.

With the variety of lock gate types that can be applied in navigation locks design, the choice of the gate type depends on a number of factors:

- Required dimensions (width of the passage, height of water levels, required lift)
- Load conditions (hydraulic loads, waves, currents, ship impact, earthquakes)
- Available space (preconditions)
- Operating conditions (capacity, locking frequency)
- Environmental considerations (salt water intrusion, pollution during construction and operation)

2.4 Rolling gate

Rolling gates are extensively used in navigation locks. As a well-proven technology, rolling gates are applied in the widest locks on earth. For example in the Panama third set of locks project, a total of sixteen rolling gates is applied.

The gate moves with a horizontal translation, perpendicularly closing the passage. In the open position, the gate is retained in a large recess next to the lock head. This also results in good accessibility, allowing for easier maintenance. With the flat gate, two-sided water retention is possible and hydraulic loads are directly transferred to the chamber walls. Because there's no rotation around a heavily loaded hinge, rolling gates are very suitable for wide locks. The gates are large and robust and provide good resistance to vessel collisions. The gates are moved by carriages guided along rails; an alternative is the use of sliding tracks (sliding gate). To reduce the load on the carriages, buoyancy chambers can be utilised. With larger water heads, the thickness of the gate increases quickly. There is a certain overweight required on the carriages to ensure stability under all conditions, especially during opening and closing of the gate. A downside is an increase in the loads on the carriages in the case of low water levels, as the volumetric displacement by the gate decreases. (Vrijburcht & Glerum, 2000)

Advantages:

- Two sided water retention possible.
- No limitation to vessel height clearance.
- Relatively easy (dry) maintenance in the gate recesses.
- Suitable for wide locks.

Disadvantages:

- Large recess space is required besides the lock head.
- Cannot be opened or closed when there's a water head difference (a small head difference is possible but undesirable).

2.4.1 Structural components

There are three main components: The gate, the gate chamber/recess and the operations building. A 3D impression of a lock with a double executed rolling gate is shown in Figure 3. Double gates increase the level of safety and reliability of operations. In the open position, the gate goes into the gate chamber, to allow for safe passage of vessels. In the closed position, the end of the gate rests in the recess on the opposite side of the gate chamber. The chamber is equipped with guides to allow for a smooth entrance of the gate into the chamber.

The gate chamber can be used as a dry dock, so maintenance and repairs can be performed without the need to remove the gates. The application of double gates allows for operations to keep going with one gate, while the other is repaired in the recess. The dimensions of the gate chamber are not only determined by the dimensions of the gate. The chamber should be long enough to allow a roller carriage to be hoisted out behind the gate and wide enough for maintenance and exchange of a roller carriage under a floating gate. Water being pushed around by the gate entering the chamber should be taken into account, as well as creating enough space for the gate to be floated into position from either the lock chamber or lock approaches.

Located near the lock head, an enclosed space is required for all the operating machinery and equipment. The operations building includes a central control room with a good view of the lock and the lock approaches.

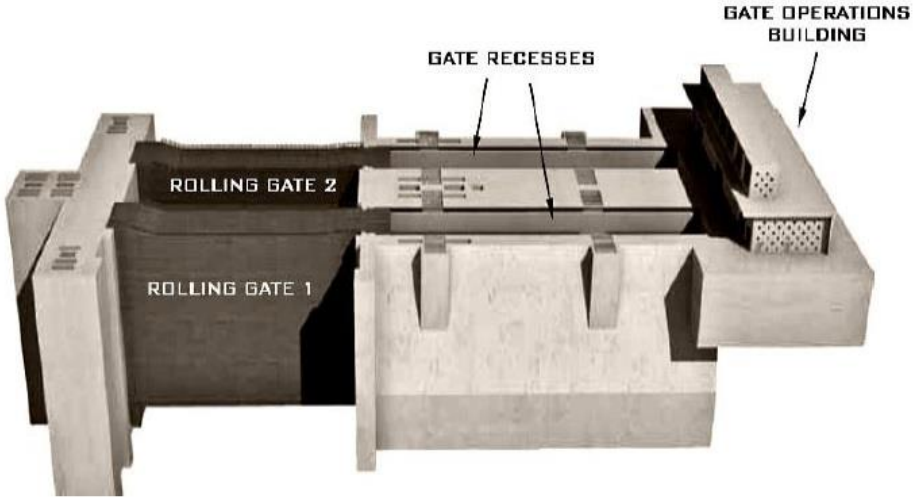

Figure 3. Impression of a rolling gate and lock head (Laukaitis & Boyce)

2.4.2 The Gate

The main dimensions of the gate depend on a variety of factors. For example the dimensions of the waterway, the category of vessels, water levels, various load cases, aesthetics and environmental conditions. The thickness of the gate depends not only on the strength and stiffness requirements but is also determined by the required support carriage width, which is needed to guarantee stability under all circumstances. As a first estimate of the thickness a ratio of 1:4 or 1:5 with the gate width can be used.

In general, the design of a rolling gate consists of a number of elements (Vrijburcht & Glerum, 2000):

- Retaining plates on both the low and high water side of the gate.
- The gate is sealed off by a bottom girder and end portals.
- The load is transferred from the retaining plates to columns, spaced out over the length of the gate.
- Horizontal girders take the load from this vertical portal of columns.
- These vertical posts and horizontal girders make up the support structure of the gate.
- From here the load goes to the end portals and is transferred to the gate chamber and recess.
- The end portals are equipped with supports.
- The gate rests on bearing on the roller carriages.
- If necessary, the gate is provided with ballast and buoyancy chambers, to relief/create an overweight.

2.4.2.1 Ballast and buoyancy tanks

The gate is equipped with ballast and buoyancy tanks for different reasons. If the gate is floated into position, ballast, trim, diving, sink and relief tanks are used. Tanks can be filled with water to slowly float it down onto the carriages. Different tanks spread out over the complete width of the gate are filled or emptied to keep the gate stable.

Ballast/buoyancy tanks can also be used during operation: (Molenaar & e.a., 2011)

- Buoyancy, offers relief of weight and friction (during opening and closing), thus reducing wear-and-tear.
- Ballast, the tanks are filled in closed position, to ensure contact pressure and stability.

2.4.2.2 Gate openings

Depending on the boundary conditions and the requirements of the gate, openings placed near the bottom of the gate can be used as a levelling system. The openings are closed by valves. It's the cheapest solution and mainly used in gates with relatively small head differences. Turbulence leads to large forces on vessels in the chamber and on the bottom of the chamber itself. Bed protection and barriers to dissipate energy directly behind the gate may be required.

2.4.2.3 Sealing

To prevent leakage of water and guarantee water tightness between the gate and the various structural components, sealing is an important aspect of the gates design. When the gate is closed, it seals against vertical supports on the sides and the sill on the bottom. Wooden beams (hard timber e.g. Azobé) or a polymer bearing surface is applied to create the seal and protect the gate. The sealing has to be flexible to be able to function under deflection.

2.4.2.4 Sliding gates

Instead of roller carriages, the gate is supported by hydrostatic bearings. Due to their water repelling profile, the hydro-bearings can be carried on a thin film of water.

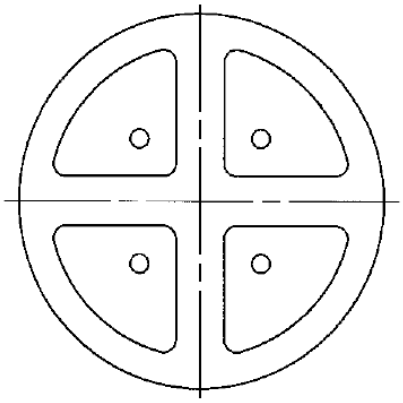

Figure 4. Hydrostatic bearing (Vrijburcht & Glerum, 2000)

This allows for the gate to slide with a relatively small required force. The required water pressure is achieved with a pump. An advantage over roller carriages is the reduction of moving and rotating parts. Inspection and maintenance of these particular parts are difficult and costly.

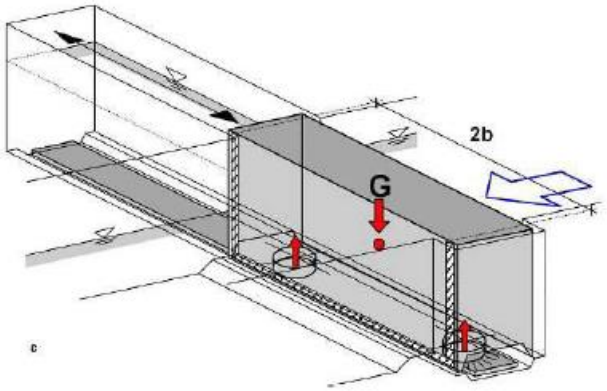

Figure 5. Sliding gate schematic (PIANC, 2014)

2.4.3 The Operating Mechanism

The operating mechanism makes the horizontal translation of the gate possible and consists of many different elements. Figure 6 shows the elements generally part of the rolling gate operating mechanism.

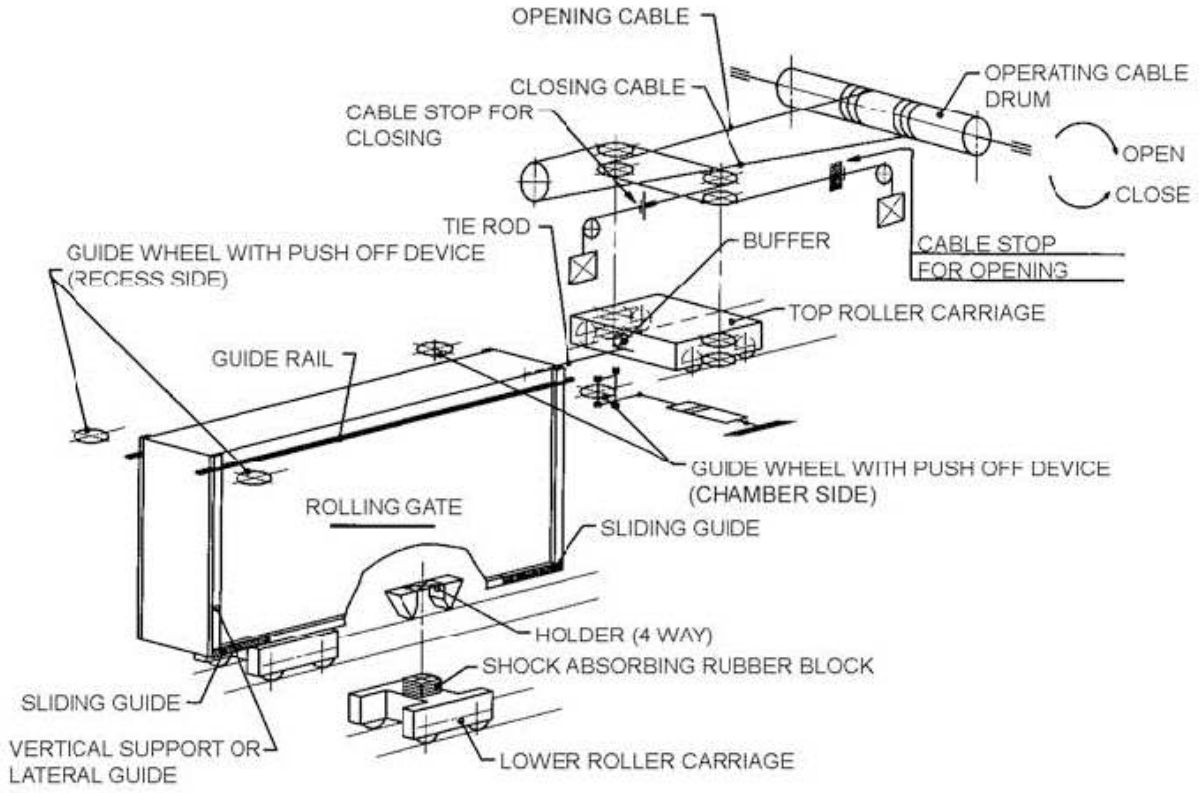

Figure 6. Operating mechanism of a rolling gate (Vrijburcht & Glerum, 2000)

The gate is pulled by a cable winch gear system. Different setups are available; a choice can be made between a one- or two-sided drive wheel, with cable drums on one or both sides. The drive system consists of a motor, brake, gearbox, drive shafts and the wire rope drums (PIANC, 2014). The cables are connected to connection points on the gate or the upper carriage. These connections are preferably above the highest water levels to limit corrosion.

In general, the rolling gate is vertically supported by two roller carriages. The two main layouts are depicted in Figure 7, two lower carriages or a wheelbarrow layout, with one lower and one upper carriage. Main advantages of the wheelbarrow system are that it reduces the number of mechanical components permanently under water and better stability during opening and closing. A second rail at the top of the gate chamber is required for the upper carriage. The two lower carriage system, on the other hand, is relatively simple. With lower construction costs, but unfavourable conditions for stability during opening and closing, and inspection and maintenance is harder, due to more components being under water. The wheels of the carriages run on rails. Placement of the gate on the carriages must be performed accurately to distribute the overweight of the gate equally over the wheels. The gate is guided horizontally by either guide wheels, sliding guides or a combination of both.

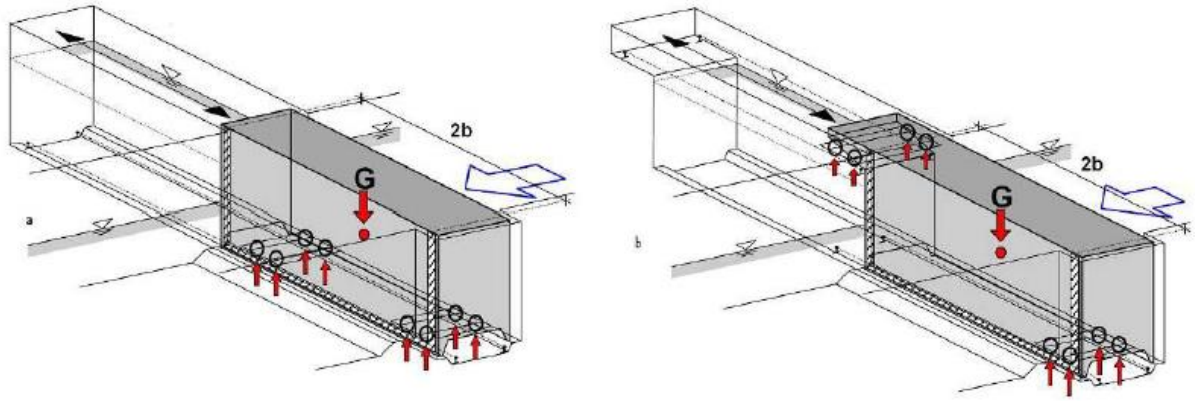

Figure 7. Rolling gate schematics – 2-lower & wheelbarrow (PIANC, 2014)

2.4.3.1 Carriages

Roller carriages are most commonly used in horizontal translation gates. The overweight of the gate is supported by the carriages. The carriages are equipped with four wheels. This can be 8 in the case of very large locks. The wheels transfer the vertical gate loads to the rails. Horizontal loads are carried by a combination of guides.

The gate can hinge around the carriage; some lateral displacement is allowed. In the case of a lower carriage, a choice can be made between one central support or two lateral movement rollers. With a single support, the gate is placed on an elastomeric bearing, or simply referred to as a rubber block. This increases the stability and results in a more equal load distribution to the wheels and the rails, even in the case of small level differences, unequal settlements or other dimensional deviations. In comparison to lateral rollers, the elastomeric bearing is less sensitive to wear, friction and contamination.

As the name suggests, lateral movement rollers allow the gate to move in a lateral direction, under small head differences. Figure 8 shows a carriage with rollers, as applied in the Kaiser Lock in the harbour of Bremen. The support system must be able to balance the lateral loads on the gate during opening and closing. Dimensions of the rollers and the base plate curvatures must therefore be chosen as such, so that the lateral rigidity of the support system is sufficient, calibrated to the required horizontal force. The moment a load is applied, the load distribution to the rails is unequal. Wear of the rail is a major problem when this arrangement is applied. (Daniel, 2011)

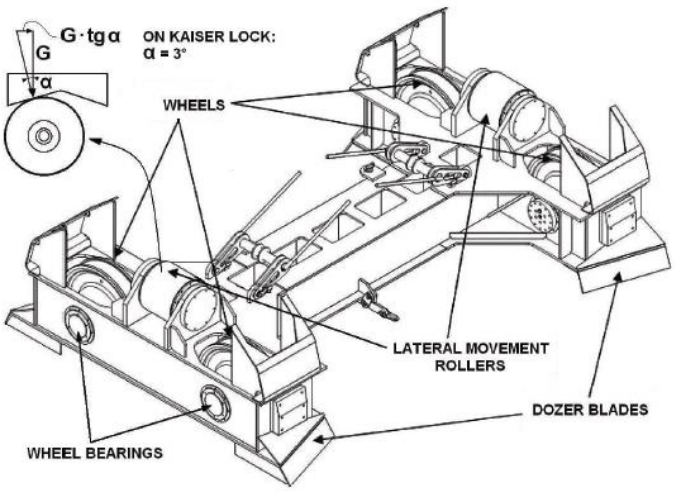

Figure 8. Carriage Kaiser Lock – Lateral rollers (PIANC, 2014)

The connection of the upper carriage to the gate is achieved by hooking the gate on two tubular rockers by a pivot hinge. The connection allows the gate to be pushed sideways against contact points. Ideally, the upper carriage is only carrying vertical loads, but with small lateral gate movements, the carriage is also carrying horizontal loads. (Daniel, 2011)

2.4.3.2 Rails

Rails support the roller carriages. Lower rails are placed in a cunette along the bottom of the lock head and gate chamber/recess. The foundation is subject to strict requirements to limit settlements, especially settlement differences along the length of the rails are detrimental to the stability of the gate and equal distribution of loads. The rails experience a lot of wear-and-tear and regular inspection and maintenance is key. Also, plastic deformation of the rails over time should be taken into account. An upper carriage requires a separate rail track along the top of the gate chamber.

2.4.3.3 Guides

In order for the gate to remain upright, centred and stable during movement a variety of guide devices is applied. These horizontal guides are required to absorb the perpendicular load the gate is exposed to. Generally, there are three support points. Two lower guides at the bottom in the cunette and one upper guide in the gate chamber. Depending on the gate and operating conditions a choice can be made between a guide wheel or a sliding/gliding guide.

Figure 9 depicts a number of options for the lower guides. From left to right, a sliding guide by means of a sliding strip on the gate, two roller guides and a single central roller guide respectively.

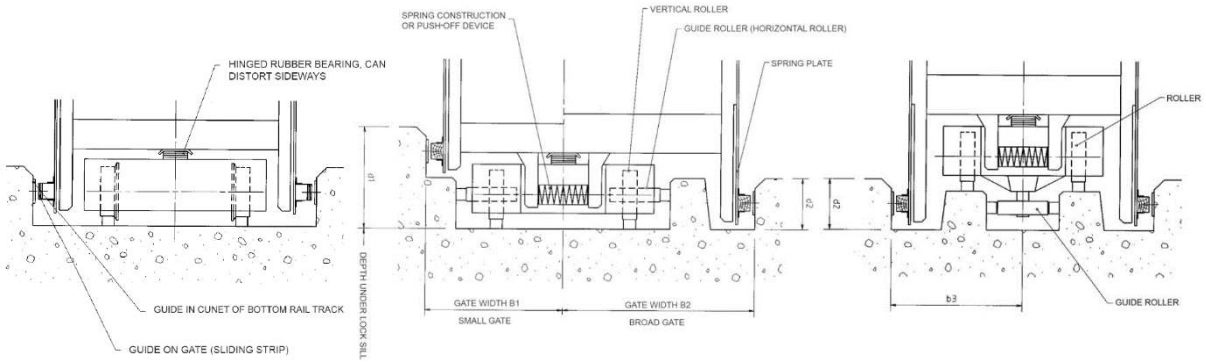

Figure 9. Lower horizontal guides (Vrijburcht & Glerum, 2000)

Wheels run on rails and a sliding guide on a track. A bearing can be placed on the wall of the gate chamber that slides along a track on the gate, or the bearing can be placed on the gate which slides on the track positioned on the wall.

In addition, push on-off devices are used to push the gate off its supports to allow the gate to move. During movements these devices also keep the gate centred. In closed position, the push on-off devices are turned off, and the gate leans against the supports due to hydraulic loads perpendicular to the gate.

2.4.4 Lifetime of structure

- Design
- Manufacturing/assembly/construction
- Operation + Maintenance
- Demolition/Recycling

2.4.4.1 Design

In the design stage of a lock and the lock gate, a program of requirements is set up listing all the conditions and requirements that have to be taken into account. These requirements can be split up in different aspects of the design (Vrijburcht & Glerum, 2000):

- *Boundary conditions;* a detailed description of the environment, existing locks, operating conditions (water levels, wind), morphology and soil characteristics.
- *Functional requirements;* requirements concerning navigation, i.e. normative vessel and quantity of traffic; structural requirements, i.e. strength, stability and reliability; water management requirements, i.e. water loss, fresh/salt and intake/discharge.
- *User requirements;* design water levels, operating and levelling times, operational management, dealing with the traffic and safety.
- *Maintenance requirements;* maintenance strategy regarding monitoring, inspection, repairs and replacements.
- *Environmental requirements (in the use and in the construction phase);* Aesthetics, used materials, recreation and pollution.
- *Codes and guidelines.*

2.4.4.2 Construction

During the construction phase, there's a lot to be considered. Focussing on the lock gate, an important aspect is the question of how and where the gate is going to be constructed and how it's going to be transported and positioned. Generally, large rolling gates are equipped with a system of buoyancy tanks allowing the gate to float and be transported to its destination. There the gate is floated down into position. As opposed to the use of a crane to lift the gate into position. When designing the gate, lock head and the gate chamber, the designer must keep the logistics of this process in mind and choose dimensions accordingly.

2.4.4.3 Operation + Maintenance

In the operation phase the lock is used and to guarantee safety and reliability requirements throughout the entire operation phase, a maintenance strategy must be implemented. The objective of the maintenance strategy is to find the economic optimum between the consequences of unavailability or failure of the gate versus the execution of planned maintenance or and resulting downtime. The life span of a lock gate is generally between 50 and 100 years. Therefore it's difficult to find this optimum. Causes for unavailability can be split up into three categories: (Vrijburcht & Glerum, 2000)

- Unplanned unavailability due to natural circumstances (extreme water levels, ice, etc.).
- Unplanned unavailability due to failure (structural, malfunctions, external influences e.g. blockages or collision).
- Planned unavailability due to planned inspection, maintenance or other planned impediments.

Another issue is the presence of debris/waste and ice. It can build up in the gate chamber and get stuck between the gate and the wall. There must be enough room in the chamber to accommodate the waste, and periodic removal is necessary. To prevent carriages from getting stuck, they are equipped with track clearers. The gate can become icebound when ice grows on its supports.

Most maintenance can be performed in the gate chamber. Dewatering of the gate chamber essentially turns it into a dry dock. To perform maintenance on roller carriages, the gate is either hoisted up or floated off of the carriages allowing them to be removed.

2.4.5 Codes and guidelines

The lock gates design is executed in accordance with the Eurocode. In addition TAW Leidraad Kunstwerken and ROK 1.3 is used to determine certain hydraulic loads.

- Eurocode 0: NEN-EN 1990 – Basis of structural design
- Eurocode 1: NEN-EN 1991 – Actions on structures
- Eurocode 3: NEN-EN 1993 – Design of steel structures
- TAW Leidraad Kunstwerken (Leidraad Kunstwerken, 2003)
- ROK 1.3 – Richtlijnen Ontwerpen Kunstwerken (ROK-1.3, 2015)

2.5 Key points – chapter 2

- Only the lock gate and in particular a rolling lock gate is considered.
- Dimensioning and checking of the lock head and foundation is outside of the scope of this thesis.
- Only a 2-lower roller carriage configuration is considered.
- In reality the gate rests on one central bearing on either end, from there the weight/loads are transferred to the wheels. In the model, the supports are modelled as if the gate is supported directly by the wheels.

3 Introducing the material

Fibre-Reinforced Polymer

Composite materials have been around for a long time and in many different forms. From mud bricks reinforced with straw to concrete reinforced with steel. A composite can be defined as a material that consists of two or more different materials. The properties of the separate materials complement each other, resulting in a composite with better properties than the individual components separately. Fibre reinforced polymers (FRPs) build on the same well-established and recognised concept of all composite materials. A fibrous reinforcement is used to add its strength to the durable, corrosion-resistant properties of a surrounding polymeric matrix.

The real development of FRP started 70 years ago. FRP found most of its application in the aerospace, maritime and automotive industry, but since then FRP has slowly penetrated other areas of application i.e. consumer products, electronics and construction. As a lightweight material, with the unique ability to 'tailor' the properties to the specific needs of the user, FRP can be a serious competitor for many traditional materials. (Kolstein, 2008)

Some of the inherent advantages of FRPs over traditional materials are (Kolstein, 2008), (GangaRao & Vijay, 2010),

- Lightweight;
- High strength-to-weight ratio;
- Relatively low in-service costs;
- High fatigue resistance;
- Excellent corrosion resistance;
- Ease of installation and assembly.

Some disadvantages are:

- Relatively higher initial costs;
- Limited experience by designers and contractors with the material;
- Lack of data on long-term field performance;
- Low stiffness compared to many traditional materials;
- Temperature is often limited to not exceed 150° C;
- Poor ductility.

This chapter elaborates on FRP, its base materials and properties. It's only an introduction to the subject. Detailed information on for instance the manufacturing processes or chemistry of materials are beyond the scope of the main report. For more elaborate information one is referred Appendix A, (Campbell, 2010) and the literature study related to (Kok, 2013).

3.1 Components

3.1.1 Fibres

Fibres can be defined as a material that has a long axis, many times greater than its other dimensions. In other words, a high aspect ratio is characteristic for fibres. The aspect ratio refers to the fibre length divided by the diameter.

The fibres used in FRP are embedded in a matrix and provide the composite with its mechanical properties. A high fibre content, with an upper limit of 60-70%, increases the strength and stiffness properties of the composite. There are many types of fibres available: Polyester, jute, sisal, nylon and born, but there is little use for these compared to the fibres that dominate the composite market: Glass, carbon and polyaramid. (Kolstein, 2008)

3.1.1.1 Glass fibres

The relatively low cost and excellent properties, like high tensile strength and a good chemical resistance, have resulted in fibreglass being the most commonly used fibre as reinforcement for composites. Typical glass properties are hardness, corrosion resistance and chemical inertness. Glass is inherently brittle. Modulus and fatigue properties are inferior to those of carbon. Glass fibre has a higher elongation to failure compared to carbon or aramid fibres.

As reinforcement, a variety of classes of glass are available: A, C, E, R and S. A 'Alkali' glass, formerly the most used for glass fibre production. C 'Chemical resistant' glass, used for surface tissue manufacture. E 'Electrical' glass, a borosilicate glass with a very low alkali content with good electrical, mechanical and chemical resistance properties. Nowadays the most commonly used for glass fibre production. R- and S 'Structural or high strength' glass, mostly applied in aerospace applications. (Kolstein, 2008) The main compound in all these glass fibres is silica (SiO_2). The different properties are achieved with the use of various oxide component in the manufacturing process. (Moen, 2014) The manufacturing process of glass fibres is discussed in Appendix A.

3.1.1.2 Carbon fibres

Carbon fibres are very lightweight and among the strongest materials today, with a very high strength and modulus. The fibres have an excellent chemical resistance, temperature tolerance and fatigue properties. The downside is a low impact resistance and brittleness of the material. Due to the relatively high costs, up to 10 times that of glass fibres, carbon fibre composites are mainly used in high-performance applications where the cost is a secondary priority. Many of these applications are in the aerospace industry. (Moen, 2014)

About 90% of carbon fibres are made from polyacrylonitrile (PAN). The remaining 10% are made from rayon or petroleum-based pitch precursors. The precursor fibre is converted to carbon fibre through controlled oxidation and carbonisation. A distinction can be made between carbon and graphite fibres. Carbon fibres generally have a carbon content between 93 to 95%. Heat treatment above 1650 °C, known as graphitization, results in graphite fibres with a carbon content exceeding 99%. (Kolstein, 2008)

3.1.1.3 Aramid fibres

Most commonly known under the brand name Kevlar, manufactured by DuPont, aramid fibres are part of the nylon family. The strength and stiffness properties of these organic fibres are between those of glass and carbon fibres, but it has the highest tensile strength-to-weight ratio. Aramid fibres are extremely tough, with the ability to absorb large amounts of energy during fracture, ideal for ballistic protection. In compression, the material can plastically deform, during tensile fracture it has the ability to defibrillate. The low compressive strength and relatively bad fatigue and creep behaviour of aramid fibres make them less useful as a construction material. (Campbell, 2010)

3.1.1.4 Properties

There is quite a lot of scatter among sources on the properties of various fibres. (Moen, 2014) reviewed a variety of sources, (Campbell, 2010), (Kolstein, 2008), (Strong, 2008), also (Zoghi, 2013) is used, resulting in the following overview of representative values.

Table 1. Representative fibre properties

Fibre	Tensile strength [MPa]	Tensile modulus [GPa]	Elongation [%]	Density [kg/m^3]	Coefficient of thermal expansion [10^{-6} °C]
E-glass	3450	72	4.9	2540	5
A-glass	3300	69	4.4	2450	-
C-glass	3310	69	5.0	2450	6.3
S-glass	4580	85	5.7	2490	2.9
R-glass	4400	85	4.8	2580	-
Carbon PAN I	2400-2700	380	0.74	1950	-0.5
Carbon PAN II	3400-4500	230	1.34	1750	-0.5
Carbon Pitch	1550	380	2.5	2000	-1
Carbon Rayon	2500	500	..	1700	-0.9
Aramid HM	3400	180	2.0	1450	-2.0
Aramid HS	4000	130	2.8	1450	-2.0

HM: High Modulus ; HS: High Strength

3.1.2 Reinforcement forms

Fibres can be applied in FRPs in a variety of ways or reinforcements forms. The fibres can be continuous filaments or discontinuous, e.g. chopped strands. Each form has different advantages and disadvantages. Application of continuous fibres can improve the strength of the composite, due to a controlled fibre orientation. Chopped strands are randomly oriented, resulting in a lower quality product, but at a lower cost and easier manufacturing.

3.1.2.1 Continuous filament rovings

Continuous filaments or fibres are supplied as a roving. The continuous filament roving is made up of one or several fibre strands parallel wound into a spool. The rovings can be processed into other products, such as mats and woven fabrics.

3.1.2.2 Mats

Mats are a reinforcement form made from chopped strands or continuous filaments rovings. Chopped strands are uniformly spread, in a random orientation, and bonded together to form the chopped strand mat (CSM). In continuous filament mats (CFM) the fibres are randomly deposited forming multiple layers.

3.1.2.3 Woven fabrics

Rovings or twisted continuous filaments (yarn) can be woven into a fabrics in different weave patterns: Plain, twill, satin, or unidirectional. A satin weave gives good mechanical properties in all directions, whereas the unidirectional weave gives the best properties in the main direction.

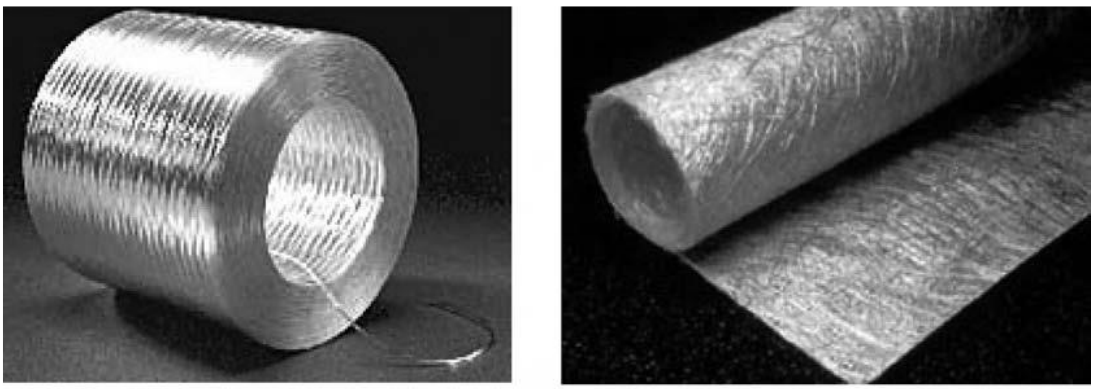

Figure 10. Glass roving and glass-reinforced mat (Campbell, 2010)

3.1.3 Matrix

The polymer matrix has a number of main functions. The matrix fixes the reinforcement fibres in the desired arrangement, transfers loads to the fibres and forms a barrier against the environment, protecting the fibres. Since the reinforcements compressive and shear strength are poor, the matrix provides the composite with these properties and prevents buckling of fibres under compressive actions. Polymer matrices can be divided into thermosets and thermoplastics. (Zoghi, 2013)

3.1.3.1 Thermoset resins

Thermosets undergo an irreversible chemical process forming covalent bonds between all molecular chains under the influence of a catalyst or heat. When the curing process is initiated, the polymers form a 3D network of crosslinks. This permanent change results in a rigid material with good chemical resistance and thermal stability. Thermosets are generally in liquid form at room temperature, making them relatively easy to process. Due to these qualities, thermosets are generally applied over thermoplastics in civil engineering applications. Most common thermoset resins include polyesters, epoxies, polyimides and phenolic. (Zoghi, 2013)

3.1.3.2 Thermoplastic resins

The molecular chains of thermoplastics are connected by weak van der Waals bonds. Thermoplastics are processed by applying heat causing the material to soften/melt. When the material cools off, it sets in the shape of the mould. The heating and cooling doesn't cause permanent chemical changes to the material, allowing reprocessing and recycling. Examples of thermoplastics are polyethylene, nylon, polypropylene (PP) and polyether-etherketone (PEEK).

3.1.3.3 Properties

The following table gives typical properties of unfilled thermoset and thermoplastic resins, according to (Mazumdar, 2002).

Table 2. Typical resin properties

Resin	Tensile strength [MPa]	Tensile modulus [GPa]	Density [kg/m^3]
Epoxy	50-110	2.5-5.0	1200-1400
Phenolic	35-60	2.7-4.1	1200-1400
Polyester	35-95	1.6-4.1	1200-1400
Nylon	55-90	1.3-3.5	1100
PEEK	100	3.5-4.4	1300-1350
Polyethylene	20-35	0.7-1.4	900-1000

3.1.3.4 Additives

To enhance specific characteristics of the composite material, additives can be used. The characteristics that can be influenced range from mechanical, electrical and thermal properties to chemical and environmental resistance. Also sizing, applying a surface finish to the fibres, can be done to improve the bond between the fibres and matrix. (Moen, 2014)

3.1.4 Core materials

As a structural element, composites are often applied in a sandwich configuration consisting of two face laminates and a thick lightweight core. The use of the core increases the structural efficiency. There are many core materials available and these can be subdivided into three categories: Solid, foam and honeycomb. (Kolstein, 2008)

3.1.4.1 Solid

The most important characteristic of solid core materials is that they are very lightweight. Wood is a material that has been used extensively in various applications. Balsa wood in particular is still in use, but synthetic materials are becoming increasingly more popular.

3.1.4.2 Foam

As a core material, foams can serve a variety of functions depending on the requirements. Higher density foams can be applied as a structural component, because of good compression and shear properties. Very low density foams can also be applied as a non-structural component, for instance to produce a specific shape FRP structure. Foams are often made from plastic materials.

3.1.4.3 Honeycomb

Thin sheet material, like fibreglass or aluminium, is shaped and connected into the required form. Due to the shape of the honeycomb structure, the structural properties are particularly good in direct compression and shear. Honeycomb cores are relatively expensive in comparison to foam cores, therefore they are most used in high performance applications.

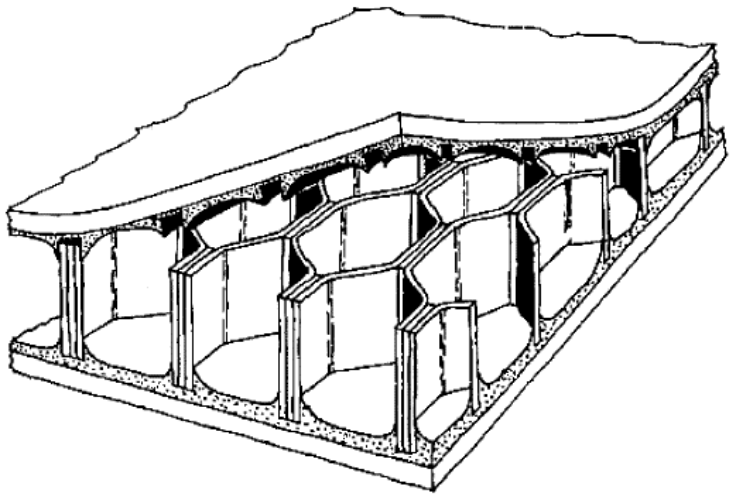

Figure 11. Honeycomb core sandwich panel (Campbell, 2010)

3.2 Manufacturing processes

For the manufacturing of FRPs, many processes are available. Each manufacturing technique requiring different material systems, processing conditions and tools. Selecting the right manufacturing process depends on the requirements for the final product. Each has its own advantages and disadvantages, in relation to processing, geometry (size and shape), cost, etc. In every composite manufacturing process, four basic steps are always involved in some way: Impregnation, lay-up, consolidation and solidification. Three main types of manufacturing processes can be distinguished: Open mould, closed mould and continuous. (Kolstein, 2008)

3.2.1 Open mould process

- **Hand laminating:** A labour intensive process, but still widely used due to flexibility and low equipment costs. A gel coat is applied in the mould, followed by the resin. Then the fibres are cut and fitted and a layer is made. Consolidation is achieved manually with a roller. The process is repeated until the specified thickness is reached.
- **Saturation:** The application process of the resin is mechanized. It is mixed and sprayed onto the mould with a spray gun controlled by an operator. Quality of the end product, concerning fibre content and thickness can be expected to be the same as hand laminating.
- **(Auto) Spray-up:** A high production output system, suitable for high-volume non-critical products, because an operator is still in control of the thickness. The fibres are cut by the

machine and simultaneously applied with resin. Auto-control of the spray gun is possible, improving the quality of the final product by taking away drawbacks of a human operator.

- **Filament winding:** Used mainly for the manufacturing of simple hollow sections, for example tanks, pressure vessels, gas bottles, etc. Continuous fibre strands are impregnated by being fed through a resin bath. The fibres are wound around a rotating mould. By adjusting the relative rotating speeds and winding angles, the fibre orientation and thickness of different layers can be controlled. Filament winding can be combined with spray-up by alternating layers. This is called **spray winding**.
- **Centrifugal casting:** Similar to filament winding, the centrifugal casting process uses a rotating mould. The difference being that reinforcement and resin are sprayed on the inside of the mould. As a result the moulded surface is on the outside, as opposed to on the inside for filament winding. The mould rotates at high speeds, consolidating the resin/fibre mixture. Problems arise with the distribution, where the more dense reinforcement moves to the outside and the inside becoming more resin-rich.

3.2.2 Closed mould process

- **Vacuum bag:** The process follows the same steps as hand laminating. After resin and reinforcement are applied a thin film is placed over the laminate. Next a rubber bag is clamped at the edges and a vacuum pump is used to evacuate the space between bag and mould. Manual rolling on the outside of the bag may be required to achieve complete consolidation. The vacuum bag process is particularly effective at bonding sandwich laminates.
- **Pressure bag:** A similar process as the vacuum bag, but higher fibre contents are achieved and consolidation is improved, by increasing the pressure up to 3.5 bar.
- **Autoclave:** The laminate is simultaneously subjected to vacuum, pressure and heat by placing a vacuum bag assembly in an autoclave. Complete consolidation and cure are achieved and the result is a very high quality product. An important advantage is that the mould can be constructed reasonably light because it is not subjected to large forces.
- **Leaky mould:** Through hand laminating, resin and fibres are applied on a female mould. The male part is pressed and clamped onto the female part. After curing, the moulds are split and the component can be extracted. The final product has accurate dimensions and a quality finish on both sides.
- **Cold press:** A dry reinforcement pack is loaded onto the female mould, followed by liquid resin. The male part of the mould goes onto the female mould and the closed mould is placed on a hydraulic press. Under pressure of at least 2 bar, the fibres are impregnated and the air is purged.
- **Hot press:** The same cold press process with liquid resin can be carried out, but also prepregs or sheet and dough moulding compounds can be used to load the base materials. These compounds contain chopped fibres and flow when subjected to heat and pressure. By applying heat, the curing process is accelerated, dramatically increases the production rate.
- **Resin injection:** Similar to the cold press process, but the mould is closed without the resin. The resin is injected through one or more injection points by an air-driven dispensing machine. This technique enables more complex shapes, but fibre content is limited.
- **Vacuum-assisted resin injection:** By creating a partial vacuum in the mould cavity before the resin is injected, disadvantages of the resin injection process are overcome. Large mouldings and a higher fibre content are now possible. The upper mould is made of a flexible material, deforming under pressure of the injected resin, allowing it to pass. After injection, the final shape is achieved by vacuum, also ensuring impregnation.

- **Injection moulding:** All the base materials are loaded into a moulding machine hopper. This dough of materials is forced into the mould by a feed screw or piston, causing degradation to the fibres. Only short, random fibres can be applied. The production rate is very high, but variable properties of parts can be expected.

3.2.3 Continuous process

- **Continuous laminating:** A highly productive manufacturing method, but limited to flat sheets and simple profiles. Two layers of release film contain the combined reinforcement and resin. The resin is applied, either by passing the reinforcement through a resin bath or by applying the resin onto the release film. To control the thickness and ensure consolidation, the sandwich of laminate and release film goes through a series of rollers. The laminate is moved through a curing oven, after which the release film is peeled off and the cured laminate is cut to the required length.
- **Pultrusion:** The reinforcement is pulled through a heated die, forming and curing it to the final shape. Impregnation of the reinforcement is realized either by pulling the reinforcement through a resin bath, or the resin is injected directly into the die. High fibre contents and very good mechanical properties, particularly in longitudinal direction, can be achieved. The final product is highly consistent, both in quality and shape, especially suitable for beams and columns.
- **Continuous filament winding:** Yarn reinforcement is continuously fed from a winding head containing several 'cheeses'. The winding head rotates around a mandrel creating a filament wound pipe. More winding heads can be used to create different fibre angles. The pipe emerges from an oven fully cured. The mandrel is designed in such a way that it collapses at the end of the process and reforms into a cylinder at the start.

3.2.4 Comparison of manufacturing processes

The following table gives an overview of a number of characteristics of the various manufacturing processes discussed.

Table 3. Comparison of manufacturing processes (Kok, 2013)

Manufacturing process	Fibre volume [%]	Size range [m²]	Processing pressure [bar]	Processing temperature [°C]	Core	Detail tolerance [mm]	Relative production costs
Open mould							
Hand laminating	13-50	0.25-2000	Ambient	Ambient	Yes	1.0-5.0	High
Saturation	13-50	0.25-2000	Ambient	Ambient	Yes	1.0-5.0	Moderate-High
Spray-up	13-21	2.0-100	Ambient	Ambient	Yes	1.0-3.0	Low
Auto spray-up	13-22	2.0-100	Ambient	Ambient	Yes	2.0-3.0	Very low
Filament winding	55-70	0.1-100	Ambient	Ambient	Yes	1.0-2.0	Moderate-Low
Spray winding	40-60	0.1-100	Ambient	Ambient	Yes	2.0-3.0	Very low
Centrifugal Casting	20-60	0.5-100	Ambient	40-60	No	1.0-3.0	Moderate-Low
Closed mould							
Vacuum bag	15-60	0.5-200	Ambient	Ambient	Yes	1.0-3.0	Very high
Pressure bag	20-70	0.5-200	1-3.5	20-70	Yes	1.0-3.0	Very high
Autoclave	35-70	0.25-5.0	1-10.0	20-140	Yes	0.5-1.0	Very high
Cold press	15-25	0.25-5.0	2.0-5.0	20-50	No	0.25-1.0	Low
Hot press	12-40	0.1-2.5	50-150	130-150	No	0.2-1.0	Very low
Resin injection	10-60	0.25-5.0	1-2.0	20-50	Yes	1.0-2.0	Moderate
Vacuum-assisted resin injection	15-60	1.0-100	1-2.0	15-30	Yes	2.0-5.0	Moderate
Injection moulding	5-10	0.01-1.0	750-1500	140	No	0.1-0.5	Very low
Continuous process							
Continuous laminating	10-25	Width <2m	Ambient	100-150	No	1.0	Very low
Pultrusion	30-65	Width <1m	Varies	130-150	No	0.2-0.5	Low
Continuous filament winding	55-70	Diameter <2m	Ambient	Ambient	No	1.0-2.0	Low

3.3 Mechanics of FRPs

Analysis and design of composite materials is a complicated process. Laminates are built up of laminae and laminae consist of matrix and fibres. To determine the properties of the laminate, first the individual plies must be investigated.

Not only are the properties of the constituents of importance, also the interface between the two. In addition, shape, size, orientation and distribution affect the laminas properties. The result is an inhomogeneous and anisotropic material, meaning that the material properties are inconsistent depending on the location and are different in all directions.

To simplify analysis, average properties of the lamina are used. A ply is considered unidirectional and homogeneous. A stress-strain relationship of the ply can be determined and from here the stress-strain relationship of the laminate. These properties can be used in the structural analysis of the composite structure.

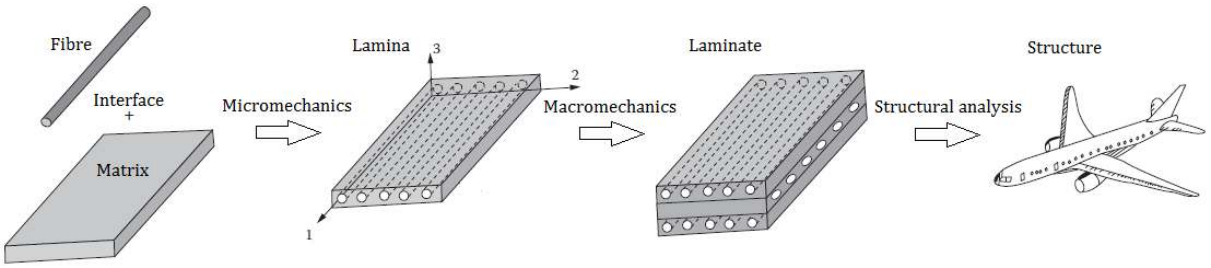

Figure 12. Levels of analysis (Zoghi, 2013)

3.3.1 Mechanics of laminae

Laminates are constructed by stacking various laminae, or plies. These laminae have a thickness in the order of 0.125 mm. To determine the properties of the laminate, first a mechanical analysis of a single lamina is required. (Kaw, 2006)

3.3.1.1 Hooke's Law

The stress-strain relationship for an FRP, an anisotropic material, follows Hooke's law and is described by a six-by-six matrix. In equation (3.1) this relationship is given in an orthogonal Cartesian coordinate system.

$$\begin{bmatrix} \varepsilon_1 \\ \varepsilon_2 \\ \varepsilon_3 \\ \gamma_{23} \\ \gamma_{31} \\ \gamma_{21} \end{bmatrix} = \begin{bmatrix} S_{11} & S_{12} & S_{13} & S_{14} & S_{15} & S_{16} \\ S_{21} & S_{22} & S_{23} & S_{24} & S_{25} & S_{26} \\ S_{31} & S_{32} & S_{33} & S_{34} & S_{35} & S_{36} \\ S_{41} & S_{42} & S_{43} & S_{44} & S_{45} & S_{46} \\ S_{51} & S_{52} & S_{53} & S_{54} & S_{55} & S_{56} \\ S_{61} & S_{62} & S_{63} & S_{64} & S_{65} & S_{66} \end{bmatrix} \begin{bmatrix} \sigma_1 \\ \sigma_2 \\ \sigma_3 \\ \tau_{23} \\ \tau_{31} \\ \tau_{21} \end{bmatrix} \tag{3.1}$$

where

ε	*normal strains*
γ	*shear strains*
σ	*normal stresses*
τ	*shear stresses*
S	*elements of the stiffness matrix*

Planes of symmetry

Assuming the lamina is orthotropic, consisting of continuous fibres with a unidirectional orientation. Three planes of symmetry are present, significantly simplifying the stiffness matrix. Shear behaviour is decoupled from normal stresses.

$$[S] = \begin{bmatrix} S_{11} & S_{12} & S_{13} & 0 & 0 & 0 \\ S_{21} & S_{22} & S_{23} & 0 & 0 & 0 \\ S_{31} & S_{32} & S_{33} & 0 & 0 & 0 \\ 0 & 0 & 0 & S_{44} & 0 & 0 \\ 0 & 0 & 0 & 0 & S_{55} & 0 \\ 0 & 0 & 0 & 0 & 0 & S_{66} \end{bmatrix} \tag{3.2}$$

Since a lamina is thin, it does not carry any out-of-plane loads and plane stress conditions can be assumed. This means, $\sigma_3 = 0, \tau_{23} = 0$ and $\tau_{31} = 0$, reducing (3.2) to

$$\begin{bmatrix} \varepsilon_1 \\ \varepsilon_2 \\ \gamma_{12} \end{bmatrix} = \begin{bmatrix} S_{11} & S_{12} & 0 \\ S_{21} & S_{22} & 0 \\ 0 & 0 & S_{66} \end{bmatrix} \begin{bmatrix} \sigma_1 \\ \sigma_2 \\ \tau_{12} \end{bmatrix} \tag{3.3}$$

Inverting equation (3.3) gives the stress-strain relationship as

$$\begin{bmatrix} \sigma_1 \\ \sigma_2 \\ \tau_{12} \end{bmatrix} = \begin{bmatrix} Q_{11} & Q_{12} & 0 \\ Q_{21} & Q_{22} & 0 \\ 0 & 0 & Q_{66} \end{bmatrix} \begin{bmatrix} \varepsilon_1 \\ \varepsilon_2 \\ \gamma_{12} \end{bmatrix} \tag{3.4}$$

where

σ_1, σ_2	*normal stresses in 1- and 2-direction, respectively.*
τ_{12}	*in-plane shear stress*
$\varepsilon_1, \varepsilon_2$	*normal strains in 1- and 2-direction, respectively.*
γ_{12}	*in-plane shear strain*
Q_{11}	*axial modulus of the ply*
$Q_{12}=Q_{21}$	*Poisson's ratio effect of transverse strain to axial stress and vice versa*
Q_{22}	*transverse modulus of the ply*
Q_{66}	*shear modulus of the ply*

The reduced stiffness matrix coefficients are given as

$$\left.\begin{aligned} Q_{11} &= \frac{E_1}{1-v_{12}v_{21}} \\ Q_{12} &= \frac{v_{21}E_1}{1-v_{12}v_{21}} \\ Q_{22} &= \frac{E_2}{1-v_{12}v_{21}} \\ Q_{66} &= G_{12} \end{aligned}\right\} \tag{3.5}$$

where

E_1	l*ongitudinal Young's modulus*
E_2	t*ransverse Young's modulus*
G_{12}	*in-plane shear modulus*
v_{12}	m*ajor Poisson's ratio*
v_{21}	*minor Poisson's ratio*

These independent engineering elastic constants can be determined through testing or they can be approximated with the use of a theoretical or semi-empirical model. Two commonly used models are rules of mixtures and the Halpin-Tsai model. (Moen, 2014)

A number of assumptions are used in these theories (Zoghi, 2013):

- Each lamina is homogeneous, linearly elastic, and orthotropic.
- The matrix and the fibres are linear elastic and homogeneous.
- The lamina is free of voids.
- The matrix and fibres interface provides a perfect bond.
- Each ply is initially in a stress-free state.
- The fibres are uniform in properties and diameter, continuous and parallel throughout.

3.3.1.2 Rules of mixtures

The rules of mixture model is simple and reasonably accurate. The properties of the lamina are determined using the properties of the individual constituents and the proportions with which they are applied in the lamina.

Volume fractions

$$V_f = v_f / v_c \tag{3.6}$$

$$V_m = v_m / v_c \tag{3.7}$$

where

V_f *fibre volume fraction*
V_m *matrix volume fraction*
$v_{f,m,c}$ *volume of the fibre, matrix and composite material, respectively*

The sum of volume fractions

$$V_f + V_m + V_v = 1.0 \tag{3.8}$$

where

V_v *volume fraction of voids*

By assuming the absence of voids this becomes

$$V_f + V_m = 1.0 \tag{3.9}$$

Longitudinal Young's Modulus

The longitudinal Young's modulus is obtained with

$$E_1 = E_f V_f + E_m V_m \tag{3.10}$$

where

E_f *modulus of elasticity of the fibres*
E_m *modulus of elasticity of the matrix*

Major Poisson's ratio

The major Poisson's ratio relates the strain in transverse direction to the strain in longitudinal direction in the case that the lamina is only loaded in the longitudinal direction.

$$v_{12} = v_f V_f + v_m V_m \tag{3.11}$$

where

v_f *Poisson's ratio of fibres*
v_m *Poisson's ratio of matrix*

The minor Poisson's ratio relates the longitudinal and transverse strains when the lamina is only loaded in the transverse direction

$$v_{21} = \frac{E_2}{E_1} \cdot v_{12} \tag{3.12}$$

3.3.1.3 Semi-empirical model of Halpin-Tsai

The rules of mixture method lacks accuracy, compared to experimental results, when predicting the in-plane shear modulus and transverse modulus. The semi-empirical model of Halpin-Tsai is more accurate predicting these properties. (Zoghi, 2013)

Transverse Young's Modulus:

$$\frac{E_2}{E_m} = \frac{1+\xi\eta V_f}{1-\eta V_f} \tag{3.13}$$

where

$$\eta = \frac{(E_f/E_m)-1}{(E_f/E_m)+\xi} \tag{3.14}$$

The term ξ is called the reinforcing factor is dependent on the following:

- Geometry of the fibres
- Packing geometry of fibres within the matrix
- Loading conditions

For example, in the case of a circular fibre geometry $\xi = 2$.

In-plane shear modulus:

$$\frac{G_{12}}{G_m} = \frac{1+\xi\eta V_f}{1-\eta V_f} \tag{3.15}$$

where

$$\eta = \frac{(G_f/G_m)-1}{(G_f/G_m)+\xi} \tag{3.16}$$

3.3.1.4 Local vs. Global coordinate system

The reduced stiffness matrix coefficients of [Q] are oriented in a local coordinate system (1-2-3), which doesn't necessarily coincide with the coordinate system of the structural element (x,y,z). The global and local stresses are related through transformation matrix [T] with the angle θ.

$$\begin{bmatrix}\sigma_1\\ \sigma_2\\ \tau_{12}\end{bmatrix} = \begin{bmatrix}\cos^2(\theta) & \sin^2(\theta) & 2\cdot\sin(\theta)\cdot\cos(\theta)\\ \sin^2(\theta) & \cos^2(\theta) & -2\cdot\sin(\theta)\cdot\cos(\theta)\\ -\sin(\theta)\cdot\cos(\theta) & \sin(\theta)\cdot\cos(\theta) & \cos^2(\theta)-\sin^2(\theta)\end{bmatrix}\begin{bmatrix}\sigma_x\\ \sigma_y\\ \tau_{xy}\end{bmatrix} \tag{3.17}$$

and

$$\begin{bmatrix}\sigma_x\\ \sigma_y\\ \tau_{xy}\end{bmatrix} = [T]^{-1}\begin{bmatrix}\sigma_1\\ \sigma_2\\ \tau_{12}\end{bmatrix} \tag{3.18}$$

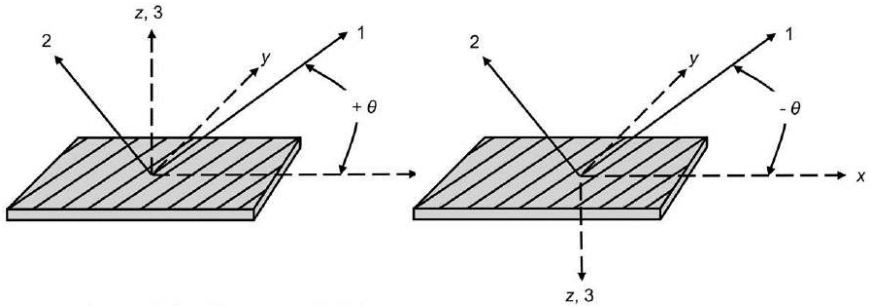

Figure 13. Material and structural coordinate systems (Campbell, 2010)

The global and local strains are also related through the transformation matrix (Kaw, 2006)

$$\begin{bmatrix} \varepsilon_1 \\ \varepsilon_2 \\ \gamma_{12}/2 \end{bmatrix} = [T] \begin{bmatrix} \varepsilon_x \\ \varepsilon_y \\ \gamma_{xy}/2 \end{bmatrix} \tag{3.19}$$

This can be rewritten as

$$\begin{bmatrix} \varepsilon_1 \\ \varepsilon_2 \\ \gamma_{12} \end{bmatrix} = [R][T][R]^{-1} \begin{bmatrix} \varepsilon_x \\ \varepsilon_y \\ \gamma_{xy} \end{bmatrix} \tag{3.20}$$

Where [R] is the Reuter matrix

$$[R] = \begin{bmatrix} 1 & 0 & 0 \\ 0 & 1 & 0 \\ 0 & 0 & 2 \end{bmatrix} \tag{3.21}$$

Combining equations (3.4), (3.18) and (3.20) gives

$$\begin{bmatrix} \sigma_x \\ \sigma_y \\ \tau_{xy} \end{bmatrix} = [T]^{-1}[Q][R][T][R]^{-1} \begin{bmatrix} \varepsilon_x \\ \varepsilon_y \\ \gamma_{xy} \end{bmatrix} \tag{3.22}$$

The result is the stress-strain relation for a lamina of arbitrary orientation.

$$\begin{bmatrix} \sigma_x \\ \sigma_y \\ \tau_{xy} \end{bmatrix} = \begin{bmatrix} \bar{Q}_{11} & \bar{Q}_{12} & \bar{Q}_{16} \\ \bar{Q}_{21} & \bar{Q}_{22} & \bar{Q}_{26} \\ \bar{Q}_{61} & \bar{Q}_{62} & \bar{Q}_{66} \end{bmatrix} \begin{bmatrix} \varepsilon_x \\ \varepsilon_y \\ \gamma_{xy} \end{bmatrix} \tag{3.23}$$

where

$$\bar{Q}_{11} = Q_{11}\cos^4\theta + 2(Q_{12} + 2Q_{66})\sin^2\theta\cos^2\theta + Q_{22}\sin^4\theta$$

$$\bar{Q}_{12} = (Q_{11} + Q_{22} - 4Q_{66})\sin^2\theta\cos^2\theta + Q_{12}(\sin^4\theta + \cos^4\theta)$$

$$\bar{Q}_{22} = Q_{11}\sin^4\theta + 2(Q_{12} + 2Q_{66})\sin^2\theta\cos^2\theta + Q_{22}\cos^4\theta$$

$$\bar{Q}_{16} = (Q_{11} - Q_{12} - 2Q_{66})\sin\theta\cos^3\theta + (Q_{12} - Q_{22} + 2Q_{66})\sin^3\theta\cos\theta$$

$$\bar{Q}_{26} = (Q_{11} - Q_{12} - 2Q_{66})\sin^3\theta\cos\theta + (Q_{12} - Q_{22} + 2Q_{66})\sin\theta\cos^3\theta$$

$$\bar{Q}_{66} = (Q_{11} + Q_{22} - 2Q_{12} - 2Q_{66})\sin^2\theta\cos^2\theta + Q_{66}(\sin^4\theta + \cos^4\theta) \tag{3.24}$$

$\bar{Q}_{ij}$ *elements of the transformed reduced stiffness matrix*

3.3.2 Mechanics of laminates

Laminates are built up of layers of laminae. The laminae are stacked under different angles and can be made with various constituent materials to achieve the required properties of the laminate. The properties of the laminate are dependent on each individual ply and the stress-strain relationship is described by classical laminate theory.

3.3.2.1 Classical laminate theory

Some assumptions are made to describe the relationship with classical laminate theory (Moen, 2014):

- Each lamina is orthotropic
- Each lamina is homogeneous
- Each lamina is elastic
- No slip between the lamina interfaces
- A straight and perpendicular line to the middle surface remains straight and perpendicular to the middle surface during deformation ($\gamma_{xz} = \gamma_{yz} = 0$)
- The lamina is thin and only subjected to in-plane loading ($\sigma_z = \tau_{xz} = \tau_{yz} = 0$)
- Displacements are continuous and small throughout the laminate ($|w| \ll |h|$)

Strain–displacement relations

The strain varies linearly along the thickness of the laminate. The following expression gives the strain at any point in the laminate. It consists of a midplane strain component and a component resulting from the curvature multiplied by the distance z from the midplane.

$$\begin{Bmatrix} \varepsilon_x \\ \varepsilon_y \\ \varepsilon_{xy} \end{Bmatrix} = \begin{Bmatrix} \varepsilon_x^0 \\ \varepsilon_y^0 \\ \gamma_{xy}^0 \end{Bmatrix} + z \begin{Bmatrix} \kappa_x \\ \kappa_y \\ \kappa_{xy} \end{Bmatrix} \tag{3.25}$$

Stress–strain relations

With the midplane strains and the curvatures, the global stresses in each ply can be determined by substituting (3.25) into (3.23) resulting in

$$\begin{bmatrix} \sigma_x \\ \sigma_y \\ \tau_{xy} \end{bmatrix} = \begin{bmatrix} \bar{Q}_{11} & \bar{Q}_{12} & \bar{Q}_{16} \\ \bar{Q}_{21} & \bar{Q}_{22} & \bar{Q}_{26} \\ \bar{Q}_{16} & \bar{Q}_{26} & \bar{Q}_{66} \end{bmatrix} \begin{bmatrix} \varepsilon_x^0 + z\kappa_x \\ \varepsilon_y^0 + z\kappa_y \\ \gamma_{xy}^0 + z\kappa_{xy} \end{bmatrix} \tag{3.26}$$

The stresses in each ply vary linearly over the thickness of that ply, but between plies jumps can occur. This is a result of the transformed reduced stiffness matrix and the fact that it changes depending on the material and orientation of the ply.

Force and moment resultants

Consider the laminate in Figure 14 consisting of N plies, with ply thickness t_k. The thickness h of the laminate is given by

$$h = \sum_{k=1}^{N} t_k \tag{3.27}$$

Integrating the global stresses in each ply gives the resultant forces per unit length in the x-y plane through the laminate thickness as (Kaw, 2006)

$$N_x = \int_{-h/2}^{h/2} \sigma_x \cdot dz$$

$$N_y = \int_{-h/2}^{h/2} \sigma_y \cdot dz$$

$$N_{xy} = \int_{-h/2}^{h/2} \tau_{xy} \cdot dz \tag{3.28}$$

Similarly, the resultant moments per unit length in the x-y plane can be found as

$$M_x = \int_{-h/2}^{h/2} \sigma_x \cdot z \cdot dz$$

$$M_y = \int_{-h/2}^{h/2} \sigma_y \cdot z \cdot dz$$

$$M_{xy} = \int_{-h/2}^{h/2} \tau_{xy} \cdot z \cdot dz \tag{3.29}$$

where

$N_{x,y}$ *normal forces*
N_{xy} *shear force*
$M_{x,y}$ *bending moments*
M_{xy} *twisting moment*

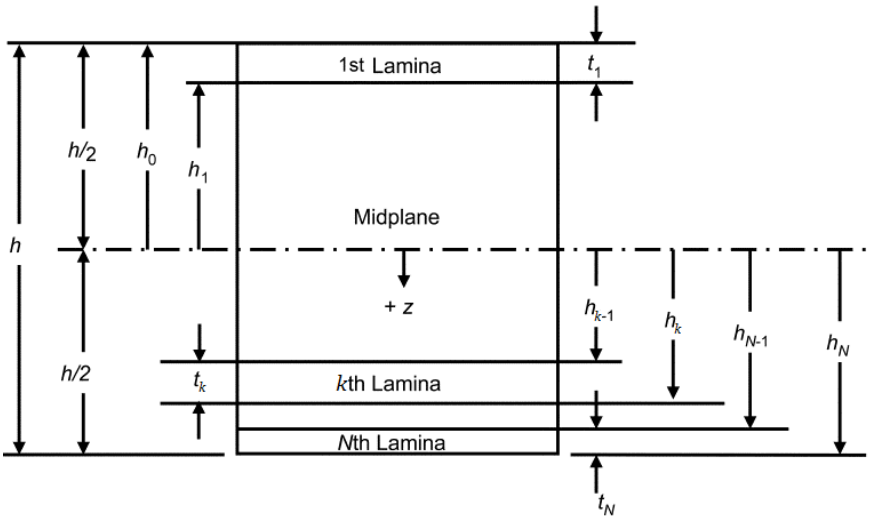

Figure 14. Laminate stacking sequence (Campbell, 2010)

Substitution of (3.26) into the resultant force and moment equations, the 6x6 so-called ABD-matrix can be found

$$\begin{bmatrix} N_x \\ N_y \\ N_{xy} \\ M_x \\ M_y \\ M_{xy} \end{bmatrix} = \begin{bmatrix} A_{11} & A_{12} & A_{16} & B_{11} & B_{12} & B_{16} \\ A_{12} & A_{22} & A_{26} & B_{12} & B_{22} & B_{26} \\ A_{16} & A_{26} & A_{66} & B_{16} & B_{26} & B_{66} \\ B_{11} & B_{12} & B_{16} & D_{11} & D_{12} & D_{16} \\ B_{12} & B_{22} & B_{26} & D_{12} & D_{22} & D_{26} \\ B_{16} & B_{26} & B_{66} & D_{16} & D_{26} & D_{66} \end{bmatrix} \begin{bmatrix} \varepsilon_x^0 \\ \varepsilon_y^0 \\ \gamma_{xy}^0 \\ \kappa_x \\ \kappa_y \\ \kappa_{xy} \end{bmatrix} \tag{3.30}$$

where

[N] *force vector [N]*
[M] *moment vector [Nm]*
[ε^0] *midplane laminate strain vector [-]*
[κ] *curvature vector [1/m]*

The elements of the stiffness matrix are calculated with

$$[A] = A_{ij} = \sum_{k=1}^{N} \left(\bar{Q}_{ij}\right)_k (h_k - h_{k-1}) \qquad \textit{extension stiffness matrix [N/m]}$$

$$[B] = B_{ij} = \frac{1}{2} \sum_{k=1}^{N} \left(\bar{Q}_{ij}\right)_k \left(h_k^2 - h_{k-1}^2\right) \qquad \textit{coupling stiffness matrix [N]}$$

$$[D] = D_{ij} = \frac{1}{3} \sum_{k=1}^{N} \left(\bar{Q}_{ij}\right)_k \left(h_k^3 - h_{k-1}^3\right) \qquad \textit{bending stiffness matrix [Nm]}$$

where

i=1,2,6 ; j=1,2,6
N *total number of plies*
h_{k-1} *distance from the top of ply k to the midplane*
h_k *distance from the bottom of ply k to the midplane*

The [B] matrix and a number of elements in the [A] and [D] matrices cause coupling effects. Tension-shear coupling is represented by terms A_{16} and A_{26}, tension-twisting coupling is represented by B_{16} and B_{26}, and flexure-twisting coupling when a moment is applied is represented by D_{16} and D_{26}.

[A] is the extensional stiffness matrix and is not affected by the stacking sequence. The terms A_{11}, A_{12}, A_{22}, and A_{66} are never negative. In the case of a balanced laminate, no tension-shear coupling exists.

[B] is the coupling stiffness matrix and in the case of a symmetric laminate [B]=0. If [B] is nonzero, the laminate will warp under a normal force or bending moment.

[D] is the bending stiffness matrix and affected the most by the stacking sequence of the laminate. The terms D_{11}, D_{12}, D_{22}, and D_{66} are always positive. No flexure-twisting coupling will exist in plies oriented at 0° or 90° orientation. This is also valid if a ply oriented at +θ at a certain distance above the midplane is balanced by a ply oriented at –θ at the same distance below the midplane. A downside of this is that the laminate will be not symmetric.

A balanced and symmetric stacking sequence is always preferred to avoid bending, twisting and warping under applied loads and moments. (Campbell, 2010)

3.3.2.2 Laminate types

Laminates are formed by laminae, stacked at various angles and bonded together.

Example of a laminate code notation:

0
30
60
30
0

A number of different laminate types are used (Campbell, 2010):

Unidirectional. All plies are oriented at a 0-degree or 90-degree angle. The result is the same as a single ply, but thicker.

Angle-ply. The laminae are stacked in a sequence that follows +θ/–θ. For example $[30°/-30°]_4$ where the subscript 4 specifies that the sequence is repeated 4 times.

Cross-ply. The laminae are stacked in a sequence, alternating between 0° and 90°.

Symmetric. The laminae stacking sequence is mirrored about the midplane of the laminate. For example $[0°,45°,-45°,90°]_s$ gives half laminate, where the s indicates that it is a symmetric laminate. The full sequence of the laminate would be [0°,45°,-45°,90°,90°,-45°,45°,0°].

Balanced. The laminae are stacked as such, that for every +θ° ply an identical ply oriented -θ° is applied. The stacking order doesn't have to be symmetrical.

Quasi-Isotropic. The laminae are stacked, consisting of three or more identical plies, with equal angles between each ply and the next.

Hybrid. Laminates build up off laminae of different materials, for example plies of glass and plies of carbon.

3.3.2.3 Laminate failure

Laminates don't fail in the same manner as for instance isotropic materials that exhibit yielding. Failure mechanisms like fibre breakage, matrix cracking, debonding and fibre pull-out do not instantly result in catastrophic failure. Different mechanisms develop and progress simultaneously and interactively, making the failure of the laminate a complex phenomenon. A conservative approach that is often used, is first ply failure. However in reality, first ply failure doesn't provide the ultimate strength of the laminate. After the first ply fails, the remaining laminae can continue to carry additional loading, successively failing at increasing strength depending on loading conditions, properties of each ply and orientation. The first ply that fails is generally oriented with the fibre direction perpendicular to the main loading direction. Next to fail are other off-angle plies and finally plies with a fibre orientation in the direction of loading. When plies start to fail delamination occurs, where the failed plies debond from the remaining plies. To analyze failure progressively, stress analysis must be repeated as different plies fail. The ultimate strength can be determined accurately.

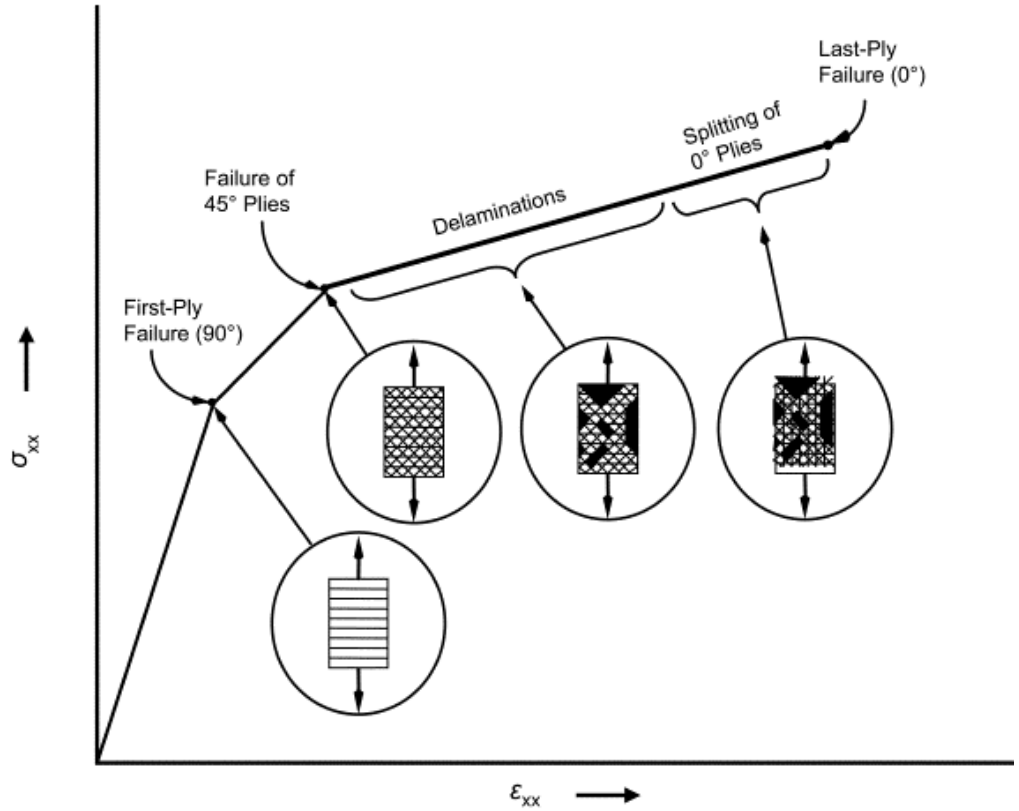

Figure 15. Progressive failure of plies (Campbell, 2010)

3.4 Joints

As for other structural materials, joints are an important aspect of the design in FRP, since joints are often weaker spots in a structural design. Joints are needed for a variety of functions (Kolstein, 2008):

- Material size is limited
- More convenient manufacturing or transportation
- Providing access
- Connecting sub-assemblies

Two main joint types are used for FRPs: mechanically fastened and adhesively bonded. These two joining methods can also be combined. Figure 16 shows a number of typical joint configurations.

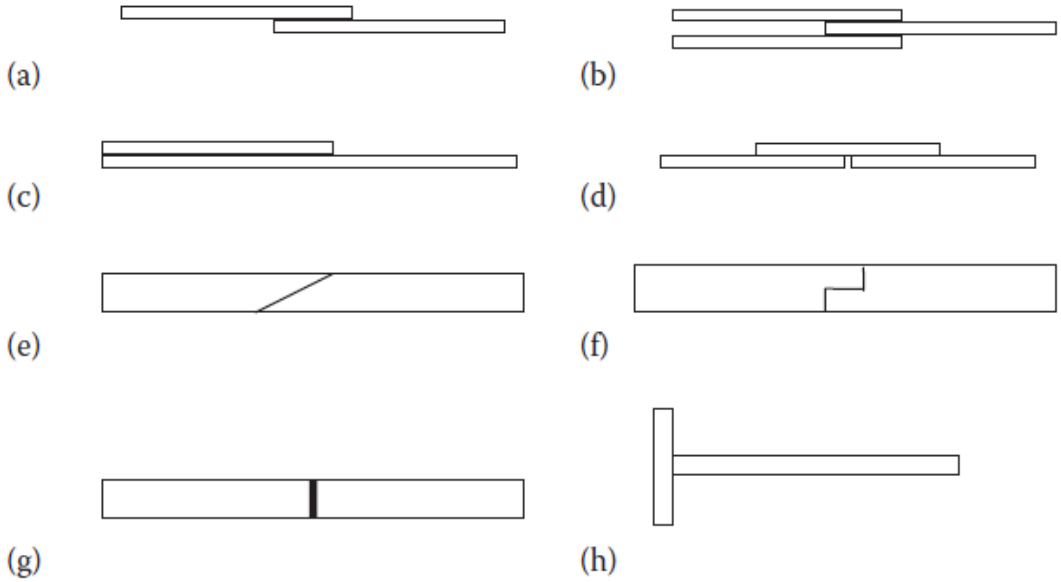

Figure 16. Typical joint configurations (Zoghi, 2013)

(a) Single-lap joint (fastened, bonded, or combined), (b) double-lap joint (fastened, bonded, or combined), (c) lap-strap joint (fastened, bonded, or combined), (d) single-strap joint (fastened, bonded, or combined), (e) scarf joint (bonded), (f) stepped joint (fastened, bonded, or combined; stepped region varies), (g) butt joint (bonded), and (h) tee joint (fastened, bonded, or combined; tee region varies)

3.4.1 Mechanically fastened

In mechanically fastened joints, two components are joined together with screws, rivets or bolts. Both metallic or FRP fasteners can be used. Some advantages and disadvantages are listed below (Campbell, 2010).

Advantages of mechanically fastened joints:

- Relatively easy joining method; no special surface preparation required
- Not as sensitive to peel stresses or residual-stress effects
- Non-destructive testing is generally not required
- Disassembly is possible
- Easier inspection, maintenance and repairs

Disadvantages of mechanically fastened joints:

- Relatively low joint efficiency; well-designed joints attain 40 to 50 percent of the base material strength
- Peak stresses concentrated in the joint area
- In-service fatigue can lead to hole elongation
- Delamination can occur during assembly due to improper hole preparation

The most common failure modes of mechanically fastened joints are given in Figure 17.

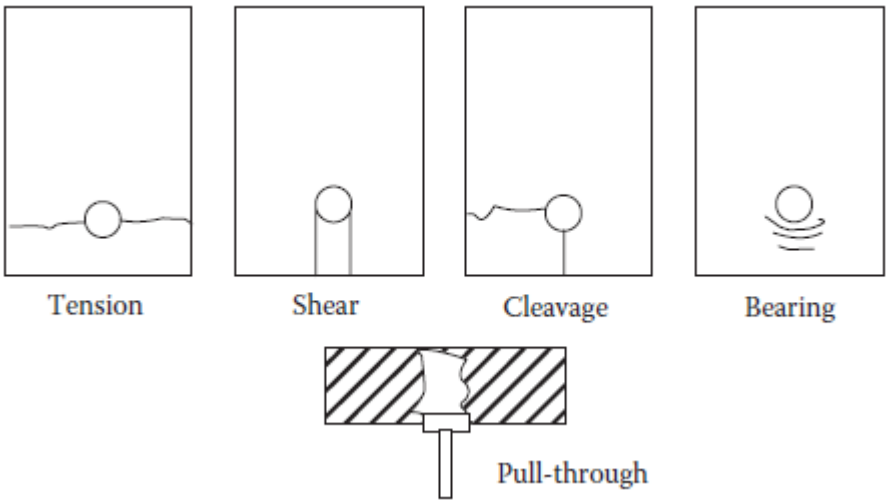

Figure 17. Fastened joint failure (Zoghi, 2013)

3.4.2 Adhesively bonded

In adhesively bonded joints, two components are joined together through an adhesive layer. Some advantages and disadvantages are listed below (Campbell, 2010).

Advantages of adhesively bonded joints:

- More uniform stress distribution, see Figure 18
- Lighter than mechanically fastened joints
- Enables sealed joints and a smooth external surface
- Stiffening effect over the entire bonded area, in comparison to point stiffening in mechanical joints

Disadvantages of adhesively bonded joints:

- Disassembly is difficult and generally results in damage
- Surface preparation is necessary for a strong connection
- There are no reliable non-destructive methods available to determine the joint strength
- Adhesive materials must be properly stored because they are perishable
- Susceptible to environmental degradation

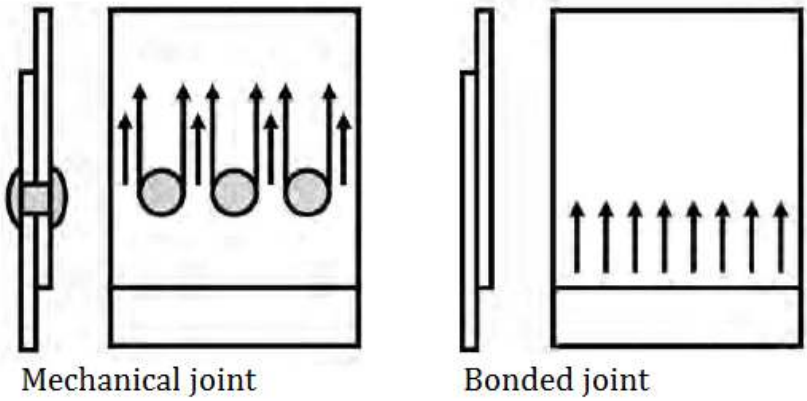

Figure 18. Load distribution mechanical and bonded joints (Campbell, 2010)

The following figure displays various failure modes in adhesively bonded joints.

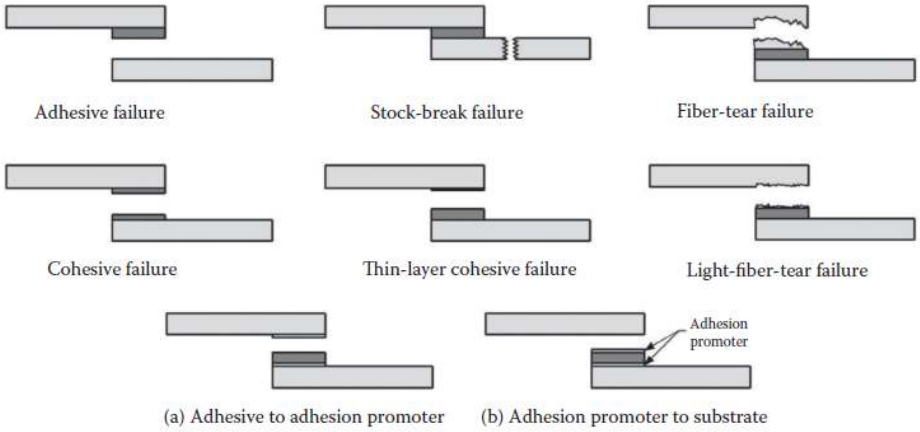

Figure 19. Failure modes in adhesively bonded joints (Zoghi, 2013)

3.4.3 Combined

Fastened-bonded joints are a combination of both methods. Even though the strength of the joint is not the sum of both individual joining methods, the overall properties of the combined joint can be a significant improvement over either method.

Some advantages of combined joints is listed below (Mosallam, 2011)

- Higher overall capacities
- Improved resistance to environmental and thermal effects
- Decreased vulnerability to peel and cleavage failures
- Improved stress distribution
- Improved fatigue and impact properties
- Increased rigidity
- Higher safety factors

3.5 FRP in lock gates

Two projects where FRP was applied in lock gates are presented here. In practice only mitre gates have been executed in FRP, one example is shown. In addition, a master thesis study of a lifting gate is discussed.

Wilhelmina canal (FiberCore Europe, 2015)
Produced by FibreCore Europe, the new Lock III in the Wilhelmina canal has the largest FRP gates built to date. The mitre gates have a height of 12.9 m, are 6.2 m wide and can withstand a head difference of 7.9 m. A low self-weight results in fast operating times and limited loading on the operating mechanism.

Figure 20. New Lock III, Wilhelmina canal (FiberCore Europe, 2015)

Eastern Scheldt storm surge barrier (Straten, 2013)
Van Straten performed a feasibility study on the application of FRP for the Eastern Scheldt storm surge barrier. A combination of E-glass and polyester was used in the design of the lifting gate with a span length of 41.5 m and a height of 22 m. The gate was designed as a straight box girder consisting of skin plates connected by horizontal plates.

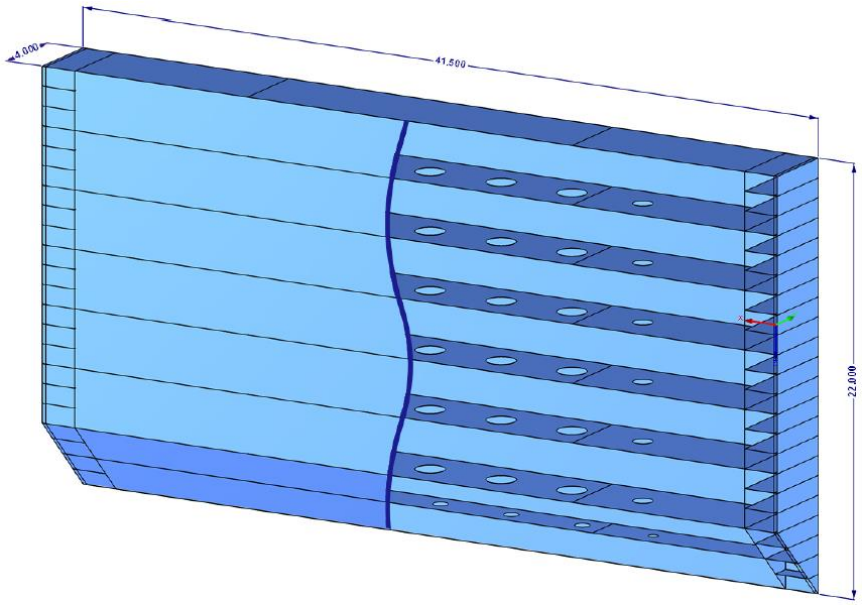

Figure 21. Final gate design (Straten, 2013)

3.6 Codes and guidelines

The design with FRP is executed in accordance with 'CUR aanbeveling 96' and the 'Eurocomp design code'. These codes are used to determine the material properties, carry out the required checks and design specific elements.

- CUR aanbeveling 96 - Vezelversterkte kunststoffen in civiele draagconstructies (CUR-96, 2003)
- Structural Design of Polymer Composites – Design Code and Handbook (EUROCOMP, 1996)

3.7 Key points – chapter 3

- Only glass fibres are considered.
- Dimensioning of joints is outside of the scope of this thesis.

Practical Part I

Foundation

- Introducing the research method
- Case study: New Lock Terneuzen
- Design input

4 Introducing the research method

Rolling gate design and stability

The research in this thesis can be roughly divided into two parts. Part A is the design of a rolling box gate and part B is focussed on the stability of the gate during movement. In part A the FRP gate design is worked out, first determining the design input (loads, laminate properties, etc.), second is the dimensioning of the box gate, performing basic checks (strength, deflection and stability) and third is a 3D model of the FRP box gate to check the gate with FEA, and performing some additional checks (fatigue and creep). Part B focusses on the stability during movement and how certain aspects of the gates design can improve the stability. Changes in the shape of the gate are implemented and the impact of these changes on the stability of the gate will be investigated.

Part A
Part B

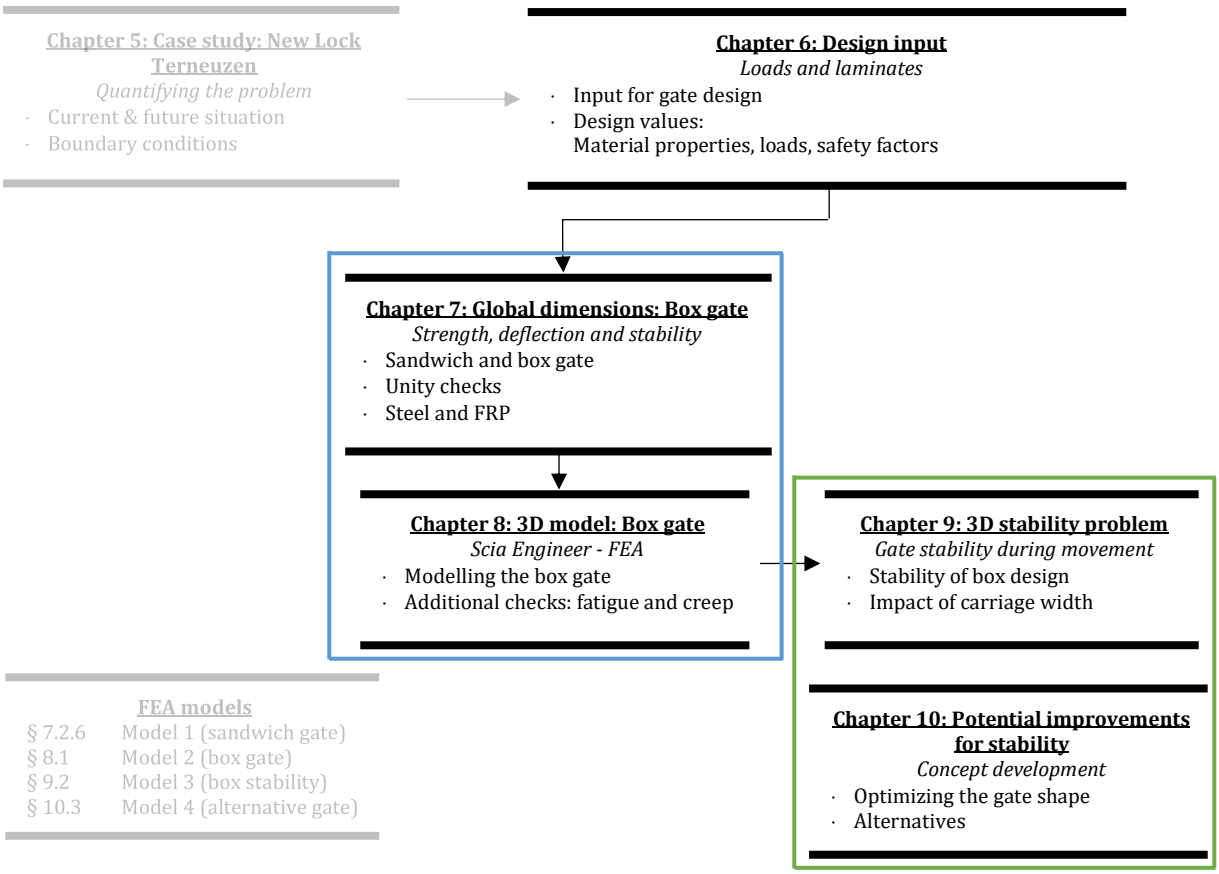

4.1 Global dimensions: Box gate (chapter 7)

The boundary conditions and design input are determined in chapters 5 and 6. From here the global dimensions of the box gate are determined with a hand calculation.

The chosen design structure is a box gate, because it is most commonly applied in rolling gates, and both a steel and FRP design is performed. The steel gate is used as a reference point to compare the FRP gate with. A number of checks; strength and deflection for the gate in closed position and stability (simplified) for the gate during movement are executed to find the global dimensions of the gate and its various structural elements. The FRP gate consists of two sandwich (two FRP skins with a foam core) retaining plates connected by multiple horizontal webs, also executed as a sandwich plate.

The stability of the gate during movement is evaluated with the principle presented in Figure 22. The support reactions follow from the vertical and moment equilibria. The resultant of these support reactions must meet the following requirement to be stable.

$$x \leq \frac{W}{6} \tag{4.1}$$

where

x	*point of action of the resultant support reaction, or eccentricity from gate centre*
W	*thickness of the gate or distance between carriage wheels*

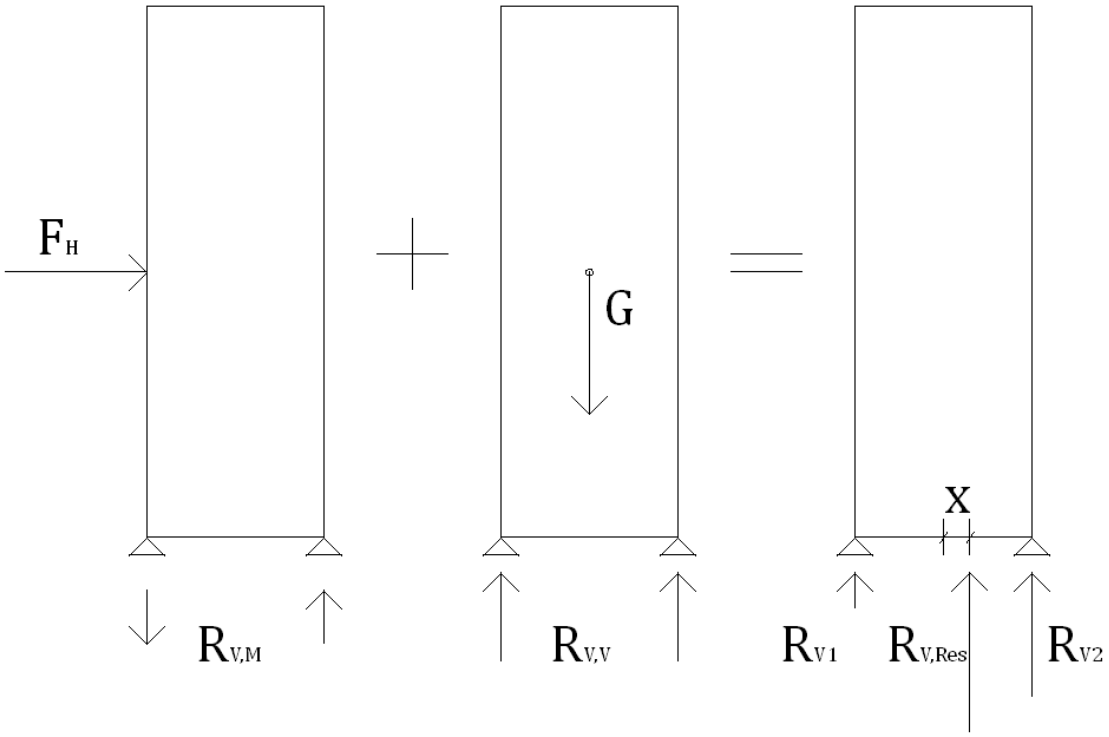

Figure 22. Stability problem

where

$R_{V,M}$	*Vertical support reactions following from the moment equilibrium*
$R_{V,V}$	*Vertical support reactions following from the vertical equilibrium*
$R_{V,Res}$	*Resultant of vertical support reactions*

4.2 3D model: Box gate (chapter 8)

The results from chapter 7 provide the necessary input for the 3D model. All models in this thesis are created with Scia Engineer. Software that allows engineers to design a structure, applying the necessary materials, easily generating the load cases and load combinations and achieve accurate results with finite elements analysis (FEA).

The laminate properties and stacking sequences for the various structural elements; retaining plates, webs and end plates are found with Kolibri. A program which allows engineers to input the desired stacking sequences resulting in the laminate properties and ABD-matrix, see expression (3.30), which serves as input for the 3D model.

The model represents the gate in closed position. The deflection and stresses of the various structural elements, i.e retaining plates, webs and end plates can be checked. Also a fatigue check and creep due to permanent ballast are performed. Ballast will always be present to sink the gate to the bottom. The required overweight for stability is achieved by a combination of self-weight and ballast.

The results from the model are presented in this chapter and give useful information on the stress distribution over the gate. These results are used to determine potential changes in the shape of the gate, elaborated on in chapter 10.

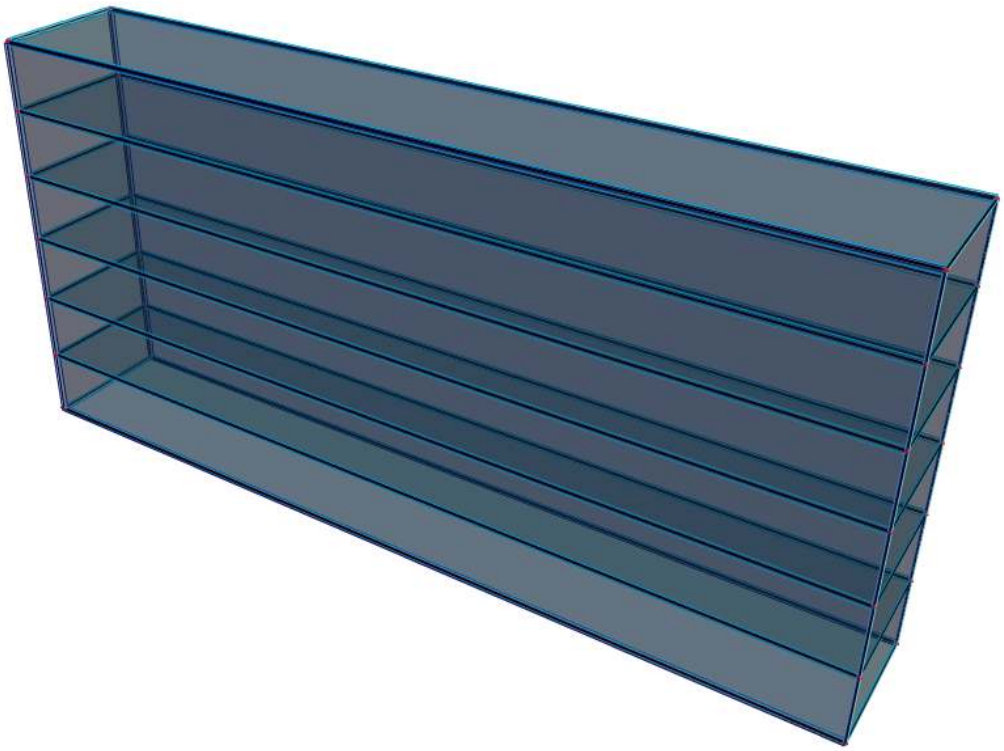

Figure 23. 3D box gate model

4.3 3D stability problem (chapter 9)

The box gate model is adjusted to represent the gate during movement. This is achieved by changing the supports, leaving the top right corner unsupported.

The stability problem is investigated according to the same principle as presented in Figure 22. The difference being the accuracy of the applied loads and the resulting support reactions. The distribution of the loads over the supports in particular.

In addition to the stability check of the designed box gate. The width between the supports, representing the carriage width, is varied (from 0.5 to 12 m) and the impact on the stability is presented in a graph. This impact is quantified by the required dead weight to guarantee stability.

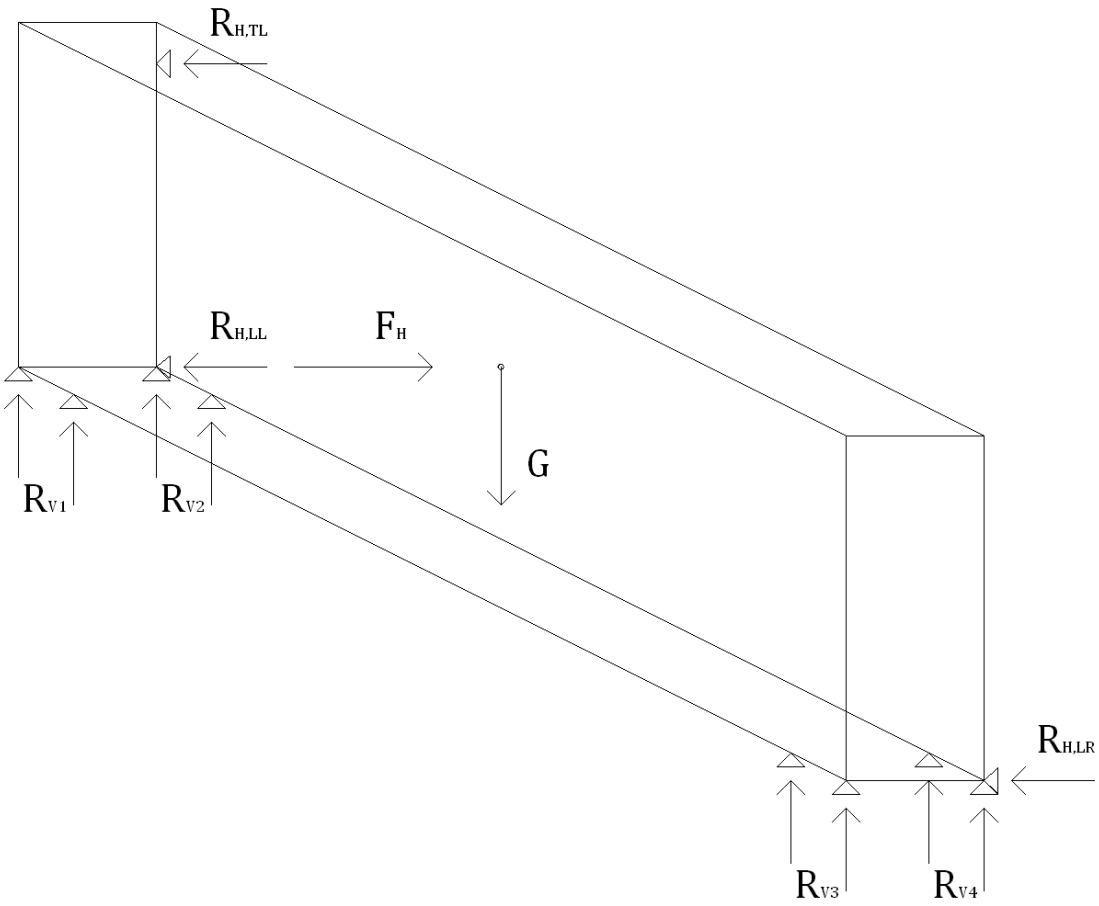

Figure 24. 3D stability problem

where

G	*Dead load (self-weight minus buoyancy)*
F_H	*All horizontal loads related to the stability load combination*
R_{V1}	*Vertical support reactions, carriage 1*
R_{V2}	*Vertical support reactions, carriage 2*
$R_{H,TL}$	*Horizontal support reaction on the gate chamber side (top left)*
$R_{H,LL}$	*Vertical support reactions on the gate chamber side (lower left)*
$R_{H,LR}$	*Vertical support reactions on the gate recess side (lower right)*

4.4 Potential improvements for stability (chapter 10)

The results from the previous chapters are used to come up with potential improvements or alternatives to the box gate design. The main objective being a gate with increased stability, which is again quantified by the overweight required. A number of ideas are conceived.

Optimizing the shape of the gate is one of these ideas and this is explored further. A variety of alternative shapes are presented in chapter 10 with the global dimensions estimated, based on the results from previous chapters. These alternative gates are modelled with the same laminate properties as applied in the box gate design. The objective with these models is to gain insight in the effects the changes have on the gates stability during movement. These designs are a first step into optimizing the rolling gate shape further.

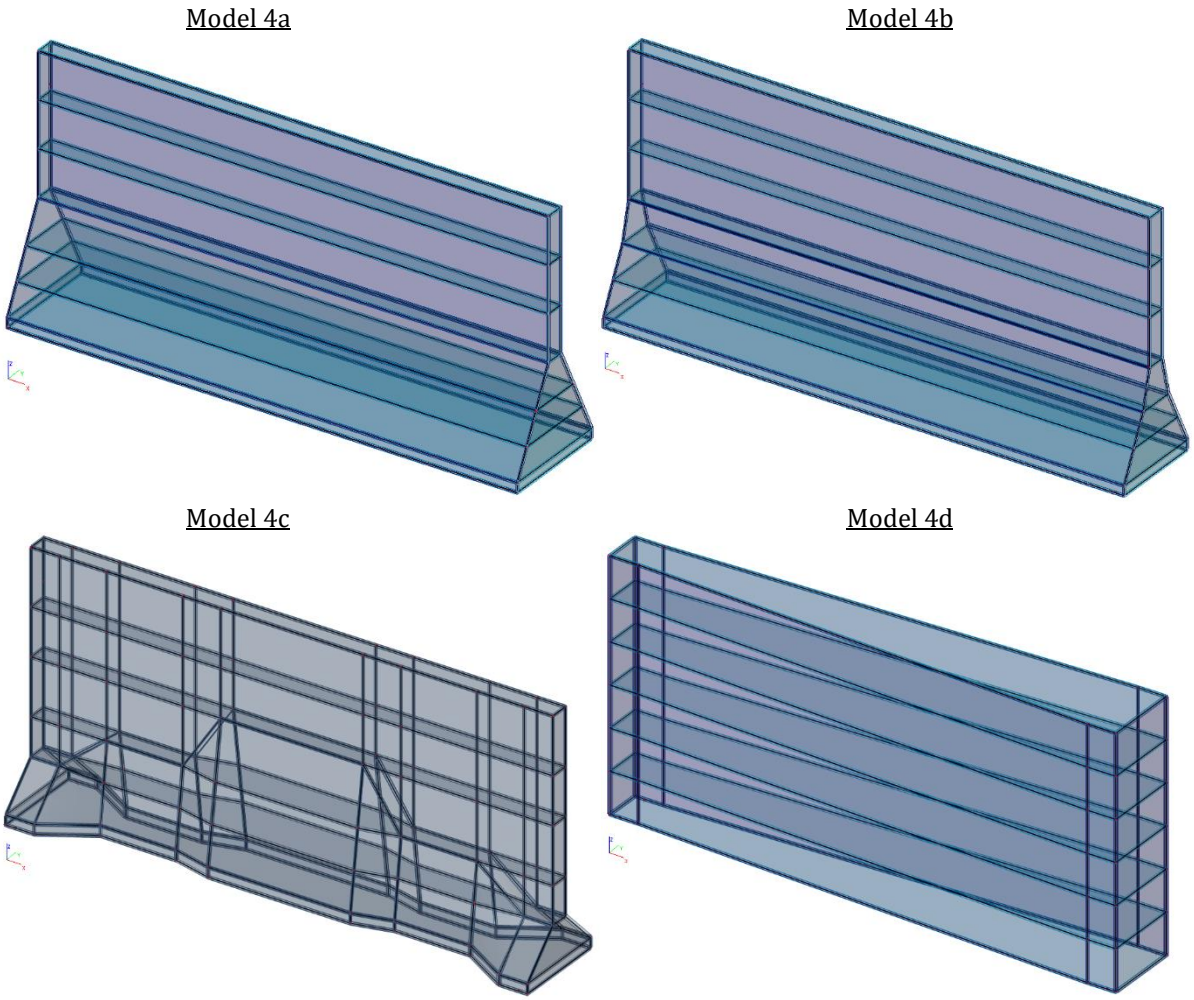

Figure 25. Alternative gate shapes

4.5 Scia Engineer models

Over the course of this thesis, a variety of 3D models are created and used to evaluate certain aspects of the gate designs. Each model is briefly discussed.

4.5.1 Model 1: Sandwich gate

The sandwich gate design in chapter 7 is modelled as a single wall element. The input for the laminate properties of this element are the combined properties of the FRP skins and the foam core. This is a simplification applied for all sandwich elements.

4.5.2 Model 2: Box gate in closed position

This is a model of the FRP box gate, representing the gate in closed position. The gate is horizontally supported along both ends of the gate. The stress and deflection results from this model are presented in chapter 8.

4.5.3 Model 3: Box gate during movement

This model represents the FRP box gate during movement. Three separate subdivisions are used for this model. The results are presented in chapter 9.

- Model 3a:
  Checking the stability of the box gate as it was designed.
- Model 3b:
  Investigate the impact of the carriage width on the stability of the gate.
- Model 3c:
  Investigate the impact of the remaining head difference on the stability of the gate.

4.5.4 Model 4: Alternative gate shapes

Four separate models are made, each with a different shape. Checks are performed in both open and closed position. The models are displayed in Figure 25.

- Model 4a:
  The narrow top leads to a very wide base. The widening starts approximately halfway down under a constant slope. The cross-section of the gate remains constant over the span of the gate.
- Model 4b:
  Similar to model 4a, but the base is not as wide. The slope, which forms the transition between the narrow top and wide base is not constant.
- Model 4c:
  The shape of the gate varies both over the height and the span. This results in buoyancy forces to be drastically reduced.
- Model 4d:
  The width of the gate gradually increases towards the end with the unsupported top corner.

4.6 Key points – chapter 4

- **Chapter 7:**

The rolling gate is designed with a box shape. The global dimensions are determined with a hand calculation. Strength and deflection checks are performed on the gate in closed position, extreme positive and negative water levels and waves apply. The stability of the gate is checked for the gate during movement/open position, a stability load case applies with maximum water levels during operation and in combination with waves.

- **Chapter 8:**

With the results from chapter 7, a 3D model (model 2) is made of the gate in closed position. Laminate stacking sequences are determined and with Kolibri the properties are found. Strength and deflection checks are performed on the various structural elements, i.e. retaining plates, webs and end plates.

- **Chapter 9:**

The model from chapter 8 is altered to represent the gate during movement (model 3). The stability of the box shaped gate can be checked in 3D, as opposed to 2D in chapter 7. In addition the carriage width and horizontal loads are varied to investigate the effects on the stability and in turn the required dead weight for stability.

- **Chapter 10:**

Based on the results of the previous chapters, solutions are presented to potentially reduce the required dead weight to meet the stability requirements. The main focus is on the shape of the gate.

– THIS PAGE IS INTENTIONALLY LEFT BLANK –

5 Case study: New Lock Terneuzen

Quantifying the problem

5.1 Lock complex Terneuzen

The lock complex Terneuzen is the gateway to the harbours of Terneuzen and Ghent and creates a shipping route between The Netherlands, Belgium and France. The complex connects the Western Scheldt and the Ghent-Terneuzen channel with multiple locks. Currently, the lock consists of three locks, the West Lock (Westsluis), the Middle Lock (Middensluis) and East Lock (Oostsluis). Each lock intersects and is crossed by two bridges. Road traffic doesn't experience much hindrance from the locks. Terneuzen is located to the east of the complex.

The West Lock is the largest of the three locks with a length of 290m, a width of 40m and the sill depth is 13.5m. The lock was built in 1968 and is the only one that allows lockage of larger maritime vessels, limited to lightered Panamax vessels with dimensions of 265x34x12.5m and approximately 92.000 DWT. The Middle Lock is the oldest and smallest of the three locks. It was completed in 1910 and thoroughly renovated in 1986. The locks dimensions are 140x18x8.63m and is primarily used for inland shipping. The East Locks dimensions are 260x24x4.5m and was built in 1968. This lock is also mainly used for inland shipping (IenM, 2016). Figure 26 gives an overview of the entire complex. From left to right respectively, the West, Middle and East Lock can be seen.

Figure 26. Lockcomplex Terneuzen (Portaal van Vlaanderen, 2016)

5.2 New Lock Terneuzen

Starting in 2004, a committee investigated the future potential of the Ghent-Terneuzen channel zone and explored possible improvements. The research revealed that, the current layout of the lock complex has a number of limitations for the channel zone Ghent-Terneuzen and the Seine-Scheldt connection (IenM, 2016):

- The capacity of the lock complex is limited, resulting in the displacement of cargo to other means of transportation.
- The limited capacity also results in increasingly longer waiting time.
- Robustness of the Ghent-Terneuzen channel is an issue. In case the locks are out of order, no alternative routes are available.
- The dimension of the Westsluis, currently the largest lock of the complex, are limited and can't accommodate larger maritime vessels.

Three main variants for the New Lock were investigated, starting in 2009.

- Maritime lock (large or small) external to the current complex
- Maritime lock integrated in the current complex
- Large, small or deep inland navigation lock

Further investigation of these variants has led to a preferred variant, the maritime lock integrated in the current complex. A maritime lock best targets the limitations of the current lock complex and integrating the lock as opposed to an external variant was considerably more economical. (IenM, 2016)

5.2.1 Description of preferred variant

The Middle Lock will be decommissioned. This allows for the New lock to be located between the West and East lock. Optimized for both maritime and inland vessels, the lock is oriented at a 5° rotation in relation to West lock. This results in the straightest possible approach from the channel.

The main dimensions of the lock chamber are as follows: A length of 427 m, measured between one inner gate and one outer gate. The width between the chamber walls is 55 m, but due to the application of floating fenders the available space could be slightly reduced. The main shipping route is excavated to a depth of -16.44 m NAP, the lock sill is also at this depth. The depth inside the lock chamber is -17 m NAP to limit negative effects caused by levelling currents. This allows vessels with a draught of 12.5 m to pass independent of the tide.

Figure 27 displays the current situation, the changes to be made and an impression of the lock complex with the New Lock. Table 4 presents various details and requirements of the preferred variant of the New Lock project.

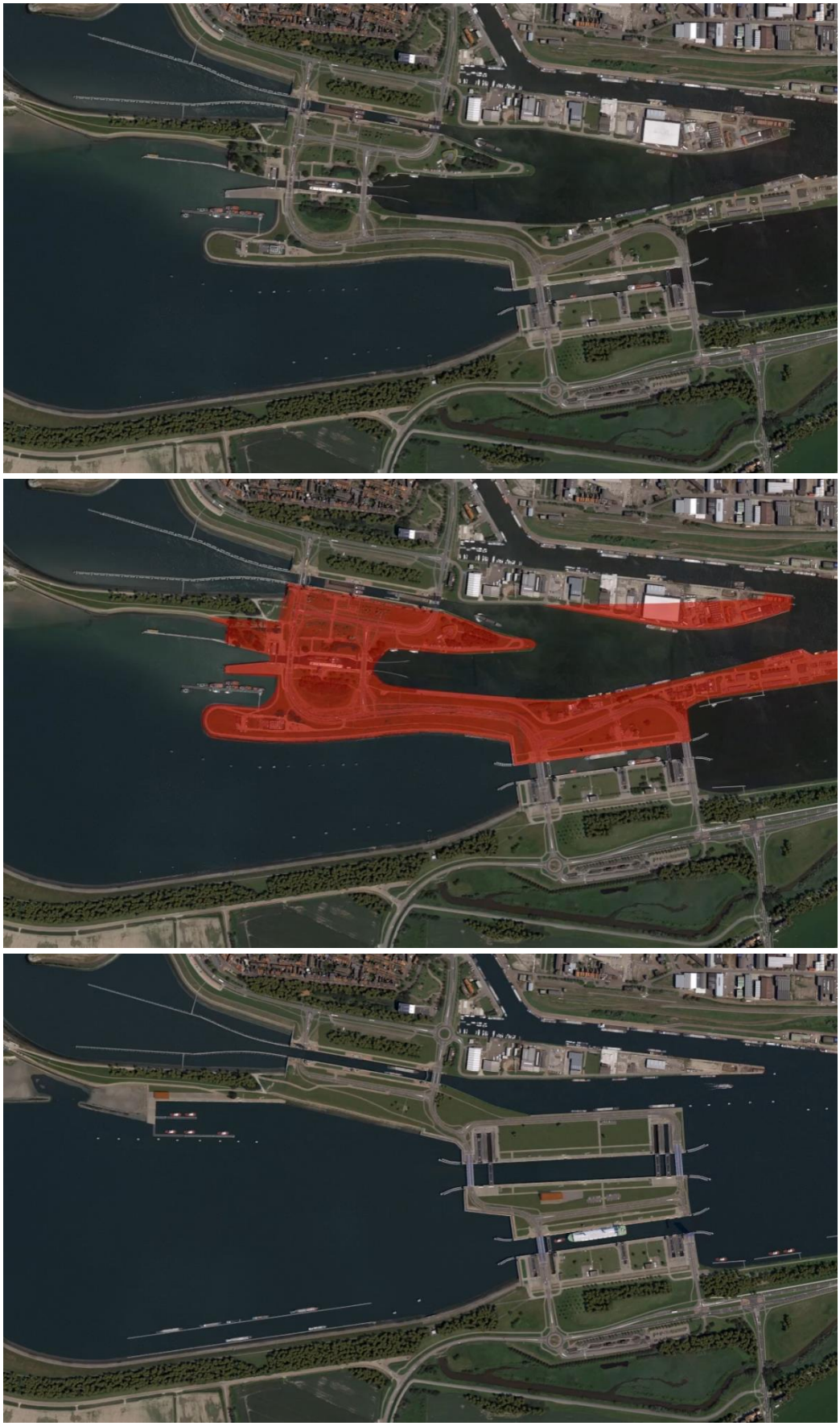

Figure 27. Lock complex Terneuzen - Current, Changes, New (impression)
(youtube/Nieuwe Sluis Terneuzen, 2015)

Table 4. Requirements of preferred variant (IenM, 2016), (VNSC, 2015)

Functional requirements	
Vessels	See section 5.2.2
Flood defence	The New Lock is part of dikering area 32, see Figure 28. Lock heads and gates are part of the primary flood defence, with a height of +7.5m and +9.5m NAP for the channel and Western Scheldt side respectively.
Fresh/Salt	Mitigating measures are applied. (Outside of scope thesis)
Intake/Discharge	Accomplished with the gates.
Levelling	Accomplished through valves in the gates. (Scope?)
Gates	Straight rolling gates in a 2x2 configuration.
Other infrastructure	
Bridges	Similar to bridges in the current complex, just outside of the lock gates.
Middle Lock	The Middle Lock is decommissioned
User requirements	
Hydraulic conditions	See section 5.2.3
Operational times	
Operating times	24 hours a day, 7 days a week
Opening gate	Western Scheldt: 4.5 min ; Channel: 4.5 min
Closing gate	Western Scheldt: 4.7 min ; Channel: 3.5 min
Waiting times	Projected waiting times are displayed in Table 7
Availability	Non-availability 1%
Design life	100 years
Maintenance requirements	
Maintenance strategy	
Spare parts	Within the lock complex (the southern point of the Schependike, located southeast to the Eastlock) an area for storage and maintenance is appointed. Essential spare part are kept here.
Redundancy	The lock is equipped with two gates per lock head. In case of maintenance on one, the other can continue to fulfil the gates function.
Environmental requirement	
Following the legal framework, the New Lock project must be executed with a m.e.r.-procedure. This insures that environmental effects are mapped thoroughly (environmental effects report) and taken into account early in the planning phases of the project.	

5.2.2 Vessel traffic

The New Lock allows the passage of larger maritime vessels with dimensions of 366x49x15m. A simulation was performed to investigate the capacity of vessel traffic. Commissioned by LievenseCSO, MARIN executed the simulation with the SIVAK model. Table 5 displays the properties of the governing vessels from this simulation.

Table 5. Governing vessel properties (VNSC, 2015)

	Tide dependent Bulk carrier		**Tide independent Bulk carrier**	**Bulk carrier Panama III**	**Containership**
	loaded	**Unloaded**			
Length [m]	366.0	366.0	265.0	248.0	366.0
Width [m]	49.0	49.0	40	32.2	49.0
Draught [m]	14.5	9.0	12.5	12.2	14.5
Displacement [ton]	214.000	133.000	110.400	78.390	179.000
Dead weight [ton]	250.000	250.000	120.000	70.000	148.760
Power [kW]	22.500	22.500	15.700	8000	72.400
Bow thruster [kW]/[ton]	-	-	2500/34	-	3.400/47

The properties used for the simulation are also used as the governing vessel properties in this thesis.

Not only the vessel classes are of importance, but also the number of vessels that are going to utilize the New Lock. In the 'Tracébesluit' a prognoses of the vessel traffic is given. Traffic is projected over time in the case that nothing change, or autonomous development, and in the case that the New Lock project is realized.

Table 6. Prognoses vessel traffic (IenM, 2016)

Traffic prognoses		Tonnage (x1000)		Vessels*	
		Maritime	**Inland**	**Maritime**	**Inland**
2020	Autonomous	37.547	39.931	12480	58916
	New Lock	42.635	45.086	12938	59540
2030	Autonomous	40.194	43.872	12051	57373
	New Lock	50.958	53.522	15347	68079
2040	Autonomous	39.689	45.960	14456	62816
	New Lock	58.709	61.386	17581	75932

*Vessels excluding recreational and passenger vessels

The total number of lockages, resulting from the simulation, for the New Lock in accordance with the prognoses of vessel traffic is found to be, 140 lockages per week (MARIN, 2015).

In addition to the traffic prognoses, the waiting times in minutes for maritime and inland vessels are projected.

Table 7. Projected waiting times

		Maritime	**Inland**
2020	Autonomous	245	67
	New Lock	57	30
2030	Autonomous	373	98
	New Lock	85	44
2040	Autonomous	529	127
	New Lock	128	66

5.2.3 Hydraulic conditions

The lock complex Terneuzen does not only connect the Western Scheldt and the Ghent-Terneuzen channel. It is also a part of Dikering area 32, Dutch Flanders, see Figure 28. Being a part of the primary flood defence system, a norm frequency of 1/4000 applies.

5.2.3.1 Ghent-Terneuzen channel

The water level of the Ghent-Terneuzen channel is regulated and equals +2.13 m NAP with a maximum deviation of + or – 0.25 m. This results in the following maximum and minimum water levels for the channel:

- Maximum channel water level: +2.38 m NAP
- Minimum channel water level: +1.88 m NAP

The water density of the channel varies between 1000 and 1008 kg/m^3 (Bonnes, 2005).

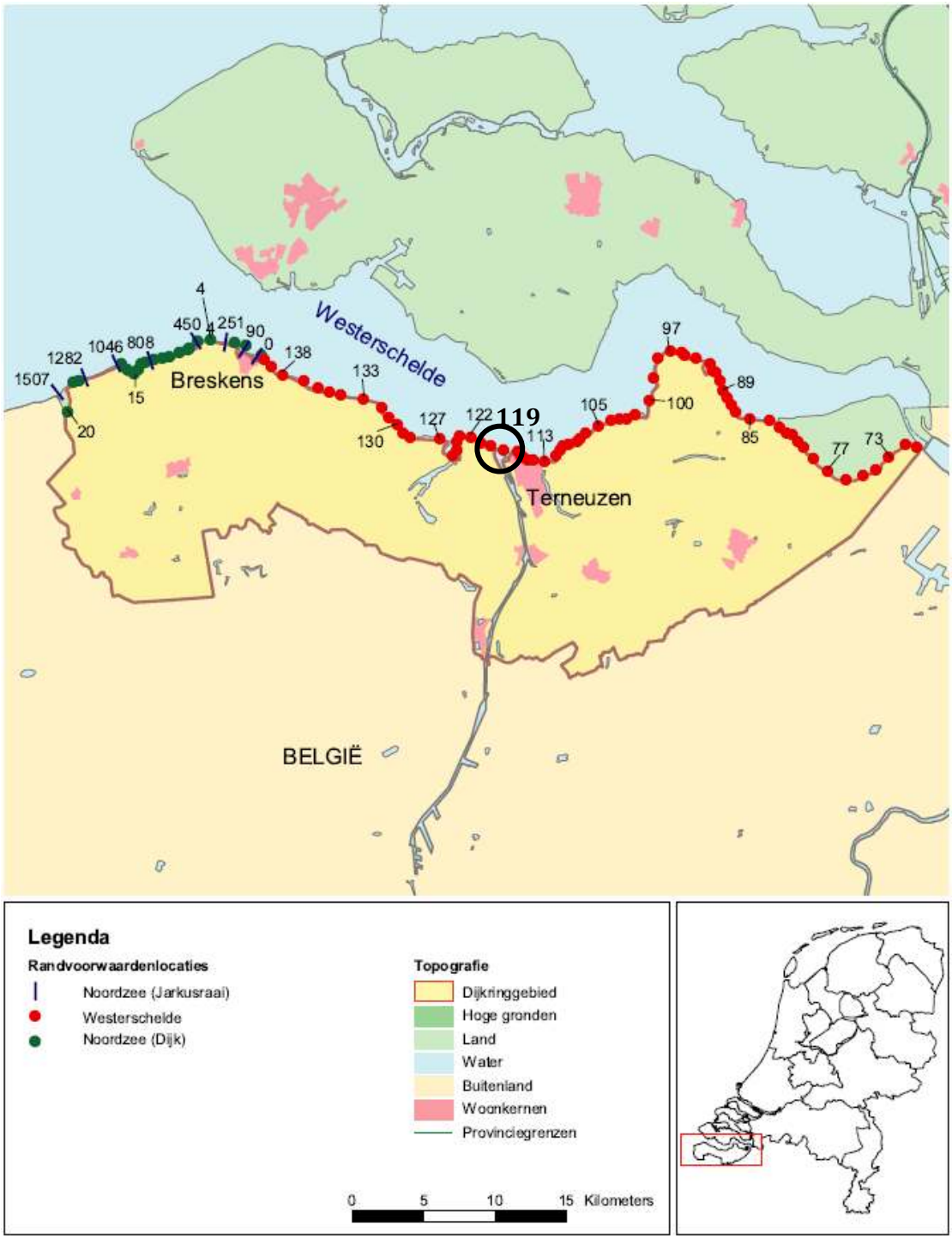

Figure 28. Dikering area 32: Dutch Flanders (Ministerie van Verkeer en Waterstaat, 2007)

5.2.3.2 Western Scheldt

The tide of the Western Scheldt follows a semi-diurnal pattern. The various tidal types and corresponding high and low water levels are displayed in Table 8. The water levels are given in cm in reference to NAP.

Table 8. Tidal types (Rijkswaterstaat, 2013)

Tidal type	HW	LW	Difference
Avg. spring tide	267	-213	480
Avg. tide	229	-189	418
Avg. neap tide	176	-156	332

Locking of vessels is shut down in the case that certain water levels are exceeded or underrun. The maximum and minimum operational water levels are:

- Maximum operational water level: +4.0 m NAP
- Minimum operational water level: -3.5 m NAP

The norm frequency water level and wave properties at the Terneuzen locations are displayed in Table 9.

Table 9. Hydraulic conditions Dutch Flanders – Western Scheldt (Ministerie van Verkeer en Waterstaat, 2007)

Location	Description	Stationing	Water level [m+NAP]	H_s [m]	$T_{m-1.0}$ [s]	B [°]
116	Terneuzen	dp403	5.8	1.50	4.6	40
117	Terneuzen	dp405	5.8	1.55	4.6	40
118	Terneuzen	dp408	5.8	1.8	4.8	50
119	Terneuzen	dp413	5.8	2.05	4.9	50

The values from location 119 are used:

$$H_s = 2.05\ m \quad T_{m-1.0} = 4.9\ s$$

Various exceedance and underrun water levels for different frequencies are given in Table 10. Also the highest and lowest recorded values are shown.

Table 10. Exceedance and underrun frequencies (Rijkswaterstaat, 2013)

Frequency [year(s)]	Exceedance HW level	Underrun LW level
1x per 10.000	600	-
1x per 5000	580	-
1x per 4000	580	-
1x per 2000	560	-
1x per 1000	540	-
1x per 500	520	-
1x per 200	500	-
1x per 100	480	-
1x per 50	460	-
1x per 20	435	-335
1x per 10	415	-325
1x per 5	400	-315
1x per 2	380	-305
1x per 1	365	-295
2x per 1	350	-285
5x per 1	330	-270
Highest known value	+496 cm : 1 feb 1953	
Lowest known value	-350 cm : 9 feb 1943	

The water density of the Western Scheldt varies between 1012 and 1020 kg/m^3 (Bonnes, 2005).

5.3 Key points – chapter 5

- Water levels

	Western Scheldt side [m]	**Channel side [m]**
Positive head	+5.8	+1.88
Negative head	-3.5	+2.38
Maximum	+4.0	+1.88
Minimum	-3.5	+2.38
Average high	+2.29	+2.13
Average low	-1.89	+2.13

- Water density

	Western Scheldt [kg/m³]	**Channel [kg/m³]**
Minimum	1012	1000
Maximum	1020	1008

- Wave properties

$$H_s = 2.05\ m \quad T_{m-1.0} = 4.9\ s$$

6 Design input

Loads and laminates

This chapter elaborates on the design input for the next part of the thesis. Actions and load combinations are quantified, partial load and material factors are presented, initial material properties are chosen and resulting properties of the lamina are calculated.

6.1 Actions

Lock gates are subjected to a variety of actions. All actions can be divided into three different categories:

- Permanent actions (G): An action that acts throughout the given reference period with negligible variation in time, e.g. self-weight.
- Variable actions (Q): An action for which the variation in time is not negligible or monotonic, in other words the variation is not always in the same direction, e.g. imposed actions, wind, waves.
- Accidental actions (A): An action which is unlikely to occur during the design working life of the structure, often of short duration but of significant magnitude, e.g. collisions, explosions.

During the design life of the lock gate, a number of operating conditions apply during which the gate is subjected to different actions or load combinations. A distinction between four situations is made (Vrijburcht & Glerum, 2000):

- Gate in closed position
- Gate in opened position
- Gate during opening and closing
- Gate during transport, assembly or repair

For all actions and circumstances, different factors (combination factors ψ, partial safety factors γ) apply.

6.1.1 Self-weight

The self-weight of the gate consists of all permanent elements, structural and non-structural. As a starting point the self-weight is estimated with a simplification of the gate. Self-weight is an important variable in the gates design. On the one hand a low self-weight is preferred, decreasing loads on the operating mechanism, but self-weight is also a critical factor for the stability of the gate.

Commercially available composite materials generally have its weight specified by the manufacturer. In the case that a laminate is designed from scratch, the density of the laminate can be determined with rules of mixtures. The presence of voids is neglected.

$$\rho_c = \rho_f V_f + \rho_m V_m \tag{6.1}$$

where

ρ_c *density of the composite*
$\rho_{f,m}$ *density of the fibre and matrix material, respectively*
$V_{f,m}$ *volume fraction of the fibre and matric material, respectively*

6.1.1.1 Buoyancy

Buoyancy forces oppose the self-weight of the gate, and vice versa. The magnitude of these forces directly depend on the gates design and can be controlled with the use of ballast and buoyancy chambers.

6.1.2 Hydrostatic pressure

A governing variable load in lock gate design is the hydrostatic water pressure, caused by water level differences. A number of operating conditions related to the hydrostatic water pressure are considered; positive head, negative head and opening/closing. The positive and negative head difference conditions both apply when the gate is in closed position.

The hydrostatic pressure at a certain depth along the gate is determined with

$$p = \rho_w \cdot g \cdot h \tag{6.2}$$

6.1.2.1 Extreme levels

Extreme and operating water levels are found in section 5.2.3. Extreme water levels are displayed in Table 11. For the calculation of the hydrostatic pressures, the most unfavourable combination of water densities on the channel and Western Scheldt side are chosen. Respectively 1000 and 1020 kg/m^3 in the case of a positive head and 1008 and 1012 kg/m^3 in the case of a negative head.

Table 11. Extreme water levels

	Western Scheldt side [m]	**Channel side [m]**
Positive head	+5.8	+1.88
Negative head	-3.5	+2.38

Water levels are in reference to NAP.

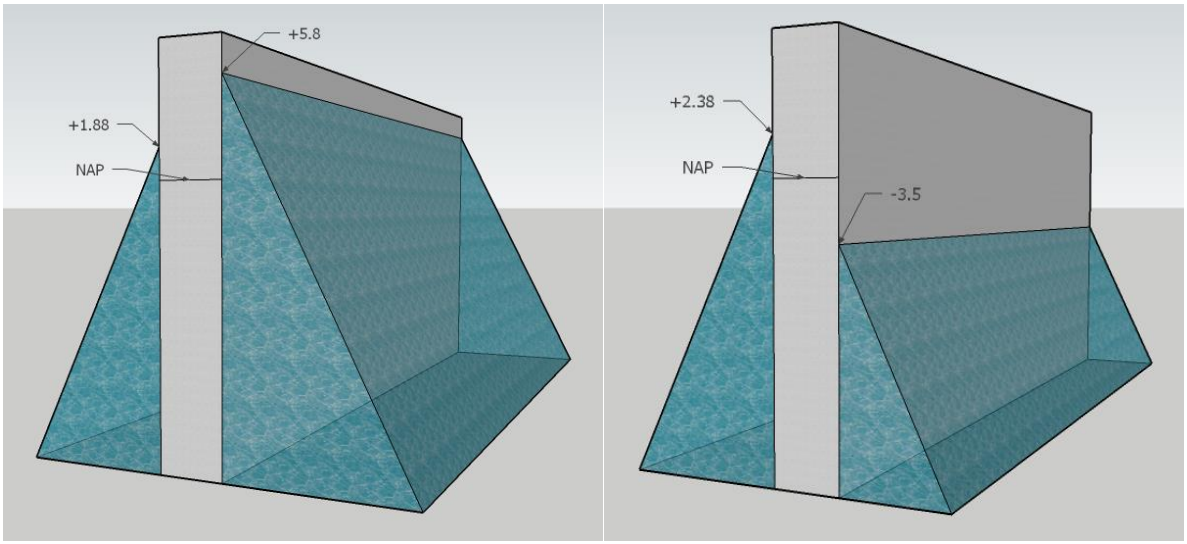

Figure 29. Positive and negative head - Schematization

6.1.2.2 Operating levels

The water levels during which the lock is operational are displayed in Table 12. Average water densities are used for the hydrostatic pressure calculations of the operating water levels. Respectively 1004 kg/m^3 for the channel and 1016 kg/m^3 for the Western Scheldt.

Table 12. Operating water levels

	Western Scheldt side [m]	**Channel side [m]**
Maximum	+4.0	+1.88
Minimum	-3.5	+2.38
Average high	+2.29	+2.13
Average low	-1.89	+2.13

Water levels are in reference to NAP.

6.1.2.3 Calculated pressures

The calculated values for the various water levels are displayed here. The calculations can be found in Appendix B. The first value corresponds with Δh, the values between brackets are the water pressures on the Western Scheldt side and the channel side.

Positive head: $p_{pos} = 42.8\ kN/m^2 \quad (p_{pos;WS} = 222.5;\ p_{pos;Ch} = 179.7)$

Negative head: $p_{neg} = 57.6\ kN/m^2 \quad (p_{neg;WS} = 128.5;\ p_{neg;Ch} = 186.1)$

Maximum: $p_{max} = 23.3\ kN/m^2 \quad (p_{max;WS} = 203.7;\ p_{max;Ch} = 180.4)$

Minimum: $p_{min} = 56.4\ kN/m^2 \quad (p_{min;WS} = 129.0;\ p_{min;Ch} = 185.4)$

Average high: $p_{hi} = 3.78\ kN/m^2 \quad (p_{hi;WS} = 186.7;\ p_{hi;Ch} = 182.9)$

Average low: $p_{lo} = 37.9\ kN/m^2 \quad (p_{lo;WS} = 145.0;\ p_{lo;Ch} = 182.9)$

Operating head: $p_{sta} = 2.71\ kN/m^2 \quad (p_{sta;WS} = 203.7;\ p_{sta;Ch} = 200.9)$

6.1.3 Waves

Wave loads are determined in accordance with the model of Sainflou, see Figure 30. The application of this model is limited to non-breaking waves, which is not a concern. This model is chosen because of its simplicity (Leidraad Kunstwerken, 2003).

The norm frequency wave properties as found in chapter 5 are used, the following is assumed concerning the design wave height

$$H_d = H_s \tag{6.3}$$

The waves are reflected by the gate, resulting in the reflected design wave height

$$H_{d,refl} = (1 + \chi) \cdot H_d \tag{6.4}$$

For a vertical wall, the reflection coefficient $\chi \approx 0.7 - 0.9$ (Leidraad Kunstwerken, 2003), but conservatively a value of 1 (full reflection) can be chosen. For breaking waves the reflection strongly decreases.

The wave length is determined with

$$L = \frac{gT^2}{2\pi}\tanh(kh) \tag{6.5}$$

where

$k = \frac{2\pi}{L}$ *wave number [rad/m]*
T wave period [s]

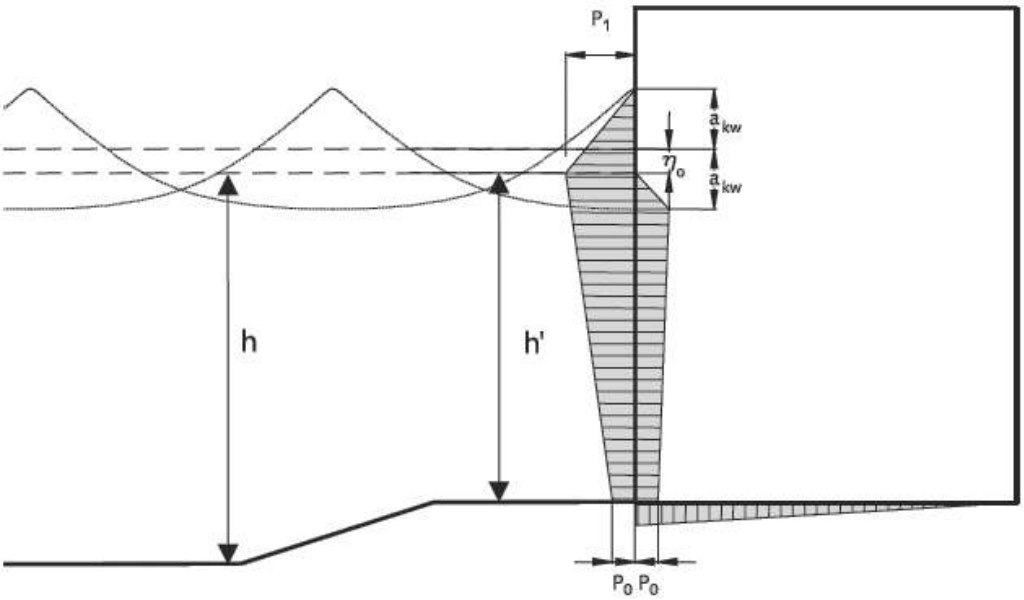

Figure 30. Model of Sainflou

The mean water level increases and is calculated with

$$\eta_0 = \frac{1}{2}ka_{kw}^2\coth(kh) \tag{6.6}$$

where

η_0 *increase of mean water level [m]*
a_{kw} *half of the wave height in front of the structure = $H_{d,refl}$/2 [m]*
h *water depth [m]*

The maximum pressure at the mean water level and the pressure at the bottom near the gate sill are respectively given by

$$p_1 = \rho g(a_{kw} + \eta_0) \tag{6.7}$$

$$p_0 = \frac{\rho g a_{kw}}{\cosh(kh')} \tag{6.8}$$

where

h' *water depth at sill*

The maximum pressure in a wave trough is given by

$$p_3 = \rho g(a_{kw} - \eta_0) \tag{6.9}$$

6.1.3.1 Wave properties

As presented in section 5.2.3.2, the following wave properties apply.

$H_s = 2.05\ m \quad T_{m-1.0} = 4.9\ s$

The calculated values for the wave pressures related to the various water level conditions are presented in Table 13. Detailed calculation can be found in Appendix B.

Table 13. Wave pressures

	p_0 [kN/m²]	p_1 [kN/m²]	p_3 [kN/m²]
Positive head	1.0	24.0	17.0
Negative head	4.4	24.0	16.7
Operating maximum	1.3	24.0	16.9
Operating minimum	4.3	24.1	16.8
Average high	1.7	24.0	16.9
Average low	3.4	24.0	16.8

6.1.4 Currents

Hydraulic structures are subjected to currents, which can be caused in different ways. A current as a result of a head difference under normal daily circumstances of the structure or in the case of failed closure of the gate. These types of currents are important for guard locks or storm surge barriers, but not really a concern in the case of a navigation lock and rolling gates in particular.

Currents can also be vessel induced. The load generated by the vessels propeller is determined with

$$F_s = \rho \cdot \frac{\pi}{4} \cdot D_0^2 \cdot u_0^2 \tag{6.10}$$

where

D_0 *effective propeller diameter*
u_0 *flow speed behind propeller*

6.1.5 Wind

Wind induced loads on the gate are expected to be negligible compared to water pressure and wave loads.

6.1.6 Vessel collision

The collision load depends on the normative vessel. Figure 31 depicts the collision surface according to NEN-EN 1991-1-7 NB.

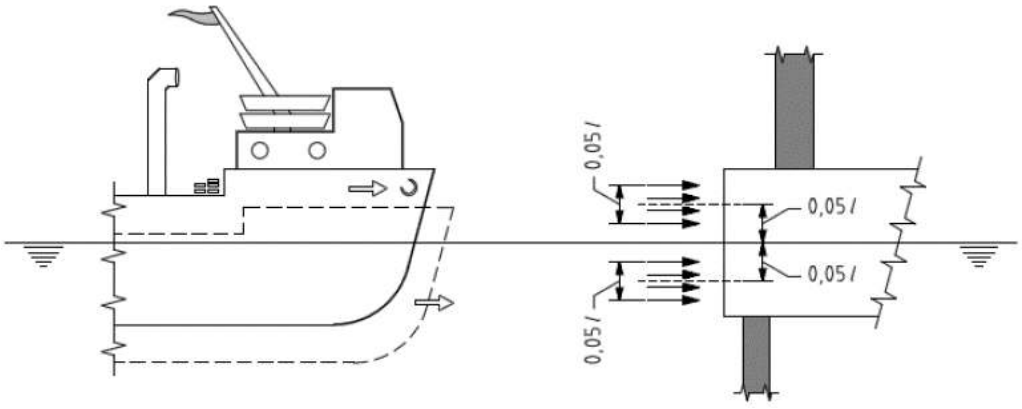

Figure 31. Collision surface

6.1.7 Ice

Ice loads can be determined conform CUR166 and can be applied as a line load at the most unfavourable location. A line load with a magnitude of 250 kN/m, for salt water, or 400 kN/m, for sweet water can be used. Also a local point load of 1.5 MN can be applied at specific structural details when subjected to ice loading. (Leidraad Kunstwerken, 2003)

6.1.8 Design values

The design value F_d of an action F can be expressed in general terms as (NEN-EN 1990)

$$F_d = \gamma_f F_{rep} \tag{6.11}$$

with

$$F_{rep} = \psi F_k \tag{6.12}$$

where

F_k	*characteristic value of the action*
F_{rep}	*relevant representative value of the action*
γ_f	*partial factor for the action taking into account unfavourable deviations from the representative values*
ψ	*1.00 or ψ_0, $\psi_1$or ψ_2*

6.1.8.1 Combination of actions

In order to ensure a certain level of safety and reliability in compliance with the specified consequence class, actions are multiplied with partial factors. Initially the combination factors ψ are set equal to 1.

Ultimate Limit State

Combinations of actions to be considered are expressed according to equations 6.10a and 6.10b of NEN-EN1990.

Equation 6.10a of NEN-EN1990

$$\sum_{j\geq 1} \gamma_{G;j} G_{k,j} + \gamma_P P + \gamma_{Q,1} \psi_{0,1} Q_{k,1} + \sum_{i>1} \gamma_{Q,i} \psi_{0,i} Q_{k,i} \tag{6.13a}$$

Equation 6.10b of NEN-EN1990

$$\sum_{j\geq 1} \xi_j \gamma_{G;j} G_{k,j} + \gamma_P P + \gamma_{Q,1} Q_{k,1} + \sum_{i>1} \gamma_{Q,i} \psi_{0,i} Q_{k,i} \tag{6.13b}$$

where

G, P, Q	*refer to permanent load, pre-stress and variable load, respectively*
γ	*partial factor*
ξ, ψ	*reduction factors*
k	*index referring to a characteristic value*
$+$	*meaning 'combine with', not a mathematical addition*
$\sum$	*meaning 'combined effect of', not a mathematical summation*

Load factors in accordance with NEN-EN1990 and consequence class 3 are used and depicted in Table 14. Load factors for hydraulic loads, i.e. water pressure due to water level differences or waves, are determined in accordance with (Leidraad Kunstwerken, 2003).

Table 14. Load factors

Load case	**Eq. 6.10a**	**Eq. 6.10b (incl. ξ)**
Permanent	1.4/0.9	1.25/0.9
Hydraulic	1.25	1.25
Variable	1.65	1.65
Accidental	1.00	1.00

Serviceability Limit State
For combinations of actions in the SLS, the frequent combination expression 6.15b of NEN-EN1990 is used.

Equation 6.15b of NEN-EN1990

$$\sum_{j\geq 1} G_{k,j} + P + \psi_{1,1} Q_{k,1} + \sum_{i>1} \psi_{0,i} Q_{k,i} \quad (6.14)$$

6.1.8.2 Load combinations
The various actions the gate is subjected to, don´t always apply simultaneously. Different combinations apply under different operational circumstances (open, closed, etc.). A number of load combinations are considered:

- *POS:* The maximum positive head difference that occurs with the norm frequency. The gate is in closed position.
- *NEG:* The maximum negative head difference that occurs with the norm frequency. The gate is in closed position.
- *ICE:* The gate in closed position subjected to an ice, line load. In the open position the gate could be subjected to an ice point load at the end of the gate.
- *COL:* A vessel collision under normal operating conditions.
- *CUR:* Addition of a current load under normal operating conditions.
- *STA:* Stability load combination with the maximum allowed head difference during operation.

Table 15. Load combinations

Load combination	POS	NEG	ICE	COL	CUR	STA
Self-weight	x	x	x	x	x	x
Average operating level			x	x	x	
Max. operating head						x
Extreme positive	x					
Extreme negative		x				
Waves	x	x		x	x	x
Current					x	
Ice			x			
Collision				x		

6.2 Laminate properties
6.2.1 Components
For the preliminary design, the chosen components and corresponding properties are taken from Table 1 and Table 2 from chapter 3.

6.2.1.1 Fibres
The most economical choice in civil engineering structures is to use a glass fibre. The initial fibre choice is E-glass with the following properties:

$$E_f = 72\ GPa \quad G_f = 30\ GPa \quad v_f = 0.22 \qquad \rho_f = 2450\ kg/m^3$$

6.2.1.2 Matrix
The initial matrix material choice is epoxy. It's not necessarily the most economical choice, but offers excellent resistance to environmental effects. The following properties are used:

$$E_m = 4.2\ GPa \quad G_m = 1.57 GPa \quad v_m = 0.34 \qquad \rho_m = 1260\ kg/m^3$$

6.2.1.3 Manufacturing method

Vacuum-assisted resin injection is chosen as the manufacturing method, because of the relatively low equipment costs, moderate production costs, good size range and achievable fibre volume. The chosen manufacturing method affects the final material properties. This influence is expressed in the partial material factor, see section 6.2.3.1.

6.2.1.4 Core

Foam is chosen as the core material, because it is relatively cheap and easy to process. A foam core is compatible with the chosen manufacturing method. There are many foams available, each with different properties, and a selection can be made to best suit the requirements for the structure or structural element. Table 16 displays the properties of three PVC foam core materials with respectively a low-, medium- and high-density. Initially the medium density foam will be used.

Table 16. Properties of foam cores (Moen, 2014)

Core	***Density [kg/m³]***	σ_t ***[MPa]***	σ_c ***[MPa]***	τ ***[MPa]***	E_c ***[GPa]***	G ***[GPa]***
LD Foam	40	0.7	0.45	0.45	0.037	0.013
MD Foam	100	2.7	2.0	1.7	0.115	0.04
HD Foam	250	7.5	6.6	4.7	0.282	0.095

6.2.2 Laminate

6.2.2.1 Lamella properties

The lamella properties are determined with rules of mixtures and the Halpin-Tsai model as discussed in chapter 3. The moduli must be multiplied with a reduction factor for uni-directional lamina, $\phi_{UD} = 0.97$ as prescribed by CUR96.

The full calculation can be found in Appendix B. The following results are obtained:

$$E_1 = 43.53\ GPa \qquad E_2 = 16.59\ GPa \qquad G_{12} = 5.10\ GPa \qquad v_{12} = 0.268 \tag{6.15}$$

The density of the lamella is determined with

$$\rho_{lam} = \rho_f \cdot V_f + \rho_m \cdot V_m = 1974\ kg/m^3 \tag{6.16}$$

6.2.2.2 Stacking sequence

Laminate stacking sequences must fulfil the requirements described in CUR96. Following these requirements allows for the application of one nominal strain limit in all directions. (CUR-96, 2003)

- Laminates must contain a minimum fibre volume of 20%.
- In every orientation (0° , +45° , 90°, -45°), a minimum of 15% of the total fibre content must be present.
- As a result, a maximum fibre volume of 40% is possible in the preferred orientation.

6.2.2.3 Laminate properties

The properties of the laminate are determined with classical laminate theory as discussed in chapter 3. To perform the calculations, software can be used, e.g. Kolibri.

6.2.3 Design values

Design value X_d of material or product property

$$X_d = \frac{X_k}{\gamma_m \cdot \gamma_c} \tag{6.17}$$

where

X_d *characteristic value of the material or product property*
γ_c *mean value of the conversion factor taking into account :*
· volume and scale effects
· effects of moisture and temperature
· any other relevant parameters
γ_m *partial factor for the material or product property taking into account:*
· possibility of unfavourable deviation from the characteristic value
· random part of the conversion factor η

6.2.3.1 Material factor

The partial material factor is determined with

$$\gamma_m = \gamma_{m,1} \cdot \gamma_{m,2} \tag{6.18}$$

where

$\gamma_{m,1}$ *equal to 1.35; partial material factor to account for uncertainties in obtaining the desired material properties*
$\gamma_{m,2}$ *partial factor to account for uncertainties related to the manufacturing method, values are in accordance with Table 17*

Table 17. Partial material factors $\gamma_{m,2}$ for different manufacturing methods (CUR-96, 2003)

Manufacturing method	**Partial material factor $\gamma_{m,2}$**	
	Postcured laminate	**Non-postcured laminate**
Spray-up	1.6	1.9
Hand lay-up	1.4	1.7
Vacuum- or pressure injection	1.2	1.4
Filament winding	1.1	1.3
Prepregging	1.1	1.3
Pultrusion	1.1	1.3

In the ultimate limit state $\gamma_m > 1.5$

With the chosen manufacturing method of vacuum-assisted resin injection and assuming a postcured laminate, the total material factor is equal to

$$\gamma_m = 1.35 \cdot 1.2 = 1.62 \tag{6.19}$$

6.2.3.2 Conversion factor

Conversion factors are applied to account for anticipated effects on the material properties related to temperature, time, environmental influences, load duration and cyclic loading. The total combined conversion factor can be determined with

$$\gamma_c = \gamma_{ct} \cdot \gamma_{cv} \cdot \gamma_{ck} \cdot \gamma_{cf} \tag{6.20}$$

where

γ_c *total combined conversion factor*
γ_{ct} *partial conversion factor accounting for temperature effects*
γ_{cv} *partial conversion factor accounting for moisture effects*
γ_{ck} *partial conversion factor accounting for creep effects*
γ_{cf} *partial conversion factor accounting for fatigue effects*

Table 18. Application of conversion factors (CUR-96, 2003)

Conversion factor	Ultimate Limit State			Serviceability Limit State		
	Strength	**Stability**	**Fatigue**	**Deflection**	**Vibration**	**Cracking**
Temperature	x	x	x	x	x	x
Moisture	x	x	x	x	x	x
Creep	x	x	-	x	-	x
Fatigue	-	x	-	x	x	x
Combined	1.43	1.57	1.43	1.57	1.57	1.57
Including creep	1.64	1.80	-	1.80	-	1.80

In accordance with (CUR-96, 2003) the separate conversion factors are determined as follows.

The partial conversion factor for temperature effects has a value of $\gamma_{ct} = 1.1$

The partial conversion factor for moisture effects equals:
- Structures permanently in dry conditions, $\gamma_{cv} = 1.0$
- Structures subject to variable conditions, alternating dry and wet periods, , $\gamma_{cv} = 1.1$
- Structures permanently in wet conditions, , $\gamma_{cv} = 1.3$

The partial conversion factor for fatigue effects has a value of $\gamma_{cf} = 1.1$. This factors only applies for stiffness related limit states.

The partial conversion factor for creep effects is determined with the following equation. This factor only applies for long-term actions.

$$\gamma_{ck} = t^n \tag{6.21}$$

where

t *load duration in hours*

n *exponent related to the fibre orientation*

- $n = 0.01$ *UD-lamina with long-term action in fibre direction*
- $n = 0.04$ *weave lamina*
- $n = 0.1$ *mat lamina*

6.2.4 Fracture criterion

As described in CUR96 the strain limits for a uni-directional lamina have been determined as follows (CUR-Aanbeveling 96 - Achtergrondrapport, 2003):

$$\varepsilon_{1tR} = 2.4\,;\ \varepsilon_{1cR} = 1.6\,;\ \varepsilon_{2tR} = 0.34\,;\ \varepsilon_{2cR} = 1.1\,;\ \varepsilon_{12R} = 0.58$$

ε_{1tR} *tension strain limit in the first principal direction*
ε_{1cR} *compression strain limit in the first principal direction*
ε_{2tR} *tension strain limit in the second principal direction*
ε_{2cR} *compression strain limit in the second principal direction*
ε_{12R} *shear strain limit in the first and second principal direction*

Provided that the requirements described in 6.2.2.2 are met, a nominal strain limit can be applied in the ultimate limit state for all direction; tension, compression and shear. This nominal strain limit is equal to 1.2%.

In the serviceability limit state, the strain limit may not exceed 0.27%, because the structure operates in wet conditions.

Limit stresses are calculated with Hooke's law:

$$\sigma = E \cdot \varepsilon \tag{6.22}$$

6.2.5 Initial laminate build up

Laminate build up and properties

Table 19. Initial laminate stacking distribution

Angle	Quasi-isotropic	One main fibre direction	Two main fibre directions
0	25%	55%	35%
+45	25%	15%	15%
90	25%	15%	35%
-45	25%	15%	15%

With Kolibri, based on classical laminate theory, the following properties are calculated for various laminate types.

Quasi-Isotropic

$$E_x = 24.12\ GPa \qquad E_y = 24.12\ GPa \qquad G_{xy} = 9.13\ GPa \qquad v_{xy} = 0.320 \qquad v_{yx} = 0.320 \tag{6.23}$$

One main fibre direction

$$E_x = 31.90\ GPa \qquad E_y = 21.51\ GPa \qquad G_{xy} = 7.52\ GPa \qquad v_{xy} = 0.305 \qquad v_{yx} = 0.205 \tag{6.24}$$

Two main fibre directions

$$E_x = 26.77\ GPa \qquad E_y = 26.77\ GPa \qquad G_{xy} = 7.52\ GPa \qquad v_{xy} = 0.245 \qquad v_{yx} = 0.245 \tag{6.25}$$

6.3 Key points – chapter 6

- Hydrostatic pressures are summarized in section 6.1.2.3.
- Wave pressures are presented in Table 13.
- Load factors are presented in Table 14.
- Material choices
  Fibre: E-glass ; Matrix: epoxy ; Manufacturing method: vacuum-assisted resin injection
  Core: medium foam core
- Material factor is found to be $\gamma_m = 1.62$ and values for the conversion factors are presented in Table 18.
- As a starting point, the properties for the one main fibre direction laminate are applied.
- A nominal strain limit of 1.2% is used.

Practical Part II

Execution

- Global dimensions: Box gate
- 3D model: Box gate
- 3D Stability Problem
- Potential Improvements

7 Global dimensions: Box gate

Strength, deflection and stability

In this chapter the first steps in the gates design are taken. Boundary conditions found in chapter 5 and 6 are summarised. Deflection and strength checks are performed on the gate in closed position. The extreme positive and negative load combinations apply here. The stability of the gate during movement is checked with the stability load combination.

The first variant to be determined is a sandwich gate, essentially a gate consisting only of two outer FRP skin plates and a (very) thick foam core. This design is mainly performed to check the calculation and to gain some insight in the magnitude of forces.

The most important section of this chapter is the determination of the global dimensions of the box shaped gate in both steel and FRP. Finally, some preliminary conclusions are drawn concerning the stability of the box gate and a comparison of steel and FRP is made.

7.1 Boundary conditions

7.1.1 Initial laminate properties

For all the laminates in the preliminary design a one main fibre direction stacking sequence is applied, see section 6.2.5.

$$E_x = 31.90\ GPa \qquad E_y = 21.51\ GPa \qquad G_{xy} = 7.52\ GPa \qquad v_{xy} = 0.305 \qquad v_{yx} = 0.205 \tag{7.1}$$

For the cores of sandwich elements a medium density foam is applied, see section 6.2.1.4.

$$E_c = 0.115\ GPa \qquad G_c = 0.04\ GPa \qquad \rho_c = 100\ kg/m^3$$

$$\sigma_t = 2.7\ MPa \qquad \sigma_c = 6.6\ MPa \qquad \tau = 4.7\ MPa \tag{7.2}$$

7.1.2 Global dimensions

The global dimensions of the gate resulting from the case study:

The span or length of the gate corresponds to the width of the lock.

$$L = 55\ m \tag{7.3}$$

The height of the gate results from the sill depth (-16.44 m NAP) and the flood defence requirement (+9.5 m NAP). The height is rounded up to 26 m to simplify further calculations and dimensioning of the gate.

$$H = 16.44 + 9.5 = 25.94\ m \approx 26\ m \tag{7.4}$$

The thickness or width, W, of the gate is determined iteratively from the design checks in the following sections.

7.1.3 Design criterion

7.1.3.1 Strength criterion

As stated in chapter 6, limit stresses are calculated with Hooke's law.

$$E_{x;d} = \frac{E_x}{\gamma_m \cdot \gamma_c} = 13770\ MPa \tag{7.5}$$

With the nominal strain limit of 1.2%, the maximum allowed stress is

$$\sigma_{max} = E_{x;d} \cdot \varepsilon = 165\ N/mm^2 \tag{7.6}$$

7.1.3.2 Deflection criterion

For the deflection, the following criterion must be met,

$$w_{max} = L/200 = 55000/200 = 275\ mm \tag{7.7}$$

7.1.3.3 Stability criterion

For this simplified stability calculation, the support reaction from the carriage has to provide a resisting moment to the moment caused by the combined horizontal loads. In order for the gate to remain stable during movement, the distance between the rotation point and the point of action of the resultant of the support reactions must meet the following requirement:

$$x \leq \frac{1}{6}W \tag{7.8}$$

7.1.4 Load combinations

For the preliminary design, the extreme positive head (POS) and extreme negative head load combination (NEG) is used for the strength and deflection checks. For the stability check the stability load combination (STA) is used. See section 6.1.2.3 for hydrostatic pressures and section 6.1.3.1 for the wave pressures.

7.1.4.1 Load combination: POS and NEG

Hydrostatic pressure + wave crest corresponding to the extreme positive head water conditions.

$$q_{POS} = 42.8 + 24.0 = 66.8\ kN/m^2 \tag{7.9}$$

Hydrostatic water pressure + wave through corresponding to the negative head water conditions.

$$q_{NEG} = 57.6 + 16.7 = 74.3\ kN/m^2 \tag{7.10}$$

7.1.4.2 Load combination: STA

The assumption is made that the self-weight is evenly distributed over the support carriages, i.e. half the weight to each carriage on either end of the gate, see Figure 32. The self-weight depends on the final dimensions of all the structural elements and is determined iteratively.

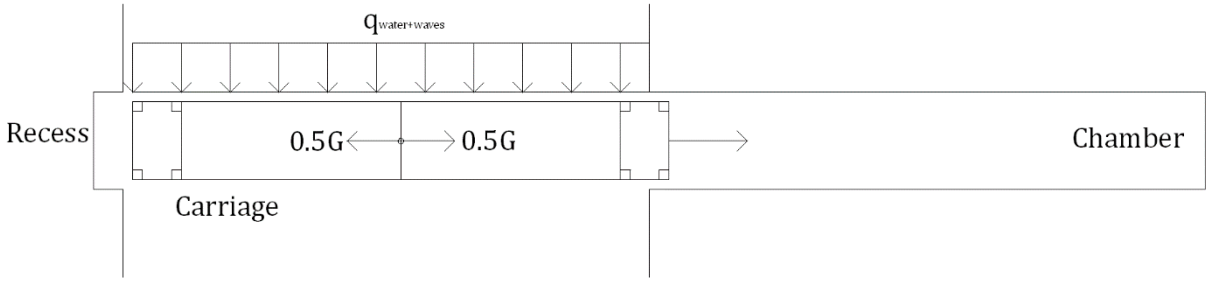

Figure 32. Gate during movement - top view

This load combination consists of the maximum allowed head difference during operation ($\Delta h = 0.28\ m$) plus the wave pressures corresponding to the maximum water level during operation. It is assumed that both wave troughs and crests are present along the span of the gate.

$$p_{STA} = 2.71\ kN/m^2 \quad p_1 = 24.0\ kN/m^2 \quad p_0 = 1.3\ kN/m^2 \quad p_3 = 16.9\ kN/m^2 \tag{7.11}$$

The loads are broken down into point loads, each working at a different distance from the point of rotation. Similarly to the self-weight, it is assumed that half of the loads need to be supported by each carriage.

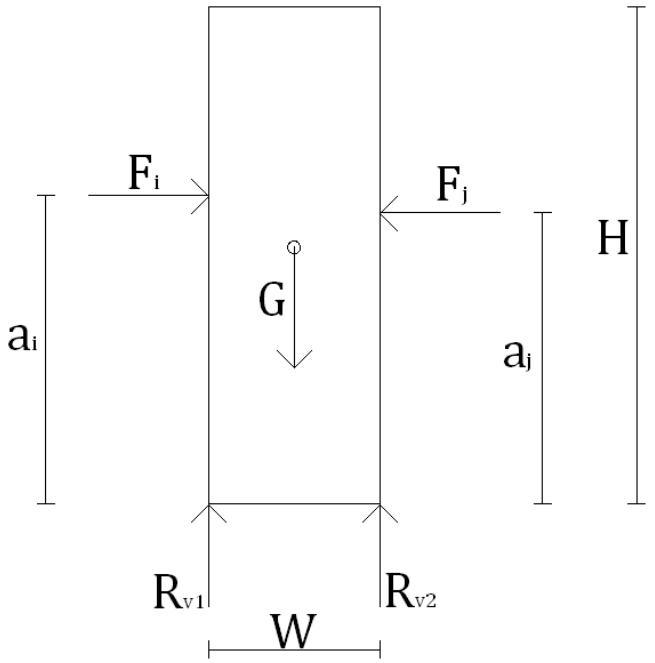

Figure 33. Stability calculation

$$F_1 = \frac{1}{2}L \cdot \left(p_{STA} \cdot (h_{NAP} + h_{ch})\right) \qquad F_2 = \frac{1}{2}L \cdot \left(\frac{1}{2}p_{STA} \cdot \Delta h\right)$$
$$F_3 = \frac{1}{4}L \cdot \left(p_0 \cdot (h_{NAP} + h_{WS})\right) \qquad F_4 = \frac{1}{4}L \cdot \left(\frac{1}{2}(p_1 - p_0) \cdot (h_{NAP} + h_{WS})\right)$$
$$F_5 = \frac{1}{4}L \cdot \left(\frac{1}{2}p_1 \cdot (a_{kw} + \eta_0)\right) \qquad F_6 = \frac{1}{4}L \cdot \left(p_0\big((h_{NAP} + h_{WS}) - (a_{kw} - \eta_0)\big)\right)$$
$$F_7 = \frac{1}{4}L \cdot \left((p_3 - p_0) \cdot \big((h_{NAP} + h_{WS}) - (a_{kw} - \eta_0)\big)\right) \qquad F_8 = \frac{1}{4}L \cdot \left(p_3 \cdot (a_{kw} - \eta_0)\right)$$

$$a_1 = \frac{1}{2}(h_{NAP} + h_{ch}) \quad a_2 = \frac{1}{3}\Delta h + (h_{NAP} + h_{ch}) \quad a_3 = \frac{1}{2}(h_{NAP} + h_{WS})$$
$$a_4 = \frac{2}{3}(h_{NAP} + h_{WS}) \quad a_5 = (h_{NAP} + h_{WS}) + \frac{1}{3}(a_{kw} + \eta_0)$$
$$a_6 = \frac{1}{2}\big((h_{NAP} + h_{WS}) - (a_{kw} - \eta_0)\big) \qquad a_7 = \frac{2}{3}\big((h_{NAP} + h_{WS}) - (a_{kw} - \eta_0)\big)$$
$$a_8 = \big((h_{NAP} + h_{WS}) - (a_{kw} - \eta_0)\big) + \frac{1}{3}(a_{kw} - \eta_0) \tag{7.12}$$

where

$F_{i;j}$	*Point load corresponding to part i of water or wave pressures (i=1..5 ; j=6..8)*
$a_{i;j}$	*Distance from point load i to the point of rotation (i=1..5 ; j=6..8)*
h_{NAP}	*16.44 m ; water depth*
h_{ch}	*+3.72 m ; water level on the channel side*
h_{WS}	*+4 m ; water level Western Scheldt side*
Δh	*0.28 m ; maximum head difference during movement*

The calculation can be found in Appendix C. The calculated values are displayed below and in Table 20.

$$a_1 = 10.08\ m \qquad a_2 = 20.33\ m \qquad a_3 = 10.22\ m \qquad a_4 = 13.63\ m$$
$$a_5 = 21.24\ m \qquad a_6 = 9.37\ m \qquad a_7 = 12.49\ m \qquad a_8 = 19.31\ m \tag{7.13}$$

7.1.4.3 Limit states

ULS: hydraulic loads, 1.25

Table 20. Limit state load combinations

Limit state	POS [kN/m²]	NEG [kN/m²]	STA [kN]							
			F_1	F_2	F_3	F_4	F_5	F_6	F_7	F_8
SLS	66.8	74.3	1502	18.63	365.4	3190	396.0	335.0	4020	395.0
ULS	83.5	92.9	1878	23.29	456.7	3987	495.0	418.7	5025	493.8

7.2 Sandwich variant

To gain some perspective about the dimensions, required laminate properties and magnitude of stresses and deflection the gate is initially designed as a large sandwich plate. In practice lock gates have been applied as a sandwich structure, but for relatively small mitre gates. The expectation is that in practice, on the scale of the New Lock a simple sandwich structure is not a realistic design.

The laminate skin and core thickness are determined iteratively. The stability check is governing and the final skin and core thicknesses are relatively thick,

$$t_s = 2 \times 300\ mm \qquad t_c = 8500\ mm \tag{7.14}$$

These values are used in the following checks. The full calculation can be found in Appendix C.

7.2.1 Strength check

The sandwich gate is simplified to a simply supported beam with a height of h=1 m. The NEG load combination is governing, so the distributed load becomes

$$q_d = q_{NEG;ULS} = 92.9\ kN/m \tag{7.15}$$

The design moment

$$M_d = \frac{1}{8} \cdot q_d \cdot L^2 = 35128\ kNm \tag{7.16}$$

The combined flexural rigidity of the sandwich profile is found with

$$EI_{tot} = \left(\frac{2E_s t_s^3}{12} + \frac{E_s t_s (t_s + t_c)^2}{2} + \frac{E_c t_c^3}{12}\right) \cdot h = 1.62 \cdot 10^8\ kNm^2 \tag{7.17}$$

To determine the stresses in the skin and the core, section moduli are calculated with

$$W_{s,c} = \frac{EI_{tot}}{h_{s,c} \cdot E_{s,c}} \tag{7.18}$$

where

z *reference to skin (s) or core (c)*

With the section moduli known, the design stresses can be determined.

$$\sigma_d = \frac{M_d}{W_{s,c}} \qquad \sigma_{d;s} = 72.6\ N/mm^2 \qquad \sigma_{d;c} = 0.245\ N/mm^2 \tag{7.19}$$

The strength criteria is easily met. This is because the skin and core thickness are very large as a result of the stability check elaborated in section 7.2.3.

$$skin: \frac{\sigma_{max;s}}{\sigma_{d;s}} = 0.44 \leq 1$$

$$core: \frac{\sigma_{max;c}}{\sigma_{d;c}} = 0.28 \leq 1 \tag{7.20}$$

7.2.2 Deflection check

The governing design load for this calculation is the negative head in the SLS limit state.

$$q_d = q_{NEG;SLS} = 74.3\ kN/m \tag{7.21}$$

The total deflection is the combined deflection due to bending and shear. The flexural rigidity is calculated with (7.17). The shear rigidity follows from,

$$\sum GA = G_s \cdot A_s + G_c \cdot A_c \tag{7.22}$$

where

$\sum GA$	*Combined shear rigidity*
G_s	*Shear stiffness of the skin (laminate)*
A_s	*Area of the skin*
G_c	*Shear stiffness of the core*
A_c	*Area of core*

The design deflection is calculated with the following expression and must meet the maximum deflection criterion. Similar to the strength check, the deflection criterion is easily met due to large skin and core thickness.

$$w_d = \frac{5}{384} \cdot \frac{qL^4}{EI} + \frac{qL^2}{8GA} \leq w_{max} \tag{7.23}$$

$$59.8 \leq 275\ mm$$

7.2.3 Stability check

For a sandwich gate, the total thickness, or width, of the gate is calculated with

$$W = 2 \cdot t_s + t_c$$

The dead weight is a result of the self-weight of the gate minus buoyancy. Densities of the skin, core and water are required. The average water density of the Western Scheldt is applied.

$$\rho_s = 1974\ kg/m^3 \qquad \rho_c = 100\ kg/m^3 \qquad \rho_w = 1016\ kg/m^3$$

Self-weight, buoyancy and dead weight are calculated as follows

$$G_{SW} = \rho_s \cdot g \cdot (2 \cdot t_s \cdot L \cdot H) + \rho_c \cdot g \cdot (2 \cdot t_c \cdot L \cdot H) = 28539\ kN$$

$$Buoyancy.ratio = \frac{G_{buoyancy}}{G_{SW}} = 0.35 \qquad G_{buoyancy} = 9942\ kN$$

$$G_{tot} = G_{SW} - G_{buoyancy} = 18598\ kN \tag{7.24}$$

With the loads found in section 7.1.4.3 the stability calculation can be performed. G_{tot} is divided by 2 and multiplied by 0.9, due to the assumption that half of the weight goes to each carriage and the load factor that applies to permanent loads, see Table 14. Solving the expressions for the vertical and moment equilibriums gives the vertical support reactions.

$$\sum V = 0 \qquad V = \frac{G_{tot} \cdot 0.9}{2} - R_{V1} - R_{V2} = 0$$

$$\sum M = 0 \qquad M = F_1 \cdot a_1 + F_2 \cdot a_2 + F_3 \cdot a_3 + F_4 \cdot a_4 + F_5 \cdot a_5 - F_6 \cdot a_6 - F_7 \cdot a_7 - F_8 \cdot a_8 + R_{V1} \cdot \frac{W}{2} - R_{V2} \cdot \frac{W}{2} \tag{7.25}$$

With the support reactions known, the distance x between the rotation point (middle of the gate) and the point of action of the resultant of the support reactions can be determined.

$$(x = 1.52) \leq \left(\frac{W}{6} = 1.52\ m\right) \tag{7.26}$$

The stability criteria is met.

7.2.4 Sandwich conclusion

From all checks performed, the stability is governing for the dimensions of the skin and core thickness. The strength and deflection criteria are easily met with these dimensions. Besides the considerable core thickness, a sandwich design is not very practical, because there is no space for ballast and buoyancy tanks.

7.2.5 Laminate properties

Applying a laminate with the majority of fibres in the main loading direction.

Table 21. Laminate stacking sequence

Angle [°]	Fibre content	Thickness [mm]
0	55	165
45	15	45
-45	15	45
90	15	45
0	Foam core	8500
90	15	45
-45	15	45
45	15	45
0	55	165
		9100

With Kolibri, the laminate properties and ABD-matrix is found and used as input for the Scia model.

$$E_x = 2.2126\ GPa \qquad E_y = 1.5324\ GPa \qquad G_{xy} = 0.5332\ GPa$$
$$v_{xy} = 0.315 \qquad v_{yx} = 0.218 \qquad \rho_{com} = 223.56\ kg/m^3 \tag{7.27}$$

$$[ABD] = \begin{bmatrix} 2.1624 \cdot 10^{10} & 4.7238 \cdot 10^{9} & 0 & 0 & 0 & 0 \\ 4.7238 \cdot 10^{9} & 1.4977 \cdot 10^{9} & 0 & 0 & 0 & 0 \\ 0 & 0 & 4.8521 \cdot 10^{9} & 0 & 0 & 0 \\ 0 & 0 & 0 & 4.0754 \cdot 10^{11} & 8.3657 \cdot 10^{10} & 2.4343 \cdot 10^{8} \\ 0 & 0 & 0 & 8.3657 \cdot 10^{10} & 2.7060 \cdot 10^{11} & 2.4343 \cdot 10^{8} \\ 0 & 0 & 0 & 2.4343 \cdot 10^{8} & 2.4343 \cdot 10^{8} & 8.8664 \cdot 10^{10} \end{bmatrix}$$

7.2.6 Scia model 1

The sandwich gate is modelled in Scia Engineer (Model 1). The gate is represented by a wall element with properties of the foam core and FRP skins combined. Downside is that the foam and FRP skins cannot be investigated separately. The supports are modelled as line supports, as opposed to nodal supports. This is done to prevent extreme peak stresses to occur near the supports.

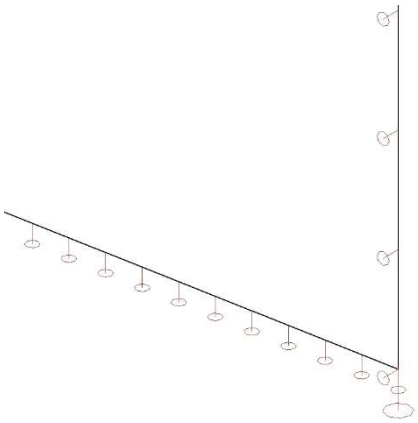

Figure 34. Line supports

The loads are modelled on the gate as surface loads corresponding to the loads determined in chapter 6. Figure 35 shows how the wave pressures are modelled on the gate. Some details and results of model 1 are presented in this section.

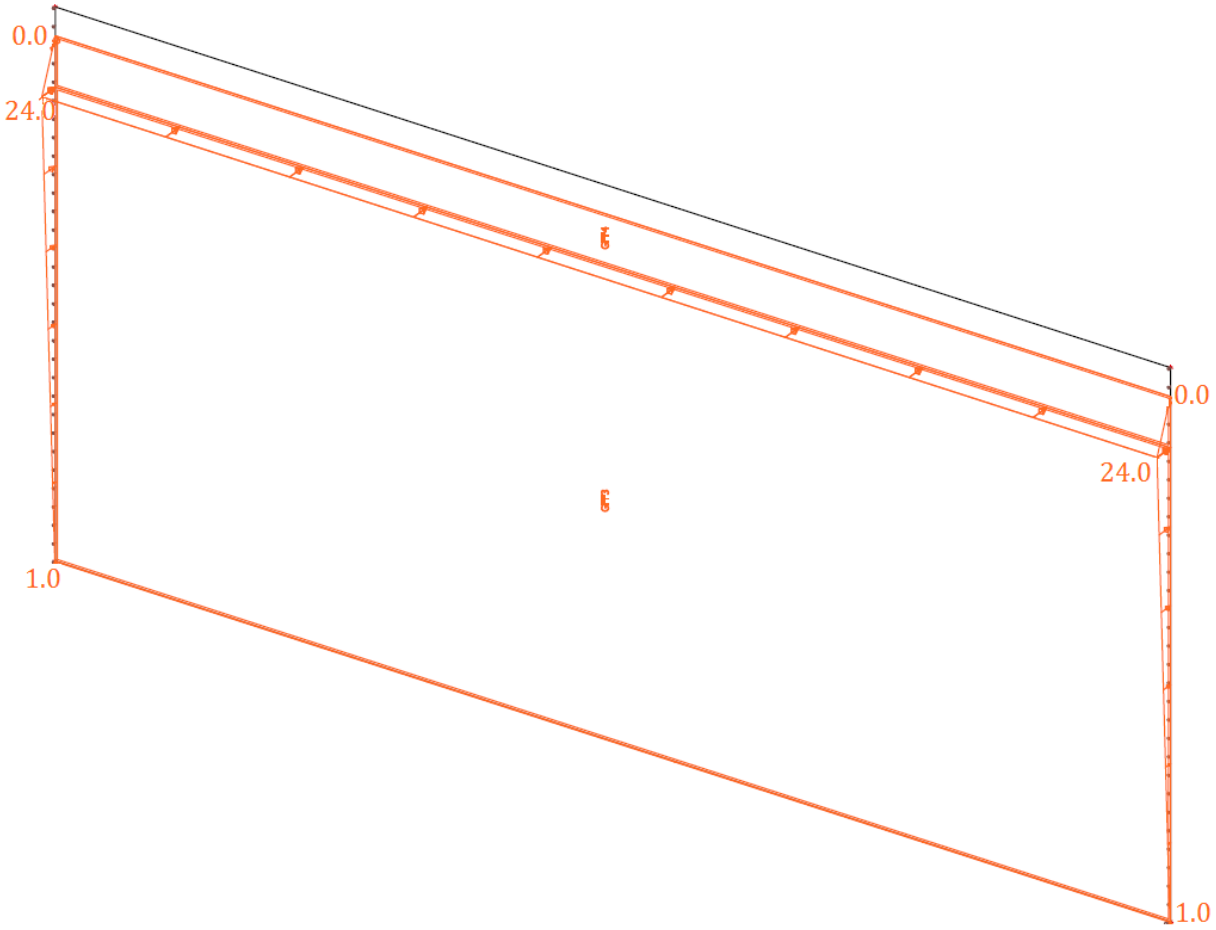

Figure 35. Model 1- Wave pressures

The largest stress found with the model is 3.7 N/mm^2. The location of this stress is mid span at a height of approximately 5 m. In the hand calculation, the stresses were calculated separately for the FRP skin and the foam core, so the model result cannot be compared to those values. If however a hand calculation is performed with the combined properties of the FRP skins and foam, a stress of 4.53 N/mm^2 is found.

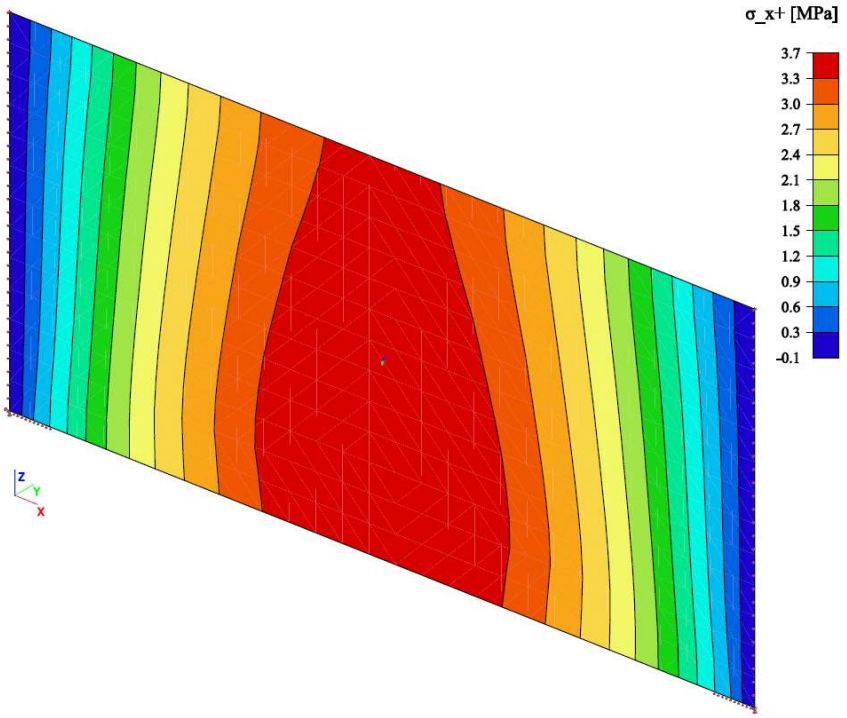

Figure 36. Model 1 – Stress

The deflection found with the model is 51.9 mm. Compared to 59.8 mm with the hand calculation. The differences between the hand calculation and the model are a result of the simplification of the gate as a simply supported beam with a height of 1 m.

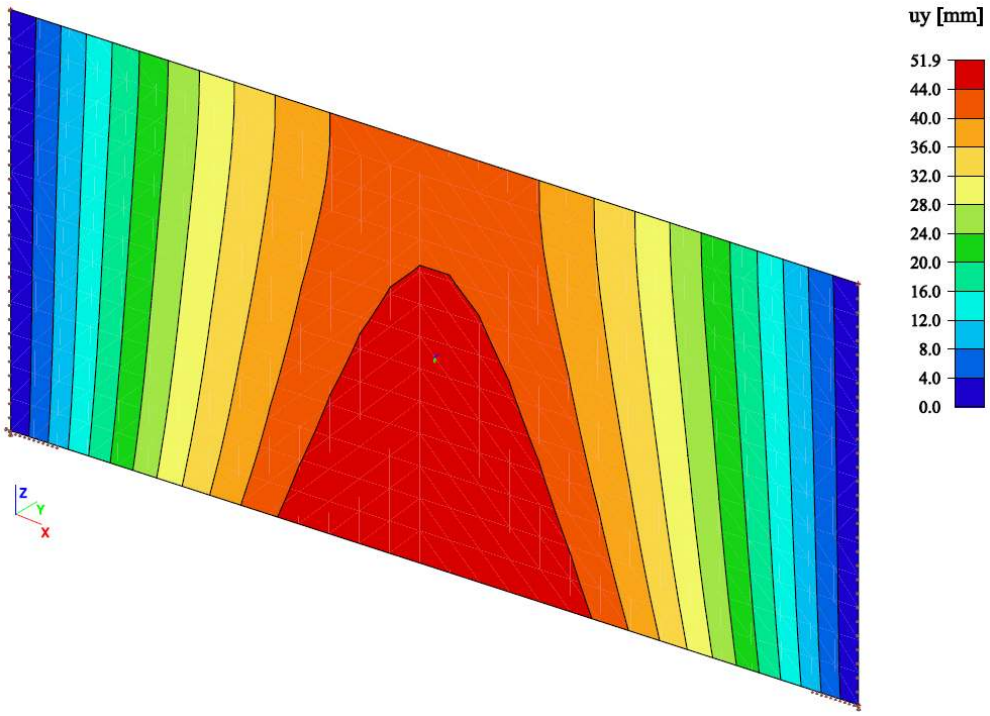

Figure 37. Model 1 - Deflection

7.3 Box variant

A box variant is chosen for the final gates design, a commonly used design for rolling gates. Both a steel and a FRP variant will be evaluated. Global and local checks as well as a stability check are performed to determine the required dimension of the various structural elements.

A cross-section of the box gate is presented in Figure 38.

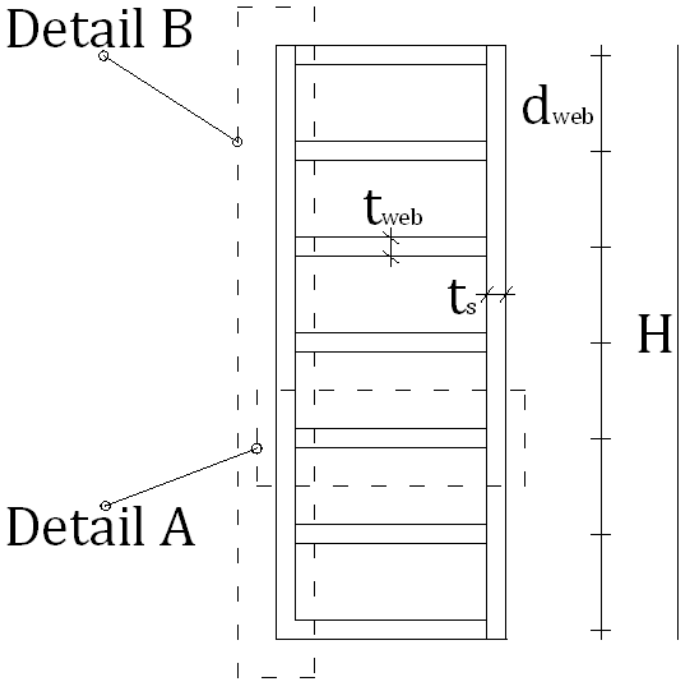

Figure 38. Box gate cross-section

where

t_s	thickness of the retaining plates
t_{web}	thickness of the webs
d_{web}	distance between webs (=4.33 m)

7.3.1 Global check

To simplify the calculation of the global checks, the specific profiles of the plates and webs are not taken into account. The objective with this calculation is to the determine the amount of material required for the structural elements.

The gate is simplified to a simply supported beam with detail A as its cross-section. Figure 39 and Figure 40 display the cross-sections of respectively the steel and FRP box gates. The height of the beam is equal to the distance between the webs, $d_{web} = 4.33\ m$. The load is also multiplied by this height to determine a uniformly distributed load over the length of the beam, $L = 55\ m$.

$$q_{d;ULS} = q_{NEG;ULS} \cdot d_{web} = 402.3\ kN/m$$

$$q_{d;SLS} = q_{NEG;SLS} \cdot d_{web} = 317.8\ kN/m \quad (7.28)$$

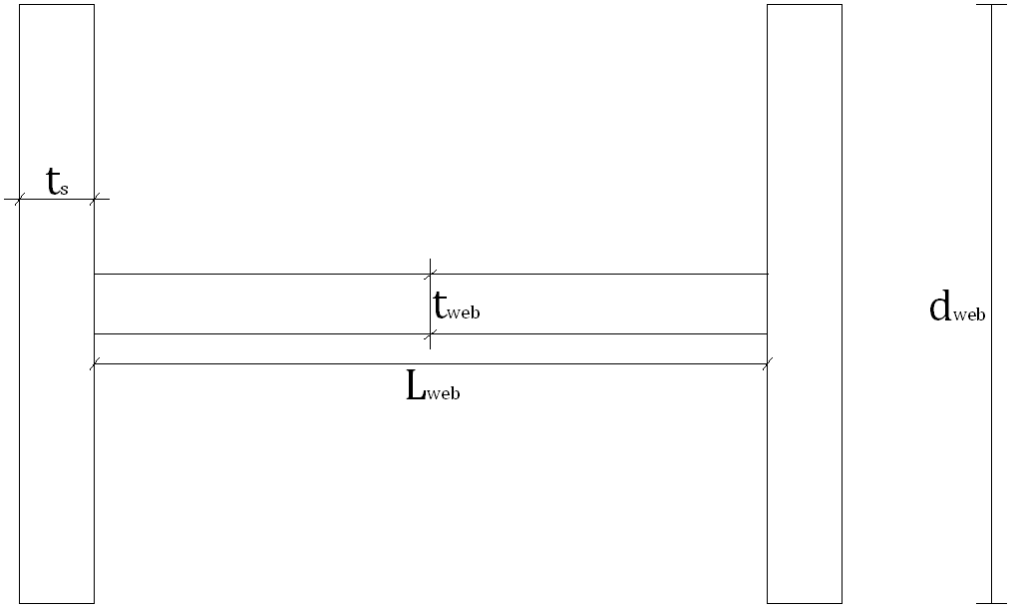

Figure 39. Detail A - Global steel cross-section

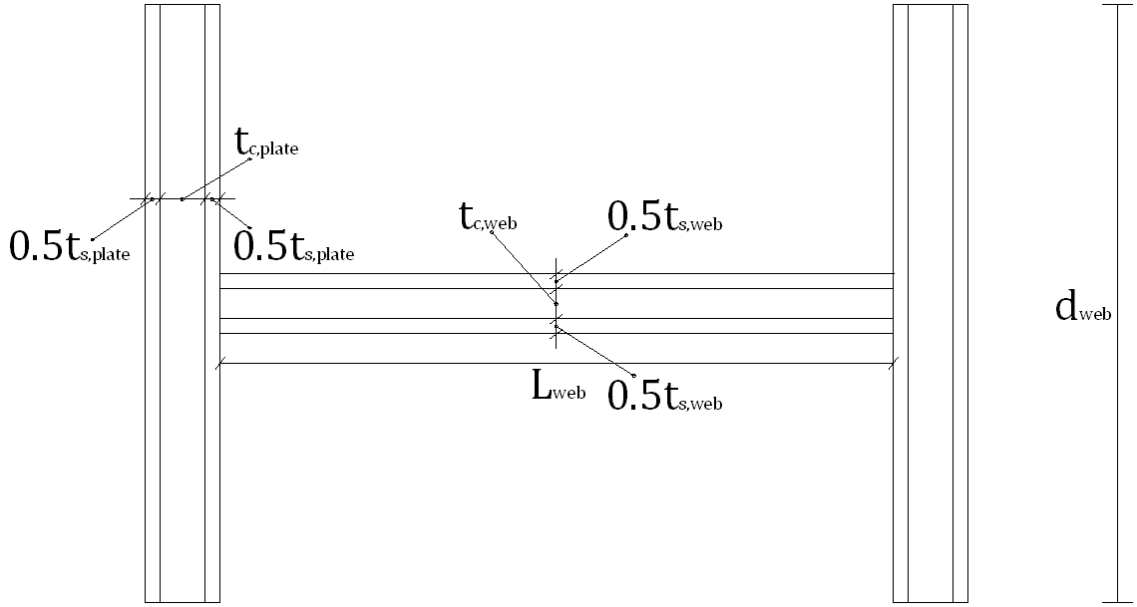

Figure 40. Detail A - Global FRP cross-section

7.3.2 Local check

For the local check, detail B from Figure 38 is simplified to a continuous multi-span beam with a length equal to the height of the gate. Consisting of 7 supports and 6 spans, the beam is loaded by a uniformly distributed load. The load is placed over the entire length of beam which is a conservative representation of the actual hydrostatic pressure and wave loading. The maximum moment can be determined and is used to check the stress in the retaining plate. The largest support reaction is used as a buckling load on the web. The web is simplified as a column.

Full calculation can be found in Appendix C.

7.3.2.1 Local maximum moment

Moments at supports

$$M_B = M_F = 165.6\ kNm \qquad M_C = M_E = 120.4\ kNm \qquad M_D = 135.5\ kNm \qquad (7.29)$$

The maximum span moment is found at a distance $x = 1.71\ m$ in the first span.

$$M_{span} = 121.7\ kNm$$

Support reactions

$$R_A = R_G = 142.5\ kN \quad R_B = R_F = 410.2\ kN \quad R_C = R_E = 347.6\ kN \quad R_D = 368.5kN \tag{7.30}$$

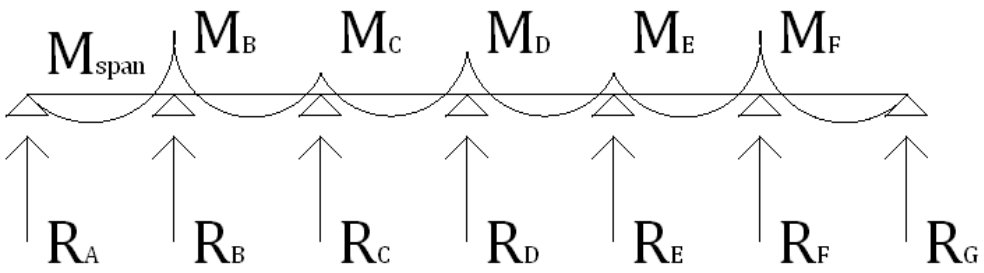

Figure 41. Local moment and support reactions

7.3.3 Steel design

The final dimensions found are as follows

$$t_s = 70\ mm \qquad t_{web} = 60\ mm \qquad L_{web} = 8000\ mm \tag{7.31}$$

7.3.3.1 Steel properties

For the steel gate design S235 is applied with the following material properties.

$$E = 210000\ MPa \qquad G = 80769\ MPa \qquad v_{xy} = 0.3$$

$$\rho_{s235} = 7850\ kg/m^3 \qquad \sigma_y = 235\ N/mm^2 \qquad \sigma_u = 360\ N/mm^2 \tag{7.32}$$

7.3.3.2 Global – Strength

The design bending moment is equal to

$$M_d = \frac{1}{8} \cdot q_{d;ULS} \cdot L^2 = 152000\ kNm \tag{7.33}$$

To calculate the stress in the retaining plates, first the moment of inertia must be determine. The assumption is made that the retaining plates are the main contribution so the influence of the webs is not taken into account.

$$I_{plate} = \left(\frac{2t_s^3}{12} + \frac{t_s(t_s+t_c)^2}{2}\right) \cdot d_{web} = 9.87 \cdot 10^{12}\ mm^4 \tag{7.34}$$

The section modulus is calculated with

$$W_s = \frac{I_{plate}}{z_s} = \frac{I_{plate}}{1/2(2t_s+L_{web})} = 2.43 \cdot 10^9\ mm^3 \tag{7.35}$$

where

z_s *distance to the outer fibre of the plate*

With the section modulus known, the design stress can be determined.

$$\sigma_d = \frac{M_d}{W_s} = 62.7\ N/mm^2$$

$$plate: \frac{\sigma_{max;s}}{\sigma_d} = \frac{235}{62.7} = 0.27 \leq 1 \tag{7.36}$$

7.3.3.3 Global – Deflection

The elastic modulus, shear modulus and the moment of inertia are known. Only the cross-sectional area must be determined.

$$A_{tot} = 2t_s \cdot d_{web} + t_{web} \cdot L_{web} = 1086200\ mm^2 \tag{7.37}$$

Substituting the values into the deflection equation gives

$$w_d = \frac{5}{384} \cdot \frac{q_{d;SLS} L^4}{EI_{plate}} + \frac{q_{d;SLS} L^2}{8GA_{tot}} \leq w_{max} \tag{7.38}$$

$$19.6 \leq 275\ mm$$

7.3.3.4 Stability check

The total thickness, or width, of the gate is calculated with

$$W = 2 \cdot t_s + web \tag{7.39}$$

Self-weight, buoyancy and dead weight are calculated as follows

$$G_{SW} = \rho_{s235} \cdot g \cdot (2 \cdot t_s \cdot L \cdot H + 7 \cdot t_{web} \cdot L \cdot L_{web}) = 29648\ kN$$

$$Buoyancy.ratio = \frac{G_{buoyancy}}{G_{SW}} = 0.30 \qquad G_{buoyancy} = 8874kN$$

$$G_{tot} = G_{SW} - G_{buoyancy} = 20774\ kN \tag{7.40}$$

Solving the expressions, see (7.25), for the vertical and moment equilibria gives the vertical support reactions.

$$R_{V1} = 3113\ kN \qquad R_{V2} = 6235\ kN \tag{7.41}$$

With the support reactions known, the distance x between the rotation point (middle of the gate) and the point of action of the resultant of the support reactions can be determined.

$$(x = 1.36\ m) \leq \left(\frac{W}{6} = 1.36\ m\right) \tag{7.42}$$

The stability criteria are met.

7.3.3.5 Local - Retaining plate

The maximum local moment was determined as

$$M_{max} = M_B = 165.6\ kNm \tag{7.43}$$

The required section modulus can be calculated with

$$W_{req} = \frac{M_{max}}{\sigma_{max}} = \frac{165.6 \cdot 10^6}{235} = 7.05 \cdot 10^5\ mm^3 \tag{7.44}$$

From the stability calculation in section 7.3.3.4 a required cross-sectional area of the retaining plate can be found.

$$A_{req} = t_s \cdot L = 70 \cdot 55000 = 3.85 \cdot 10^6\ mm^2 \tag{7.45}$$

Fulfilling both these requirements a steel profile can be chosen. The profiles are placed side to side over the span of the retaining plate. The combined cross-sectional area of the profiles A_{com}, must be equal or greater than A_{req}. The section modulus of the profile must be equal or greater than W_{req}. Figure 42 displays how the steel profiles form the retaining plate. This calculation is done to get an idea of the final steel plate, since it is not just a thick slab of steel.

A HEA550 profile is chosen, the following properties apply.

$$W_{HEA550} = 4.146 \cdot 10^6\ mm^3 \geq W_{req}$$

$$A_{com} = 3.88 \cdot 10^6\ mm^2 \geq A_{req} \tag{7.46}$$

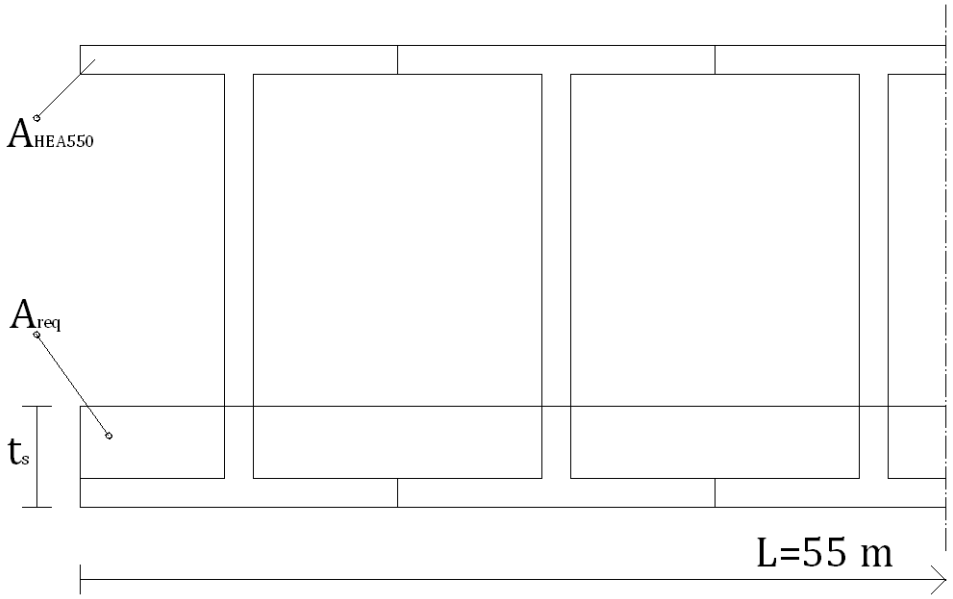

Figure 42. Steel profile retaining plate – top view

7.3.3.6 Local – Webs

The local normal force in the web was determined as

$$N_{cr} = R_B = 410.2\ kN \tag{7.47}$$

Simplifying the web as a column, the required moment of inertia can be determined with the expression for buckling.

$$N_{cr} = \frac{\pi^2 EI}{(KL)^2} = \frac{\pi^2 EI_{req}}{(KL_{web})^2} \tag{7.48}$$

where

N_{cr}	*Critical buckling load (column)*
E	*Modulus of elasticity*
I	*Moment of inertia of column cross-section*
L	*Length of the column*
K	*Effective length factor (= 1.0)*

Following the same method as the local retaining plate calculation, with the required moment of inertia and a material volume requirement from the stability calculation a profile can be chosen for the web.

A HEA500 profile is chosen, the following properties apply.

$$(I_{HEA500} = 8.697 \cdot 10^8\ mm^4) \geq (I_{req} = 1.27 \cdot 10^7\ mm^4)$$

$$(V_{com} = 202.7\ m^3) \geq (V_{req} = 184.8\ m^3) \tag{7.49}$$

7.3.4 FRP design

The final values have been determined iteratively with the checks in the following sections. The full calculation can be found in Appendix C.

$$t_{s;plate} = 280\ mm \qquad t_{c;plate} = 200\ mm \tag{7.50}$$

$$t_{s;web} = 200\ mm \qquad t_{c;web} = 200\ mm \qquad L_{web} = 8000\ mm$$

For the FRP box, two end plates are added to the design. A shear calculation is performed to determine the dimensions of this structural element.

$$t_{s;end} = 80\ mm \qquad t_{c;end} = 80\ mm \tag{7.51}$$

7.3.4.1 Global - Strength

The design bending moment is equal to

$$M_d = \frac{1}{8} \cdot q_{d;ULS} \cdot L^2 = 152000\ kNm \tag{7.52}$$

For the moment of inertia, only the laminate skins are taken into account. The contribution of the foam cores is neglected.

$$I_{skin} = \left(\frac{2t_{s;plate}^3}{12} + \frac{t_{s;plate}(t_{s;plate}+L_{web})^2}{2}\right) \cdot d_{web} = 4.16 \cdot 10^{13}\ mm^4 \tag{7.53}$$

The section modulus is calculated with

$$W_s = \frac{I_{skin}}{z_s} = \frac{I_{plate}}{1/2\left(2t_{s;plate}+L_{web}\right)} = 9.71 \cdot 10^9\ mm^3 \tag{7.54}$$

where

z_s *distance to the outer fibre of the retaining plate*

With the section modulus known, the design stress can be determined.

$$\sigma_d = \frac{M_d}{W_s} = 15.7\ N/mm^2$$

$$plate\text{:}\ \frac{\sigma_{max;s}}{\sigma_d} = \frac{165}{15.7} = 0.09 \leq 1 \tag{7.55}$$

7.3.4.2 Global – Deflection

The cross-sectional area must be determined. Again, the contribution of the foam cores is not taken into account.

$$A_{tot} = 2t_{s;plate} \cdot d_{web} + t_{s;web} \cdot L_{web} = 1086200\ mm^2 \tag{7.56}$$

Substituting the values into the deflection equation gives

$$w_d = \frac{5}{384} \cdot \frac{q_{d;SLS}L^4}{EI_{skin}} + \frac{q_{d;SLS}L^2}{8GA_{tot}} \leq w_{max} \tag{7.57}$$

$$82.7\ mm \leq 275\ mm$$

7.3.4.3 Shear check – End plate

The combined shear modulus of the end plate is calculated with

$$G_{end} = \left(\frac{G_{xy}}{\gamma_m \cdot \gamma_c} \cdot t_{s;end} \cdot d_{web} + \frac{G_c}{\gamma_m \cdot \gamma_c} \cdot t_{c;end} \cdot d_{web}\right) / A_{end} \tag{7.58}$$

The design shear force is determined as follows

$$V_d = \frac{1}{2} q_{d;ULS} L = 11062\ kN \tag{7.59}$$

The shear stress check can be performed

$$\left(\tau_d = \frac{V_d}{A_{end}} = 16.0\ N/mm^2\right) \leq (\tau_{max} = \varepsilon_{ULS} \cdot G_{end} = 19.6\ N/mm^2) \tag{7.60}$$

7.3.4.4 Stability check

The total thickness, or width, of the gate is calculated with

$$W = 2 \cdot t_{s;plate} + 2 \cdot t_{c;plate} + L_{web} = 8960\ mm \tag{7.61}$$

Self-weight, buoyancy and dead weight are calculated as follows

$$G_{SW} = \rho_s \cdot g \cdot \left(2 \cdot t_{s;plate} \cdot L \cdot H + 7 \cdot t_{s;web} \cdot L_{web} \cdot L\right) + \rho_c \cdot g \cdot \left(2 \cdot t_{c;plate} \cdot L \cdot H + 7 \cdot t_{c;web} \cdot L_{web} \cdot L\right) + \rho_s \cdot g \cdot \left(t_{s;end} \cdot W \cdot H\right) + \rho_c \cdot g \cdot \left(t_{c;end} \cdot W \cdot H\right) = 28981\ kN$$

$$Buoyancy.ratio = \frac{G_{buoyancy}}{G_{SW}} = 0.35 \qquad G_{buoyancy} = 10140 kN$$

$$G_{tot} = G_{SW} - G_{buoyancy} = 18841\ kN \tag{7.62}$$

Solving the expressions, see (7.25), for the vertical and moment equilibriums gives the vertical support reactions.

$$R_{V1} = 2821\ kN \qquad R_{V2} = 5657\ kN \tag{7.63}$$

With the support reactions known, the distance x between the rotation point (middle of the gate) and the point of action of the resultant of the support reactions can be determined.

$$(x = 1.49\ m) \leq \left(\frac{W}{6} = 1.49\ m\right) \tag{7.64}$$

The stability criteria is met.

7.3.4.5 Local - Retaining plate

The maximum local moment and the required section modulus are determined as

$$M_{max} = M_B = 165.6\ kNm \qquad W_{req} = \frac{M_{max}}{\sigma_{s;max}} = 1.00 \cdot 10^6\ mm^3 \tag{7.65}$$

To calculate the section modulus of the retaining plate, the combined flexural rigidity and the total thickness of the retaining plate must be determined.

$$EI_{plate} = E_{s;d} \cdot d_{web} \left(t_{s;plate} \left(\frac{\left(t_{s;plate} + t_{c;plate}\right)}{2} \right)^2 + \frac{2}{12} \frac{{t_{s;plate}}^3}{2} \right) + \frac{1}{12} E_{c;d} \cdot d_{web} \cdot {t_{c;plate}}^3$$

$$t_{tot;plate} = t_{s;plate} + t_{c;plate} = 480\ mm \tag{7.66}$$

With these values known the section modulus can be found.

$$W_s = \frac{EI_{plate}}{\left(\frac{t_{tot}}{2}\right) \cdot E_{s;d}} = 2.99 \cdot 10^8\ mm^3 > W_{req} \tag{7.67}$$

7.3.4.6 Local – Webs

Substituting all known values in the buckling expression gives the required flexural rigidity of the web.

$$N_{cr} = \frac{\pi^2 EI}{(KL)^2} = \frac{\pi^2 EI_{req}}{(KL_{web})^2} \qquad EI_{req} = \frac{N_{cr} \cdot {L_{web}}^2}{\pi^2} \tag{7.68}$$

$$EI_{tot;web} = E_{s;d} \cdot w_{column} \left(t_{s;web} \left(\frac{t_{s;web} + t_{c;web}}{2} \right)^2 + \frac{2}{12} {\frac{t_{s;web}}{2}}^3 \right) + E_{c;d} \cdot \frac{1}{12} w_{column} \cdot {t_{c;web}}^3$$

where

w_{column} *is an assumed width of the simplified column*

Due to relatively large dimensions of the web laminate, the required flexural rigidity is easily met.

$$EI_{tot;web} > EI_{req} \tag{7.69}$$

7.3.5 Box gate preliminary conclusion

For all designs, the stability calculation was found to be governing. In other words, a minimum self-weight was required and not necessarily the lightest gate design could be achieved. As a result, the self-weight of each gate is very similar. However, the amount of material that is necessary to attain the self-weight required for stability is very different. The table below presents the volume of steel and the volume of FRP and core material that was used in both box gate designs. It can be seen that the volume of materials in the FRP gate is considerably larger.

The masses are calculated with the following values:

$$\rho_{s235} = 7850 \ {}^{kg}/_{m^3} \ ; \ \rho_{lam} = 1974 \ {}^{kg}/_{m^3} \ ; \ \rho_{core} = 100 \ {}^{kg}/_{m^3} \tag{7.70}$$

To estimate the costs of the materials the following values were used (Moen, 2014),

$$P_{s235} = 1.5 \ {}^{€}/_{kg} \ ; \ P_{lam} = 4 \ {}^{€}/_{kg} \ ; \ P_{core} = 1 \ {}^{€}/_{kg} \tag{7.71}$$

Table 22. Volume of material applied - steel vs. FRP

	V_Retaining [m³]	V_Web [m³]	V_End [m³]	V_Total [m³]	Mass [kg]	Cost [€]
Steel box						
Steel	200	185	*	385	3.022.250	4.533.375
* End plates were not dimensions in this calculation						
FRP box						
FRP	801	616	19	1435	2.832.690	11.330.760
Foam	572	616	19	1206	120.600	120.600

In the case that the other checks (strength and deflection) are assumed to be governing over the performed stability check. The required dimensions of the gates are very different. The results are presented in Table 23. Each column gives the dimensions required and self-weight of the gate in the case that respectively strength, deflection or stability are assumed governing.

Table 23. Dimensions for varying governing checks

	Strength	**Deflection**	**Stability**
Sandwich			
t_s [mm]	100	225	300
t_c [mm]	2100	4550	8500
SW $[kN]$	8484	18844	28539
Steel box			
t_s [mm]	60	50	70
t_{web} [mm]	40	40	60
L_{web} [mm]	2500	2450	8000
SW $[kN]$	16179	13918	29648
FRP box			
$t_{s;plate}$ [mm]	100	200	280
$t_{c;plate}$ [mm]	100	100	200
$t_{s;web}$ [mm]	100	100	200
$t_{c;web}$ [mm]	100	100	200
L_{web} [mm]	2100	5000	8000
SW $[kN]$	7464	15274	28981

What can be seen in the table is that the dimensions of all structural elements can be significantly reduced when stability isn't the governing criteria. The dimensions of the webs of the FRP box gate can be reduced to 50% of the dimensions required when stability is governing. When comparing the steel and FRP box it's interesting to see that for steel, the required dimensions are very similar when either strength or deflection is assumed governing. This is not the case for the FRP box gate. Strength criteria allows for smaller dimensions in comparison to the deflection criteria. Choosing a laminate with a higher stiffness could reduce this difference.

7.4 Key points – chapter 7

- The stability criteria are found to be governing, resulting in very conservative design from a strength or deflection perspective.
- The FRP box gate has dimensions of 55 m x 26 m x 8.96 m (LxHxW).
- The dimensions of the retaining plates: skin:280 mm, core: 200 mm.
  The dimensions of the webs: skin: 200 mm, core: 200 mm.
- Considerably more material is required when comparing the FRP to the steel box gate. The same can be said for the material costs. A rough estimate gives €11.5 and €4.5 million for the FRP and steel gate respectively.
- Purely looking at strength and deflection a gate in steel is more effective. Required dimensions for either criteria give similar results. For the FRP gate, the deflection criteria requires much larger dimensions than strength criteria. A stiffer laminate could reduce this difference.

– THIS PAGE IS INTENTIONALLY LEFT BLANK –

8 3D model: Box gate

Scia Engineer - FEA

In this chapter the FRP box gate dimensioned in the previous chapter is investigated with a 3D model, referred to as model 2. Model 2 represents the FRP box gate in closed position. The gate is modelled in Scia Engineer and with the model, deflections and stresses of the various structural elements can be checked with finite element analysis. In addition a fatigue check due to a stress range caused by the locking cycle and a creep calculation of the webs due to permanent ballast are performed. All the results are presented here.

8.1 Model 2: FRP Box Gate - closed position

8.1.1 Laminate properties

With the dimensions found in the preliminary design, stacking sequences are chosen for each structural element. For each element the laminate properties and ABD-matrix are determined with Kolibri and the values found are used as input for the box gate Scia model, Model 2. The determination of the laminate properties with Kolibri can be found in Appendix D.

8.1.1.1 Retaining plates

The dimensions of the retaining plates can be found in expression (7.50).

$t_{s;plate} = 280\ (2 \times 140)\ mm \qquad t_{c;plate} = 200\ mm$

Applying a laminate with the majority of fibres in the main loading direction, results in a laminate with the stacking sequence presented in Table 24.

Table 24. Laminate stacking sequence – Retaining plates

Angle [°]	Fibre content [%]	Thickness [mm]
0	55	77
45	15	21
-45	15	21
90	15	21
0	Foam core	200
90	15	21
-45	15	21
45	15	21
0	55	77
		480

The following laminate properties are found with Kolibri.

$$E_x = 18.654\ GPa \qquad E_y = 12.598\ GPa \qquad G_{xy} = 4.4035\ GPa$$
$$v_{xy} = 0.305 \qquad v_{yx} = 0.206 \qquad \rho_{com} = 1193.2\ kg/m^3 \tag{8.1}$$

Analysis of the laminate in Kolibri gives the ABD-matrix. These values are required in the model to describe the orthogonality of the plate.

$$[ABD] = \begin{bmatrix} 9.5556 \cdot 10^9 & 1.9701 \cdot 10^9 & 0 & 0 & 0 & 0 \\ 1.9701 \cdot 10^9 & 6.4534 \cdot 10^9 & 0 & 0 & 0 & 0 \\ 0 & 0 & 2.1137 \cdot 10^9 & 0 & 0 & 0 \\ 0 & 0 & 0 & 3.3108 \cdot 10^8 & 5.2887 \cdot 10^7 & 1.7345 \cdot 10^6 \\ 0 & 0 & 0 & 5.2887 \cdot 10^7 & 1.7003 \cdot 10^8 & 1.7345 \cdot 10^6 \\ 0 & 0 & 0 & 1.7345 \cdot 10^6 & 1.7345 \cdot 10^6 & 5.7392 \cdot 10^7 \end{bmatrix} N, m$$

With the laminate properties and the ABD-matrix known, the retaining plates can be modelled in Scia, see Figure 43.

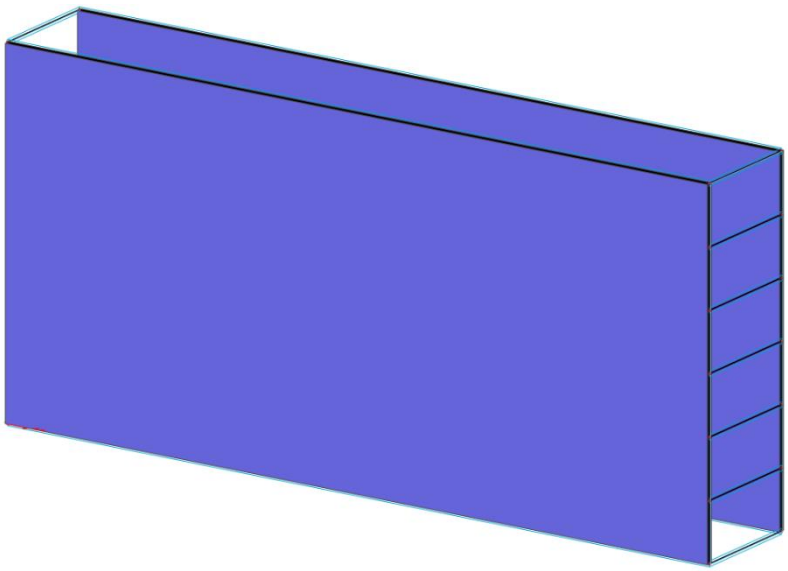

Figure 43. Model 2 - Retaining plates

8.1.1.2 Webs

The dimensions of the webs can be found in expression (7.50).

$t_{s;web} = 200\ (2 \times 100)\ mm$ $\qquad$ $t_{c;web} = 200\ mm$

Applying a laminate with the quasi-isotropic stacking sequence the following laminate is found.

Table 25. Laminate stacking sequence - Webs

Angle [°]	Fibre content [%]	Thickness [mm]
0	25	25
45	25	25
-45	25	25
90	25	25
0	Foam core	200
90	25	25
-45	25	25
45	25	25
0	25	22
		400

The following laminate properties are found with Kolibri.

$E_x = 12.117\ GPa$ $\qquad$ $E_y = 12.117\ GPa$ $\qquad$ $G_{xy} = 4.5868\ GPa$

$v_{xy} = 0.321$ $\qquad$ $v_{yx} = 0.321$ $\qquad$ $\rho_{com} = 1037\ kg/m^3$

(8.2)

Analysis of the laminate in Kolibri gives the ABD-matrix.

$$[ABD] = \begin{bmatrix} 5.4029 \cdot 10^9 & 1.7334 \cdot 10^9 & 0 & 0 & 0 & 0 \\ 1.7334 \cdot 10^9 & 5.4029 \cdot 10^9 & 0 & 0 & 0 & 0 \\ 0 & 0 & 1.8347 \cdot 10^9 & 0 & 0 & 0 \\ 0 & 0 & 0 & 1.4158 \cdot 10^8 & 3.9694 \cdot 10^7 & 2.5967 \cdot 10^6 \\ 0 & 0 & 0 & 3.9694 \cdot 10^7 & 1.1042 \cdot 10^8 & 2.5967 \cdot 10^6 \\ 0 & 0 & 0 & 2.5967 \cdot 10^6 & 2.5967 \cdot 10^6 & 4.2146 \cdot 10^7 \end{bmatrix} N, m$$

With the laminate properties and the ABD-matrix known, the webs can be modelled in Scia, see Figure 44.

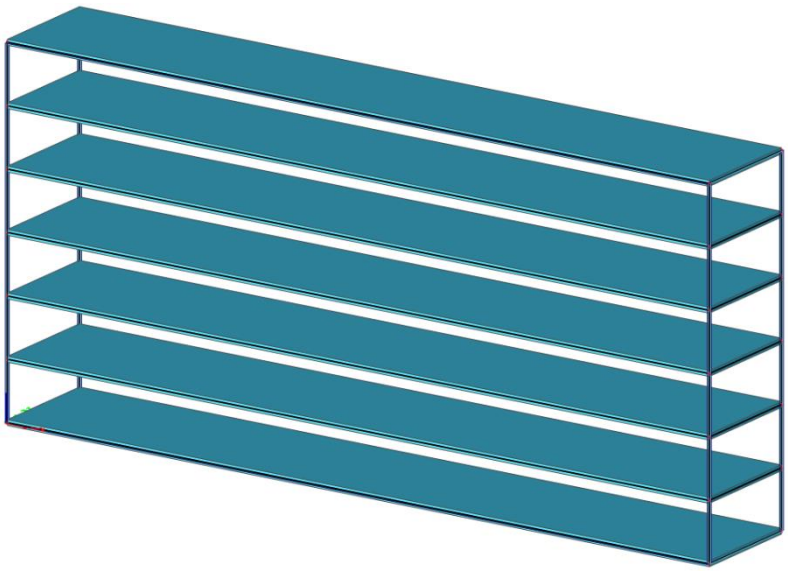

Figure 44. Model 2 - Webs

8.1.1.3 End plates

The dimensions of the end plates can be found in expression (7.51).

$t_{s;end} = 80\ (2 \times 40)\ mm$ $t_{c;end} = 80\ mm$

Applying a laminate with a stacking sequence with the majority of fibre in two main directions gives the laminate build up presented in Table 26 for the end plates.

Table 26. Laminate stacking sequence – End plates

Angle [°]	Fibre content [%]	Thickness [mm]
0	15	6
45	35	14
-45	35	14
90	15	6
0	Foam core	80
90	15	6
-45	35	14
45	35	14
0	15	6
		160

The following laminate properties are found with Kolibri.

$E_x = 10.620\ GPa$ $E_y = 10.620\ GPa$ $G_{xy} = 5.3936\ GPa$

$v_{xy} = 0.405$ $v_{yx} = 0.405$ $\rho_{com} = 1037\ kg/m^3$

(8.3)

Analysis of the laminate in Kolibri gives the ABD-matrix.

$$[ABD] = \begin{bmatrix} 2.0321 \cdot 10^9 & 8.2245 \cdot 10^8 & 0 & 0 & 0 & 0 \\ 8.2245 \cdot 10^8 & 2.0321 \cdot 10^9 & 0 & 0 & 0 & 0 \\ 0 & 0 & 8.6297 \cdot 10^8 & 0 & 0 & 0 \\ 0 & 0 & 0 & 8.2588 \cdot 10^6 & 3.0238 \cdot 10^6 & 3.2573 \cdot 10^5 \\ 0 & 0 & 0 & 3.0238 \cdot 10^6 & 6.9027 \cdot 10^6 & 3.2573 \cdot 10^5 \\ 0 & 0 & 0 & 3.2573 \cdot 10^5 & 3.2573 \cdot 10^5 & 3.1808 \cdot 10^6 \end{bmatrix} N.m$$

With the laminate properties and the ABD-matrix known, the end plates can be modelled in Scia, see Figure 45.

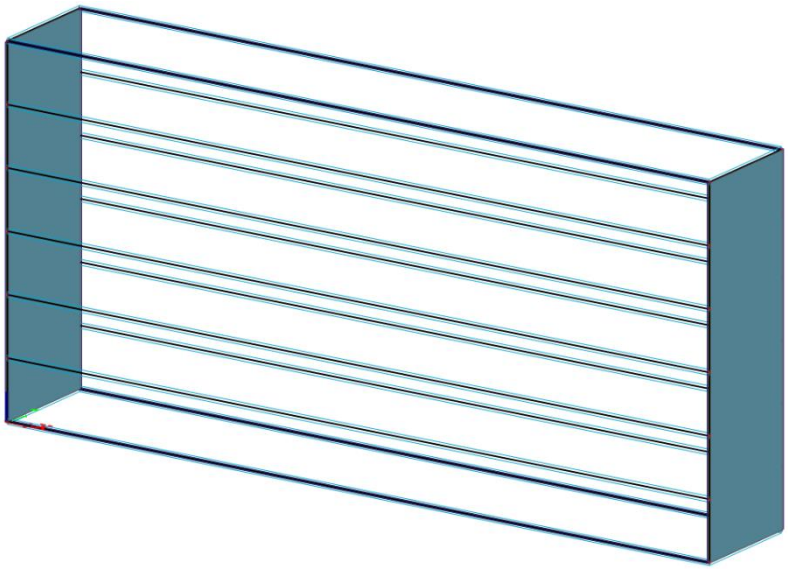

Figure 45. Model 2 - End plates

Combining all structural elements gives the complete modelled structure. An overview is presented in Figure 46.

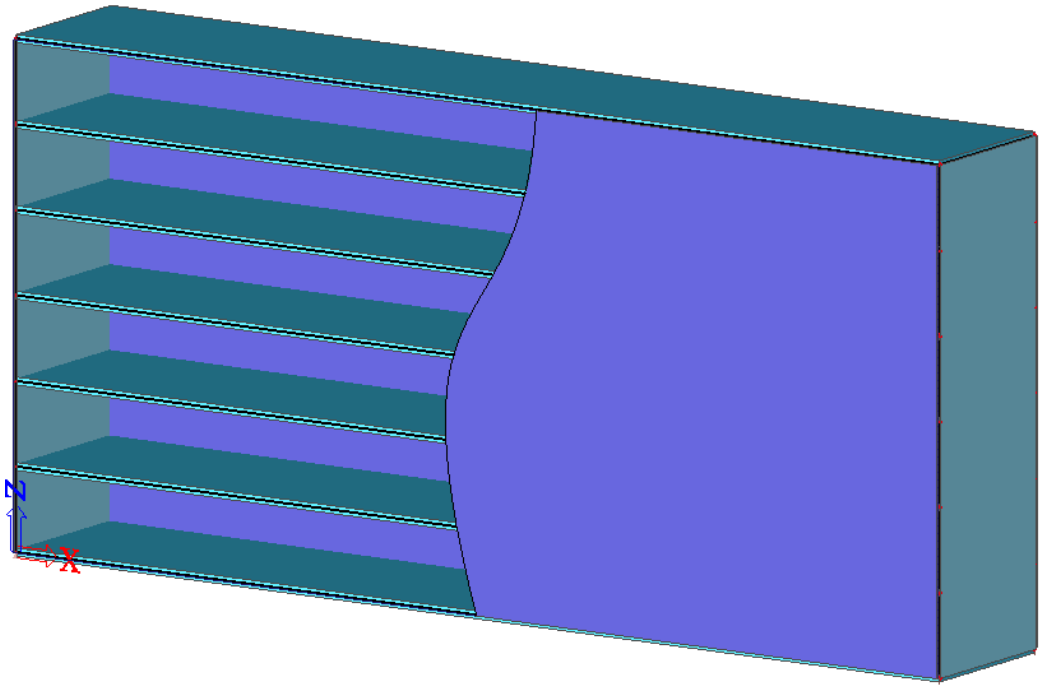

Figure 46. Model 2 - Gate overview

Retaining plates *Webs* *End plates*

8.1.2 Supports

In reality the gate is vertically supported, the z-direction, by two carriages. In the model these are represented by line supports with a length of 3 m in each bottom corner of the gate. The gate is in closed position and in practice the gate would be forced onto its horizontal supports, in the y-direction. Generally a number of nodal supports would represent these horizontal supports, but to prevent unrealistically high peak stresses a line support is applied in the model. A nodal support is added to prevent translation in the x-direction.

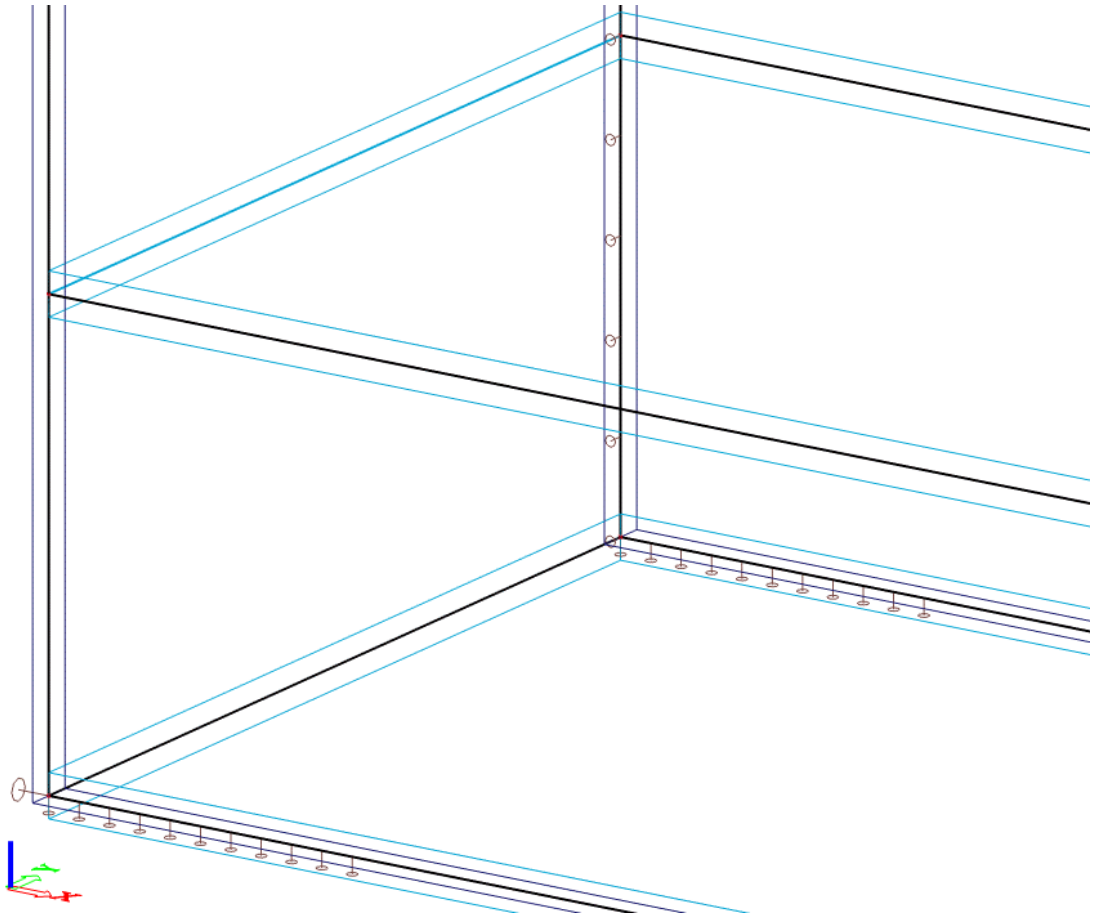

Figure 47. Model 2 - Supports

8.1.3 Loads

The loads and load combinations applied are all in accordance with the values found in chapter 6.

8.1.3.1 Self-Weight

Scia calculates the self-weight of the structure from the densities entered for the material input and the dimensions of the structure. To account for buoyancy, the self-weight load case is multiplied with 0.65 ($= 1 - buoyancy.ratio$). The applied buoyancy ratio can be found in chapter 7, see expression (7.62).

8.1.3.2 Hydraulic loads

Figure 48 shows a cross-section of the gate and presents the modelling of hydraulic loads, see also Figure 29. The left image shows the extreme negative hydrostatic pressure and the right the corresponding wave pressure load. Both of these loads are modelled as a non-uniform surface load, see Figure 49. On the left side of the gate is the Western Scheldt, on the right side of the gate is the lock chamber.

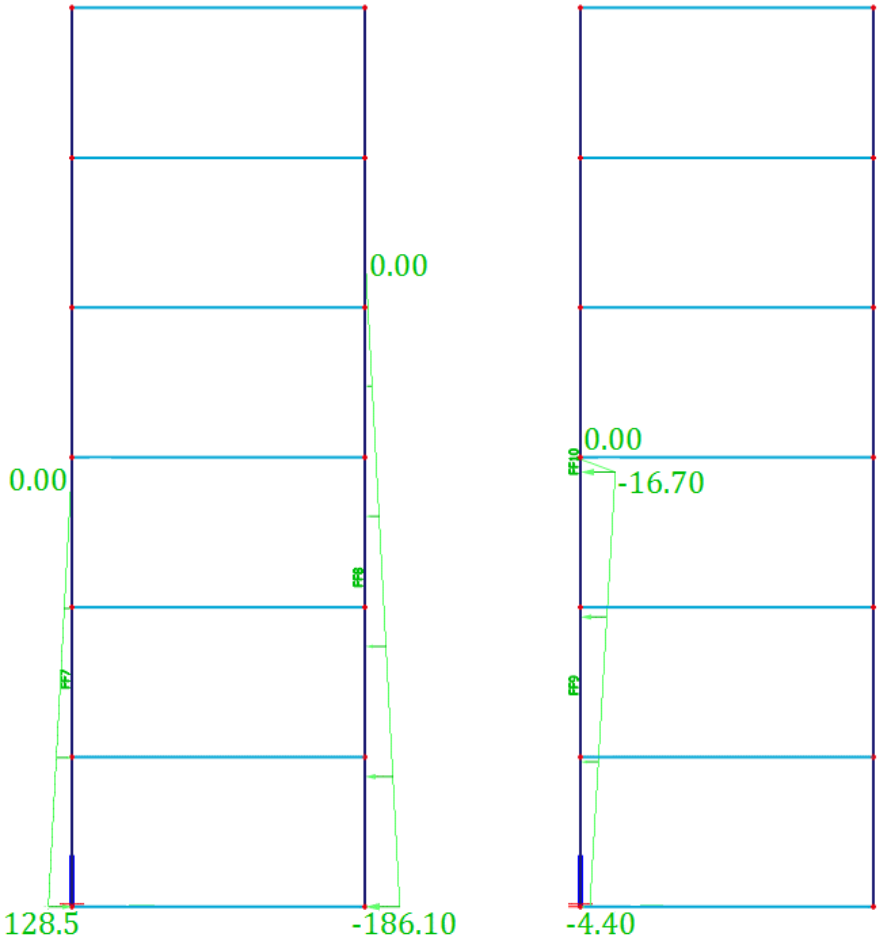

Figure 48. Model 2 - Hydraulic loads (Extreme negative)

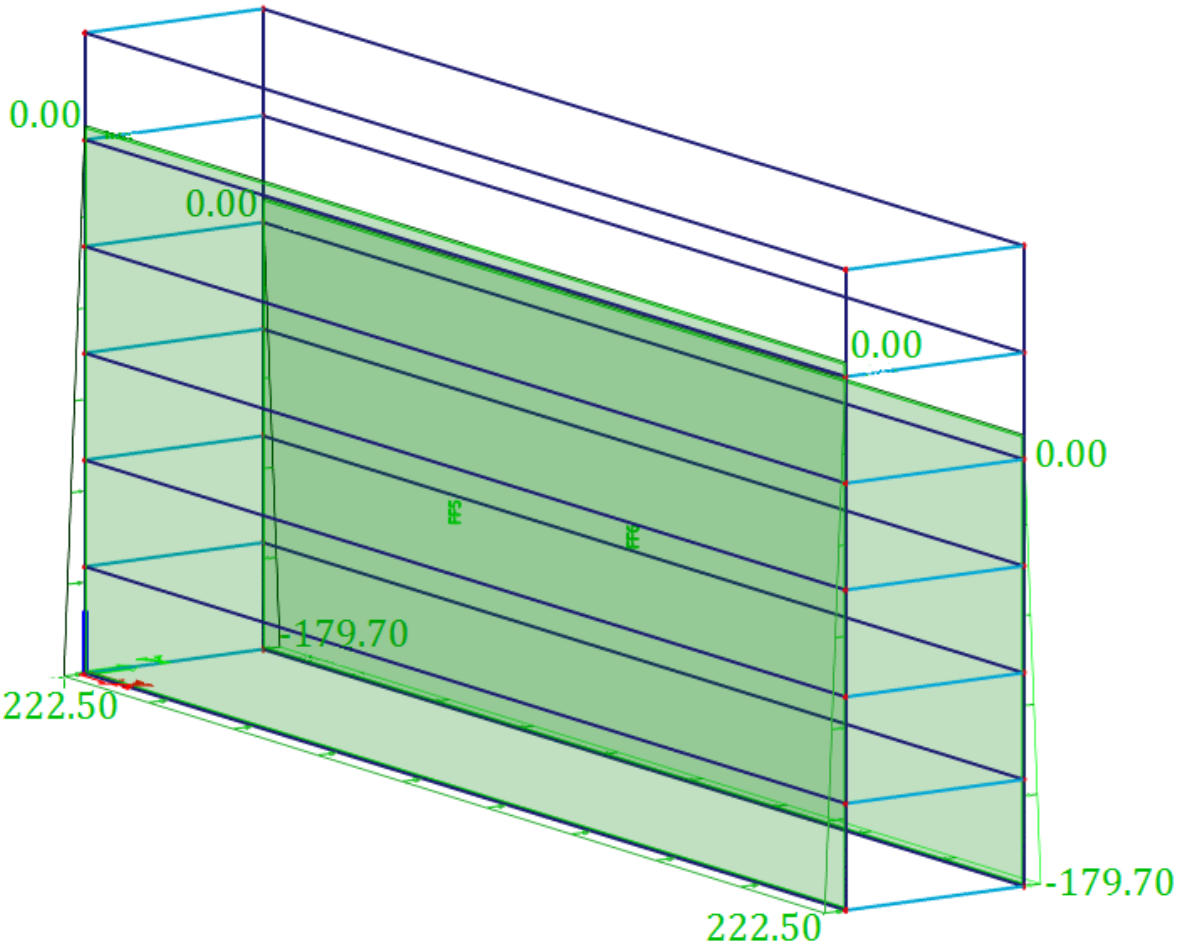

Figure 49. Model 2 - Surface load - Hydrostatic pressure positive head

8.2 Strength and deflection checks

Various deflection and strength checks are performed with the model. The governing cases for each structural element are presented here. More checks can be found in Appendix D.

8.2.1 Retaining plate checks

The maximum allowed deflection and stresses of the retaining plates are calculated with the corresponding laminate properties. Also the required partial material factors are taken into account.

Maximum allowed deflection

$$w_{max} = 108\ mm \tag{8.4}$$

Maximum stresses

$$\sigma_{x;max} = 96.6\ N/mm^2 \qquad \sigma_{y;max} = 65.3\ N/mm^2 \qquad \tau_{xy;max} = 22.8\ N/mm^2 \tag{8.5}$$

8.2.1.1 Deflection

Deflection in the global y-direction of retaining plates caused by the extreme negative head load combination. The largest deflection occurs in the 'back' retaining plate at mid-span at a height of approximately 3 m and is equal to 28.1 mm.

Unity check: $^{28.1}/_{108} = 0.26$

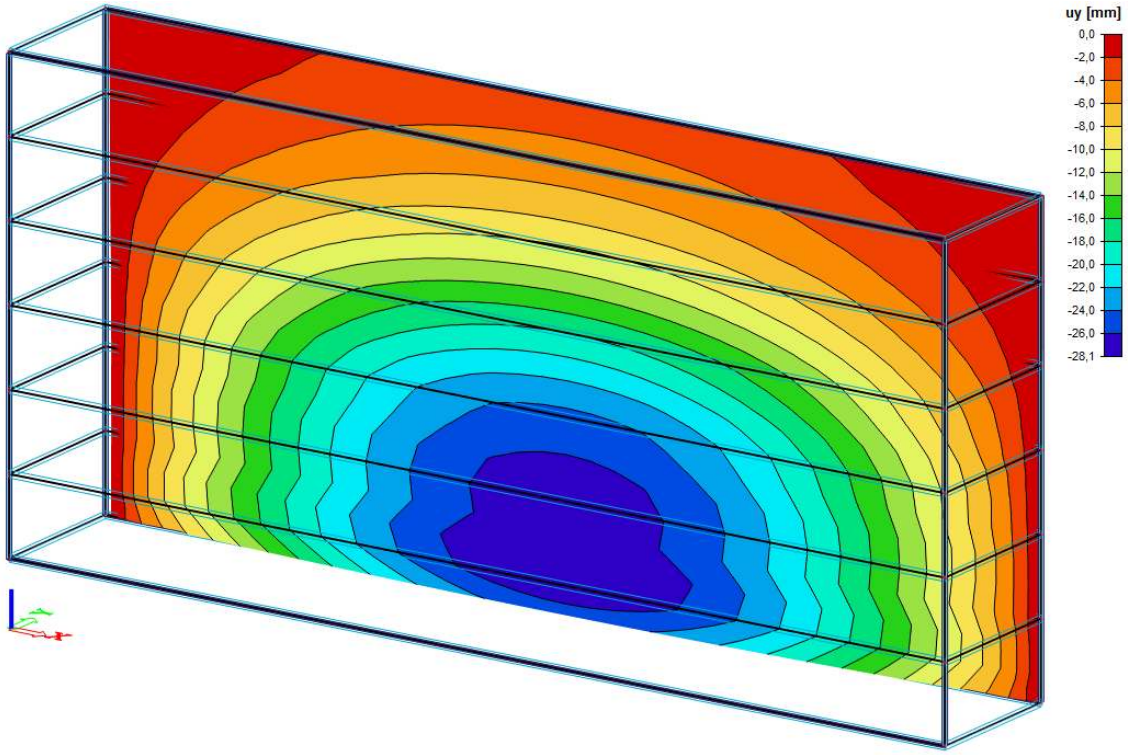

Figure 50. deflection uy – negative head – 'back' retaining plate

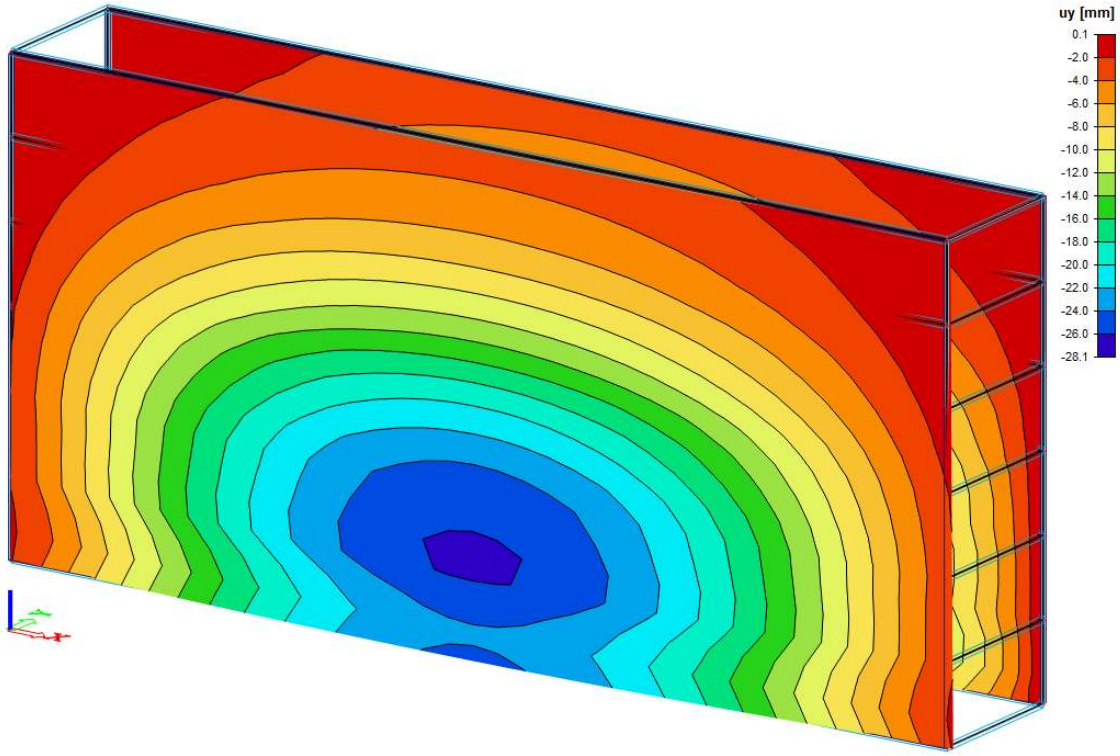

Figure 51. Deflection uy – negative head – 'front' retaining plate

8.2.1.2 Stresses

Stress in the retaining plates in local x-direction caused by the extreme negative load combination.

Unity check: $^{7.7}/_{96.6} = 0.08$

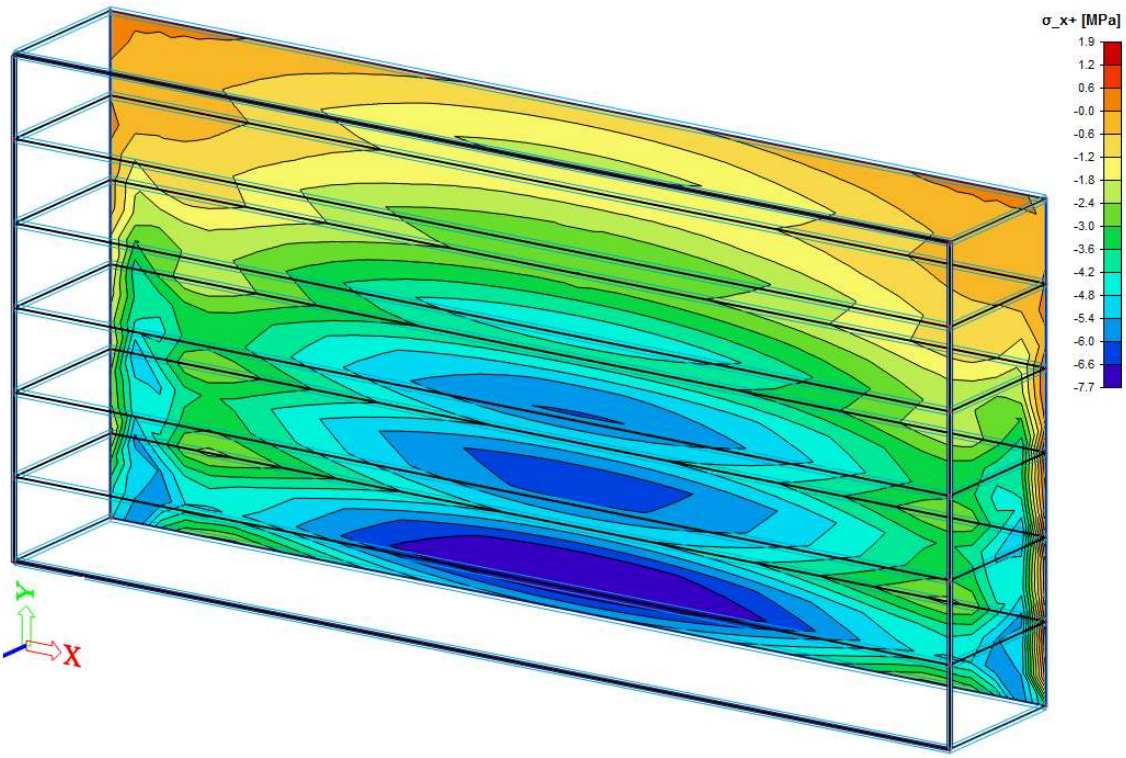

Figure 52. SigmaX– negative head – 'back' retaining plate

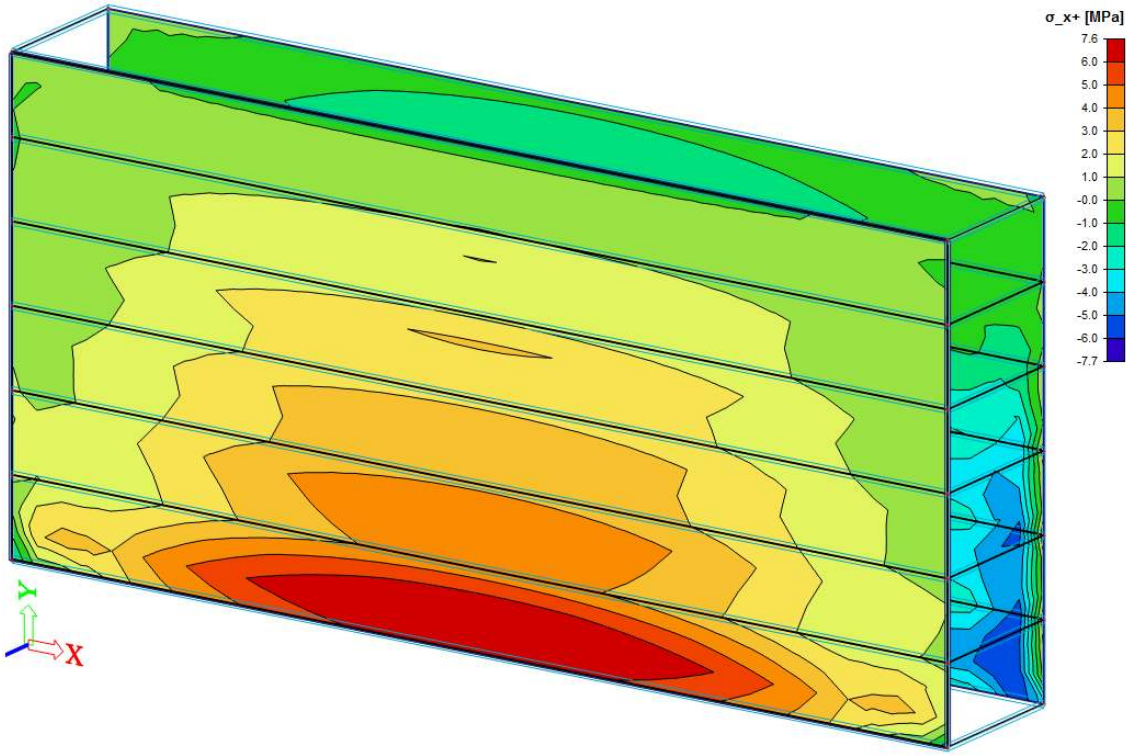

Figure 53. SigmaX – negative head – 'front' retaining plate

Stress in the retaining plates in local y-direction caused by the extreme negative load combination.

Unity check: $^{9.4}/_{65.3} = 0.14$

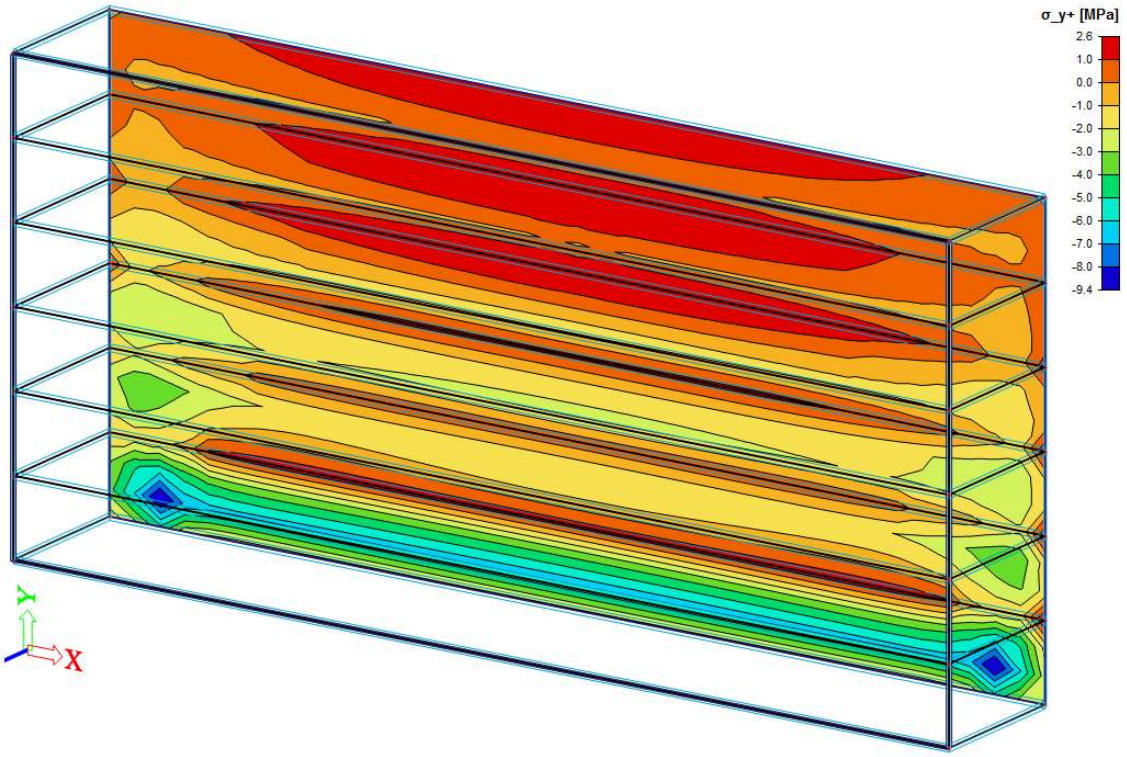

Figure 54. SigmaY– negative head – 'back' retaining plate

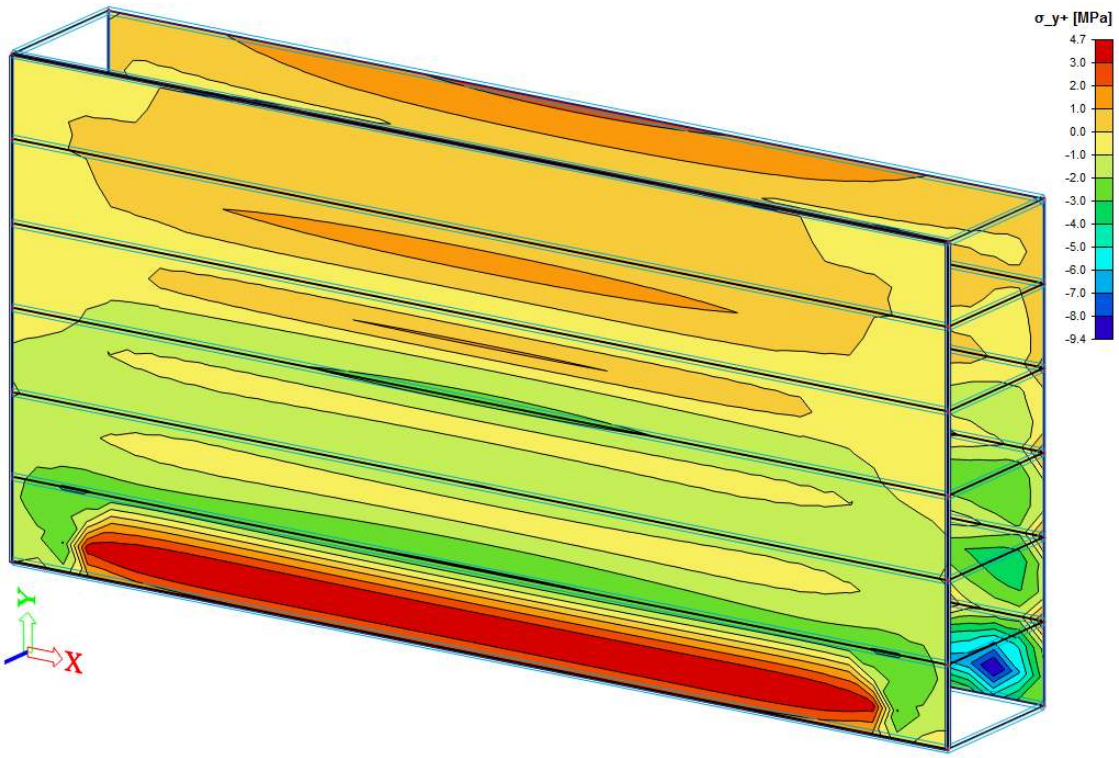

Figure 55. SigmaY– negative head – 'front' retaining plate

Shear stress in the retaining plates caused by the extreme negative load combination.

Unity check: $^{2.8}/_{22.8} = 0.12$

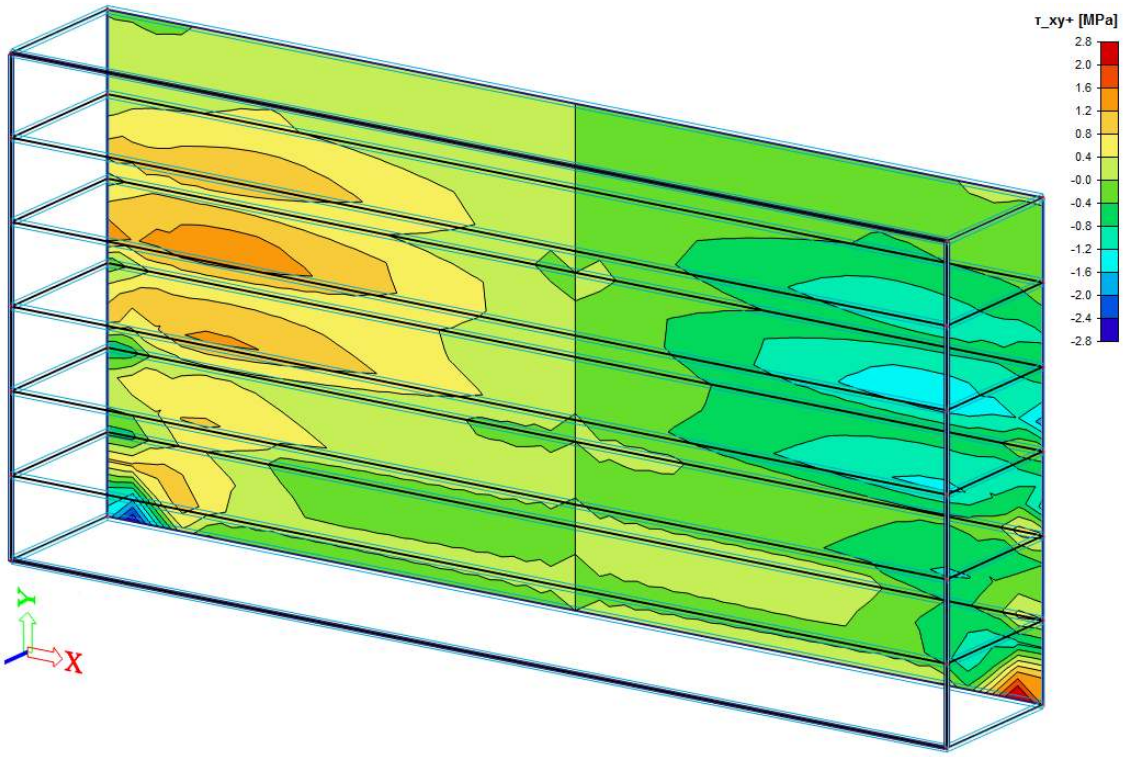

Figure 56. TauXY – negative head – 'back' retaining plate

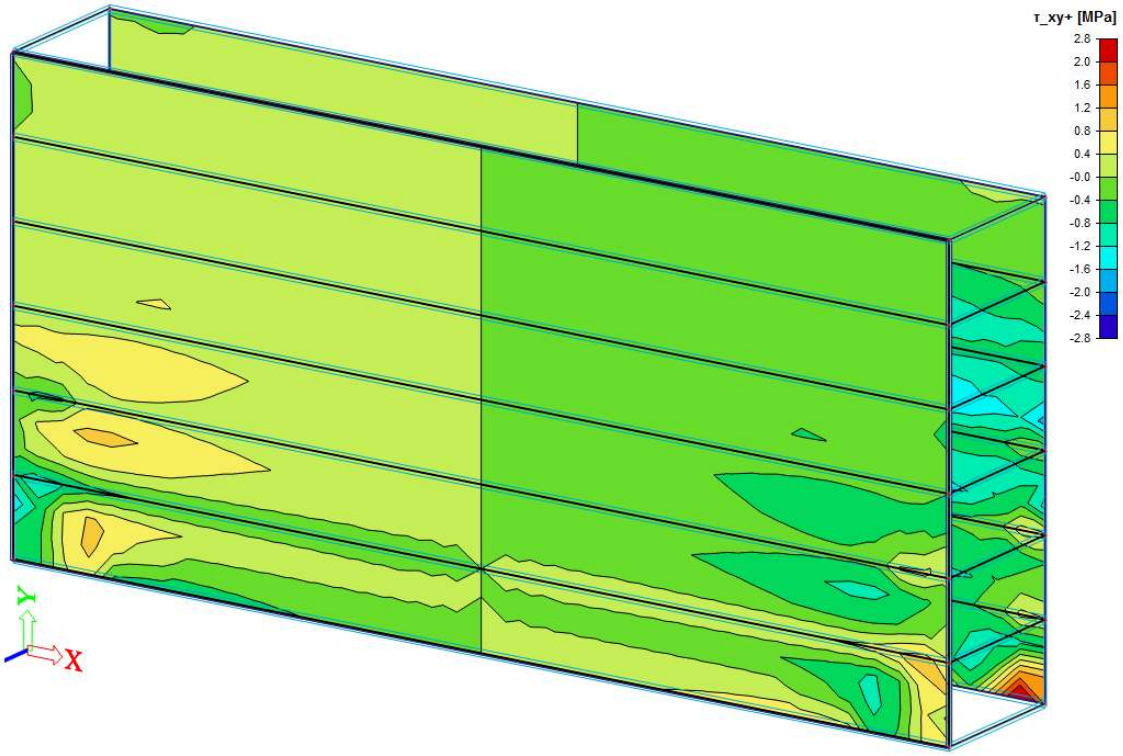

Figure 57. TauXY– negative head – 'front' retaining plate

8.2.2 Web checks

With the laminate properties of the webs, the maximum allowed deflection and stresses are calculated. The length used for the maximum deflection is 8 m, corresponding to the length of the web.

Maximum allowed deflection

$$w_{max} = 15.7\ mm \tag{8.6}$$

Maximum stresses

$$\sigma_{x;max} = 62.8\,N/mm^2 \qquad \sigma_{y;max} = 62.8\,N/mm^2 \qquad \tau_{xy;max} = 23.8\,N/mm^2 \tag{8.7}$$

8.2.2.1 Deflection

Deflection of webs in z-direction caused by the extreme positive load combination.

Unity check: $^{7.5}/_{15.7} = 0.48$

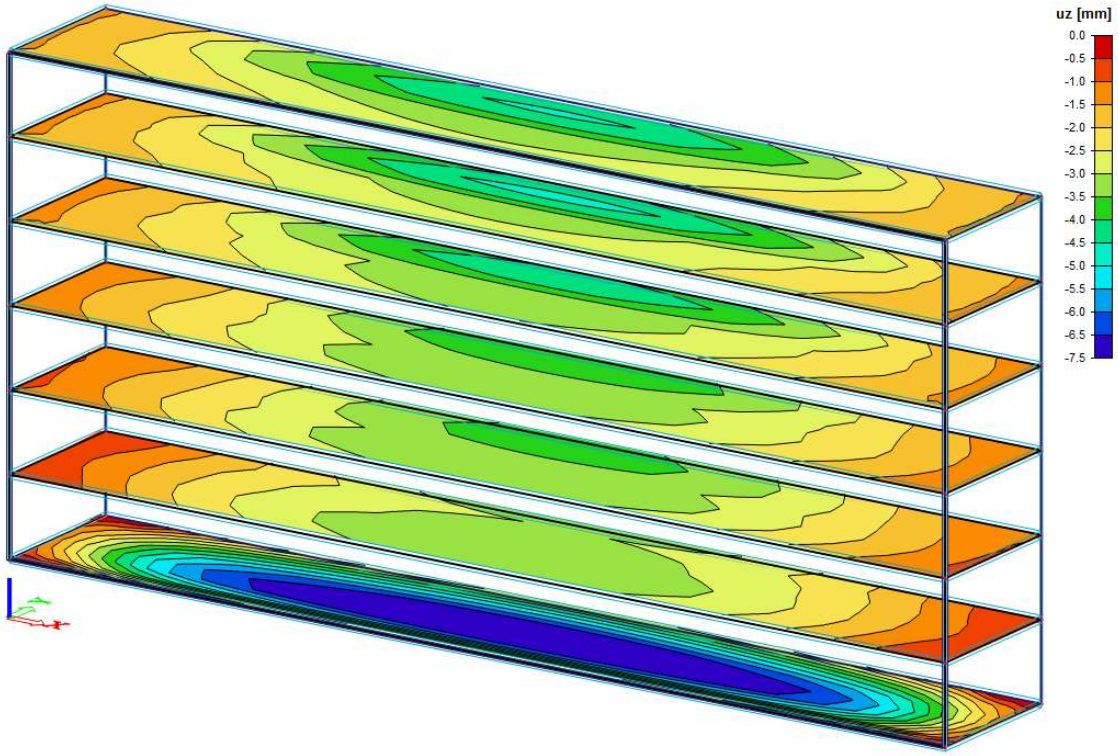

Figure 58. Deflection uz - positive head - webs

8.2.2.2 Stresses

Stresses in the webs in x- and y-direction caused by the extreme negative load combination.

Unity check: $^{6.4}/_{62.8} = 0.10$

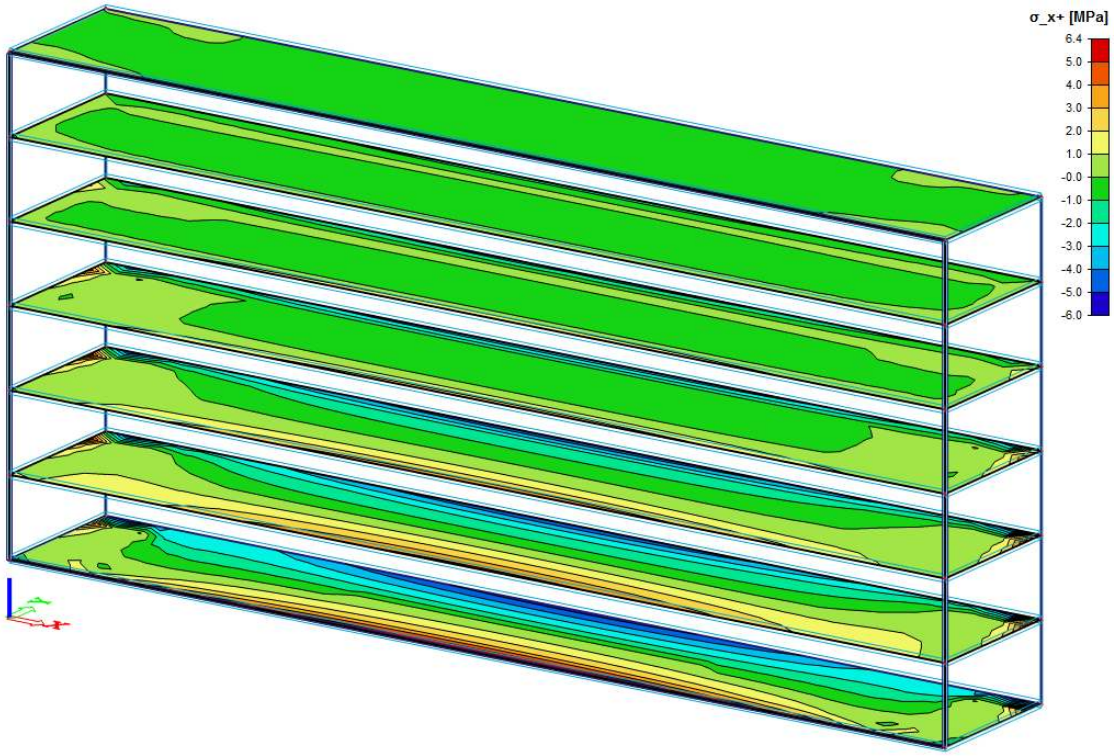

Figure 59. SigmaX – negative head – webs

Unity check: $^{7.6}/_{62.8} = 0.12$

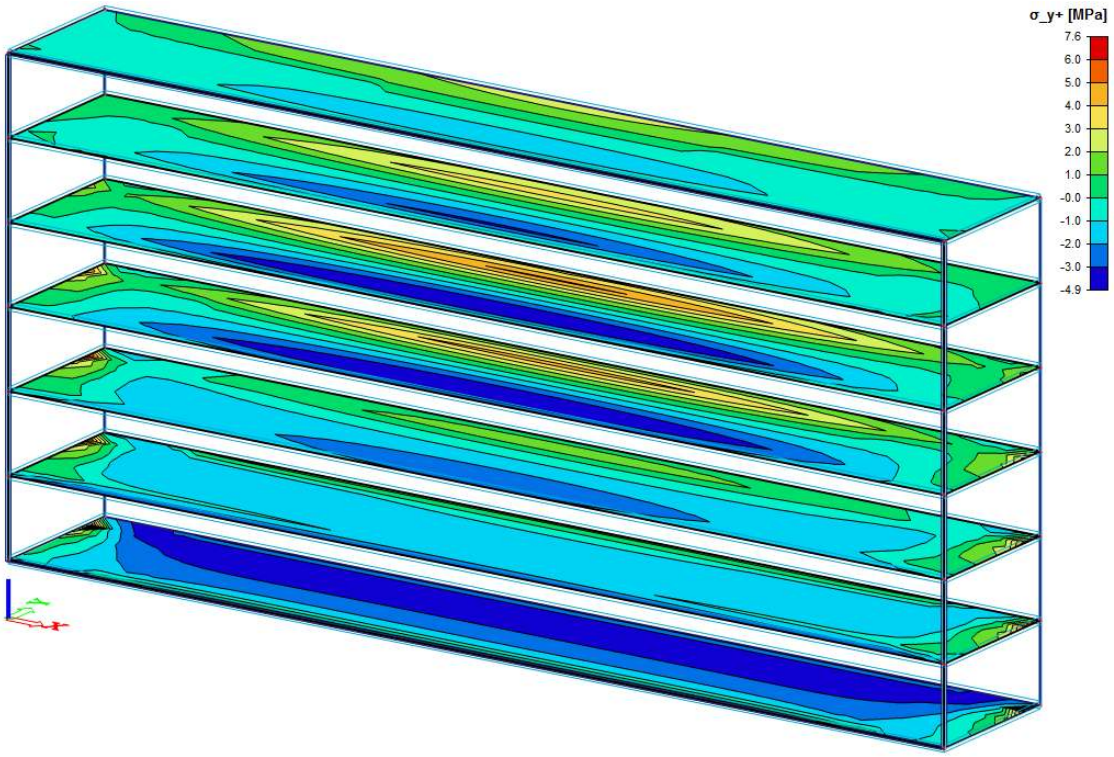

Figure 60. SigmaY – negative head – webs

Shear stress in the webs caused by the extreme negative load combination.

Unity check: $^{4.0}/_{23.8} = 0.17$

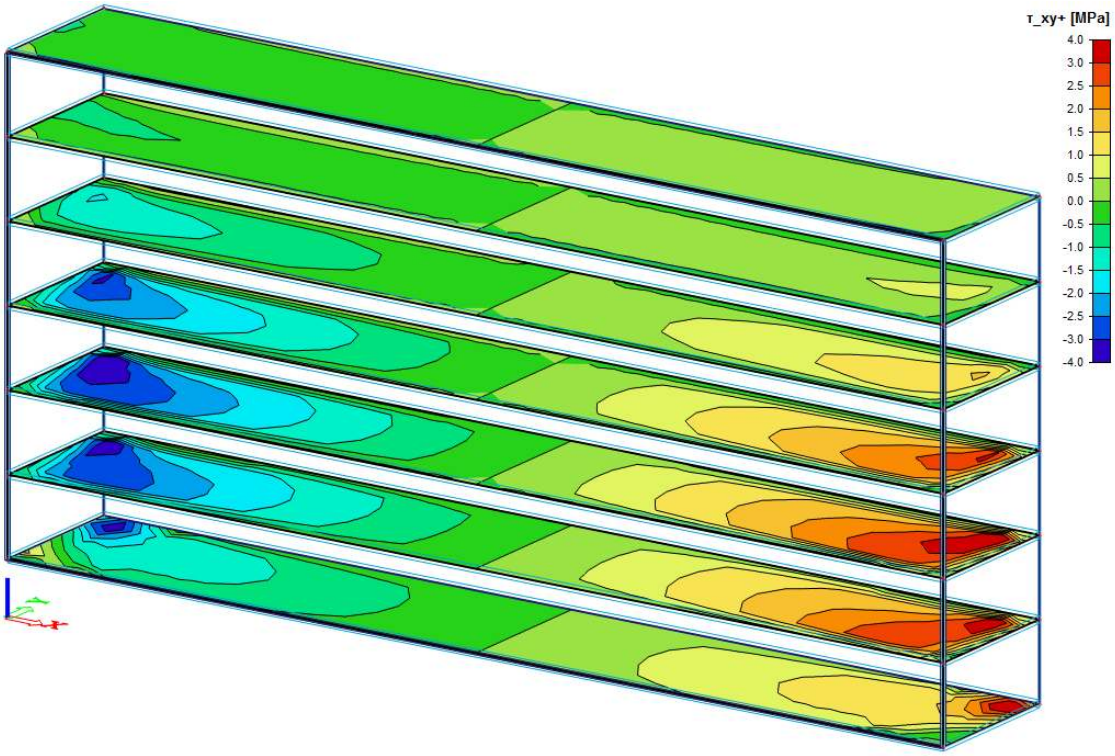

Figure 61. TauXY - negative head – webs

8.2.3 End plate checks

With the laminate properties of the end plates, the maximum allowed stresses are calculated.

$$\sigma_{x;max} = 55.0\,N/mm^2 \qquad \sigma_{y;max} = 55.0\,N/mm^2 \qquad \tau_{xy;max} = 27.9\,N/mm^2 \tag{8.8}$$

Stress in the end plates in local x-direction caused by the extreme negative load combination.

Unity check: $^{6.9}/_{55.0} = 0.13$

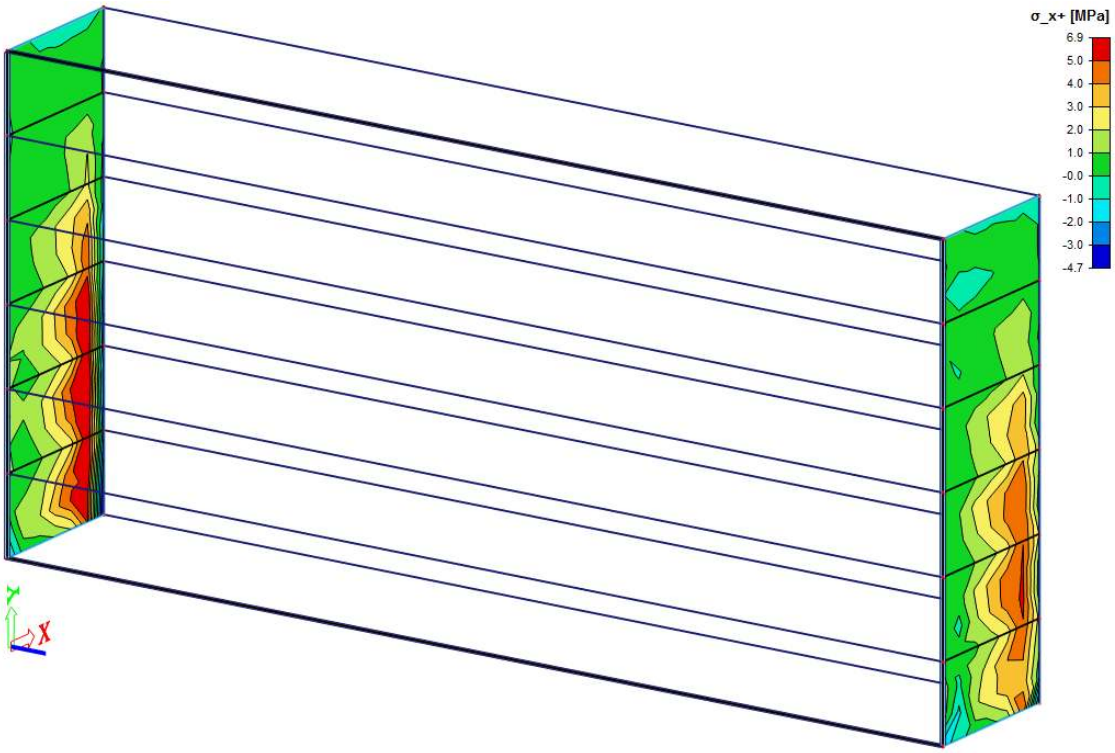

Figure 62. SigmaX - negative head - end plates

Stress in the end plates in local y-direction caused by the extreme positive load combination.

Unity check: $^{8.1}/_{55.0} = 0.15$

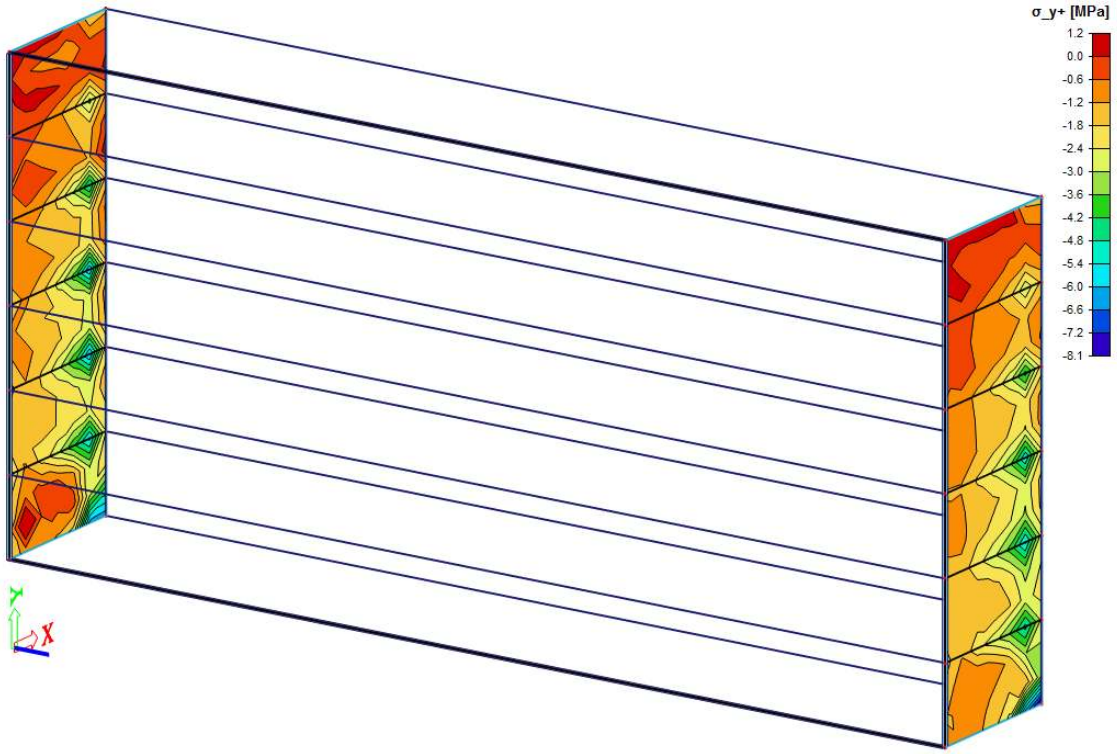

Figure 63. SigmaY - positive head - end plates

Shear stress in the end plates caused by the extreme positive load combination.

Unity check: $^{8.1}/_{27.9} = 0.30$

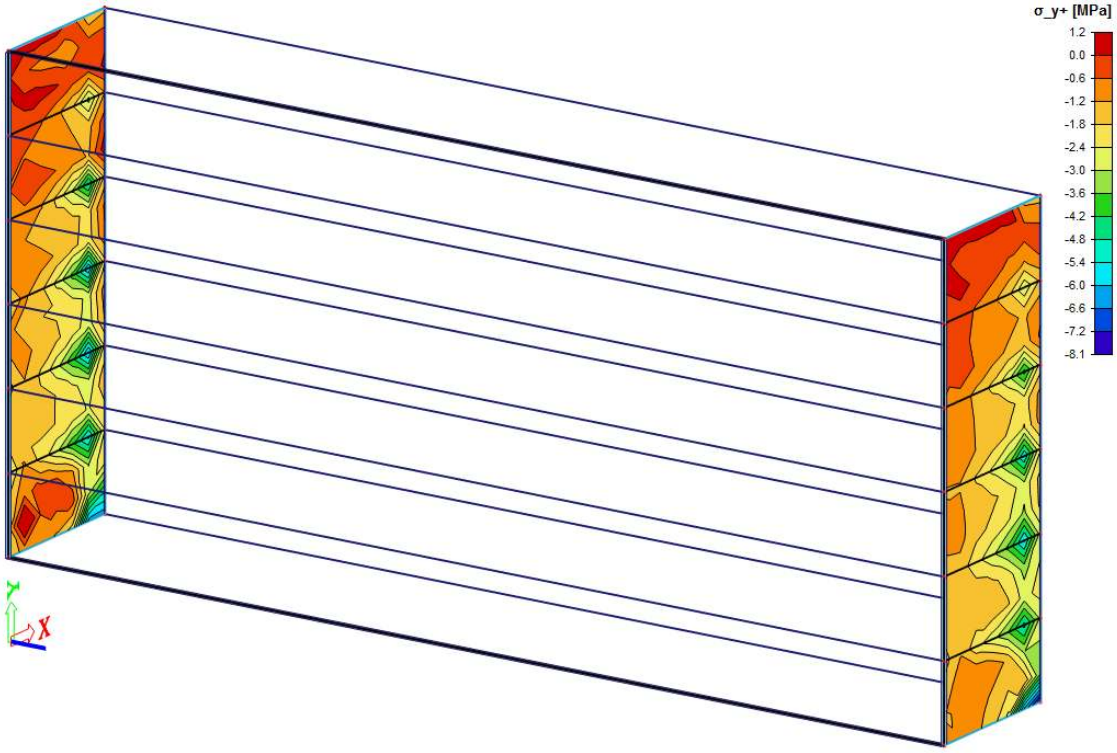

Figure 64. TauXY - positive head - end plates

8.2.4 Fatigue check

A simple fatigue check is performed. To determine a fatigue stress range, only the average low tide (Lo) load case is taken into account, 6.1.2.3. The average high tide (Hi) load case is also checked, but the hydraulic conditions during the Hi-load combination don't contribute to the fatigue stress range, because the water levels during average high tide are very similar to the water level on the channel side. In other words, a locking cycle does not result in a varying stress.

8.2.4.1 Stress range

The stress range follows from the variation of stress that occurs during the locking cycle. Figure 65 shows the hydrostatic pressures on the gate during a locking cycle when average low tide applies. In the image on the left, the water level in the lock chamber is equal to the water level in the channel (stress A). In the image on the right, the water level in the lock chamber is equal to the water level in the Western Scheldt (stress B). The stresses in the gate during both these situation is found with the model and shown in Figure 66 and Figure 67.

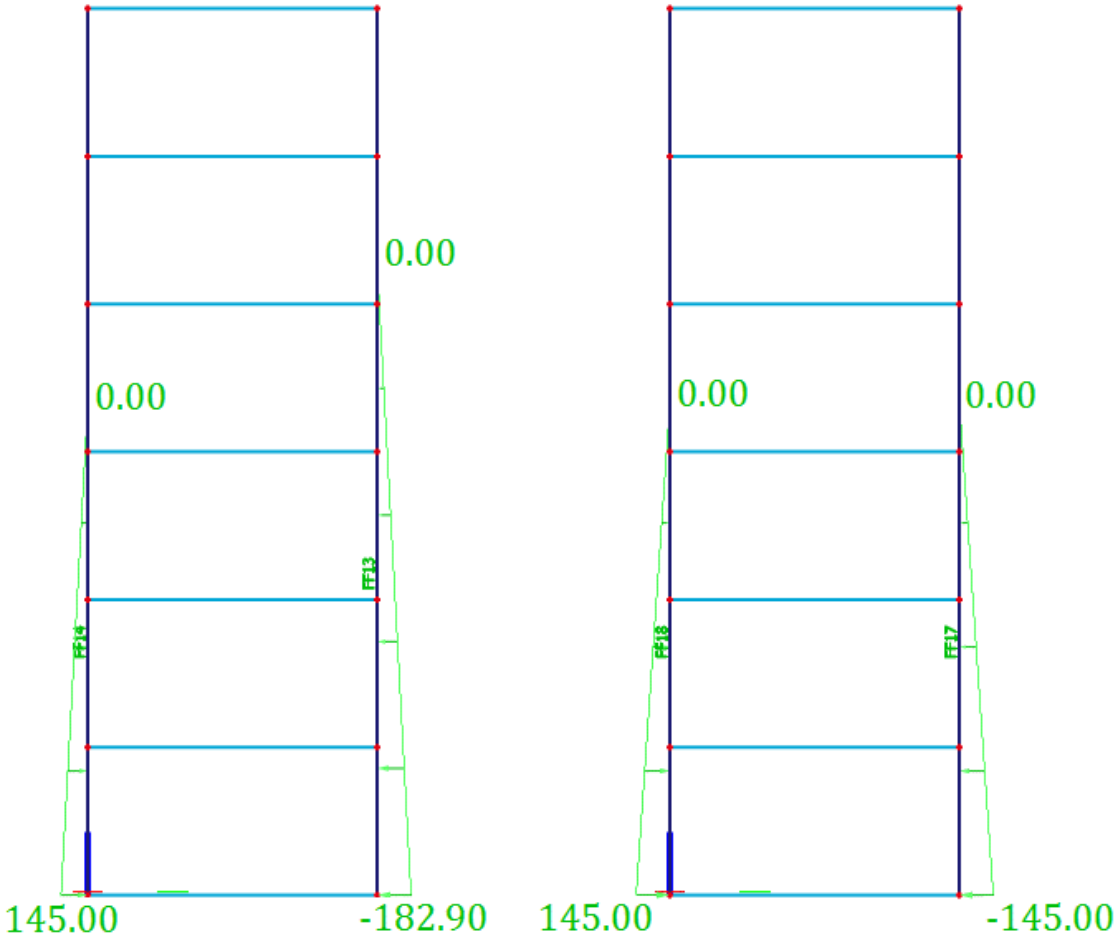

Figure 65. Hydraulic load - average low tide

Water level in chamber equal to the water level on the channel side.

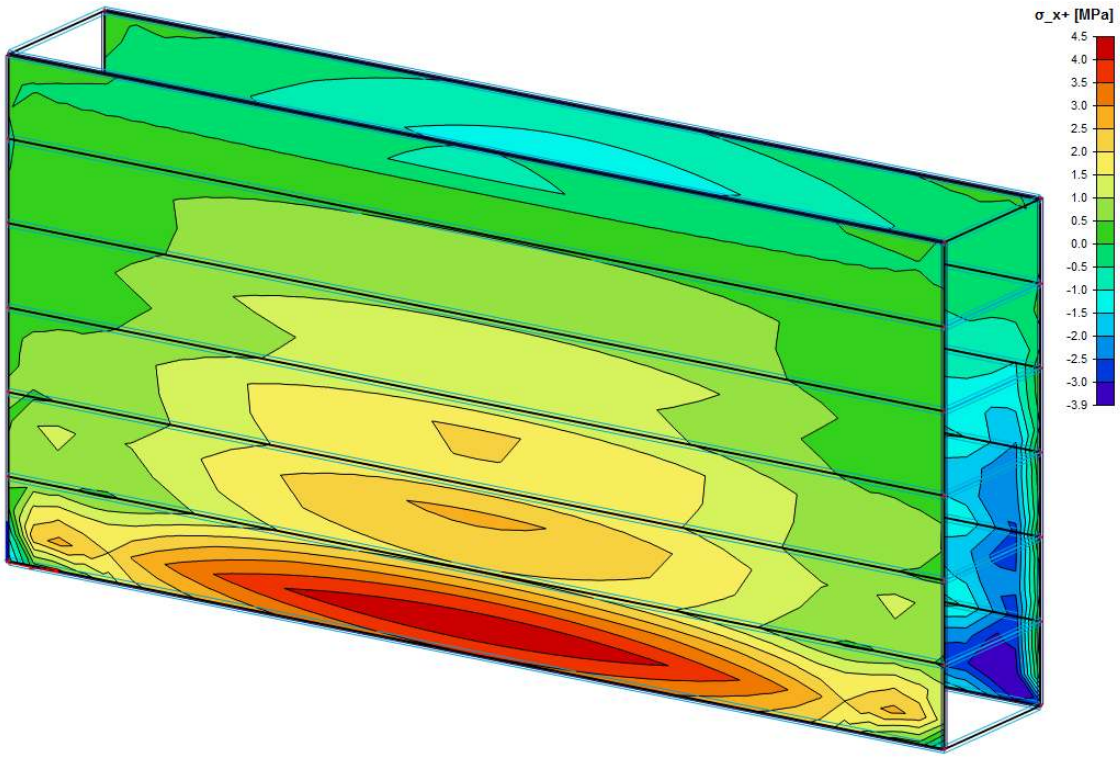

Figure 66. Fatigue stress A

Water level in chamber equal to the water level on the Western Scheldt side.

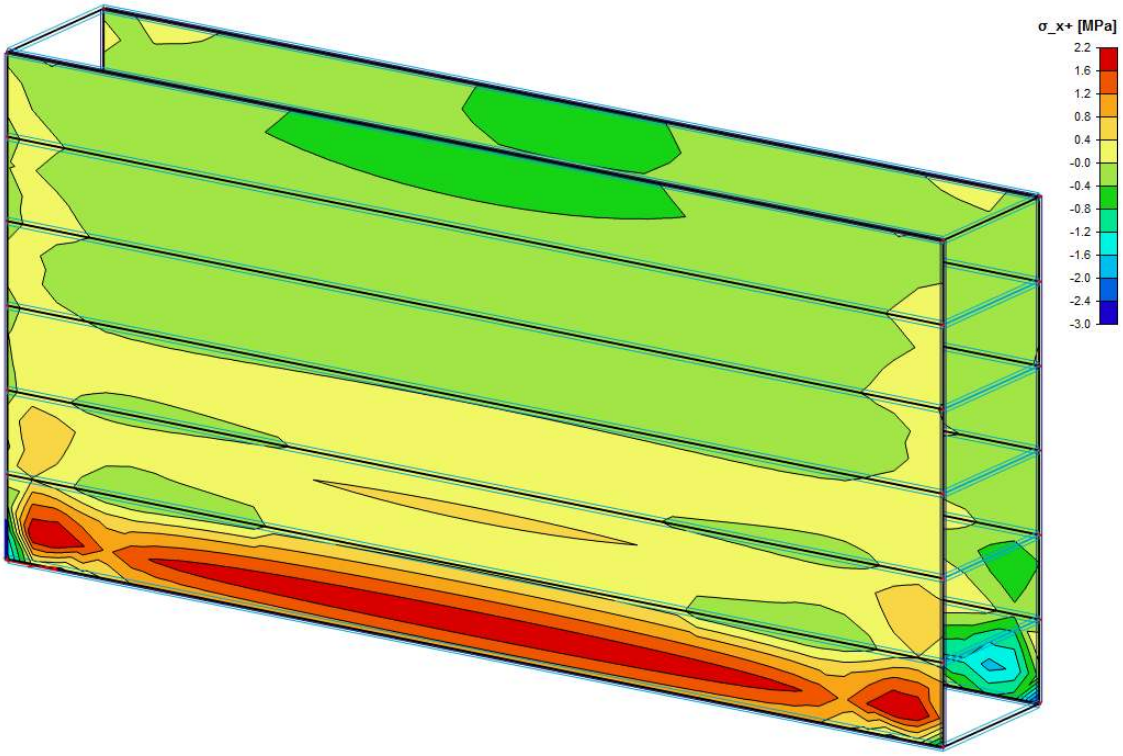

Figure 67. Fatigue stress B

8.2.4.2 Fatigue calculation

Miner's sum is used to calculated the accumulated fatigue damage as a result of the total number of cycles at each stress range. (Zorgdrager, 2014)-The calculation can be found in Appendix D.

$$N = \left(\frac{\Delta S}{\sigma_{fat}}\right)^k \tag{8.9}$$

with

$$\Delta S = stress.A - stress.B = 4.5 - 2.2 = 2.3 \ N/mm^2 \tag{8.10}$$

$$\sigma_{fat} = \frac{\varepsilon_{max} \cdot E_x}{\gamma_m \cdot \gamma_{c;fat}} = 96.6 \ \ N/mm^2 \tag{8.11}$$

where

N	*number of cycles to failure at a specific stress range*
ΔS	*stress range*
σ_{fat}	*Maximum fatigue stress*
k	*coefficient related to S-N curve slope =–9*

The number of cycles, n, during the lifetime of the structure can be determined with the value of 140 lockages per week, see section 5.2.2. For simplicity, the assumption is made that half of the lockages take place during high tide and half during low tide, so 70 lockages per week for this particular stress range.

$$n = 3.64 \cdot 10^5 \qquad N = 4.08 \cdot 10^{14}$$

$$D = \sum n/N < 1 \tag{8.12}$$

It's clear that with these values fatigue won't be a problem. That is because the stresses that occur in the structure during normal operation are relatively small.

8.2.5 Conclusion

For all the design checks performed, the requirements are easily met. This is because the dimensions of the structural elements are conservative as a result of the preliminary design and in particular the stability check.

If the stability could be made less of an issue, the gates dimensions or laminate properties of the different elements could drastically be reduced and a more optimal design could be made. In chapter 10 potential improvements or alternatives are conceptualized.

Another option is to vary with the applied ballast in the ballast tanks depending on the operating conditions. Ballast/weight is added during the conditions when stability is at risk. During average operating conditions some ballast is removed. The result would be a lighter gate. The application of ballast/buoyancy tanks is discussed in the next section.

8.3 Ballast/buoyancy

Ballast and buoyancy tanks are required, regardless of the application during the operating phase of the structure. Buoyancy is required for the gate to be floated into position during construction or for maintenance, repairs and replacement.

Ballast is required to sink the gate into position and, in combination with the weight of the gate, achieve the necessary overweight for stability.

8.3.1 Permanent ballast

The total self-weight of the gate found in the model is 30072 kN. If the gate is considered to be a completely watertight box, the total buoyancy force would be 100400 kN. In other words, the gate would float up until the buoyancy force equals the self-weight.

The minimum permanent ballast required to sink the gate is equal to

$$ballast_{min} = (100396 - 30072) = 70324\ kN \tag{8.13}$$

This means that with the current dimensions of the gate, a significant portion of the gate must be permanently filled with water.

Ballast tanks are added between the webs. Global dimensions of the permanent ballast tank is chosen to be $(L = 53) \times (W = 6) \times (H = 4.33)\ [m]$. The tank could be divided into smaller compartments, but further detailing is outside of the scope of this thesis.

In Figure 68 the permanent ballast load on a web is shown. The calculation can be found in Appendix D.

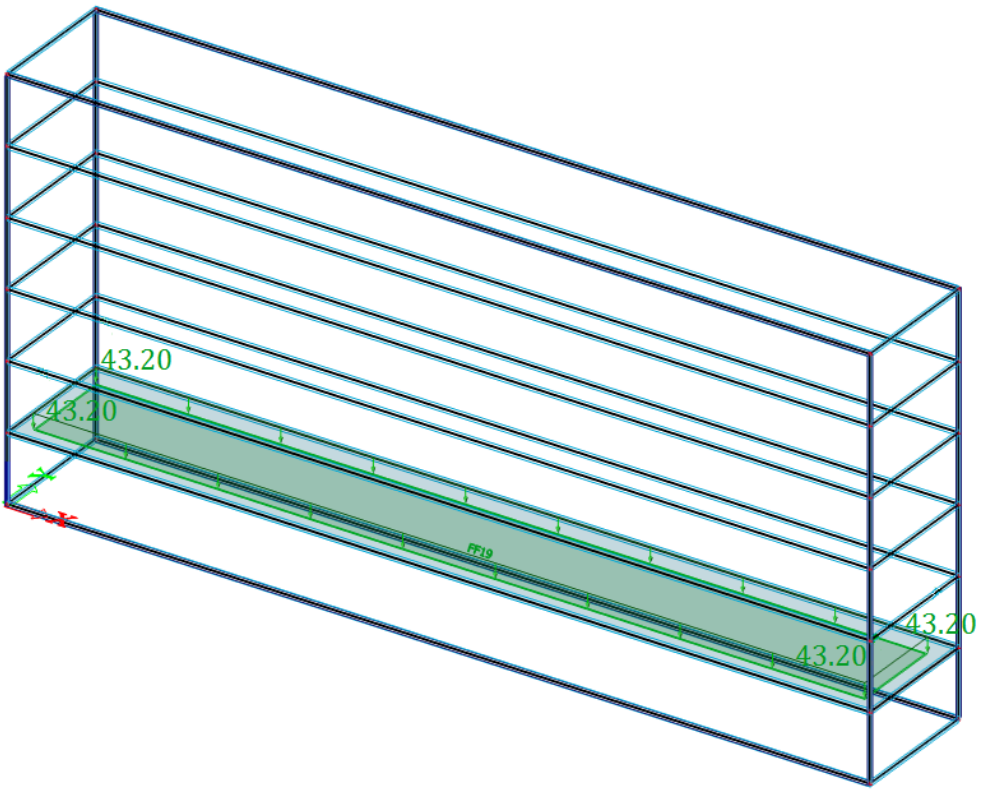

Figure 68. Permanent ballast load on web

8.3.2 Creep of the web

The permanent ballast load causes additional deformation of the webs. This deformation is presented in Figure 69. Over the entire lifetime of the structure the self-weight and the permanent ballast may cause creep deformation. The creep deformation is calculated as follows. (Zorgdrager, 2014)

The initial deflection follows from the model

$$u_{z;0} = 13.7\ mm \tag{8.14}$$

With a creep factor of $C = 1.15$ for Uni-directional plies (Zorgdrager, 2014) the stiffness of the web at the end of the lifetime of the structure can be calculated.

$$E_{x;\infty} = \left(\frac{E_x}{\gamma_m \cdot \gamma_c}\right)/C = 4155\ MPa \tag{8.15}$$

With these values know, the creep deformation can be determined

$$u_{z;creep} = u_{z;0} \cdot \left(\frac{E_x}{\gamma_m \cdot \gamma_c}/E_{x;\infty} - 1\right) = 2.06\ mm \tag{8.16}$$

The total deformation equals

$$u_{z;0} = u_{z;0} + u_{z;creep} = 15.76\ mm \tag{8.17}$$

The maximum allowed deformation of the webs is, see (8.6)

$$w_{max} = 15.7\ mm$$

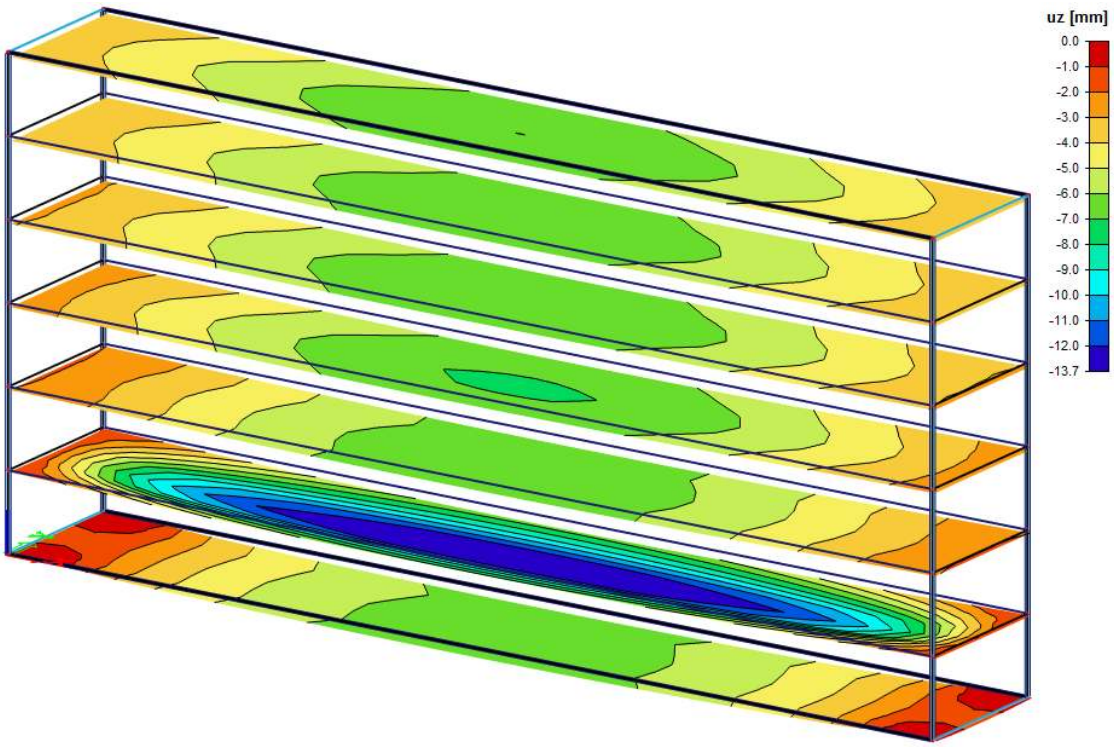

Figure 69. Deflection of web - Permanent ballast

8.4 Key points

- Deflection criteria are easily met with a unity check of 0.26. The largest deflection occurs at mid-span at a height of 3 m from the bottom.
- Strength criteria are easily met in all structural elements.
- Fatigue doesn't cause any problems, because the variation of stresses caused by the locking cycle is relatively small.
- When a ballast load is added onto the webs, the deflection criteria of the webs are just met.

9 3D Stability Problem

Gate stability during movement

In this chapter the stability of the gate during movement is evaluated with the Scia model from the previous chapter with some changes. This model is referred to as model 3. The supports are changed to represent the gate during movement and the stability load case is added. In addition, the overweight required for stability is calculated while varying the support carriage width and for a variety of water head differences. These results are plotted in graphs.

9.1 Stability during movement

The figure below displays the 3D stability problem. The support system consists of two carriages, each with four wheels. In the figure the width of the carriage, i.e. the distance between supports is equal to the width of the gate. The gate is horizontally supported at both lower ends and near the top at the gate chamber side.

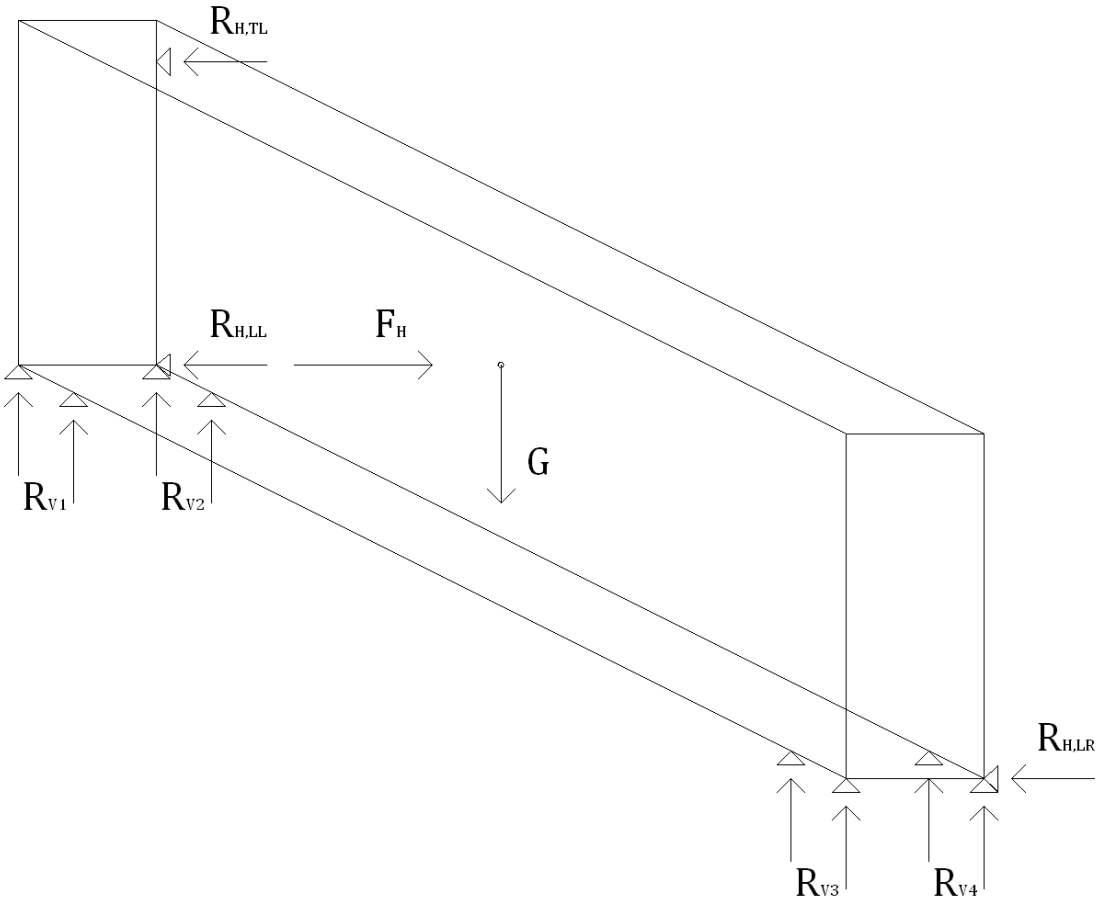

Figure 70. 3D stability problem

where

G	*Dead weight (self-weight minus buoyancy)*
F_H	*All horizontal loads related to the stability load combination*
$R_{H,LL}$	*Horizontal support reaction at bottom of the gate chamber side (lower left)*
$R_{H,TL}$	*Horizontal support reaction at the top of the gate chamber side (top left)*
$R_{H,LR}$	*Horizontal support reaction at the bottom of the gate recess side (lower right)*
R_{V1}	*Vertical support reactions 1*
R_{V2}	*Vertical support reactions 2*
R_{V3}	*Vertical support reactions 3*
R_{V4}	*Vertical support reactions 4*

9.1.1 Stability calculation

The calculation is performed by following the same steps applied in chapter 7, but the vertical support reactions are found with the model. Again, the resultant of the support reactions must meet the stability requirement. The model accurately determines the distribution of all combined loads over the supports, taking into account deflections of the gate that affect this distribution.

The point of action of the resultant is calculated with

$$x = \frac{(R_{v2}+R_{v4})\cdot W_{car}}{G} - \frac{1}{2}W_{car} \tag{9.1}$$

where

x	*point of action resultant support reaction*
R_{vi}	*combined support reaction i=2,4*
W_{car}	*width of the support carriage/distance between supports*
G	*Dead weight*

Again, the stability requirement is

$$x \leq \frac{W_{car}}{6} \tag{9.2}$$

9.1.2 Required dead weight calculation

From the vertical equilibrium it follows that

$$R_{V1} + R_{V2} + R_{V3} + R_{V4} = G \tag{9.3}$$

To simplify this calculation it is assumed that the dead weight is evenly distributed over the vertical supports. So the supports reactions as a result of the dead load will be

$$R_{V1,G} = R_{V2,G} = R_{V3,G} = R_{V4,G} = \frac{1}{4}G \tag{9.4}$$

The required dead weight can be found by solving the following equation

$$\left(\frac{W_{car}}{2} + x\right)\cdot G = \left(R_{V2,STA} + R_{V2,G}\right)\cdot W_{car} + \left(R_{V4,STA} + R_{V4,G}\right)\cdot W_{car} \tag{9.5}$$

with

$x = \frac{W_{car}}{6}$

$R_{V2,STA}$ *support reaction as a result of the horizontal loads*

This becomes,

$$\left(\frac{2\cdot W_{car}}{3}\right)\cdot G = \left(R_{V2,STA} + \frac{G}{4}\right)\cdot W_{car} + \left(R_{V4,STA} + \frac{G}{4}\right)\cdot W_{car} \tag{9.6}$$

$$G_{req} = G = \left(R_{V2,STA} + R_{V4,STA}\right)\cdot 6 \tag{9.7}$$

9.2 Model 3 – FRP box gate during movement

The 3D model of the FRP box gate is changed to represent the gate during movement. The support carriages are modelled as four supports in the z-direction. Initially the carriage width i.e. the distance between supports, is chosen at 8 m, approximately the thickness of the gate. Horizontally, the y-direction, the gate is supported at both lower ends and at the top on the gate chamber end. This leaves one side, horizontally unsupported at the top.

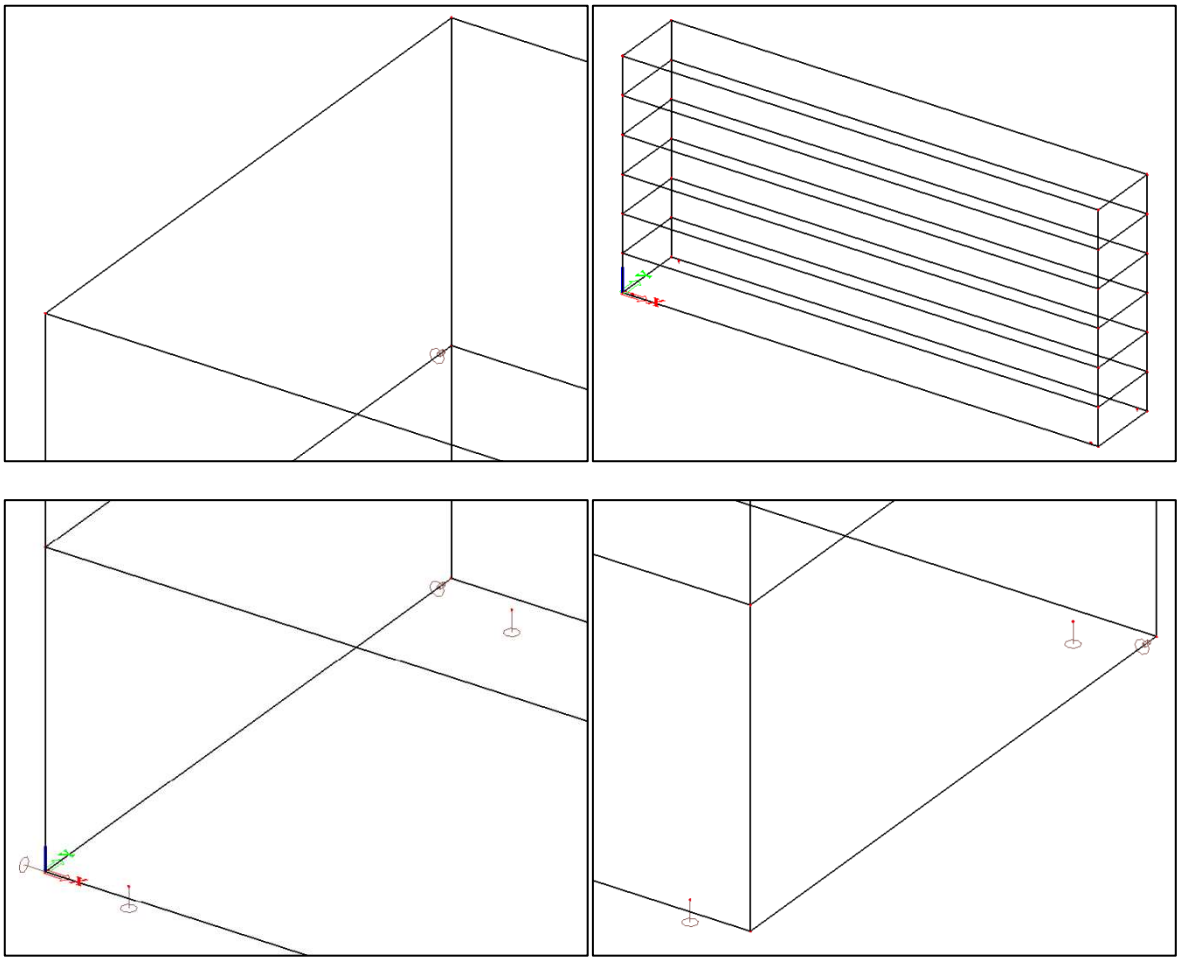

Figure 71. Model 3 – Overview and Supports

9.2.1 Stability load combination

The gate is loaded by the stability load combination, consisting of the self-weight, hydrostatic pressure as a result of Δh and wave loads. The values for these loads can be found in 6.1.2.3. The modelled hydraulic loads are displayed in the figure below.

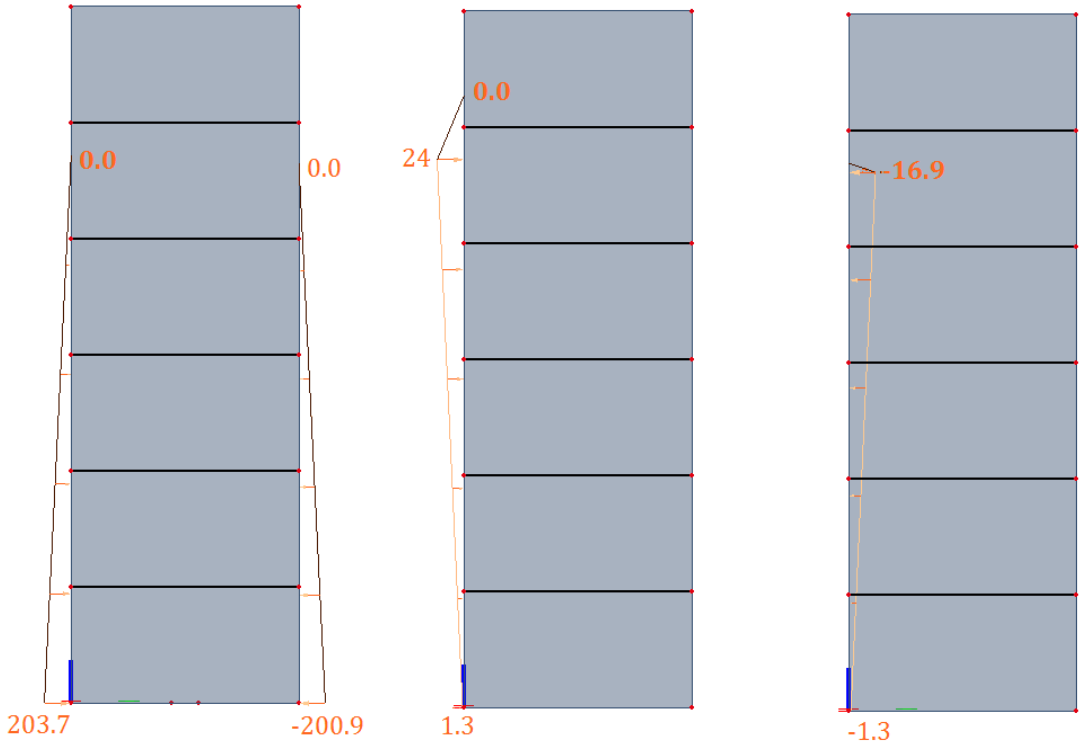

Figure 72. Model 3 - Stability load combination

9.2.2 Model 3a – Box gate stability

The objective with this model is to check the stability of the FRP box gate.

It was found that the application of rigid supports in the y-direction lead to unrealistic results when the carriage width was decreased. Caused by deflections of the gate, the support reaction in the lower left support resulted in a significant contribution to the stabilizing moment. In turn resulting in an unrealistically large decrease of the vertical support reactions and the required dead weight for stability. In Figure 73, a graph is presented of the required dead load for various carriage widths.

To get accurate results with the model, the supports are modelled as flexible supports. This makes sense, because in practice the gate is forced onto the horizontal supports and small translations occur. Flexible supports in the model mimic this phenomenon. The first step is to calibrate the stiffness of these supports.

Table 27. Required dead weight with corresponding carriage width - rigid supports

W_{car} [m]	1	2	3	4	5	6	7	8
DW_{req} [kN]	5282	5036	5860	6829	9186	11509	15546	19733

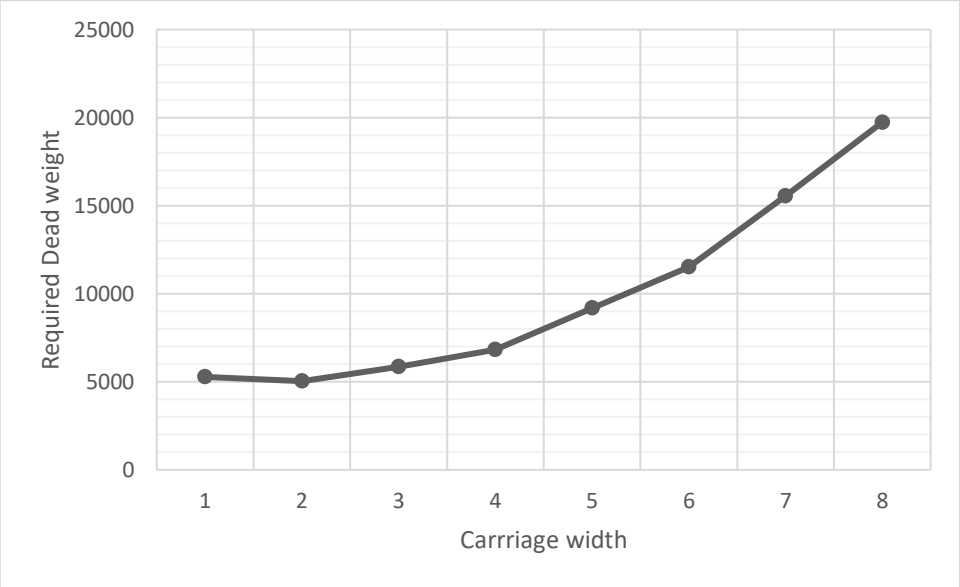

Figure 73. Graph - Dead Weight vs width - rigid supports

9.2.3 Model 3b – Dead weight vs. carriage width

The objectice with this model is to investigate the impact of the width of the support carriages on the stability of the gate. The distance between the vertical support is changed in the model and with the support reactions, the required dead weight can be calculated. The results are presented in graph. The figure below displays how the carriage width is reduced in the model. The width is also increased, resulting in a carriage wider than the gate. The connection from the gate to these supports is achieved by adding an infinitely stiff beam.

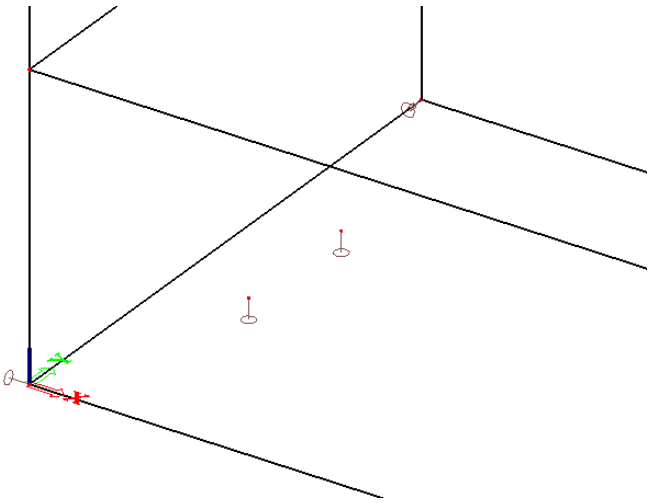

Figure 74. Model 3b - reducing carriage width

9.2.4 Model 3c – Dead weight vs. Δh

The objective with this model is to gain insight into the magnitude of the impact on the stability caused by a remaining head difference during movement. Hydrostatic pressure load cases are added for $\Delta h = 5, 10, \dots, 95, 100\ cm$. The required dead weight is calculated for each combination and plotted in a graph. The carriage width is set to the initial value of 8 m.

9.3 Box gate stability

As stated in section 9.2.2 the first step is to calibrate the stiffness of the supports. Through trial-and-error the stiffness's of the flexible horizontal supports are chosen as such, that the translations in the y-direction at the supports are all equal to 10 mm. The following stiffness's are obtained.

Lower left: $0.50 \cdot 10^2\ MN/m$

Top left: $3.20 \cdot 10^2\ MN/m$

Lower right: $3.70 \cdot 10^2\ MN/m$

In Figure 75 the deflection of the gate in y-direction is displayed. Keep in mind that the image views the gate from the 'back' side.

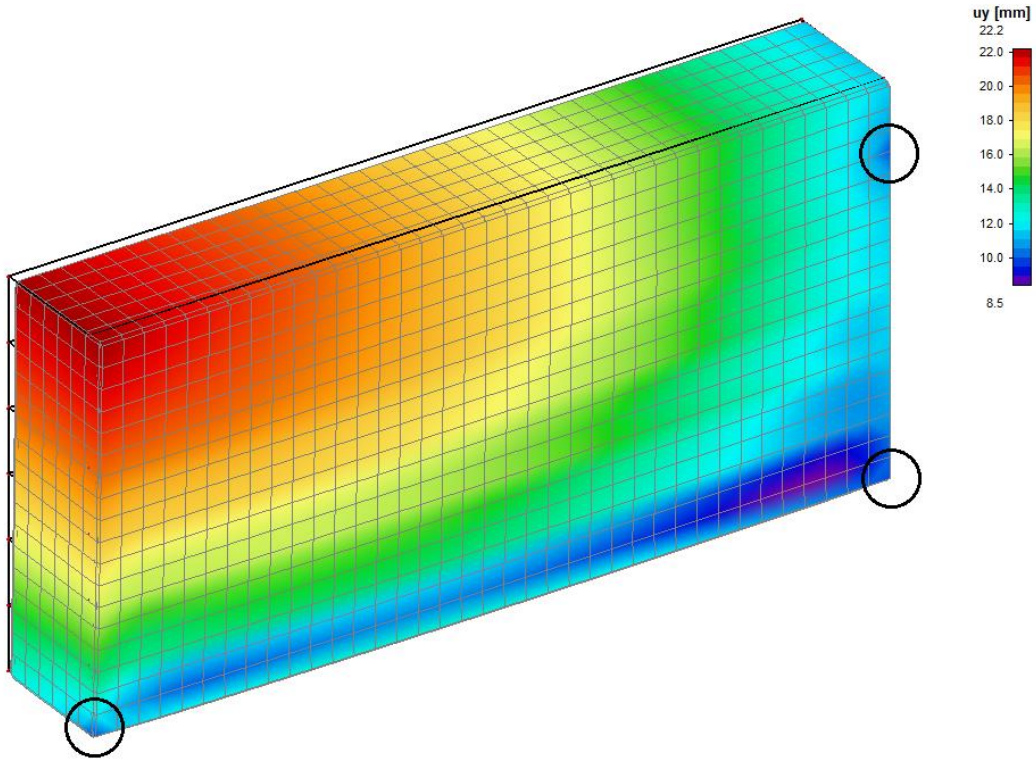

Figure 75. Model 3a - Deflection uy

○ *Location of horizontal supports*

9.3.1 Support reactions

With the supports calibrated, the correct support reactions can be determined with the model. The results are shown in Table 28.

Table 28. Calibrated support reactions

	Total incl. SW	**Total excl. SW**
Vertical	**[kN]**	**[kN]**
R_{V1}	3501.59	-932.93
R_{V2}	5369.61	932.93
R_{V3}	2068.93	-2365.89
R_{V4}	6802.27	2365.89
Horizontal		
$R_{H;LL}$	-501	-500.31
$R_{H:TL}$	-3209.55	-3210.23
$R_{H:LR}$	-3710.54	-3710.54

9.3.2 Stability check

The point of action is calculated with (9.1), giving the following results for the stability check.

$$x = 1.49\ m \qquad x_{max} = 1.33\ m$$

$$x/x_{max} = 1.12 \rightarrow Not\ stable \tag{9.8}$$

9.3.3 Conclusion – 3a

According to the check performed, the gate is not stable under all conditions. The easiest solution would be to add more ballast to achieve stability. However, it would be better to optimize the design of the gate. One solution would be to reduce buoyancy by changing the shape of the gate. For example by making the gate narrower towards the top.

The reason the gate is unstable with this calculation, but stable with the 2D calculation from chapter 7 is that deflections of the gate have a negative impact on the stability. This effect was not taken into account in the 2D calculation.

A significant difference can be seen in the distribution of the vertical support reactions to achieve a stabilizing couple. In the 2D calculation, it was assumed that the vertical supports at both ends of the gate would contribute half of the stabilizing moment. It can be seen that a significantly larger portion goes to the recess end of the gate. This is not really a problem for the stability calculation, because all reaction forces are taken into account, but in practice this uneven distribution of loads could lead to an uneven rate of wear-and-tear of certain parts.

An argument could be made that the stability criteria of W/6 is too conservative, since one end of the gate is horizontally supported at the top.

9.4 Dead weight vs. carriage width

The distance between the vertical supports is changed as described in section 9.2.3. For each distance the required dead weight is calculated with (9.7).

9.4.1 Model 3b – Results

The values in the table below are displayed in the graph in Figure 76. The graph shows the dead weight required for stability for the corresponding carriage width. The carriage width is also the distance between the vertical supports. The calculations of these values can be found in Appendix E.

Table 29. Required dead weight corresponding with carriage width

W_{car} [m]	0.5	1	1.5	2	2.5	3	3.5	4	4.5	5	5.5	6
DW_{req}	22888	20771	19142	18118	18271	18596	19013	18799	19035	20237	20269	20300

W_{car} [m]	6.5	7	7.5	8	8.5	9	9.5	10	10.5	11	11.5	12
DW_{req}	20308	20466	20224	19792	19350	17997	16362	14680	13090	11661	10410	9940

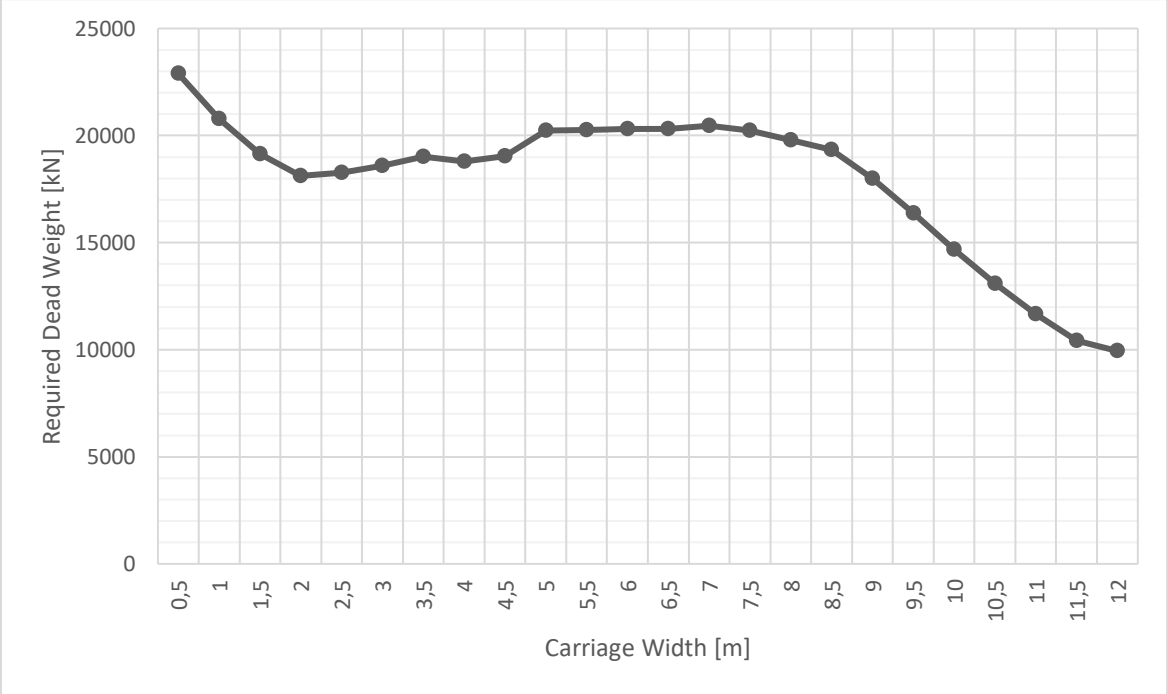

Figure 76. Graph – Dead Weight vs Width – calibrated supports

9.4.2 Conclusion – 3b

Looking at Figure 76, starting from the initial width of 8 m, when the width is increased the required dead weight goes down i.e. the gate becomes more stable. When the width is decreased, the required dead weight goes up slightly and flattens out quite quickly.

There is little change until the 4-5 m point, where a significant drop occurs. This is because the lower left horizontal support reaction becomes positive. Deflection of the unsupported top right corner becomes so large, that the deflection of the lower left side goes in the opposite direction. The gate pivots around the top left and lower right supports. With the top left horizontal support reaction a couple is generated and the contribution to the stabilizing moment significantly increases. This moment will also introduce torsion in the entire gate and wear-and-tear will increase at the horizontal supports.

The required dead weight keeps going down until eventually the horizontal contribution can no longer counter the decreasing carriage width, which leads to the vertical support reaction to start increasing again.

When the horizontal supports are calibrated for a translation in the y-direction of 50 mm, the following stiffness's are obtained:

Lower left: $0.11 \cdot 10^2\ MN/m$

Top left: $0.63 \cdot 10^2\ MN/m$

Lower right: $0.74 \cdot 10^2\ MN/m$ (9.9)

What can be seen in the resulting graph is that the horizontal contribution to the stabilizing moment doesn't increase much when narrowing the carriage width. As a result the required dead weight continuously increases when reducing the carriage width.

Table 30. Required dead weight corresponding with carriage width - calibrated supports 50 mm

W_{car} [m]	1	2	3	4	5	6	7	8
DW_{req}	59877	43541	36922	31832	28633	25407	22871	20570

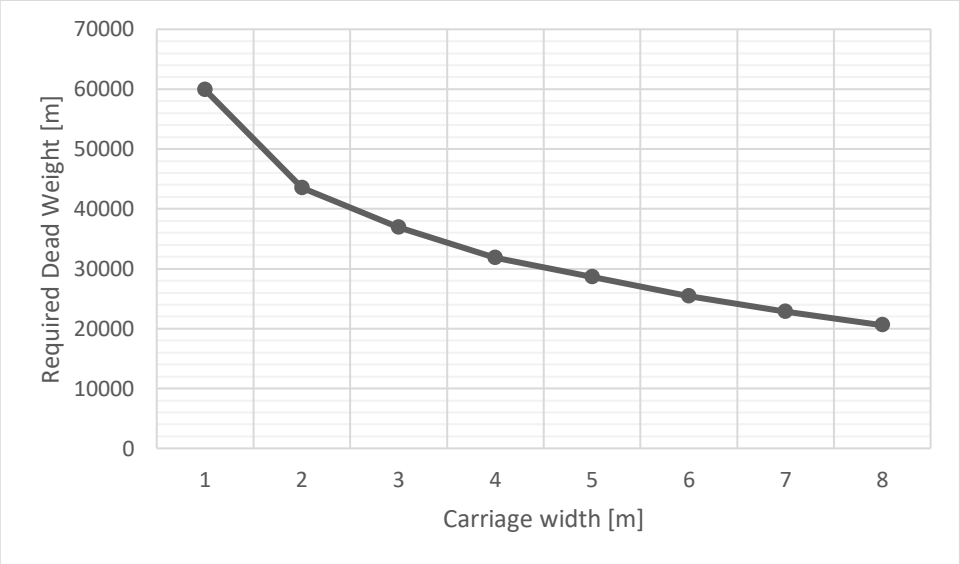

Figure 77. Graph - Dead Weight vs. width - calibrated supports 50mm

9.4.3 Horizontal support reactions

The graph and table on the next page show the distribution of the horizontal loads over the three horizontal supports for a carriage width of 0.5 to 12 m. The distribution over the left and right side remains the same regardless of the carriage width. However the distribution over the lower and top left support changes drastically. The main reason for this, is the deflection of the gate. For a decreasing carriage width, the deflections increase. At 4.5 m, what was also seen in Figure 76, deflection of the top right corner results in the gate to pivot around the top left and lower right supports causing deflection of the lower left support in the opposite direction. The resulting support reaction works in the same direction as the resultant of horizontal loads on the gate, significantly increasing the support reaction in the top left support.

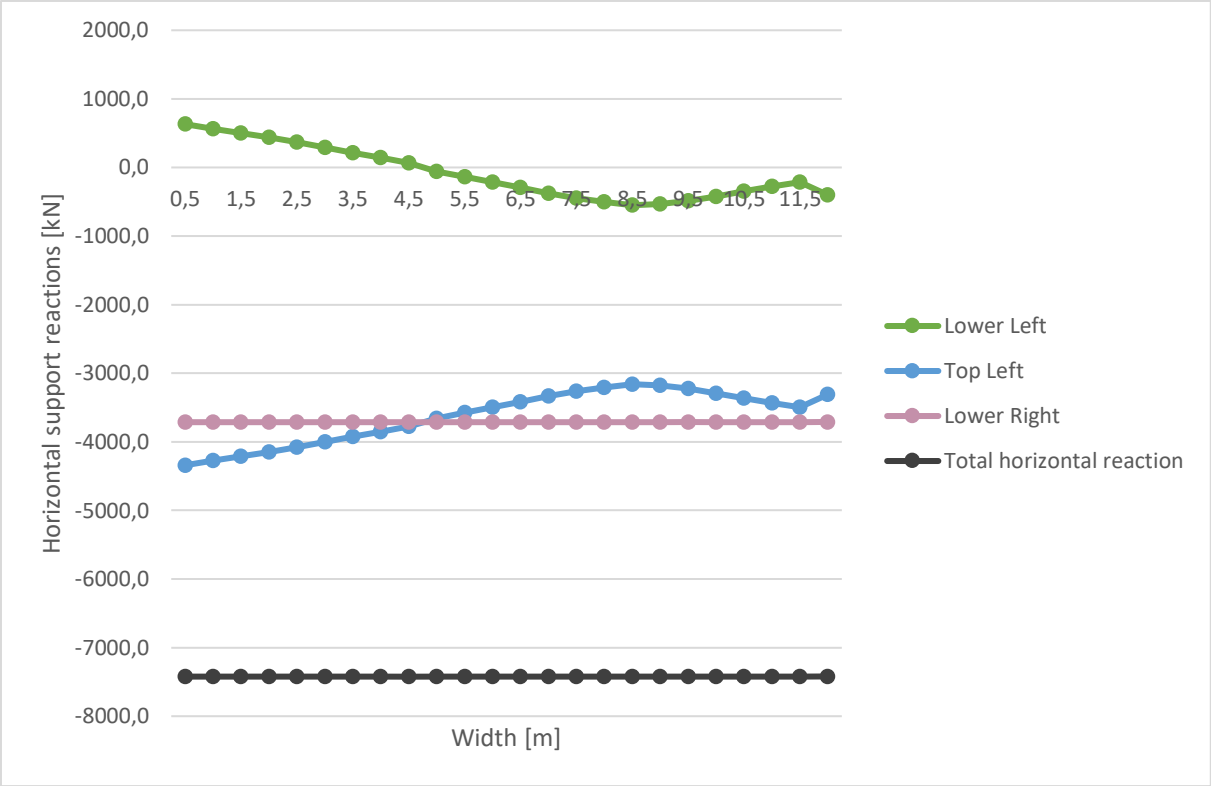

Figure 78. Graph - Horizontal support reactions

Table 31. Model 3b - Horizontal support reactions

W_{car} [m]	Lower left support [kN]	Top left Support [kN]	Lower right support [kN]	Total horizontal reaction [kN]
0.5	630.9	-4341,4	-3710,54	-7421,1
1.0	559,8	-4270,3	-3710,54	-7421,1
1.5	499,2	-4209,8	-3710,54	-7421,1
2.0	441,8	-4152,3	-3710,54	-7421,1
2.5	369,8	-4080,3	-3710,54	-7421,1
3.0	292,6	-4003,1	-3710,54	-7421,1
3.5	210,4	-3921,0	-3710,54	-7421,1
4.0	144,1	-3854,7	-3710,54	-7421,1
4.5	64,1	-3777,6	-3710,54	-7424,1
5.0	-55,2	-3655,4	-3710,54	-7421,1
5.5	-134,2	-3576,3	-3710,54	-7421,1
6.0	-213,8	-3496,7	-3710,54	-7421,1
6.5	-292,8	-3417,7	-3710,54	-7421,1
7.0	-380,1	-3330,5	-3710,54	-7421,1
7.5	-446,8	-3263,7	-3710,54	-7421,1
8.0	-501,0	-3209,6	-3710,54	-7421,1
8.5	-550,8	-3159,9	-3711,23	-7421,8
9.0	-533,6	-3176,9	-3710,04	-7420,5
9.5	-485,5	-3225,3	-3711,34	-7422,1
10.0	-420,5	-3290,3	-3710,25	-7421,0
10.5	-349,6	-3360,9	-3711	-7421,5
11.0	-280,1	-3430,4	-3711,22	-7421,7
11.5	-215,4	-3495,3	-3710,27	-7421,0
12.0	-399,5	-3310,9	-3709,95	-7420,3

9.4.4 Contribution to stabilizing moment

The horizontal contribution to the stabilizing moment is calculated by multiplying the support reaction in the top left with the arm towards the rotation point. In the model the top left support was placed at the height of the upper web. The distance from this web to rotation point, located at the bottom of the gate, is 21.66 m (=26−4.33m).

$$M_{sta:hor} = R_{h:TL} \cdot 21.66\ [m] \tag{9.10}$$

The vertical contribution results from the two couples of vertical support reactions on both ends of the gate. These couples work over an arm equal to the carriage width.

$$M_{sta:vert.} = W_{car} \cdot (R_{v2} + R_{v4}) \tag{9.11}$$

The total stabilizing moment is equal to

$$M_{sta:tot} = M_{sta:hor.} + M_{sta:vert.} \tag{9.12}$$

The following table and graph show the horizontal and vertical support reactions, both moment contributions and total stabilizing moments for all carriage widths.

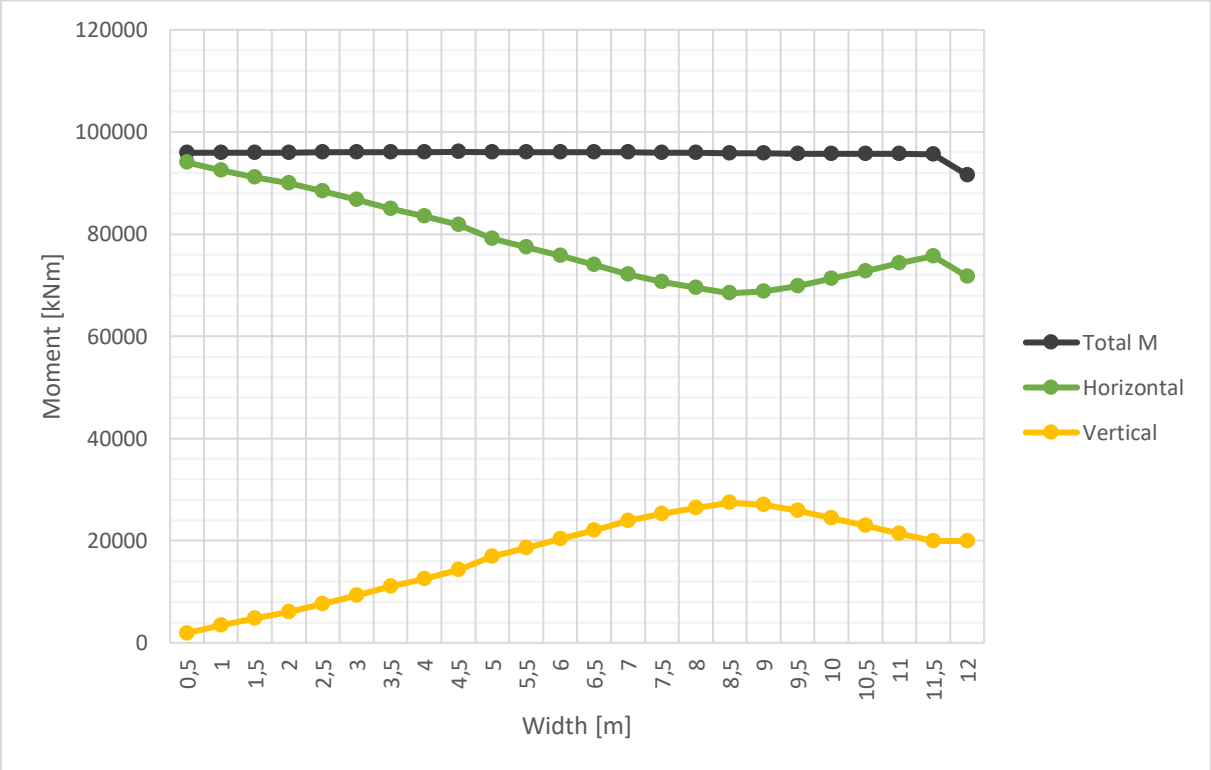

Figure 79. Graph - Stabilizing moment contributions

Table 32. Model 3b - Moment contributions

W_{car} [m]	TL [kN]	Rv2 [kN]	Rv4 [kN]	Hor. [kNm]	Vert. [kNm]	Total M [kNm]
0.5	-4341,4	1754,95	2059,63	94035	1907	95942
1.0	-4270,3	1586,66	1875,15	92495	3462	95957
1.5	-4209,8	1456,94	1733,35	91184	4785	95969
2.0	-4152,3	1373,59	1646,14	89939	6039	95979
2.5	-4080,3	1377,48	1667,72	88379	7613	95992
3.0	-4003,1	1392,57	1706,83	86708	9298	96006
3.5	-3921,0	1411,69	1757,1	84929	11091	96019
4.0	-3854,7	1383,18	1750,03	83492	12533	96025
4.5	-3777,6	1383,36	1789,05	81823	14276	96098
5.0	-3655,4	1437,97	1934,92	79176	16864	96040
5.5	-3576,3	1407,46	1970,64	77463	18580	96042
6.0	-3496,7	1366,33	2016,97	75739	20300	96039
6.5	-3417,7	1307,75	2076,9	74028	22000	96028
7.0	-3330,5	1223,13	2187,94	72138	23877	96015
7.5	-3263,7	1093,47	2277,22	70692	25280	95973
8.0	-3209,6	932,93	2365,89	69519	26391	95909
8.5	-3159,9	724,6	2500,33	68443	27412	95854
9.0	-3176,9	748,11	2251,34	68812	26995	95807
9.5	-3225,3	799,06	1927,95	69859	25907	95766
10.0	-3290,3	802,71	1644	71268	24467	95735
10.5	-3360,9	768,46	1413,23	72796	22908	95704
11.0	-3430,4	715,95	1227,51	74302	21378	95680
11.5	-3495,3	658,37	1076,69	75709	19953	95662
12.0	-3310,9	639,98	1016,76	71713	19881	91594

9.4.5 Deflection of unsupported corner

The carriage width also has an effect on the deflection of the top right corner. With a narrowing carriage width, the deflections become larger. The maximum allowed deflection of this corner including material factors, $\gamma_m = 1.62$ and $\gamma_c = 1.57$ see section 6.2.3, can be determined with

$$\frac{H}{200} \cdot \left(\frac{1}{\gamma_m \cdot \gamma_c}\right) = u_{y,TR:max}(200) = \frac{26000}{200} \cdot \left(\frac{1}{\gamma_m \cdot \gamma_c}\right) = 51.1\ mm$$

$$\frac{H}{250} \cdot \left(\frac{1}{\gamma_m \cdot \gamma_c}\right) = u_{y,TR:max}(250) = \frac{26000}{250} \cdot \left(\frac{1}{\gamma_m \cdot \gamma_c}\right) = 40.9\ mm \quad (9.13)$$

Depending on the chosen criteria, there is a limit to narrowing the carriage width. The table below presents the deflection of the unsupported (top right) corner in the y-direction for a number of carriage width.

Table 33. Deflection uy - unsupported corner

W_{car} [m]	**2**	**4**	**6**	**8**
Uy [mm]	53.8	44.0	32.2	22.2

The figure below shows the deflection in y-direction for a carriage width of 4 m. If a criteria of H/250 is applied, a carriage width of 4 m would not meet these requirements.

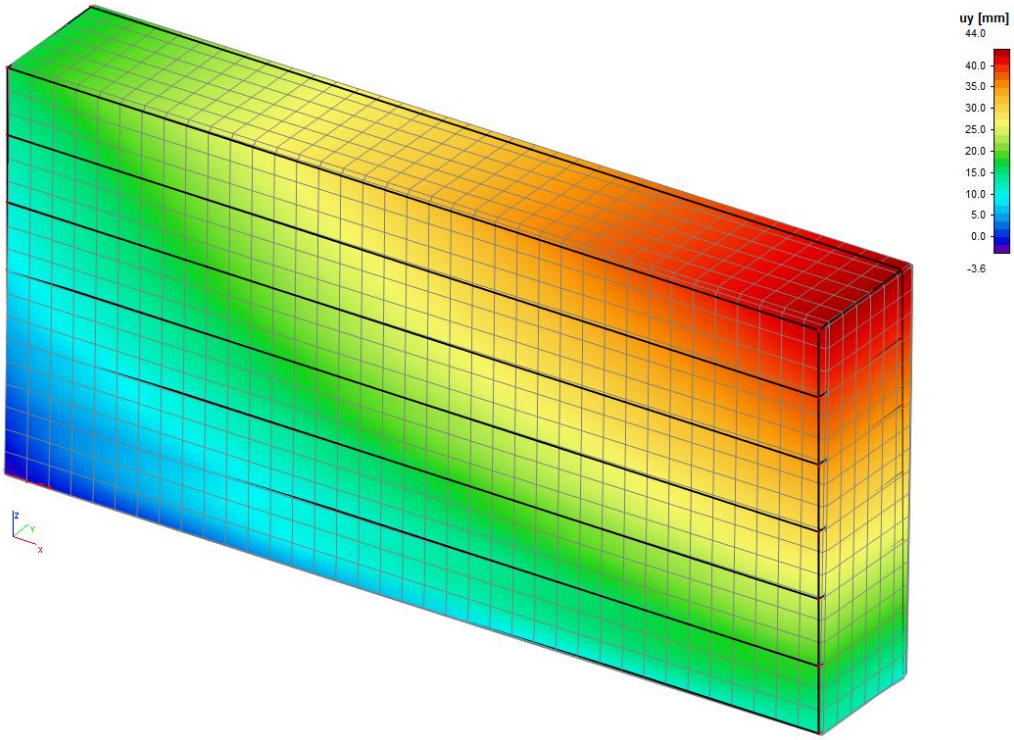

Figure 80. Model 3b - Deflection uy - Width 4 m

9.5 Dead weight vs. Δh

The hydrostatic load cases are added to the model as described in section 9.2.4. For each Δh the required dead weight is calculated with (9.7).

9.5.1 Added load cases

The hydrostatic pressure on the Western Scheldt side remains the same for all added Δh load cases. The water level and hydrostatic pressure are as follows

$$h_{WS} = 4 + h_{NAP} = 4 + 16.44 = 20.44\ m$$

$$p_{WS} = 203.72\ kN/m \tag{9.14}$$

The water levels and hydrostatic pressures on the lock chamber or channel side are calculated with

$$h_{Ch} = 4 - \Delta h + h_{NAP}$$

$$p_{Ch} = \rho_w \cdot g \cdot h_{Ch} \tag{9.15}$$

The results are presented in the table below. Calculations of all these values can be found in Appendix E.

Table 34. Δh - load cases

Δh [cm]	**H_{Ch} [m]**	**P_{Ch} [kN/m]**
5	20.39	203.23
10	20.34	202.73
15	20.29	202.23
20	20.24	201.73
25	20.19	201.23
30	20.14	200.73
35	20.09	200.24
40	20.04	199.74
45	19.99	199.24
50	19.94	198.74
55	19.89	198.24
60	19.84	197.74
65	19.79	197.25
70	19.74	196.75
75	19.69	196.25
80	19.64	195.75
85	19.59	195.25
90	19.54	194.75
95	19.49	194.26
100	19.44	193.76

9.5.2 Model 3c – results

The values in the table below are displayed in the graph in Figure 81. The graph shows the dead weight required for stability for the corresponding carriage width. The calculations of these values can be found in Appendix E.

Table 35. Required dead weight corresponding with carriage width

Δh [cm]	**5**	**10**	**15**	**20**	**25**	**30**	**35**	**40**	**45**	**50**
DW_{req} [kN]	16864	17529	18181	18820	19448	20063	20676	21268	21849	22418

Δh [cm]	**55**	**60**	**65**	**70**	**75**	**80**	**85**	**90**	**95**	**100**
DW_{req} [kN]	22976	23522	24065	24587	25098	25644	26130	26604	27075	27471

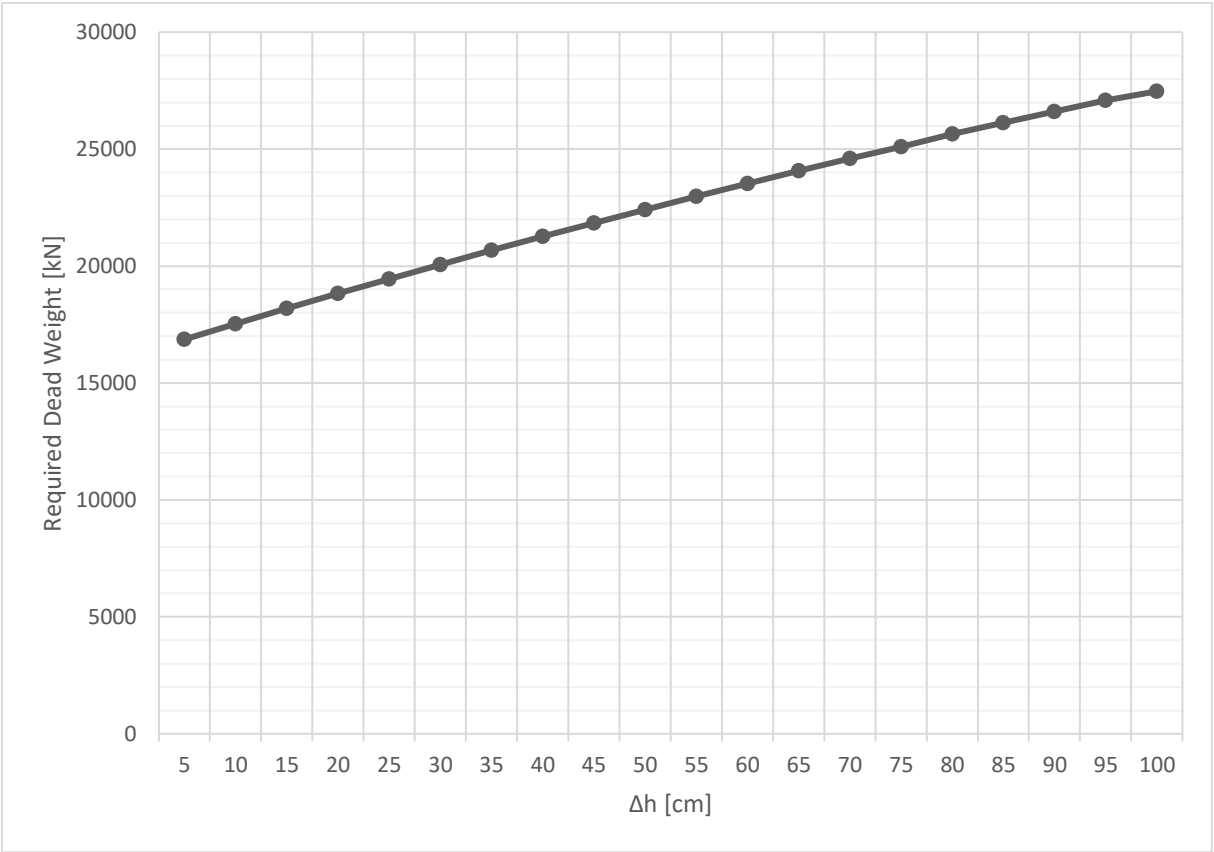

Figure 81. Graph – Dead Weight vs Δh

9.5.3 Conclusion – 3c

As expected, the graph shows that with an increasing Δh, the required dead load increases. However, this relation is not completely linear. It slowly levels off with in an increasing Δh. The difference in required weight between a remaining head difference of 5 cm and 30 cm is over 3000 kN, which is a significant difference. In practice, during operating conditions when stability is at risk. For instance during high water and high waves, the Δh could strictly be controlled and be kept limited to decrease the risk of instability.

It should be kept in mind that a large head difference will result in currents the moment the gate opens. With an increasing head difference, dynamics will become more important for the stability problem.

9.6 Key points

- The FRP box gate is found to be unstable as opposed to the hand calculation. This could be explained by deflections of the gate negatively affecting the stability of the gate.
- Increasing the distance between the carriage wheels results in a significant decrease of the required dead weight for stability. The moment remains equal, arm increases and thus the force decreases.
- The stability of the gate is achieved by the combined moments generated by the horizontal support reaction at the top left and couples of vertical support reactions. As a result narrowing the distance between the vertical support reactions, doesn't necessarily lead to an increase in the vertical reaction forces.
- Deflection of the unsupported corner essentially causes the gate to pivot around the top left and lower right supports. This reduces the load taken by the lower left support, eventually even switching direction. This in turn results in a significant increase of the horizontal moment contribution and reduction of the vertical moment contribution. This phenomenon could be taken advantage of to reduce the required dead weight.
- The horizontal moment contribution results in torsion in the gate.
- The chosen horizontal supports, rigid or flexible, have a considerable impact on the behaviour of the gate. Rigid supports will quickly shift the vertical to horizontal moment contributions when deflections increase, this could be taken advantage of to allow for a lighter gate. With flexible supports, this shift from vertical to horizontal decreases.

10 Potential improvements for stability

Concept development

In this chapter potential improvements or alternatives to the box gate are presented. The concepts are based on results found in previous chapters. The expected pros, cons and challenges are discussed. The shape of the gate is evaluated in more detail with 3D models. These models are referred to as model 4. Again, strength and deflection checks are performed on the gate in closed position loaded by the extreme positive and negative load combinations, and the stability of the gate during movement is evaluated. The stability load combination is modelled as presented in section 9.2.1. The results are compared to the original box shaped gate.

10.1 Evaluation of results

From all the results from previous chapters a number of conclusions can be drawn. With this information, concepts to improve the design of the box gate can be worked out. The conclusions are summarized below.

- The box gate is not the most efficient shape.
- Material is added just for weight to guarantee stability under all conditions.
- A minimum amount of weight is required to overcome buoyancy and sink the gate unto its supports. This is a limiting factor for weight reduction.
- A wider base, or a larger distance between vertical supports improves the stability of the gate during movement.
- The horizontal contribution to the stabilizing moment can play a large role in the gates stability.
- Strength and deflection criteria require a lot less material and a smaller gate thickness. The chosen stability criteria lead to very conservative dimensions of the gate.
- Deflection and deformation of the gate affect the distribution of loads over the supports.
- The box shape results in a large buoyancy force working on the gate. An alternative shape could reduce this force considerably. The buoyancy forces calculated for the box gate are presented in the next section.

Buoyancy forces – box gate

To calculate the buoyancy forces working on the gate the volume of displaced water is calculated. The water level of +4 m NAP is used in this calculation, because this is the maximum water level during movement. The density of water is

$$\rho_w = 1016\ kg/m^3 \tag{10.1}$$

Displaced water volume equals

$$V_{buo-box} = L \cdot W \cdot H = 55 \cdot 8.96 \cdot 20.44 = 10073\ m^3 \tag{10.2}$$

This results in a total buoyancy force of

$$F_{buo-box} = V_{buo-box} \cdot \rho_w \cdot g/1000 = 100396\ kN \quad (10.3)$$

10.2 Potential improvements/alternatives

Based on the results the following possible improvements/alternatives to the box gate design are introduced.

- Optimize the shape of the gate
  - Wide base – narrow top
  - Varying gate thickness over the gate span
  - Asymmetrical shape to manipulate the distribution of loads over the supports.
- Buoyancy-based stability
- Asymmetrical distribution of material and/or ballast

10.2.1 Shape of the gate

Possible changes to the gate shape are listed below.

- Wider base to improve stability
- Narrow towards the top to reduce buoyancy
- Further narrowing of the gate to reduce buoyancy forces by strengthening the internal support structure of the gate, e.g. by adding a number of vertical slabs or a truss structure.
- Vary the thickness of the gate over the span; wide at both ends, to accommodate wide support carriages; narrow where the strength and deflection criteria allows it; slightly wider at mid-span where the largest deflection occurs in closed position.

10.2.1.1 Varying thickness over height

Many shape variations can be applied for the gates cross-section. The two criteria are a wide base and a narrow top. The base-top transition can be gradual or abrupt, straight or curved. A gradual transition would also lead to a more gradual stress distribution. An abrupt transition would lead to a more concentrated stress at the transition. The objective is to reduce the thickness as much as the strength and deflection criteria allow to maximize the reduction of buoyancy forces. Figure 82 displays a few of the many potential shapes. Any variation is possible and should optimized for the requirements of a specific gate.

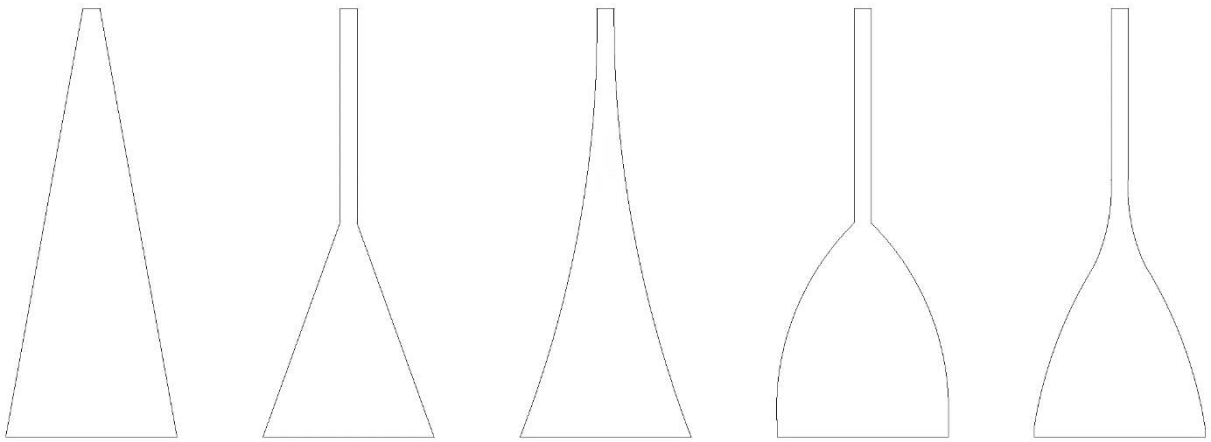

Figure 82. Potential wide base gate shapes

10.2.1.2 Varying thickness over the span

The gate is not required to have an equal thickness over the entire span of the gate. It might be beneficial to have a gate that is thicker at mid-span and gradually gets narrower towards either end. However, at both ends, the gate must be wide enough to accommodate the support carriages.

10.2.1.3 Pros and cons

The expected pros and cons of the wide base-narrow top shape are as follows.

Pros

- Significant increase of the stability
- Significant decrease of buoyancy forces, resulting in less required ballast.
- More efficient design, so less material wasted.

Cons

- Weight reduction remains limited because the gate must overcome the buoyancy.
- The narrow top leaves the gate vulnerable for vessel collisions. A solution should be implemented to achieve fast dissipation of significant amounts of energy, which is involved during a vessel collision.
- More complex lock head design.

10.2.2 Buoyancy-based stability

As opposed to gravity-based stability, where the gates stability is achieved by a certain overweight, buoyancy-based stability could be applied. The gate, by adding ballast, is sunk into position and 'hooked' on the supports. When the ballast is removed, the buoyancy forces on the gate will be greater than its gravity forces. The gate wants to float up, but this is now prevented by the supports.

The stability calculation will generally be the same as the gravity-based gate. However instead of a certain overweight, the buoyancy must meet a minimum requirement. Obviously a lighter gate would be beneficial and this is where the full potential of the lightweight qualities of FRP might be achieved.

A challenge is the support system. Most importantly: How are you going to 'hook' the gate to its supports? Just like the roller carriages, the wear-and-tear and required maintenance should be kept minimal. The gate must form a strong connection to the support system, but should be able to disconnect for maintenance, repairs or replacement. The support system could be integrated in the gate, i.e. the gate hooks onto the rail. Or a separate system, similar to a roller carriage, hooks onto the rail and the gate connects to this separate support system.

Figure 83 shows a simplification of the buoyancy-based concept. This is a very interesting solution for the lightweight versus stability problem and should be investigated in detail. However, this is outside of the scope of this thesis.

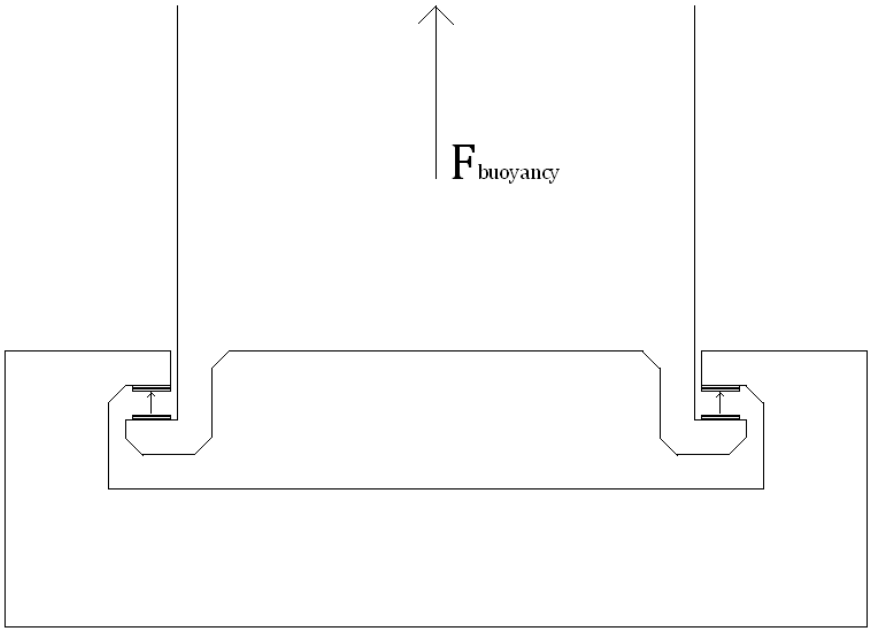

Figure 83. Buoyancy-based support system

10.2.2.1 Pros and cons

The expected pros and cons of the buoyancy-based stability concept are as follows.

Pros

- Weight reduction of the gate is not limited by buoyancy forces that have to be overcome.
- The lightweight properties of FRP can potentially be optimized, because the stability improves with a reducing self-weight.

Cons

- More complex support system.
- Maintenance is more difficult to perform.
- Getting the gate into position is more challenging.

10.2.3 Asymmetrical distribution

Lock gates are generally loaded differently from either side and therefore don't necessarily have to be symmetrical. The gate could be designed with more or heavier material on one side. This would result in an uneven distribution of the self-weight, generating a stabilizing couple which could benefit the stability during movement. This uneven distribution could also be achieved by an asymmetrical distribution of ballast.

10.2.3.1 Pros and cons

The expected pros and cons of an asymmetrical ballast or material distribution are as follows.

Pros

- Relatively simple way to increase the stability.
- Ballast can be changed according to the circumstances in real-time.

Cons

- For either case, uneven distribution also means uneven settlements or wear-and-tear. This could be a bigger problem than the initial stability problem.

10.2.4 Combination

Improvements and alternatives could be combined to find an optimum solution.

10.3 Model 4 - Wide base gate

To investigate the impact of a wide base gate to the stability during movement a number of 3d models are made with Scia Engineer. The designs are kept relatively simple and the dimensions are not optimized. The same material and laminate properties as for the box gate are applied. The objective here is not to find the very best solution, but evaluate the impact of changes in the gates design on the stability of the gate during movement.

10.3.1 Model 4a – 4b

The first two design are similar to each other. Both are narrow at the top half of the gate, 2 m, and then get wider towards the base, 12 and 10 m respectively. The base dimensions are rather extreme and may not necessarily be the optimum solution, but it will give an interesting result to evaluate the impact of the wider base.

10.3.1.1 Global dimensions

The cross-sections of model 4a and 4b are presented in Figure 84. The dimensions are given in meters. The required thickness or the height where the transition starts are estimated based on strength and deflection results from chapter 8.

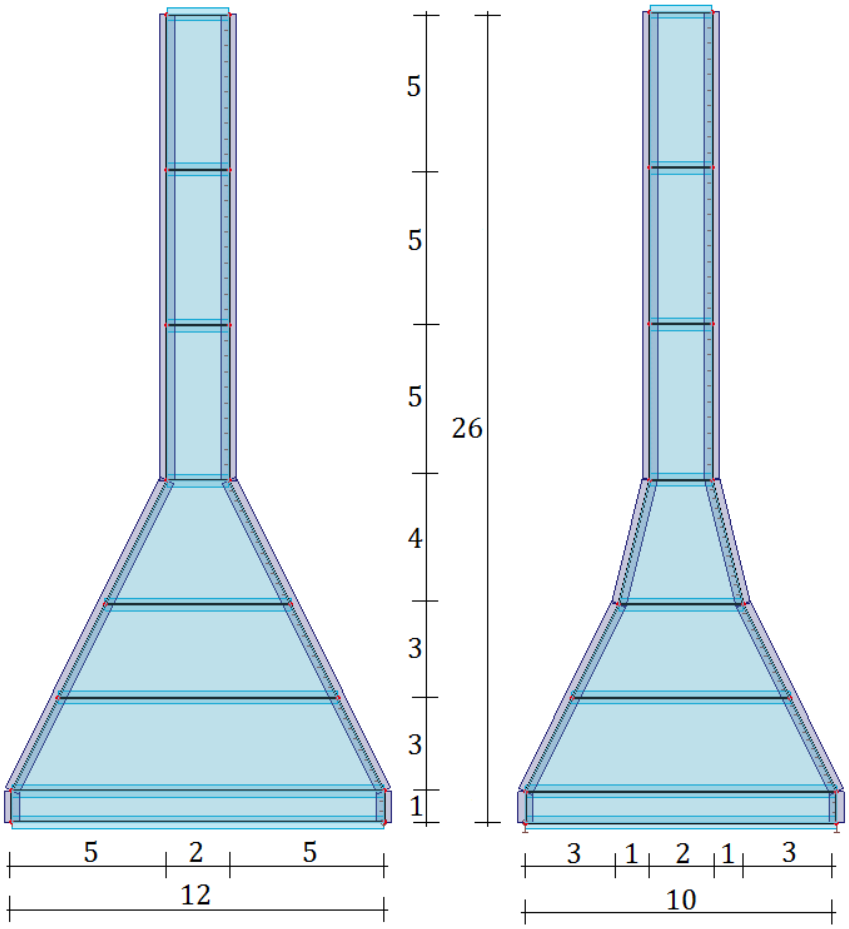

Figure 84. Model 4a (left) and 4b (right) - cross-section

Similar to the box gate, only horizontal webs are applied to allow for a better comparison to the box gate.

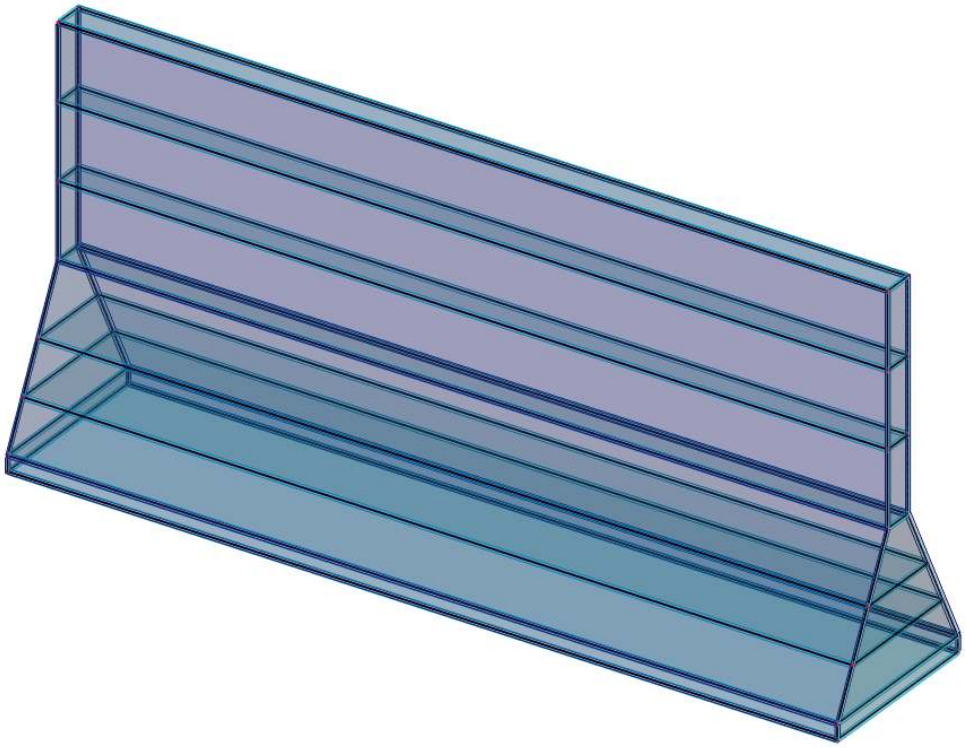

Figure 85. Model 4a - Overview

10.3.1.2 Closed gate checks

From the models, the maximum stresses in the various structural elements are found. The results are presented in Table 36 and Table 37.

Model 4a

Table 36. Model 4a - stress results

	σ_x $[N/mm^2]$	σ_y $[N/mm^2]$	τ_{xy} $[N/mm^2]$
Retaining plate			
Max	96.6	65.3	22.8
Model	10.4	7.8	3.9
Unity checks	0.11	0.12	0.17
Webs			
Max	62.8	62.8	23.8
Model	10.4	7.3	3.3
Unity checks	0.17	0.12	0.14
End plate			
Max	55.0	55.0	27.9
Model	6.8	7.3	4.6
Unity checks	0.12	0.13	0.16

Model 4b

Deflection criteria of section 8.2.1 are met, see the figure below.

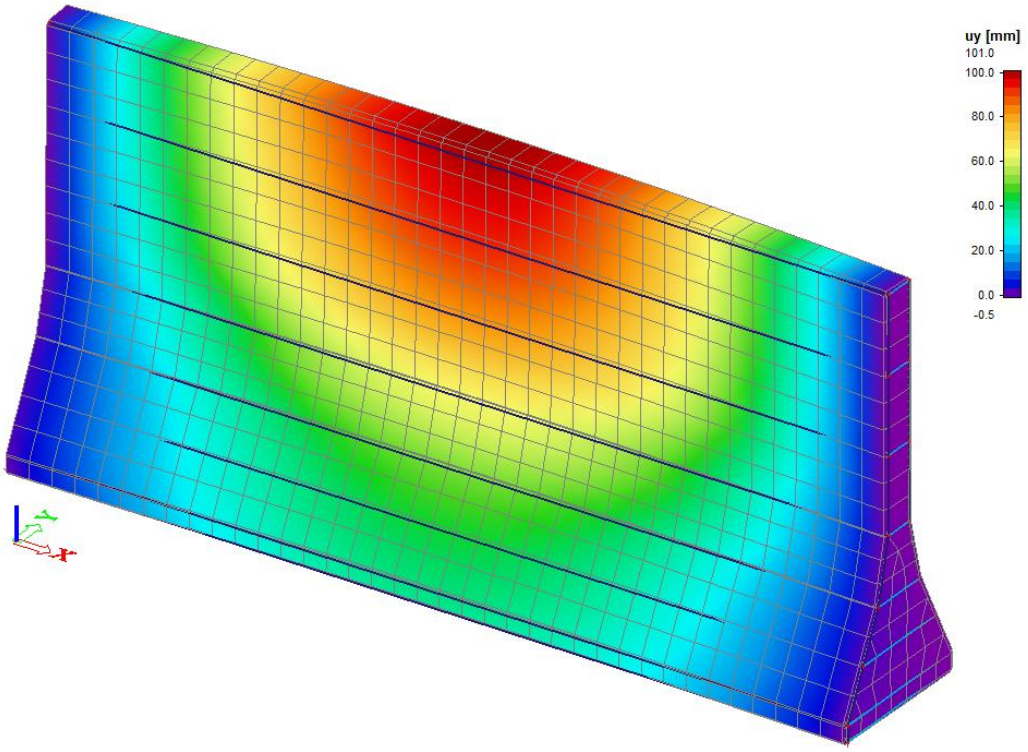

Figure 86. Model 4b - Deflection uy - Gate in closed position

For both gates, it can be seen that the stress criteria are still easily met. The main reason for this is that the laminate properties of all structural elements are on the conservative side.

Table 37. Model 4b - stress results

	σ_x $[N/mm^2]$	σ_y $[N/mm^2]$	τ_{xy} $[N/mm^2]$
Retaining plate			
Max	96.6	65.3	22.8
Model	13.8	7.2	4.5
Unity checks	0.14	0.11	0.20
Webs			
Max	62.8	62.8	23.8
Model	13.8	8.6	3.9
Unity checks	0.22	0.14	0.16
End plate			
Max	55.0	55.0	27.9
Model	9	8.6	8.2
Unity checks	0.16	0.16	0.29

10.3.1.3 Stability check

The stability of the gate during movement is evaluated with the same approach that was used for the box gate, see section 9.1. The support reactions from model 4a and 4b are presented in Table 38 and Table 39 respectively.

Model 4a

Table 38. Model 4a - support reactions

	Total incl. SW	Total excl. SW
Vertical	**[kN]**	**[kN]**
R_{V1}	3577.69	-494.28
R_{V2}	4588.49	494.28
R_{V3}	1115.83	-2963.64
R_{V4}	7050.35	2963.64
Horizontal		
$R_{H;LL}$	-1231.39	-1223.33
$R_{H:TL}$	-2633.66	-2641.69
$R_{H:LR}$	-3865.02	-3865.02

From the model, the following self-weight is found

$$SW = 25127\ kN \tag{10.4}$$

Applying the applicable partial factors and deducting buoyancy, the remaining dead weight is

$$DW = 16332\ kN \tag{10.5}$$

The value for the x (distance to point of action) is found to be,

$$x = 2.55\ m \tag{10.6}$$

With a distance between the support reaction at 12 m the following applies

$$\frac{2.55}{(12/6)} = 1.28 > 1.00 \tag{10.7}$$

With the chosen stability criteria, the gate is not stable.

Required dead weight is calculated

$$DW_{req} = 20748\ kN \tag{10.8}$$

Model 4b

Table 39. Model 4b - support reactions

	Total incl. SW	Total excl. SW
Vertical	**[kN]**	**[kN]**
R_{V1}	3151.36	-494.28
R_{V2}	4277.31	494.28
R_{V3}	202.33	-2963.64
R_{V4}	7226.67	2963.64
Horizontal		
$R_{H;LL}$	-1173.97	-1223.33
$R_{H:TL}$	-2639.81	-2641.69
$R_{H:LR}$	-3812.82	-3865.02

From the model, the following self-weight is found

$$SW = 22858\ kN \tag{10.9}$$

Applying the applicable partial factors and deducting buoyancy, the remaining dead weight is

$$DW = 14858\ kN \tag{10.10}$$

The value for the x is found to be,

$$x = 2.74\ m \tag{10.11}$$

With a distance between the support reaction at 10 m the following applies

$$\frac{2.55}{(10/6)} = 1.65 > 1.00 \tag{10.12}$$

With the chosen stability criteria, the gate is not stable.

Required dead weight is equal to

$$DW_{req} = 24368\ kN \tag{10.13}$$

10.3.1.4 Buoyancy forces

The buoyancy forces working on the gate during maximum operating water conditions are calculated.

Model 4a

Displaced water volume equals

$$V_{buo-4a} = 55 \cdot \left(12 \cdot 1 + 2 \cdot \tfrac{1}{2} \cdot 5 \cdot 10 + 2 \cdot 19.44\right) = 5548\ m^3 \tag{10.14}$$

This results in a total buoyancy force of

$$F_{buo-4a} = V_{buo-4a} \cdot \rho_w \cdot g/1000 = 55301\ kN \tag{10.15}$$

Model 4b

Displaced water volume equals

$$V_{buo-4b} = 55 \cdot \left(10 \cdot 1 + 2 \cdot \tfrac{1}{2} \cdot 3 \cdot 6 + 2 \cdot \tfrac{1}{2} \cdot 1 \cdot 4 + 4 \cdot 6 + 13.44 \cdot 2\right) = 4558\ m^3 \tag{10.16}$$

This results in a total buoyancy force of

$$F_{buo-4b} = V_{buo-box} \cdot \rho_w \cdot g/1000 = 45433\ kN \tag{10.17}$$

10.3.1.5 Lock head

One major challenge that arises with this gate shape is the lock head. Instead of simple straight walls, the lock head must now accommodate a gate which is drastically wider at the bottom in comparison to the top.

- If the head would follow the shape of the gate, getting the gate into position would be significantly more difficult. The gate could not be floated into the gate chamber and simply be sunk into position, because the wide base would not fit through the narrow top.
- If the lock head would just have straight walls, some type of construction must be applied to connect the gate to the walls of the lock head to achieve horizontal supports.

10.3.2 Conclusion 4a & 4b

A wider base improves the stability, but does not necessary reduce the overweight required to achieve stability. The shape of the gate affects how the loads are distributed over all the supports.

The box shape results in a much larger horizontal support reaction at the top left support. A narrow top and a wide base shape results in a much larger horizontal support reaction in the lower left support. The lower left horizontal support reaction doesn't contribute to a stabilizing moment as opposed to a large contribution of the top left support. In this case study the top left support has a particularly large contribution to the stabilizing moment, because the gate is relatively high. This results in a large arm for the stabilizing moment of the top left support.

The buoyancy forces are reduced significantly compared to the box gate. For model 4b the force is reduced to 45% of the box gate value.

10.3.3 Model 4c

In this design the gate thickness will vary over both the height and the span of the gate. Again, the same laminate properties are applied for all structural elements; retaining plates, webs and end plates.

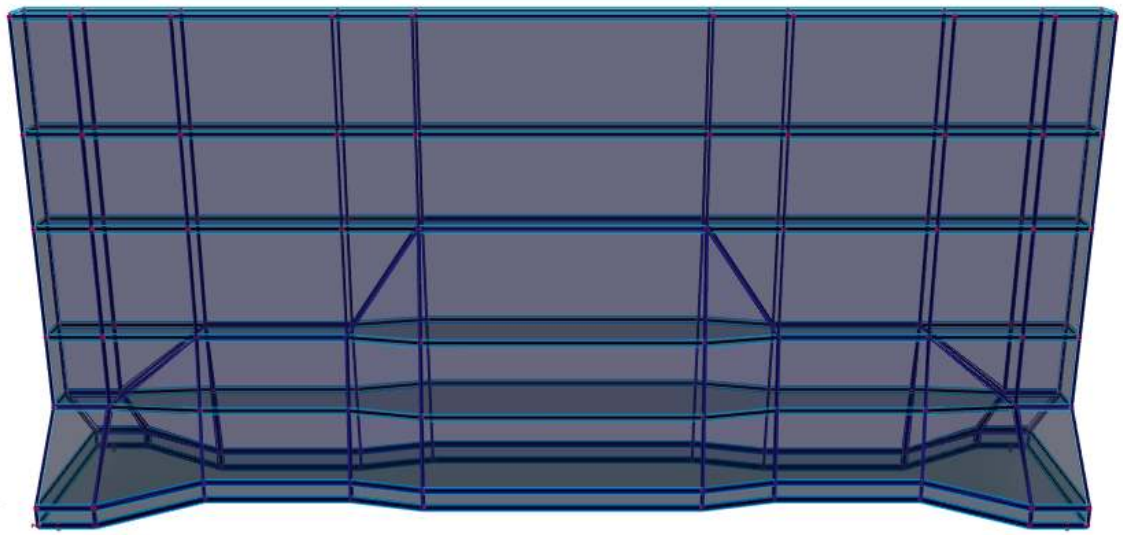

Figure 87. Model 4c - Front view

10.3.3.1 Global dimensions

Dimensions are chosen based on the results found with previous calculations and models. The shape of the gate is not optimized. It's only to get an idea of the effects of the change of shape. In Figure 88 the gate is viewed from the side.

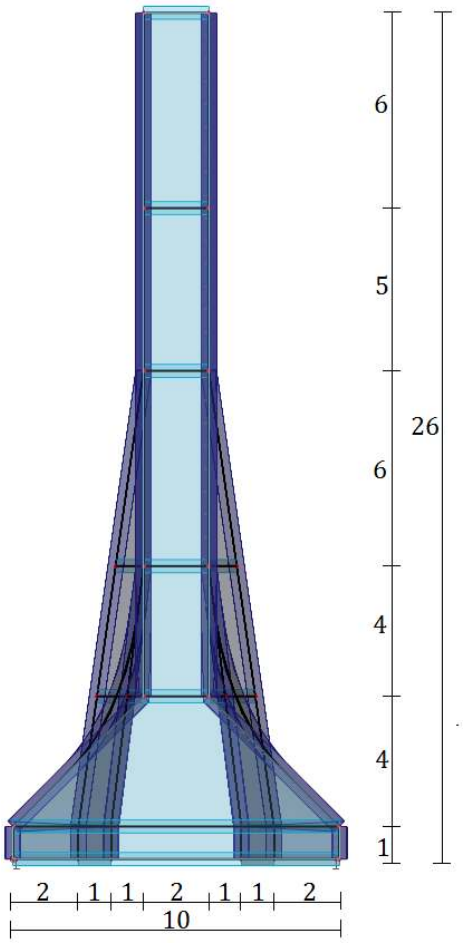

Figure 88. Model 4c - side view

In Figure 89 the gate is viewed from the top. This particular shape was chosen because,

- Very wide at both ends to accommodate for a wide carriage width.
- Quickly narrowing the width to reduce buoyancy.
- Slightly wider at mid-span to meet strength and deflection criteria.

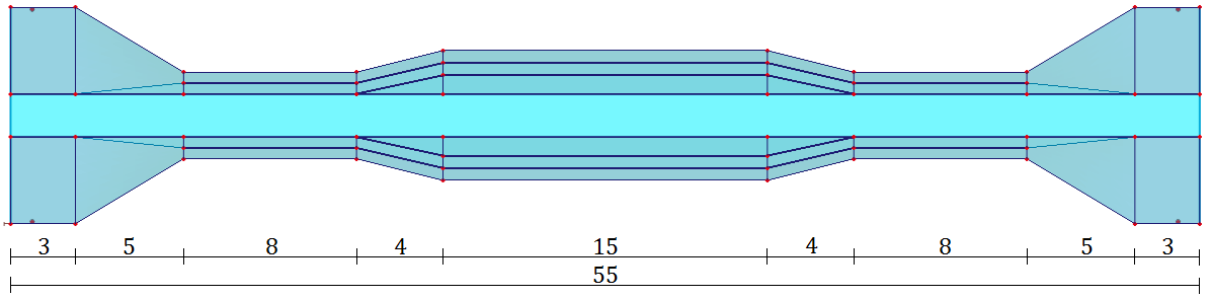

Figure 89. Model 4c - top view

10.3.3.2 Closed gate checks

The deflection criteria are not met. This could be solved by improving the laminate properties, mainly of the retaining plates at mid-span. The gate shape could also be changed to increase the thickness, again mainly around mid-span.

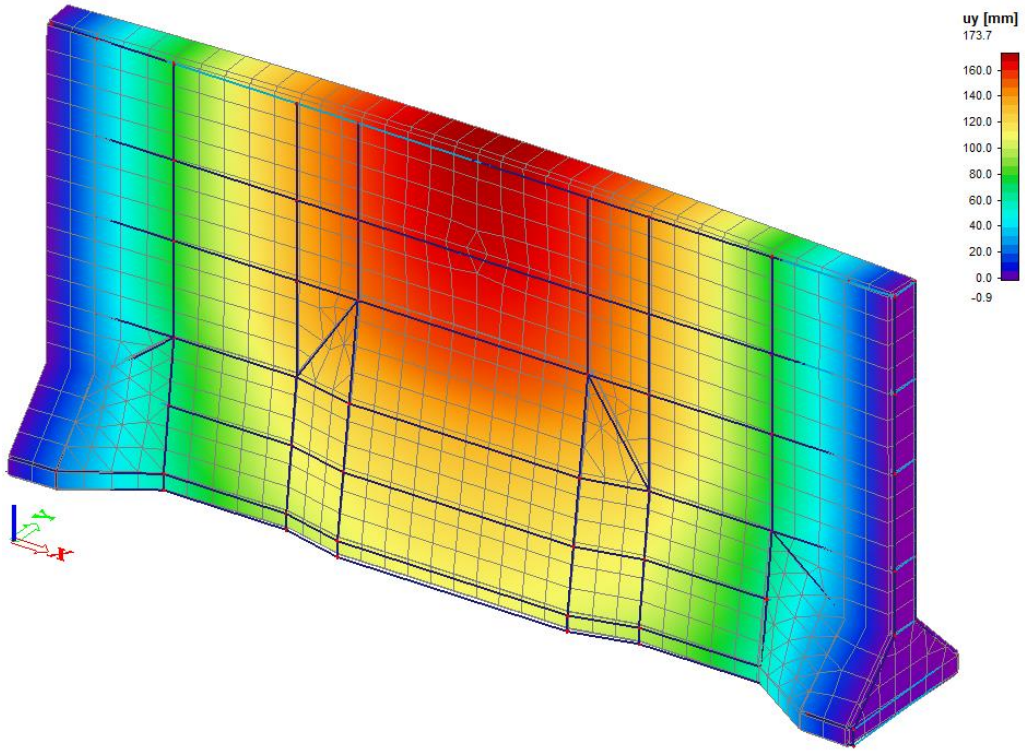

Figure 90. Model 4c - Deflection uy - Gate in closed position

The stress results are presented in the table below. In Figure 91 the stresses in the x-direction I the retaining plates are presented. It can be observed that the largest stresses occur in areas where the gate transitions between different cross-sectional shapes.

Table 40. Model 4c - stress results

	σ_x $[N/mm^2]$	σ_y $[N/mm^2]$	τ_{xy} $[N/mm^2]$
Retaining plate			
Max	96.6	65.3	22.8
Model	31.1	10.1	6
Unity checks	0.32	0.15	0.26
Webs			
Max	62.8	62.8	23.8
Model	26.2	13.8	7.1
Unity checks	0.42	0.22	0.30
End plate			
Max	55.0	55.0	27.9
Model	10.4	6.2	4.2
Unity checks	0.19	0.11	0.15

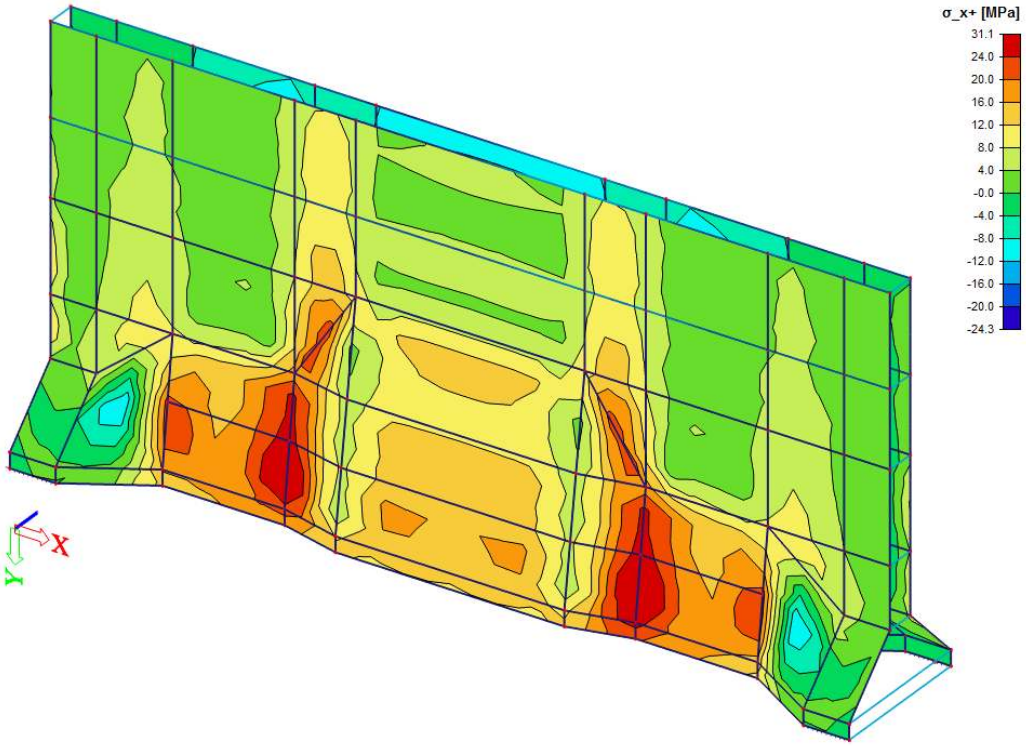

Figure 91. Model 4c - sigmaX - retaining plates

10.3.3.3 Stability check

Again, the stability of the gate is evaluated. When comparing the results of the various gates, it should be kept in mind that there are significant differences in the self-weight of the gates.

Table 41. Model 4c - support reactions

	Total incl. SW	**Total excl. SW**
Vertical	**[kN]**	**[kN]**
R_{V1}	2500.36	-723.91
R_{V2}	3974.89	723.91
R_{V3}	177.41	-3054.26
R_{V4}	6297.79	3054.26
Horizontal		
$R_{H;LL}$	-1036.52	-1027.8
$R_{H:TL}$	-2732.52	-2741.24
$R_{H:LR}$	-3767.98	-3767.98

From the model, the following self-weight is found

$$SW = 19924\ kN \tag{10.18}$$

Applying the applicable partial factors and deducting buoyancy, the remaining dead weight is

$$DW = 12950\ kN \tag{10.19}$$

The value for the x is found to be,

$$x = 2.93\ m \tag{10.20}$$

With a distance between the support reaction at 10 m the following applies

$$\frac{2.55}{(10/6)} = 1.76 > 1.00 \tag{10.21}$$

With the chosen stability criteria, the gate is not stable.

Required dead weight is equal to

$$DW_{req} = 22669\ kN \tag{10.22}$$

10.3.3.4 Buoyancy

Model 4c

Viewed from the top, see Figure 89, the gate can be mirrored through the centre. One half of the gate can be split into 5 sections with different cross-sections. Three constant sections (I,II,III) and two sections (IV,V) that form the transitions I-II and II-III. The displaced volumes are calculated separately for each section.

Displaced water volumes of the separate section are found to be

$$V_I = 3 \cdot \left(10 \cdot 1 + 2 \cdot \tfrac{1}{2} \cdot 4 \cdot 4 + 19.44 \cdot 2\right) = 195\ m^3 \tag{10.23}$$

$$V_{II} = 8 \cdot \left(4 \cdot 1 + 2 \cdot \tfrac{1}{2} \cdot 1 \cdot 8 + 19.44 \cdot 2\right) = 407\ m^3 \tag{10.24}$$

$$V_{III} = 7.5 \cdot \left(6 \cdot 1 + 2 \cdot \tfrac{1}{2} \cdot 2 \cdot 14 + 19.44 \cdot 2\right) = 547\ m^3 \tag{10.25}$$

$$V_{IV} = \tfrac{5}{2} \cdot \left(\tfrac{V_I}{3} + \tfrac{V_{II}}{8}\right) = 289\ m^3 \tag{10.26}$$

$$V_V = \tfrac{4}{2} \cdot \left(\tfrac{V_{II}}{8} + \tfrac{V_{III}}{7.5}\right) = 248\ m^3 \tag{10.27}$$

The total displaced volume equals

$$V_{buo-4c} = V_I + V_{II} + V_{III} + V_{IV} + V_V = 3370\ m^3 \tag{10.28}$$

This results in a total buoyancy force of

$$F_{buo-4b} = V_{buo-4c} \cdot \rho_w \cdot g/1000 = 33593\ kN \tag{10.29}$$

10.3.4 Conclusion 4c

The required dead weight did not reduce as expected in comparison to the box gate. When comparing the support reactions it can be seen that the horizontal support reaction in the top left is considerably larger for the box design. For all designs with a wider base, this means that the horizontal contribution to the stabilizing moment is reduced. The total moment remains the same, so the difference must be taken by a larger vertical contribution. The increased stability due to a wide base is negated by a larger vertical couple to achieve stability. The result is that the required weight is not reduced.

A positive aspect of this design is that the buoyancy force is reduced to a third of the original box gate value.

10.3.5 Model 4d

One final shape alternative is investigated. In this case, the thickness of the gate is not varied over the height, but only over the span. The gate is relatively narrow at the gate chamber end and gradually widens towards the opposite end. The expected result is that the horizontal contribution to the stabilizing moment remains rather large and that the increased width on the opposite end benefits the required vertical couple. The figure below gives an overview of model 4d.

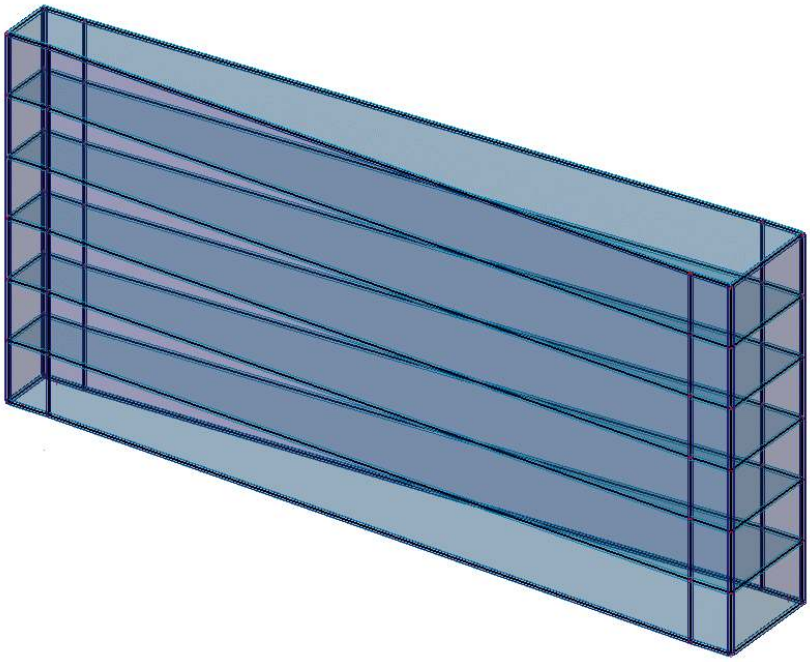

Figure 92. Model 4d - Overview

10.3.5.1 Global dimensions

In Figure 93 the gate is viewed from the top.

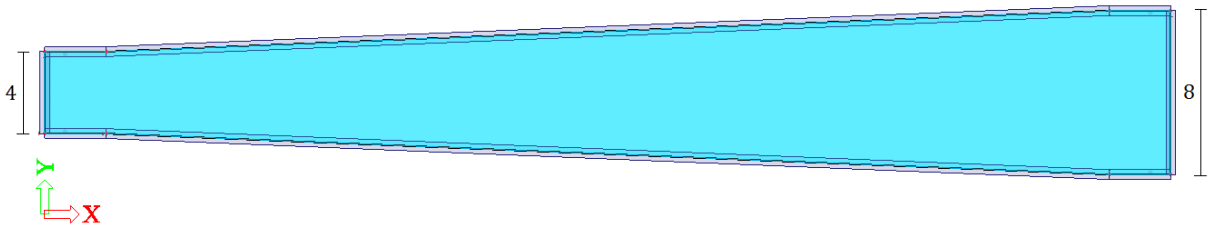

Figure 93. Model 4d - Top view

10.3.5.2 Closed gate checks

Table 42. Model 4d - stress results

	σ_x $[N/mm^2]$	σ_y $[N/mm^2]$	τ_{xy} $[N/mm^2]$
Retaining plate			
Max	96.6	65.3	22.8
Model	10.4	7.2	4.3
Unity checks	0.11	0.11	0.19
Webs			
Max	62.8	62.8	23.8
Model	8.5	4.7	4.5
Unity checks	0.14	0.07	0.19
End plate			
Max	55.0	55.0	27.9
Model	7.6	6.7	3.6
Unity checks	0.14	0.12	0.13

10.3.5.3 Stability

As expected, the distribution of loads over the horizontal supports (highlighted in green) is beneficial for the horizontal contribution to the stabilizing moment. It's interesting to see, that this primarily affects the vertical support reactions on the left side (highlighted in yellow). The distribution of self-weight over the vertical supports is also affected by the change in shape. The narrow end results in a considerably uneven distribution, negatively impacting the stability.

Table 43. Model 4d - support reactions

	Total incl. SW	Total excl. SW
Vertical	**[kN]**	**[kN]**
R_{V1}	3224.7	-206.2
R_{V2}	4150.51	206.2
R_{V3}	741.43	-3541.8
R_{V4}	7678.94	3541.8
Horizontal		
$R_{H;LL}$	-613.11	-594.39
$R_{H:TL}$	-3100.13	-3118.85
$R_{H:LR}$	-3713.35	-3713.35

In the figure below the distribution of the self-weight over the vertical supports is shown.

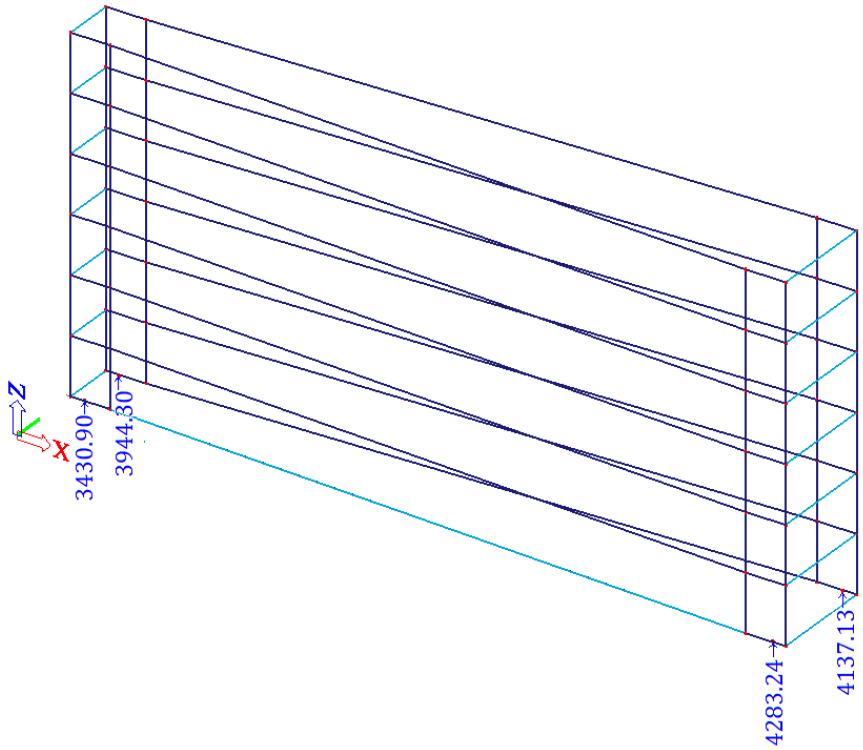

Figure 94. Model 4d - Support reactions Rz due to Self-Weight only

From the model, the following self-weight is found

$$SW = 24301\ kN \tag{10.30}$$

Applying the applicable partial factors and deducting buoyancy, the remaining dead weight is

$$DW = 15796\ kN \tag{10.31}$$

The value for x is calculated slightly different, because the carriage widths on either end is different. The value for the x is found to be,

$$x = 1.87\ m \tag{10.32}$$

With a distance between the support reaction at 10 m the following applies

$$\frac{1.87}{(8/6)} = 1.41 > 1.00 \tag{10.33}$$

With the chosen stability criteria, the gate is not stable.

Required dead weight is equal to

$$DW_{req} = 21869\ kN \tag{10.34}$$

10.3.5.4 Buoyancy

Model 4d

Displaced water volume equals

$$V_{buo-4d} = (3 \cdot 4 + 3 \cdot 8 + 49 \cdot 6) \cdot 20.44 = 6745\ m^3 \tag{10.35}$$

This results in a total buoyancy force of

$$F_{buo-4d} = V_{buo-4d} \cdot \rho_w \cdot g/1000 = 67229\ kN \tag{10.36}$$

10.3.6 Conclusion 4d

The change in shape of the gate had the expected effects on the distribution of loads over the supports. However, the dimensions were clearly not optimal. The width of the gate on the narrow end should be larger. This should even out the distribution of self-weight over the vertical supports, without too much impact on the horizontal distribution.

On the opposite end, a wider base-narrow top cross-section could be applied. This would benefit the vertical support reactions by increasing the arm of the couple. The transition from one end to the other requires optimization. This is outside of the scope of this thesis.

10.4 Stabilizing moment contributions

In the following table the horizontal and vertical moment contributions are compared for the various gate designs. The gates have different shapes and as a result the horizontal loads (hydrostatic and wave pressures) work over slightly different surface areas. This explains the differences between the values of the total stabilizing moments. The calculations of the moments is the same as in chapter 9, section 9.4.4. Except for the vertical contribution of model 4d, because the widths are different on both ends of the gate and therefor a different arm for the couple applies, 4 and 8 m respectively.

Table 44. Moment contributions - comparison of models

Gate	Width [m]	LL [kN]	TL [kN]	Rv2 [kN]	Rv4 [kN]	Hor. [kNm]	Vert. [kNm]	Total M [kNm]
3a	8	-501	-3210	933	2366	69519	26391	95909
4a	12	-1231	-2634	494	2964	57045	41495	98540
4b	10	-1174	-2640	553	3509	57178	40613	97792
4c	10	-1037	-2733	724	3054	59186	37782	96968
4d	4 - 8	-613	-3100	206	3542	67149	29159	96308

The figure below presents the vertical and horizontal contribution and the combined total stabilizing moments for the various gate designs.

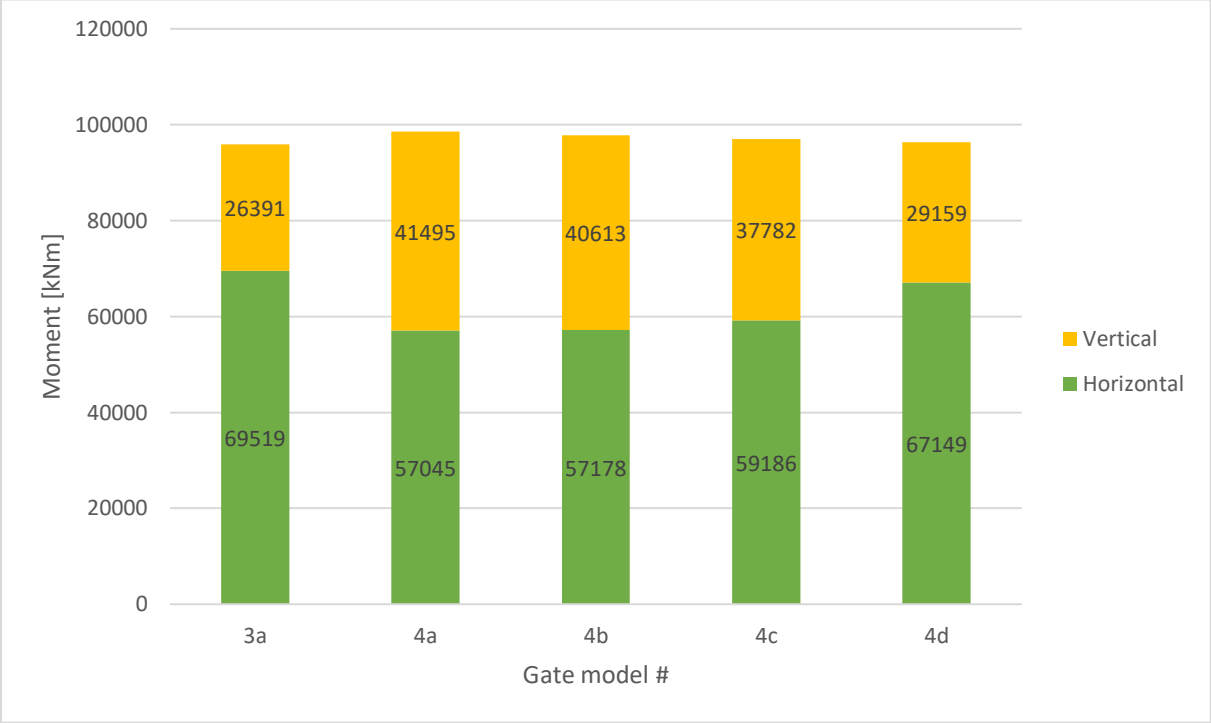

Figure 95. Graph - Vertical and horizontal contributions to moment

10.5 Deflection of unsupported corner

The shape of the gate plays a large part in the deflections of the gate. The largest deflections in the y-direction are checked for all models and compared to the box gate.

Table 45. Deflection uy - unsupported corner

Gate	uy [mm]	x-coordinate of uy [m]
3a	22.2	55.00
4a	30.0	37.16
4b	34.5	37.16
4c	55.0	39.00
4d	20.8	41.61

An interesting result is the deflection of model 4d, compared to the box gate. The average width over the span of the gate is much smaller than the box gate, yet the deflection that occurs is smaller.

The model results of the deflection in y-direction of all the models can be found in Appendix F.

10.6 Dynamics

In this research, the stability of the gate during movement was evaluated as a static problem. However, since the gate is in motion, dynamics can play an important role in the gates stability. A number of dynamic phenomena could be of importance for the stability of the gate during movement.

- Added mass
- Vessel collision
- Vortex induced vibrations
- Vibrations due to waves

With the Scia models, modal analysis can be performed and the eigenvalues of the various gate designs can be determined. It should be noted that a structure behaves differently when it is surrounded by water. For example, added mass resulting from the water that moves with the structure. This added mass can affect the eigenfrequencies of the structure. The added mass should also be taken into account when dimensioning the operating machinery. The forces exerted on the gate when pulled through the water play an important role in the stability.

The table shows 10 eigenmodes with the corresponding eigenfrequencies [Hz].

Table 46. Eigenfrequencies of the various models

	3a	4a	4b	4c	4d
1	1.89	1.72	1.74	1.54	1.95
2	2.64	2.31	2.31	2.18	2.76
3	3.45	3.46	3.55	2.87	3.75
4	4.63	4.39	4.39	4.13	4.69
5	6.41	5.96	5.97	5.69	7.37
6	8.41	6.46	6.81	6.45	9.07
7	9.52	8.71	8.44	7.79	9.20
8	10.67	9.23	9.03	9.10	10.51
9	10.81	10.27	11.40	10.50	11.43
10	12.73	11.84	12.27	11.28	12.50

10.6.1 Moving through the water

When the gate is pulled through the water, very large volumes of water are pushed out of the way. This causes turbulence and the creation of vortices along the gate. If the frequency of the vortex induced vibrations coincide with the eigenfrequency of the gate, these vortices can have a negative effect on the stability. This phenomenon is schematized in Figure 96.

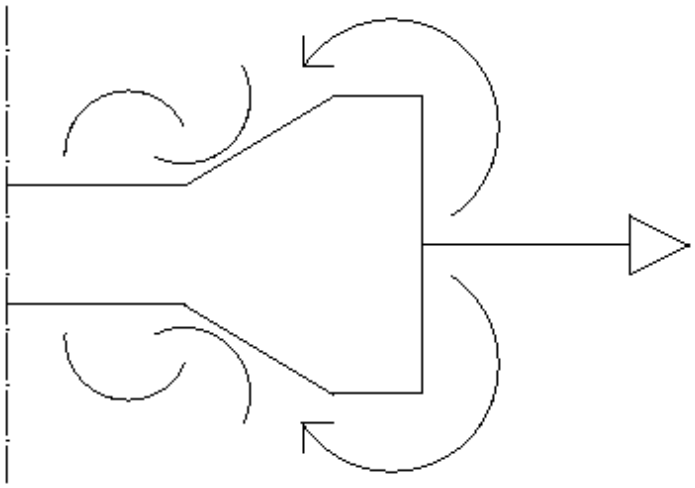

Figure 96. Gate moving through water (top view)

The vortex shedding frequency can be estimated with the so-called Strouhal number. Generally, Strouhal is used to calculate vortex shedding around an object in a flow. So the situation is somewhat reversed, because the object is moving though the water. The following expression is used to gain some perspective about the frequency of vortex induced vibrations.

$$St = \frac{f \cdot D}{U} \tag{10.37}$$

where

St	*Strouhal number (=0.2)*
f	*frequency*
D	*Diameter*
U	*Flow velocity*

The diameter is chosen equal to half the width of the gate. To determine a flow velocity, the time it takes for the gate to close is used to calculate the velocity of the gate moving through the water. The closing time is 4.7 min, see Table 4. Considering the entire process of closing the gate including starting up and slowing down till closure, between these two moment the velocity will be constant. According to Design of Locks (Vrijburcht & Glerum, 2000), the movement time regardless of lock width doesn't exceed 120 s. The constant part of the closing process is assumed to be 120 s. The distance travelled is equal to the span of the gate (=55m). The velocity is found

$$U = \frac{55}{120} \approx 0.46 \ {}^{m}/_{s} \tag{10.38}$$

The vortex shedding frequency can now be determined.

$$f = \frac{St \cdot U}{D} = 0.0092 \tag{10.39}$$

This frequency is very low in comparison to the eigenfrequencies found with the Scia model. The velocity of the gate moving through the water is probably not fast enough to really affect the stability of the gate during movement.

10.6.2 Vessel collision

A special load case, not considered in this thesis, is a vessel collision. During a vessel collision, enormous forces are exerted on the gate in a short time span. If this would occur during opening or closing of the gate, this sudden burst of energy can have serious consequences on the stability of the gate. Measures to quickly dissipate large amounts of energy should be applied to prevent this.

10.7 FRP – Optimizing the material

The chosen material can play an important role in finding the optimum gate shape. To achieve the desired shape, stronger base materials could be applied. Another improvement is the use of different laminates depending on the requirements at a specific position in the gate. For example, apply a stronger laminate for the retaining plates at mid-span, compared to the materials applied at both ends.

However, in order for the material to be optimized, the required dead weight to guarantee stability under all conditions must be brought down first. In other words, other aspects of the gates design, one of which is the shape, must be optimized first. If the weight can't be reduced significantly, the lightweight quality of FRP cannot be utilized fully.

10.8 Key points

- For all the gates, strength criteria were still easily met.
- Deflection becomes a problem. The gate shape of model 4c did not meet deflection criteria. This can be solved by increasing the gate thickness around mid-span or improving the laminate properties.
- The main objective of the shape changes was to decrease the required dead weight for stability. However, the changes did not have the desired effect. The wide base, narrow top design was thought to improve the vertical moment contribution (increase arm, reduce force). An increase of the deflection of the unsupported corner was also expected to have a positive effect on the horizontal moment contribution (due to pivoting of the gate), but it was seen that the horizontal load was increasingly taken by the lower left support. An explanation could be the increased surface are towards the base of the gate.
- Model 4d performed relatively well for strength and deflection. On average the gate is much narrower than the box shape gate, but the performance is similar. An interesting change was observed in the distribution of the self-weight of the gate over the vertical supports. So far this distribution was almost equal over all four supports. This was not the case for model 4d. The uneven distribution of the self-weight had a negative effect on the stability of the gate during movement.
- Required dead weight increased for all investigated shape changes. The main reason was an disadvantageous distribution of the total stabilizing moment (horizontal + vertical).

Concluding Part

Conclusions and Recommendations

11 Conclusions and recommendations

In this chapter, the research performed in this thesis and the results found are evaluated. The conclusions are drawn and the research questions are answered. Finally some recommendations are made regarding this research and potential future research related to the subject matter of this thesis.

11.1 Conclusions

It was established that the stability of the gate during movement is an important and sometimes critical aspects of a rolling lock gate design. It is also seen that FRPs are becoming a more commonly used building material in many civil engineering applications including locks. One quality of FRPs is the fact that it has a high strength to weight ratio. However, an important factor in the stability of the rolling lock gates is self-weight. A minimum weight is required to counter the moment caused by horizontal loads during opening and closing. If FRPs were to be applied in rolling lock gates an optimization of lightweight versus stability will be required. The objective of this thesis was to investigate the technical feasibility of the FRP rolling lock gate and how the gates design is affected by the stability criteria.

11.1.1 Box gate design

To quantify the problem a case study was chosen: New Lock Terneuzen. A rolling lock gate is set to be constructed to improve the connection between Ghent-Terneuzen. The rolling gates will be very large, with a span of 55 m and a height of approximately 26 m.

For the initial design a box shaped gate was chosen. The global dimensions of the gate and its structural elements were determined with a hand calculation. The stability problem was simplified to a 2D cross-section of the gate determining equilibria between horizontal loads and vertical support reactions. The gate was horizontally loaded by a remaining head difference and waves, the stability criteria were found to be governing. This lead to a gate with conservative dimensions. Consisting of two retaining plates, executed as a sandwich with a skin thickness of 280 mm and a foam core of 200 mm. The retaining plates are connected by horizontal webs, evenly spread out over the height of the gate. Also executed as sandwich plates, the skin thickness of the webs was 200 mm and the foam core thickness was 200 mm. The global thickness of the gate, measuring from the outer edges of the retaining plates, was 8960 mm.

A 3D model was made with Scia Engineer to check the structure with finite element analysis. Because of the conservative dimensions found, fatigue was not a problem. The results from this model were also used to estimate the dimensions of gates with alternative shapes.

11.1.2 FRP vs Steel

The same gate was also dimensioned in steel. When comparing the steel and FRP box gates, the results showed that significantly more material had to be used for the FRP gate to meet all requirements. It should be noted that both designs were not optimized. However, it can be concluded that the required dead weight for stability must be brought down drastically for FRP to be a viable option for a rolling lock gate of this scale. The table below presents the volumes of material used in both gate designs, the mass and roughly estimated material costs.

Table 47. Volume of applied material - Steel vs FRP

	Volume [m³]	Mass [kg]	Cost [€]
Steel box			
Steel	385	3.022.250	4.533.375
FRP box			
FRP	1435	2.832.690	11.330.760
Foam	1206	120.600	120.600

11.1.3 Carriage width vs. stability

With the Scia model, the stability problem was also evaluated in 3D. The horizontal and vertical support reactions could be determined and with these values known, the stability was checked. In addition, the distance between supports, resembling the width of support carriages, was varied from 0.5 to 12 m. As expected, with a wider carriage width, the stability improved and the required dead weight reduced. However, when the carriage with was narrowed, the results weren't necessarily as expected. A smaller distance between vertical supports, means reducing the arm of the couple and thereby increasing the required dead weight, because the stabilizing moment remains the same. However, other aspects related to the stability are affected as well. The distribution of loads over the supports, horizontal loads in particular, resulted in a significant increase in the horizontal contribution to the stabilizing moment. As a result, the vertical contribution decreases. Improving the stability of the gate, but more importantly reducing the required dead weight is not as straightforward as it seems. Deflections of the gate and distribution of loads play a crucial role when optimizing the design for stability.

11.1.4 Effects of shape changes

From the results found, potential improvements to the box gate were conceptualized. Optimizing the shape of the gate could improve stability, reduce required dead weight and make FRP a more appealing choice for rolling gate design. The main idea was a gate with a wide base to accommodate wide support carriages. A wide base in combination with a box shape results in considerable buoyancy forces, so to limit the buoyancy the thickness of the gate will be reduced towards the top of the gate where strength and deflection criteria allows it. Four models with various shapes were created to investigate the effects of the shape changes.

The applied shape changes did not have the desired effect, i.e. the required dead weight for stability did not go down. Against expectation, the required weight went up. The distribution over the horizontal supports is significantly influenced by the shape of the gate, similar to the response when narrowing the carriage width. This distribution weighs so heavy on the results, because the gate is relatively high. In other words, the horizontal support reaction working at the top of the gate generates a very large moment. If the contribution to the stabilizing moment shifts more towards the vertical supports, the required dead weight increases dramatically due to the fact that the arm is much smaller. For the gates with a wider base, the vertical contribution to the stabilizing moment is significantly larger in comparison to the box gate. It should be added that the shape changes are not optimized and were rather extreme, for example gate 4a goes from 12 m at the base to 2 m towards the top. Smaller and more subtle changes in the shape could prove to give

better results. The table below presents the division of moment contributions, vertically and horizontally.

Table 48. Comparison of moment contributions and required dead weight

Gate	Width [m]	Hor. [kNm]	Vert. [kNm]	Required Dead weight [kN]
3a	8	69519	26391	19792
4a	12	57045	41495	20748
4b	10	57178	40613	24368
4c	10	59186	37782	22669
4d	4 - 8	67149	29159	21869

It should also be considered that an irregular and asymmetrical shaped gate complicates other aspects of the gates design. The lock head becomes much more complex. Manufacturing will be more difficult, because structural elements of various shapes and sizes will be required. As opposed to a box, where many elements will be the same in shape and size.

11.1.5 Final conclusion

The primary research questions were as follows:

- *Is it technically feasible to use fibre-reinforced polymers in rolling lock gates?*
- *How do requirements for stability during movement* affect the rolling gates design in FRP?*

* Movement refers to opening and closing of the gate.

The application of FRP in rolling gate design is technically feasible. However from a stability point of view it's questionable if FRP is the better choice over traditional materials. In the chosen case study, the amount dead weight required for stability is significant, and the lightweight quality of FRP cannot be taken advantage of. Laminates are designed much thicker when compared to the dimensions required to meet strength and deflection criteria. In other words, material is added primarily for the sake of adding weight.

Reducing the required dead weight was proven to be much harder than anticipated. Even though a wide base is advantageous to the stability of a structure, the required weight is not necessarily reduced. The applied loads, shape of the gate, location of supports and deflections all affect the distribution of loads over the supports of the gate. In a structure of this scale, even small differences can have a significant impact on the stability of the gate and the dead weight required to achieve this stability.

The required dead weight to meet the stability criteria must be brought down in order for FRP to be a viable option.

11.2 Recommendations

The recommendations are divided into two sections. In the first section recommendations are made regarding this research specifically. The second section gives recommendations regarding future research related to or based on the findings in this research.

11.2.1 Recommendations for this research

- Determine the loads related to a rolling gate during movement more accurately and in more detail. The stability load case has a large impact on the results concerning the required dead weight.
- Include the dynamic behaviour of the rolling gate when moving through the water.
- Determine the accuracy of the applied supports in the models. How accurate are the flexible horizontal supports and do vertical supports resemble the distribution of forces with support carriages in reality?
- Include detailed analysis of the support carriages and operating machinery. Forces generated by pulling the gate play a role in the stability during movement. These forces were not taken into account in this research.
- Take other aspects of the gates design into consideration when comparing steel and FRP. For example: Fatigue behaviour, corrosion, maintenance and lifetime costs.
- Investigate the potential advantages of a lighter gate. It is expected that wear-and-tear of operating mechanism parts could be significantly reduced. The question is if the benefits are large enough.
- Evaluate other case studies. With different dimensions and loads the results could be quite different.
- Detailed design of the FRP rolling gate. Dimension joints, support carriages, lock head, locking valves.
- In the models, the material properties were defined as the combined properties of the laminate skin and core. A more detailed approach to the interaction between the two and a closer look at failure mechanisms of the laminate is recommended.
- More detailed determination of stability criteria. The applied criteria of x=W/6 is a conservative rule of thumb.

11.2.2 Recommendations for future research

- Optimize the shape of the gate to bring down the required dead weight for stability, also optimize the base materials and laminates to achieve the required shape.
- Further investigate the distribution of loads over the vertical and horizontal supports. What could be changed in the design to achieve the most advantageous distribution.
- Investigate other load cases that are important for the stability of the gate. This research was limited to normal operation loads. Special load cases, vessel collision in particular should be investigated in detail.
- Investigate other operating mechanism layout, for example a wheelbarrow layout.
- In depth analysis of a buoyancy-based stability (FRP) rolling gate. Making a gate as lightweight as possible is beneficial in this case, as opposed to gravity-based stability. New challenges arise, but from a stability perspective it shows promise.

Bibliography, figures, tables

Bibliography

Bonnes, J. (2005). *Flexibele zeesluis als nieuwe maritieme toegang kanaal Gent Terneuzen.* TU Delft.

Campbell, F. (2010). *Structural Composite Materials.* ASM International.

CUR-96. (2003). *Aanbeveling 96 Vezelversterkte Kunststoffen in Civiele Draagconstructies, CUR-commissie C124.* CUR.

CUR-96. (2003). *Aanbeveling 96 Vezelversterkte Kunststoffen in Civiele Draagconstructies, CUR-commissie C124.* CUR.

CUR-Aanbeveling 96 - Achtergrondrapport. (2003). *Vezelversterkte kunststoffen in civiele draagconstructies.* Civieltechnisch Centrum Uitvoering Research en Regelgeving.

Daniel, R. A. (2011). *Contact Behavior of Lock Gates and Other Hydraulic Closures.* Lap Lambert Academic Publishing.

Doeksen, J. (2012). *Gate Design For Large, High Head Locks.* Technische Universiteit Delft, DHV.

EUROCOMP. (1996). *Structural Design of Polymer Composites.* (J. L. Clarke, Ed.) E & FN Spon.

FiberCore Europe. (2015). Retrieved from http://www.fibercore-europe.com/

GangaRao, H., & Vijay, P. (2010). *Feasibility Review of FRP Materials for Structural Applications.* Constructed Facilities Center, Dept. of Civil & Env. Engineering.

IenM. (2016). *Ontwerp Tracébesluit Nieuwe Sluis Terneuzen.* Ministerie van Infrastructuur en Milieu.

Kaw, A. (2006). *Mechanics of Composite Materials 2nd Edition.* Taylor & Francis Group.

Kok, L. (2013). *Feasibility Study for FRP in Large Hydraulic Structures.* Witteveen+Bos, TU Delft.

Kolkman, P., & Jongeling, T. (1996). *Dynamisch Gedrag van Waterbouwkundige Constructies, Deel A.* Rijkswaterstaat.

Kolkman, P., & Jongeling, T. (1996). *Dynamisch Gedrag van Waterbouwkundige Constructies, Deel B.* Rijkswaterstaat.

Kolkman, P., & Jongeling, T. (1996). *Dynamisch Gedrag van Waterbouwkundige Constructies, Deel C.* Rijkswaterstaat.

Kolstein, M. (2008). *Fibre Reinforced Polymer (FRP) Structures.* Technische Universiteit Delft.

Laukaitis, A., & Boyce, V. (n.d.). *Unlocking the Potential of the Panama Canal.*

Leidraad Kunstwerken. (2003). *Technische Adviescommissie voor de Waterkeringen.*

MARIN. (2015). *Capaciteitsonderzoek Nieuwe Grote Zeesluis Kanaal Gent-Terneuzen.*

Mazumdar, S. K. (2002). *Composites Manufacturing: Materials, Product and Process Engineering.* CRC Press.

Ministerie van Verkeer en Waterstaat. (2007). *Hydraulische Randvoorwaarden primaire waterkeringen (HR2006).*

Moen, J. (2014). *Feasibility study on heavy-traffic FRP bascule bridges.* Technische Universiteit Delft, Witteveen+Bos.

Molenaar, W., & e.a. (2011). *Lecture Notes, CT3330 Hydraulic Structures - Locks.* Hydraulic Engineering, Faculty of Civil Engineering, TU Delft.

Molenaar, W., Baars, S. v., Kuijper, H., & e.a. (2008). *Manual Hydraulic Structures.* Technische Universiteit Delft.

Mosallam, A. (2011). *Design Guide for FRP Composite Connections.* American Society of Civil Engineers.

PIANC. (2014). *Report No 138, Mechanical and Electrical Engineering lessons Learnt from Navigation Stuctures.*

Portaal van Vlaanderen. (2016). Retrieved from http://www.portaalvanvlaanderen.nl/

Rijkswaterstaat. (2013). *Kenmerkende waarden Getijgebied 2011.* RWS Centrale Informatievoorziening.

ROK-1.3. (2015). *Richtlijnen Ontwerpen Kunstwerken - versie 1.3, Rijkswaterstaat.*

Straten, R. v. (2013). *Feasibility study on fibre reinforced polymer slides in the Eastern Scheldt storm surge barrier.* Technische Universiteit Delft, Witteveen+Bos.

Strong, A. B. (2008). *Fundamentals of Composite Manufacturing - Materials, Methods and Applications.* Society of Manufacturing Engineers.

TAW. (1997). *Leidraad Waterkerende Kunstwerken en Bijzondere Constructies.* Technische Adviescommissie voor de Waterkeringen.

VNSC. (2015). *Deelrapport MER Verkeer en Vervoer.* Vlaam-Nederlandse Scheldecommissie.

Vrijburcht, A., & Glerum, A. e. (2000). *Ontwerp van Schutsluizen.* Bouwdienst Rijswaterstaat.

Waterloopkundig laboratorium. (1981). *Krachten op de roldeur tijdens het vóórtrekken.*

youtube/Nieuwe Sluis Terneuzen. (2015). Retrieved from https://www.youtube.com/watch?v=9fy2hOOkpZw

Zoghi, M. (Ed.). (2013). *The International Handbook of FRP Composites in Civil Engineering.* CRC Press.

Zorgdrager, A. (2014). *Feasibility Study on the Application of fiber-reinforced polymers in large lock gates.* TU Delft, Iv-Infra.

Figures

Tables